ISTANBUL TECHNICAL UNIVERSITY ★ GRADUATE SCHOOL OF SCIENCE ENGINEERING AND TECHNOLOGY

DEVELOPMENT OF ALTERNATIVE FISCHER-TROPSCH CATALYSTS FOR CONVERSION OF SYNTHESIS GAS INTO LIQUID FUELS

PhD THESIS

Murat BARANAK

Chemical Engineering Department

Chemical Engineering Doctorate Program

NOVEMBER 2014

ISTANBUL TECHNICAL UNIVERSITY ★ GRADUATE SCHOOL OF SCIENCE ENGINEERING AND TECHNOLOGY

DEVELOPMENT OF ALTERNATIVE FISCHER-TROPSCH CATALYSTS FOR CONVERSION OF SYNTHESIS GAS INTO LIQUID FUELS

PhD THESIS

Murat BARANAK
(506042006)

Chemical Engineering Department

Chemical Engineering Doctorate Program

Thesis Advisor: Prof. Dr. Hüsnü ATAKÜL

NOVEMBER 2014

İSTANBUL TEKNİK ÜNİVERSİTESİ ★ FEN BİLİMLERİ ENSTİTÜSÜ

SENTEZ GAZINDAN SIVI YAKIT ÜRETİMİNE YÖNELİK ALTERNATİF FISCHER TROPSCH KATALİZÖRLERİNİN GELİŞTİRİLMESİ

DOKTORA TEZİ

Murat BARANAK
(506042006)

Kimya Mühendisliği Anabilim Dalı

Kimya Mühendisliği Programı

Tez Danışmanı: Prof. Dr. Hüsnü ATAKÜL

KASIM 2014

Murat Baranak, a **Ph.D.** student of ITU **Graduate School of Science Engineering and Technology** student ID 506042006, successfully defended the **thesis** entitled "**DEVELOPMENT OF ALTERNATIVE FISCHER-TROPSCH CATALYSTS FOR CONVERSION OF SYNTHESIS GAS INTO LIQUID FUELS**", which he prepared after fulfilling the requirements specified in the associated legislations, before the jury whose signatures are below.

Thesis Advisor :	**Prof. Dr. Hüsnü ATAKÜL** İstanbul Technical University	.....
Jury Members:	**Prof.Dr. Ahmet SİRKECİOĞLU** İstanbul Technical University	.....
	Prof. Dr. Melkon TATLIER İstanbul Technical University	.....
	Prof. Dr. Ahmet Erhan AKSOYLU Boğaziçi University	.....
	Prof. Dr. İsmail BOZ İstanbul University	.....

Date of Submission : 15 September 2014
Date of Defense : 12 November 2014

FOREWORD

First, I would like to express my gratitude to my thesis supervisor Prof. Dr. Hüsnü ATAKÜL who have supported me throughout my thesis with his invaluable guidance and experience. He was always very positive and kind within the passing years.

I also have to acknowledge Prof. Dr. Ahmet Erhan AKSOYLU, Prof. Dr. Ahmet SİRKECİOĞLU for accepting to be a member of the examining committee and for devoting their valuable time to read my thesis.

The support provided by TÜBİTAK project is gratefully acknowledged. This work was financially supported by The Scientific and Technological Research Council of Turkey (TÜBİTAK) through the project TÜBİTAK 1007-108G043 "Liquid Fuel Production from Coal and Biomass Blends". The financial support provided by İstanbul Technical University Research Fund project is also acknowledged.

I would like to thank Betül Gürünlü for her great effort and help. I have also thank to Assoc. Prof. Dr. Alper Sarıoğlan, who helped and advised me throughout my thesis. Special thanks to Mevlüt Oranlı and Hüseyin Çamkerten for their technical support.

I would like to thank my "large family", especially my mother and my father, since all of them have paid me great attention and made me feel that they have been always standing spiritually just behind me, which has given me great confidence.

Even though I am not capable of expressing my thankfullness, I wish to thank to my dearest family members and my wife, Ayşe for her support, patience, encouragement and trust in me Also I have to express my love to my daughter and son, Zeynep Duru and Emin.

September 2014

Murat BARANAK
(Chemical Engineer)

TABLE OF CONTENTS

Page

ABBREVIATIONS

AGR	: Acid gas removal unit
ASU	: Air separation unit
BPD	: Barrel per day (159 lt /day)
CCS	: Carbon capture and sequestration
CTL- OT	: Coal to liquid process, once through FT reactor (w/o :recycle)
CTL- RC	: CTL process with FT tail gas recycle line w/o reformer reactor
CTL-RC-SR	: CTL-RC process having steam reformer reactor on recycle line
F	: Mass flow rate (kmol/h)
FID	: Flam Ionization detector
FT	: Fischer – Tropsch
GC	: Gas chromotography
GTL	: Gas to Liquid Process
HC	: Hydrocarbons
H_2/CO	: Hydrogen to carbonmonoxide molar ratio
ICP	: Inductively coupled plasma
LHV	: Lower heating value (kJ/kg)
$\dot{m}$	: Mass flow rate (kg/h)
SEM	: Scanning electron miscroscoby
SR	: Steam reforming reactor
S:C	: Steam to carbon molar ratio of steam reforming reactor
TCD	: Thermal conductivity detector
TGA	: Thermo gravimetric analysis
TOS	: Time on stream
WGS	: Water gas shift reactor
$X_{FT,CO}$	: FT reactor CO conversion
XRD	: X-ray diffraction
$X_{TOT,CO}$	: FT synthesis subsystem overall CO conversion
$X_{SR,C}$	: Steam reformer reactor carbon conversion
$W_{elec.}$	: Electrical power (kWe)
α	: Anderson schulz flory chain propagation probability
$\mu_{th,gas.}$	: Process liquid fuel (gasoline) thermal efficiency
$\mu_{th,elec.}$	: Process electrical efficiency
$\mu_{th,tot.}$	: Process total efficiency (liquid fuel + electric)
$\mu_{C.}$	: Carbon efficiency

LIST OF TABLES

Page

LIST OF FIGURES

Page

DEVELOPMENT OF ALTERNATIVE FISCHER-TROPSCH CATALYSTS FOR CONVERSION OF SYNTHESIS GAS INTO LIQUID FUELS

SUMMARY

Fischer Tropsch Synthesis is becoming more attractive and feasible as the crude oil prices increase. Environmental and strategic concerns have also encouraged this interest. A major limitation of the Fischer-Tropsch technology is the low selectivity of the conventional catalysts towards targeted compounds, i.e. gasoline. This research study was conducted in order to acquire insight of highly selective Fischer Tropsch catalysts. In particular, emphasis was given zeolite supported iron based bi-functional Fischer Tropsch catalysts. This thesis basically consists of two types of studies: 1. Experimental. 2. Process simulation.

In the first section, the effects of types of zeolites, which were used as supports, on the selectivity and activity of iron-based Fischer Tropsch catalysts were investigated. Five different zeolites, namely ZSM-5, mordenite, beta, Zeolite Y and ferrierite were used as supports in the preparation of the iron-based bi-functional FT catalysts. Totally seven catalysts, six bi-functional and one base iron, catalyst were prepared by using ZSM-5 (Z), mordenite (M) , beta (B) and ferrierite (F) and zeolite Y as support and investigated for their performances in the FT synthesis. They were designated as SFeZ, SFeM, SFeB, SFeF, SFeY5, SFeY80 and BFe. Catalysts were characterized by BET, ICP, TGA and XRD analyses methods. The acidities of the the catalysts were determined by n-butyl amine desorption TGA analyses. Activity tests of catalysts were carried out in a pressurized fixed bed type reactor. The performances of the catalysts were tested at three different temperatures with a fixed H_2/CO ratio. The gas and liquid phase products from the FT reactor were analyzed by using gas chromatography instruments. All catalysts studied were found to be active in FT reactions. The support type and their pore structure was found to have a considerable impact on the activities and selectivities of catalysts. The ZSM-5 supported catalyst displayed the highest selectivity toward gasoline range hydrocarbons, while the highest reactant conversions were obtained with Beta supported catalysts. The percentage of gasoline range hydrocarbons in the entire products, including both gas and liquid phases, from FT synthesis by ZSM-5 supported catalyst, was determined to be 74%.

In the second section of this dissertation, low acidity ZSM-5-supported iron catalysts were synthesized for use in Fischer–Tropsch conversion. The low acidity ZSM-5 was particularly chosen aiming to synthesize a catalyst having lower selectivity for the light and higher selectivity for the gasoline range hydrocarbon components. Selective surface dealumination was also applied to ZSM-5 and the resulting zeolite was used as a support in the synthesis of an iron catalyst in order to obtain a catalyst with enhanced selectivity for gasoline. Two different preparation techniques were used for the catalyst synthesis; i. impregnation, ii. physical mixture. Catalysts with different iron loading degrees (4%, 9%, 18%) were synthesized and tested. The effect of

operating temperature, pressure, the hydrogen to carbon monoxide ratio (H_2/CO) of the feed gas and the gas hourly space velocity (GHSV) on the catalyst FT synthesis performances were also studied, in the scope of the study.

ZSM-5 supported catalysts were synthesized by using incipient wetness impregnation method and a hybrid catalyst was prepared by physical admixing of ZSM-5 and base iron. The performances of catalysts were compared based on the activity, selectivity and hydrocarbon yields. The catalytic activities of the catalysts were found to be considerably affected by the catalyst preparation method, the catalyst iron percentage and the reaction temperature. All catalysts displayed a CO conversion higher than 40% at 553 K. The selectivity toward the gasoline range (C5–C11) hydrocarbons of catalyst prepared by impregnation method varied between 50% and 74%. The selectivity of the hybrid catalyst, on the other hand, toward the same fraction was about 45%. No wax was detected in the products during the FT process carried out by using zeolite-supported iron catalysts. The iron catalyst prepared with dealuminated ZSM-5 displayed higher gasoline range hydrocarbon selectivity in comparison with ZSM-5-supported catalysts with same iron content. Results of a 260 h time-on-stream test, carried out for one of the supported iron catalysts with 9 wt.% Fe (SFeZ9), indicated that the catalyst was stable without any activity loss.

In order to determine an optimum process lay-out and operating conditions for coal-to- gasoline process, without product-up grading after Fischer Tropsch reactor using bi-functional FT catalysts, a simulation study has been carried out. Three coal- to-gasoline processes were simulated, parametrically studied and compared: 1.Coal–to-Liquid process (CTL-OT) with no tail gas recycling, 2.Coal-to- Liquid Process with tail gas recycling (CTL-RC), 3. Coal-to- Liquid Process with tail gas recycling and Processing (CTL-RC-SR) which includes both tail gas recycling and a steam reformer reactor catalytically converting the tail gas into syngas which fed to FT. Although, each process consisted of basic steps of syngas production, syngas purification and FT Synthesis, they were different in respect of re-using of the unused syngas from FT reactor (tail gas) and the targeted final products, i.e. gasoline and electricity. A bi-functional catalyst was used in the FT reactor. FT products obtained with this catalyst is overwhelmingly rich in C5-C11 range HC known as gasoline. Therefore, upgrading of the raw liquid product from FT reactor is no longer needed. The tail gas recycling ratio and pressure, the temperature, the steam to carbon ratio (S/C) of the reformer reactor and conversion/selectivity of the FT reactor were determined to be critical parameters and their effects on processes' performances were addressed.

Simulation results indicated that CTL-RC-SR has the maximum gasoline production efficiency of %50, followed by CTL-RC (31.4%) and CTL-OT (22.3%). A reversal tendency was determined in the electrical efficiencies which are, in descending order, CTL-OT (22.6%) > CTL-RC (15.8) > CTL-RC-SR (0.5%).

SENTEZ GAZINDAN SIVI YAKIT ÜRETIMINE YÖNELIK ALTERNATIF FISCHER TROPSCH KATALIZÖRLERININ GELIŞTIRILMESI

ÖZET

Ham petrol fiyatlarının artmasına bağlı olarak, Fischer Tropsch (FT) sentezi günümüzde daha fazla ilgi çekmekte ve ekonomik olarak uygulanabilir hale gelmektedir. Ekonomik ve stratejik faktörlerde bu ilginin artmasına katkı sağlamaktadır. FT sentezinin en önemli kısıtlarından bir tanesi halen kullanılmakta olan katalizörlerin hedeflenen ürünlere, örneğin benzin aralığındaki hidrokarbonlara karşı olan seçiciliklerinin düşük olmasıdır. Geleneksel FT reaktörlerinde elde edilen hidrokarbon ürünler metandan kırk karbonlu hatta daha uzun hidrokarbonlara kadar değişen geniş bir dağılım göstermektedir. Seçicilik problemini aşabilmek için, FT reaktörleri uzun zincirli vaks üretimini maksimize edecek şartlarda çalıştırılmaktadırlar. FT reaktörü sonrasında uygulanan ürün iyileştirme aşamasında ise elde edilen ham sıvı ürün ("syn-crude") parçalama, izomerizasyon... vb. çeşitli operasyonlardan geçirilerek benzin, dizel ve çeşitli kimyasallara dönüştürülmektedir. FT reaktöründe seçiciliğin arttırılması ve bu iki aşamalı prosesin tek aşamada gerçekleştirilebilmesi, FT aktif katalizörlerle hidroizomerizasyonu/parçalamayı gerçekleştirme özelliklerine sahip katalizörlerinin bir arada kullanılması yoluyla sağlanabilir. Zeolitler, FT reaktörlerine bu ikinci katalitik fonksiyonun eklenmesi amacıyla kullanılabilecek katalitik malzemelerin başında gelir.

FT aktif metaller (demir, kobalt) ile zeolitin birlikte kullanıldığı katalizörlerde; aktif metali FT reaksiyonları vasıtasıyla hidrokarbon zincirlerinin oluşmasını sağlar, zeolit ise parçalama ve izomerizasyon reaksiyonları yoluyla oluşan hidrokarbonların zincir uzunluğunu düzenler. Bunun yanı sıra, zeolit kanalları içerisinde gerçekleşen reaksiyonlar sonucunda ortaya çıkan ürünlerin zincir uzunlukları doğal olarak kanal boyutlarıyla sınırlanmış olmaktadır. Bu iki katalitik fonksiyona birden sahip olan bu katalizörler "*bi-fonksiyonel (bi-functional)*" katalizörler olarak isimlendirilmektedir.

Bu tez çalışmasında, sıvı ürünler, özellikle benzin grubu hidrokarbonlara karşı yüksek seçiciliğe sahip alternatif FT katalizörlerinin geliştirilmesi amaçlanmıştır. Çalışmada zeolit destekli demir bazlı FT katalizörleri üzerine yoğunlaşılmıştır. Tez temel olarak iki tip çalışmayı içermektedir: i. Deneysel çalışma. ii. Proses simülasyonu.

Deneysel çalışmada, demir ve çeşitli zeolitler kullanılarak bi-funsiyonel zeolit-destekli katalizörler sentezlenmiş ve incelenmiştir. Çalışmada destek malzemesi olarak ZSM-5 (Z), mordenit (M), beta (B), Zeolit Y (Y) ve ferrierite (F) olmak üzere beş farklı tip zeolit kullanılmıştır. Sentezlerde, silika alümina oranları farklı iki farklı tip Zeolit Y kullanılmıştır. Bu kapsamda, altı tanesi bi-fonksiyonel biri baz demir (desteksiz) olmak üzere, toplam yedi adet katalizör sentezlenmiş, karakterize edilmiş ve bunların FT sentezindeki performansları incelenmiştir. Sentezlenen katalizörler kullanılan zeolitin tipine bağlı olarak SFeZ, SFeM, SFeB, SFeF, SFeY5, SFeY80 ve BFe (baz demir) olarak isimlendirilmiştir. Sentezlenen katalizörler, XRD, BET, ICP,

SEM ve TGA gibi çeşitli analiz yöntemleri kullanılarak karakterize edilmiştir. Sentezde kullanılan taze zeolitlerin asiditeleri n-bütil amin desorpsiyonu TGA yöntemi ile belirlenmiştir. FT sentezinden elde edilen gaz ve sıvı faz ürünlerinin bileşim analizleri gaz kromatografi cihazları kullanılarak yapılmıştır. Katalizörlerin FT aktivite/performans testleri ise basınçlı sabit yatak tipi bir reaktör kullanılarak gerçekleştirilmiştir. Çalışmanın bir bölümünde, katalizör testleri sabit basınç ve önceden belirlenmiş bir gaz bileşimi için üç farklı sıcaklıkta gerçekleştirilmiştir.

Elde edilen deneysel sonuçlara göre, sentezlenen bütün katalizörlerin FT sentezinde aktivite gösterdikleri belirlenmiştir. Ancak katalizörlerin aktivite dereceleri, beklendiği gibi farklı olmuştur. Kullanılan zeolitin tipi ve yapısının katalizörlerin aktivite ve seçiciliklerini etkiledikleri görülmüştür. Sonuçlar, sentezlenen zeolit destekli demir katalizörlerin baz demir katalizöre kıyasla daha yüksek FT akitivitesi, daha düşük CO_2, vaks ve hafif hidrokarbon seçiciliği, daha yüksek benzin grubu hidrokarbon seçiciliği ve daha düşük aktif metal gereksinimi gibi önemli avantajlara sahip olduğunu göstermiştir ZSM-5 destekli demir katalizör (SFeZ) benzin aralığındaki hidrokarbonlara karşı en yüksek seçiciliği gösterirken, en yüksek dönüşüm değerleri beta destekli katalizörlerden (SFeB) elde edilmiştir. ZSM-5 destekli katalizörle yürütülen FT sentezinden benzin aralığındaki hidrokarbonların üretilen tüm hidrokarbon ürünler içindeki oranı %74 olarak saptanmıştır.

Tezin ikinci bölümünde, ZSM-5 içerikli demir bazlı katalizörler üzerinde yoğunlaşılmıştır. Çalışma kapsamında katalizörler iki farklı yöntem kullanılarak sentezlenmiştir: i. impregnasyon, ii. fiziksel karışım. Farklı demir yükleme oranlarına sahip (%4, %9, %18) katalizörler sentezlenmiş ve test edilmiştir. Bunun yanı sıra, taze ZSM-5 zeolitine seçici yüzey de-alüminasyonu işlemi uygulanmış ve elde edilen de-alümine zeolit destekli demir esaslı FT katalizörün sentezinde kullanılmıştır. Sentezlenen katalizörler yine daha önce belirtilen yöntemler kullanılarak karakterize edilmişlerdir. Sıcaklık, basınç, boşluk hızı, sentez gazının bileşimi gibi parametreler temel alınarak katalizörlerin FT sentezi aktiviteleri testleri değişik koşullarda gerçekleştirilmiştir.

ZSM-5 destekli katalizörler emdirme yöntemiyle, hibrit katalizörler ise ZSM-5 ile baz demirin fiziksel olarak karıştırılması yoluyla sentezlenmiştir. Katalizörlerin performansları aktivite, seçicilik ve hidrokarbon üretimleri temel alınarak karşılaştırılmıştır. Katalizörlerin katalitik aktivitelerinin katalizör sentez yöntemi, katalizörlerin demir oranı ve reaksiyon işletme koşullarından önemli ölçüde etkilendiği gözlenmiştir. Sentezlenen bütün katalizörler 553 K'de %40'ın üzerinde bir CO dönüşümü sağladığı görülmüştür. Emdirme yöntemi ile hazırlanan katalizörlerle gerçekleştirilen FT sentezlerinde üretilen sıvı ürünlerde benzin aralığındaki hidrokarbonların oranı %50 ile % 74 arasında değişirken, hibrit katalizörde bu oranı %45 olarak saptanmıştır. Zeolit içerikli katalizörler ile yapılan sentezlerde vaks oluşumu gözlenmemiştir. De-alümine edilmiş ZSM-5 kullanılarak sentezlenen demir bazlı katalizör, benzin aralığındaki hidrokarbonlara karşı, aynı oranda demir içeren ZSM-5 destekli katalizöre göre daha yüksek bir seçicilik göstermiştir. Katalizördeki demir oranını artması, beklenildiği gibi katalizör aktivitesinin artmasını sağlamıştır. Sıcaklık ve basıncın artışı ile boşluk hızının düşüşü de, aynı şekilde, reaksiyon aktivitesinin artmasına yol açmıştır. Basınç artışının hidrokarbon seçiciliğini ağır hidrokarbonlara kaydırdığı, boşluk hızının ise incelenen koşullarda seçicilik üzerinde etkili olmadığı görülmüştür. %9 demir içeren katalizör ile 260 saat süren bir ömür testi gerçekleştirilmiş ve test boyunca kaydadeğer bir aktivite kaybı gözlenmemiştir.

Bi-fonksiyonel FT katalizörleri kullanan FT tesisleri için optimum proses tasarımı ile işletme şartlarının belirlenebilmesi amacıyla, tez kapsamında bir proses simülasyonu çalışması yapılmıştır. Üç farklı kömürden benzin üretim prosesinin benzetimi yapılarak, proseslerin performansları parametrik olarak incelenmiş ve karşılaştırılmıştır. İncelenen prosesler şunlardır: 1. Tek geçişli kömürden benzin üretim prosesi (CTL-OT), 2. Artık gazın FT reaktörüne geri beslendiği kömürden benzin üretim prosesi (CTL-RC), 3. Artık gazın sentez gazına dönüştürülerek geri beslendiği kömürden benzin üretim prosesi (CTL-RC-SR). İncelenen bütün prosesler sentez gazı üretimi, gaz temizleme ve FT sentezi gibi temel proses aşamalarından oluşmalarına rağmen, FT artık gazının değerlendirilmesi ve hedeflenen son ürünler (elektrik, benzin vb.) açısından birbirlerinden ayrılmaktadırlar. Simülasyon çalışmasının sonuçları, bi-fonksiyonel FT katalizörlerinin yüksek benzin seçiciliğine sahip olmaları sayesinde, FT prosesinden ürün iyileştirme (product up-grading) aşamasının kaldırılmasının ve sistemin basitleştirilmesinin mümkün olduğunu göstermiştir. Artık gaz geri besleme oranı, buhar reformlama reaktörünün basınç, sıcaklık ve su buharı karbon oranı (S/C) ile FT reaktörünün dönüşüm ve seçiciliği proseslerin performansını etkileyen kritik parametreler olarak belirlenmiş ve sistem performansına etkileri parametrik olarak incelenmiştir.

Simülasyon çalışması sonucunda, en yüksek benzin üretim verimi (%50.2) CTL-RC-SR prosesiyle elde edilmiştir. CTL-RC ve CTL-OT prosesleri sırasıyla %31.4 ve %22.3 benzin üretim verimi değerleri ile bu prosesi takip etmektedirler. Elektrik üretim verimlerinde ise beklenildiği gibi benzin veriminin tersine bir eğilim görülmüş ve prosesler şu şekilde sıralanmıştır : CTL-OT (%22.6) > CTL-RC (%15.8) > CTL-RC-SR (%0.5). Alternatif proseslerin CO_2 emisyonları (kg CO_2/GJ FT yakıtı) açısından karşılaştırıldıklarında en yüksek emisyonu CTL-OT prosesinde oluştuğu görülmüştür. Emisyonlar temel alındığında prosesleri şu şekilde sıralanmaktadır: CTL-OT (135.1) > CTL-RC (80.3) > CTL-RC-SR (26.8).

1. INTRODUCTION

Fischer Tropsch Synthesis, which converts synthesis gas into high quality fuels and chemicals, is becoming more attractive and feasible as the crude oil prices climb above 100 $/barrel and keep increasing (Sudiro and Bertucci, 2009; Dry, 2002). Major uncertainties remain on future prices, but the age of cheap oil is definitively over, justifying FT process. Depletion of oil reserves and increasing environmental concerns have also stimulated this interest. For the countries having coal and/or natural gas but no crude oil reserves, (like South Africa and Turkey) this technology can be regarded politically and strategically important option as well.

A major limitation of the Fischer-Tropsch (FT) technology is the low selectivity of the conventional catalysts towards targeted compounds. Conventional Fischer Tropsch reactor produces so called "syn-crude" containing a wide range of hydrocarbons, ranging from C1 (methane) to C40 and even higher. The well-known Anderson–Schulz– Flory (ASF) kinetics of the FT reaction imposes a limit to the maximum selectivity of 48% attainable for gasoline-range products in the produced hydrocarbons (Botes and Bohringer 2004). It was claimed that by using fixed and fluidized bed reactors at 613 K, a maximum 40% of gasoline in output hydrocarbons could be obtained (Dry, 2002). The primary FT products can be up-graded by using down-stream conversion units enhancing the yield of the desired products.

The product up-grading section of a Fischer Tropsch plant can be regarded as a refinery, processing FT syn-crude, to produce liquid fuels and chemicals. The up-grading section to produce gasoline is generally composed of a syn-crude fractionating unit, a hydrocracking unit, a catalytic (Pt/zeolite) reforming, isomerization and oligomerization reactors (Liu et al, 2011; Dry, 2002). A hydrogen production system should also be installed to feed hydrocrackers and isomerization reactors. The overall complexity of gasoline production makes it less attractive in comparison of the diesel fuel option (Dry, 2002). The cost of the product up-grading section can make up to 15% of the total investment cost of an FT plant.

More than 95% of the transportation fuels is supplied by crude oil. More than 55% of the refined oil is used to produce fuels, especially gasoline and diesel (Sudiro and Bertucci, 2009). Due to the high gasoline demand all over the world and its higher prices in respect to diesel, FT process has become a more favorable option for the gasoline production (Forghani et al, 2009).

The direct production of high octane gasoline through FT reactions is a great challenge related to catalyst and process development. This may be overcome by the use of metal/zeolite bifunctional catalysts, which can enhance the selectivity of the synthesis toward the desired products, i.e. gasoline range hydrocarbons (Martinez, 2007; Forghani et al, 2009; Liu et al, 2011). In the FT process by these catalysts, the active metal (i.e. iron) phase catalyzes FT products consisted of wide range of hydrocarbons with considerable amount of heavy hydrocarbons. These first raw products are then converted into gasoline-range products through various mechanisms such as hydrocracking, olefin oligomerization, and branching that are induced by the zeolite component of the catalyst. On the other hand, the formation of heavy hydrocarbons is considerably hindered by zeolite due to its shape selectivity properties.

The acidity, surface area, pore structure and cation exchange capability of the zeolite support are crucial factors affecting the catalytic performance of zeolite–metal FT catalysts with respect to oligomerization, isomerization as well as hydrocracking reactions. The efficiency and selectivity of a supported zeolite catalyst are closely related to the dispersion and particle size of the active metal component and to the nature of the interaction between the metal and the support.

In the thesis study, bi-functional FT catalysts have been studied with a special focus on zeolite supported iron based catalysts. The main goal of the study was to develop bi-functional FT catalysts with high selectivity towards gasoline range hydrocarbons as well as acceptable activity and durability.

This thesis consists of 6 major chapters: 1. Introduction, 2. Literature Survey, 3. Experimental, 4. Results and Dıscussion, 5. Simulation of the Coal-to-Liquid fuel Processes, 6. Conclusions.

Chapter 2 includes a comprehensive literature survey on Fischer Tropsch Synthesis and catalysis with focus on the bi-functional catalysts. Chapter 3 presents the details of the experimental work carried out.

The Results and Discussion section – Chapter 4, consists of four parts. In the first part, the effect of zeolite type on the catalyst performance was studied. ZSM-5, faujasite, mordenite, ferrierite and beta zeolites were used as supports in the synthesis of iron based FT catalysts. Iron was used as the FT active metal, in the all catalysts synthesized and studied in order to take the advantage of low methane and high olefin selectivity of this metal. The synthesized catalysts were characterized by using X-ray diffraction (XRD), N_2 physisorption, inductively coupled plasma (ICP), n-butyl amine TGA, scanning electomicroscopic (SEM) techniques. A pure iron catalyst was also synthesized and tested to be used as a reference basis. Activity, selectivity and hydrocarbon yields of the catalysts were investigated by means of the activity tests, carried out in a pressurized fixed bed type reactor.

The zeolite ZSM-5 containing catalysts, giving the maximum gasoline selectivity, among alternative zeolites studied, were detailedly investigated in Section 4.2. The ZSM-5 had a very high silica to alumina ratio (280), resulting in a low acidity of the zeolite. The effects of iron loading and preparation method on the catalysts' performences were studied. Zeolite-supported catalysts were synthesized by using incipient wetness impregnation method while the hybrid catalyst was prepared by physical admixing of ZSM-5 and base iron. Selective surface dealumination was also applied to zeolite and the resulting zeolite was used as a support for the catalyst in order to enhance its selectivity. To be used as basis for comparison, an iron and a conventional iron catalyst were also synthesized and tested in the scope of the study. A parametric research on the steady state FT activities, selectivities and stabilities of zeolite containing iron based catalysts was carried out. Effects of operating conditions on the ZSM-5 supported bi-functional catalyst were also studied. Activity tests have been conducted to investigate the effects of operating temperature and pressure, feed gas composition and gas hourly space velocity. Moreover, a 260 h time on stream test was carried out to determine the stability of the catalyst.

Depending on the characteristics of these bi-functional catalysts, the process scheme and operating conditions of the FT process can be different to some extent. The main goal of the Fischer Tropsch process utilizing metal – zeolite bi-functional catalyst

would be to obtain high gasoline yields with a relatively simple process and a lower investment cost. A process simulation study was also conducted aiming to investigate different of coal-to-liquid fuel processes. Typical Turkish coal (SOMA lignite) was used as the coal feedstock. Three coal- to- gasoline processes were simulated, parametrically studied and compared. Because of the selectivity of the catalyst towards heavy hydrocarbons products was very low, the product upgrading section could be eliminated. The recycling ratio, the recycling pressure, the temperature/S:C ratio of the reformer reactor and conversion/selectivity of the FT reactor were determined to be critical parameters and their effects on process performances were addressed. The description and results of the simulation study are given in Chapter 5.

Chapter 6 summarizes the major conclusions that are drawn from the research.

2. LITERATURE SURVEY

2.1 Fischer Tropsch Synthesis - The Motivation

Currently the world's fuel and chemical production is based predominantly on petroleum crude oil. Fuels from crude oil supply about 96–98% of the worldwide energy demand for transportation (land, sea and air transportation) and more than 55% of the oil extracted is refined to produce fuels. Estimates of oil availability span from 40 to 60 years, at the present rate of consumption (Dry, 2002; Sudiro and Bertucci, 2009). Sooner or later, a time will come when mankind will have to look for a replacement for petroleum.

Since crude oil reserves are rapaciously being consumed, their costs are rising. From 1945 to 2008 the oil price rose from $12/barrel to more than $100/barrel, Figure 2.1 (Sudiro and Bertucci, 2009; Url-1). Major uncertainties remain on future prices, but the age of cheap oil is definitively over.

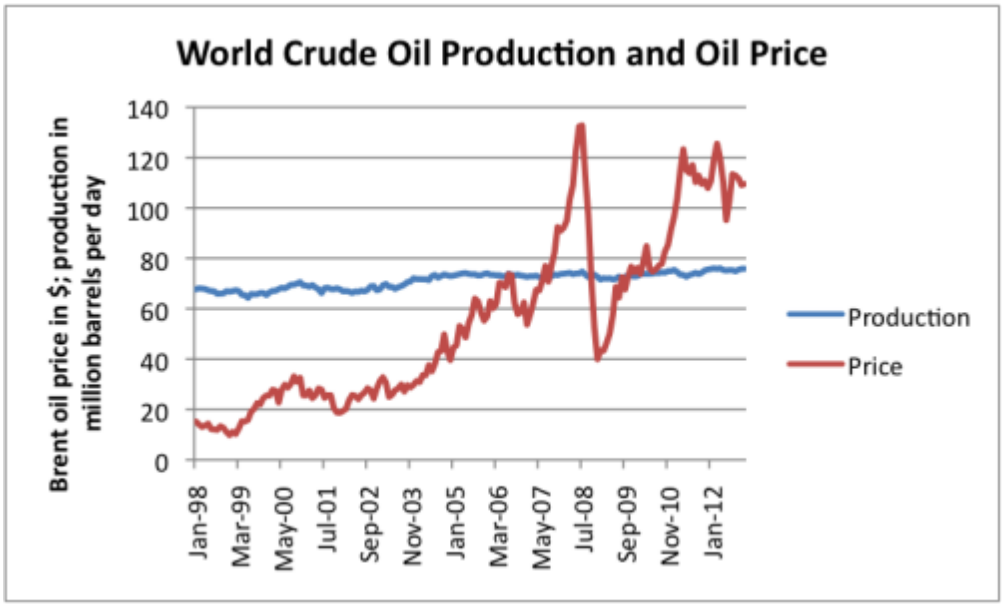

Figure 2.1: World crude oil production and oil price between 1998 – 2012.

The Fischer Tropsch synthesis provides a remarkable alternative way of producing fuels and chemicals from natural gas, coal and biomass. The Fischer Tropsch Synthesis is becoming more attractive and feasible as the crude oil prices climb up. It was estimated that the FT process would be economically preferable when the oil price was above approximately US$20 per barrel (Steynberg et al., 1999). Nowadays, as mentioned above, its price is over 100 $/barrel and keeps increasing. Besides, the presently known reserves of methane and coal exceed that of crude oil by factors of about 1.5 and 25, respectively (Dry, 2002). Moreover, their reserves are more homogeneously distributed around the world. Increasing environmental concerns have also stimulated the interest on the FT synthesis. For the countries having coal and/or natural gas but no crude oil reserves, this technology can be regarded politically and strategically important option as well.

The Fischer Tropsch Synthesis can be considered as a crucial energy technology for Turkey, a country with lack of crude oil but large coal reserves. Turkey, with its developing economy, has increasingly depended on the imported crude oil and related products. Its energy import has risen from 66% in 2000 to 73% in 2007. It is clear that Turkey dependency on the foreign energy will keep increase in the future in parallel to its economic and population growth. Among the imported energy sources, the highest portion belongs to the petroleum and natural gas. Data provided by the Turkish Statistics Institute in Figure 2.2, shows the variation in the amount of crude oil imported by Turkey over the years (Yalınkılıç, 2013). In 2007, 12 billion $ was spent for oil imported. The production of liquid fuels and petroleum-derived chemical from domestic resources like coal will contribute to decrease the foreign dependency, increase energy security and facilitate the economic growth.

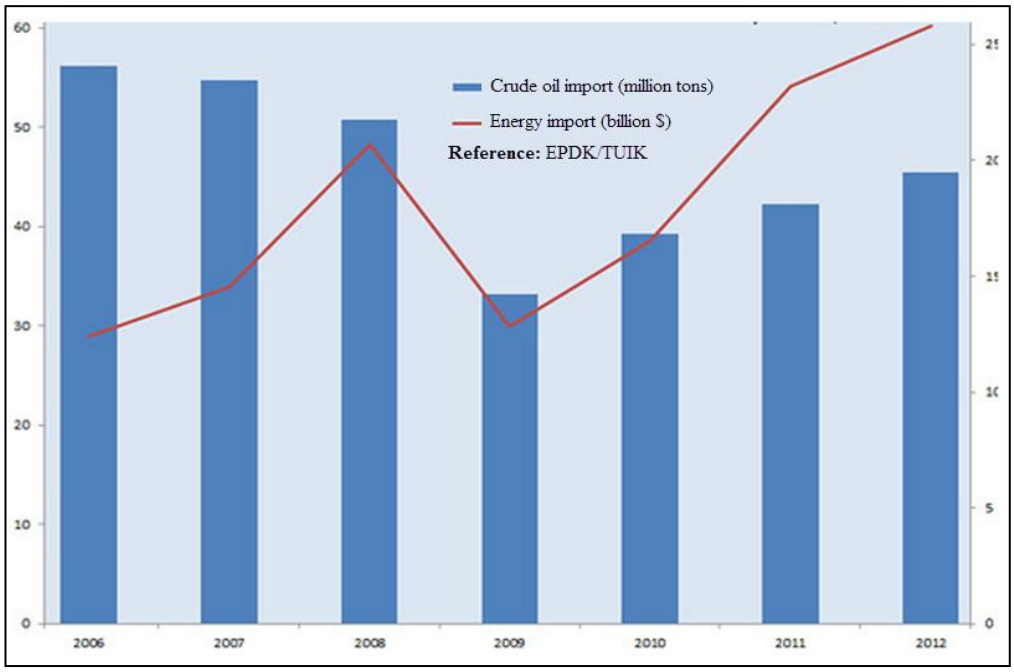

Figure 2.2 : Crude oil import of Turkey between 2006-2012.

2.2 Fischer Tropsch Synthesis - The Process

Fischer Tropsch processes mainly consist of four steps: 1. synthesis gas (syngas) production, 2. syngas purification, 3. Fischer Tropsch (FT) Synthesis and 4. product up-grading. The block diagram of Fischer Tropsch process is given in Figure 2.3 (Laan, 1999).

Synthesis gas can be produced from coal, biomass or natural gas. If the coal or biomass is used as raw material, syngas production is accomplished via gasification unit. Gasification reactor converts the coal feedstock to syngas via reactions taking place in substoichiometric oxygen conditions. For the processes utilizing natural gas feedstock, reforming reactors, i.e. autothermal reforming, steam reforming, partial oxidation, are used for syngas production.

Synthesis gas from gasifier contains some impurities like particulates, tar, NH_3, sulfur compounds (H_2S, COS etc.), aromatic compounds (benzene, toluene, xylene; known as BTX) that are needed to be removed before it introduced to the catalytic reactors.

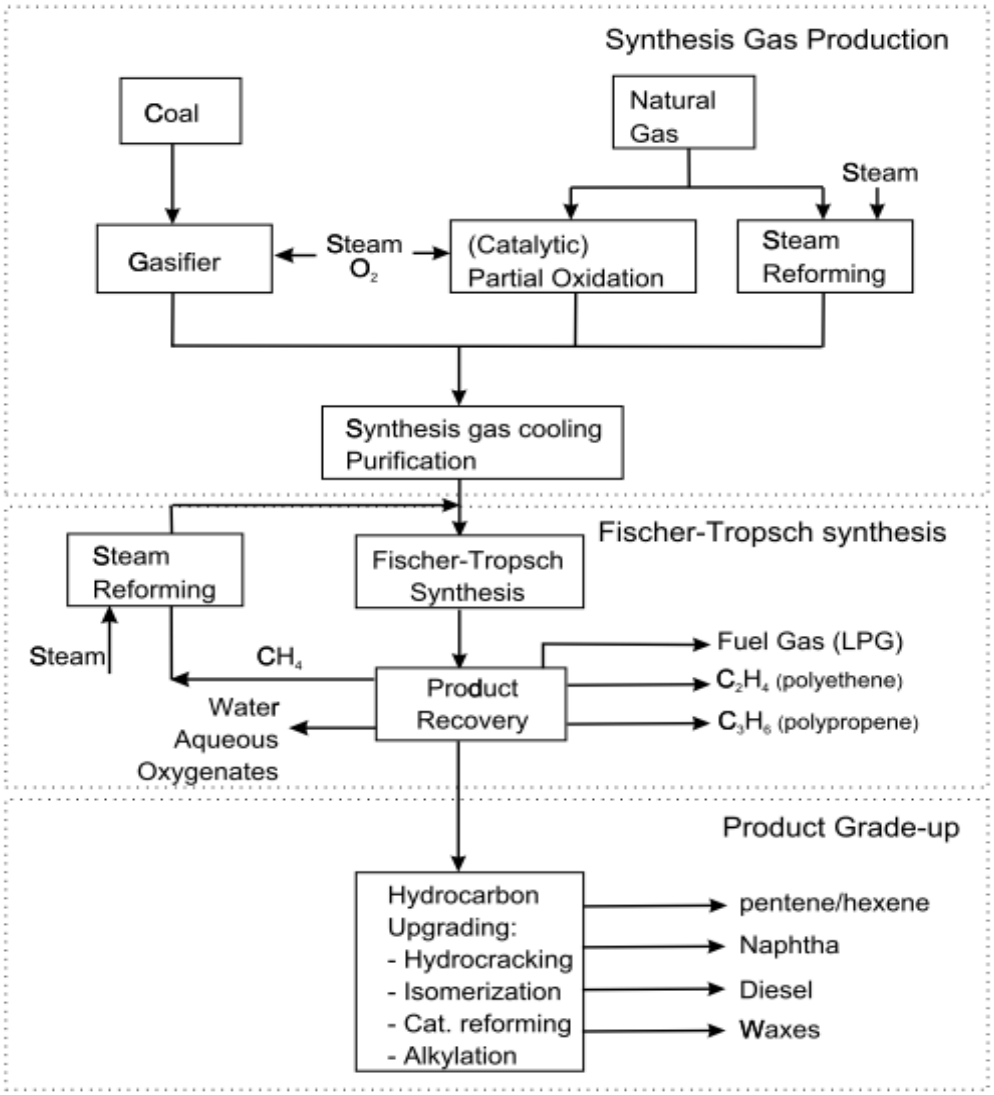

Figure 2.3 : Fischer tropsch syntesis overall process scheme.

The typical Fischer Tropsch catalysts are very sensitive to impurities, even with small concentration. In commercial operation, catalysts are periodically replaced or regenerated after a certain time. The definition of gas cleaning is, based on economic considerations: investment in syngas cleaning versus decrease of reaction rate. Therefore, there is no specific data on maximum acceptable pollutant levels, and the acceptable levels may be different according to the source. The limit concentrations of various impurities/contaminents required in Fischer Tropsch synthesis process , and technologies used to remove them from synthesis gases are listed in Table 2.1 (Gonzalez and Fierro, 2010).

Table 2.1 : The pollutant limit values for FT process and relevant purification technologies.

Contaminant	Limit Value	Removing Technology
Soot (dust, char, ash)	0 ppb	Cyclones, Metal Filters, wet scrubbers
Alkaline (halide metals)	<10 ppb	Active coal bed
Tar	< dew point	Thermal tar cracker, oil scrubber
BTX	< dew point	
Halide compounds (HCl, HBr, HF)	<10 ppb	Aqeous scrubber, active coal
Nitrogen compounds (NH3, HCN)	<1ppm	Aqeous scrubber (NH_3), Active coal bed and hydrolysis (HCN)
Sulphur compounds (H_2S, COS)	<1ppm	ZnO Guard bed; Claus unit (H_2S) Active coal bed and hydrolysis (COS)

With respect to the other possible constituents (CO_2, N_2, CH_4 and higher hydrcarbons) of the FT feed, there are no specific limitations. Required specifications are determined by economic considerations. Nevertheless, an upper limit around of 15 vol.% is considered to be acceptable for the concentration of inert gases, although lower concentrations are preferred if possible because the presence of inert compounds requires larger reactors and higher total gas pressures (Gonzalez and Fierro, 2010).

A water gas shift reactor (WGS) can be integrated into the process in order to control and adjust the hydrogen to carbon monoxide (H_2/CO) ratio to the stoichiometric consumption level in the FT reactor (Dry, 2002). The required H_2 to CO ratio for the cobalt-based FT catalysts is approximately 2.15. This ratio, however, can be slightly lower for the iron-based catalysts as they perform WGS reaction in addition to the FT reactions (Spath, 2003).

The purified and conditioned syngas is fed to Fischer Tropsch reactor. In FT reactor the synthesis gas, comprising mainly hydrogen and carbon monoxide, is converted to hydrocarbons. The global FT reaction may be expressed by the following equation (Kim et al., 2009):

$$nCO + 2nH_2 \rightarrow -(CH_2)n- + nH_2O, \ (\Delta H \approx -165 \text{ kJ/mol CO}) \quad \textbf{(2.1)}$$

Although FT reaction is described by a single global reaction, equation 1, a wide range of hydrocarbons are produced in the conventional FT reactors. These hydrocarbon products can be classified as paraffins, olefins, oxygenates (alcohols, aldehyds, ketones) and aromatics. The reactions, occuring in the course of Fischer Tropsch synthesis, may be expressed with the following equations (Spath, 2003). The main parameters affecting the product composition are reactor temperature and pressure, feed gas composition, catalyst type and catalyst composition.

Methanation: $CO + 3\ H_2 \rightarrow CH_4 + H_2O$ **(2.2)**

Parrafin synthesis: $CO + (2n+1)H_2 \rightarrow Cn\ H_{2n+2} + n\ H_2O$ **(2.3)**

Olefin synthesis : $CO + 2nH_2 \rightarrow C_n\ H_{2n} + n\ H_2O$ **(2.4)**

Alcohol synthesis: $CO + 2nH_2 \rightarrow C_n\ H_{2n+1}OH + (n-1)\ H_2O$ **(2.5)**

The water gas shift and the Boudouard reactions are also realized in the FT reactor depending on the catalyst used in the process. The WGS reaction (6) occurs on the Fe based FT catalysts and affects the hydrogen, CO consumption rates and needed H_2 to CO ratio of FT inlet synthesis gas. The Boudouard reaction (7) is a disproportionation reaction of carbon monoxide into carbon dioxide and carbon. This reaction causes carbon deposition on the catalyst surfaces, leading to catalyst deactivation.

Water-gas shift reaction: $CO + H_2O \rightarrow H_2 + CO_2$ **(2.6)**

Boudouard reaction: $2CO \rightarrow C(s) + CO_2$ **(2.7)**

The hydrocarbon products obtained from conventional FT reactors can have a wide spectrum, ranging from C1 to C40 or even higher. The product distributions for conventional FT catalysts are generally well correlated with so called the "*Anderson Schulz Flory* (ASF)" distribution. The FT product selectivity and "Anderson Schulz Flory" (ASF) distribution will be addressed in detail in Section 2.4.5.

The product up-grading section can be regarded as a refinery, processing FT "syn-crude", to produce liquid fuels and chemicals. The up-grading section of a conventional FT process generally contains following unit operations (Dry, 2002; Liu et al., 2011).

- Syn-crude fractionating unit,
- Hydrocracking unit,
- Catalytic reforming unit.
- Isomerization
- Alkylation
- Hydrotreatment,

Furthermore, a hydrogen production system can also be required to supply hydrogen needed for hydrocrackers and isomerization reactors.

The liquid fuels produced via Fischer Tropsch Synthesis have a set of advantages over the fuels derived from crude oil.

- FT fuels have lower sulfur, nitrogen, heavy metal and aromatic contents,
- The FT kerosene and jet fuel combustion characteristics are better.
- The FT diesel oil has superior combustion characteristics and can be used for blending with low quality diesel.
- The linear α-olefins obtained by FT process are very valuable products for the chemical industry.

2.3 Fischer Tropsch Reactors

The FT reactions are highly exothermic; therefore it is important to remove the heat of reaction from the catalyst particles. Overheating of the catalyst particles would result in an increased deactivation rate due to sintering and fouling as well as an undesirable high methane production. For large-scale commercial FT reactors heat removal and temperature control are the most important design features to obtain an optimum product selectivity and long catalyst lifetimes. High heat exchange rates can be achieved by turbulent syngas flow with high linear velocities through the narrow and long packed catalyst beds or using a catalytic fluidized bed reactor.

Currently two FT operating modes are applied. 1. The high-temperature (300–350°C) processes with iron-based catalysts. These processes aiming at produce gasoline and linear olefins of low molecular weights. 2. The low-temperature (200–240°C) process with either iron or cobalt catalysts is used for the production of linear waxes of high molecular weights. Over the years, basically four different FT reactor designs have been developed for these operating modes and used commercially. Figure 2.4 and Figure 2.5 depicts the types of Fischer-Tropsch synthesis reactors (Dry, 2002).

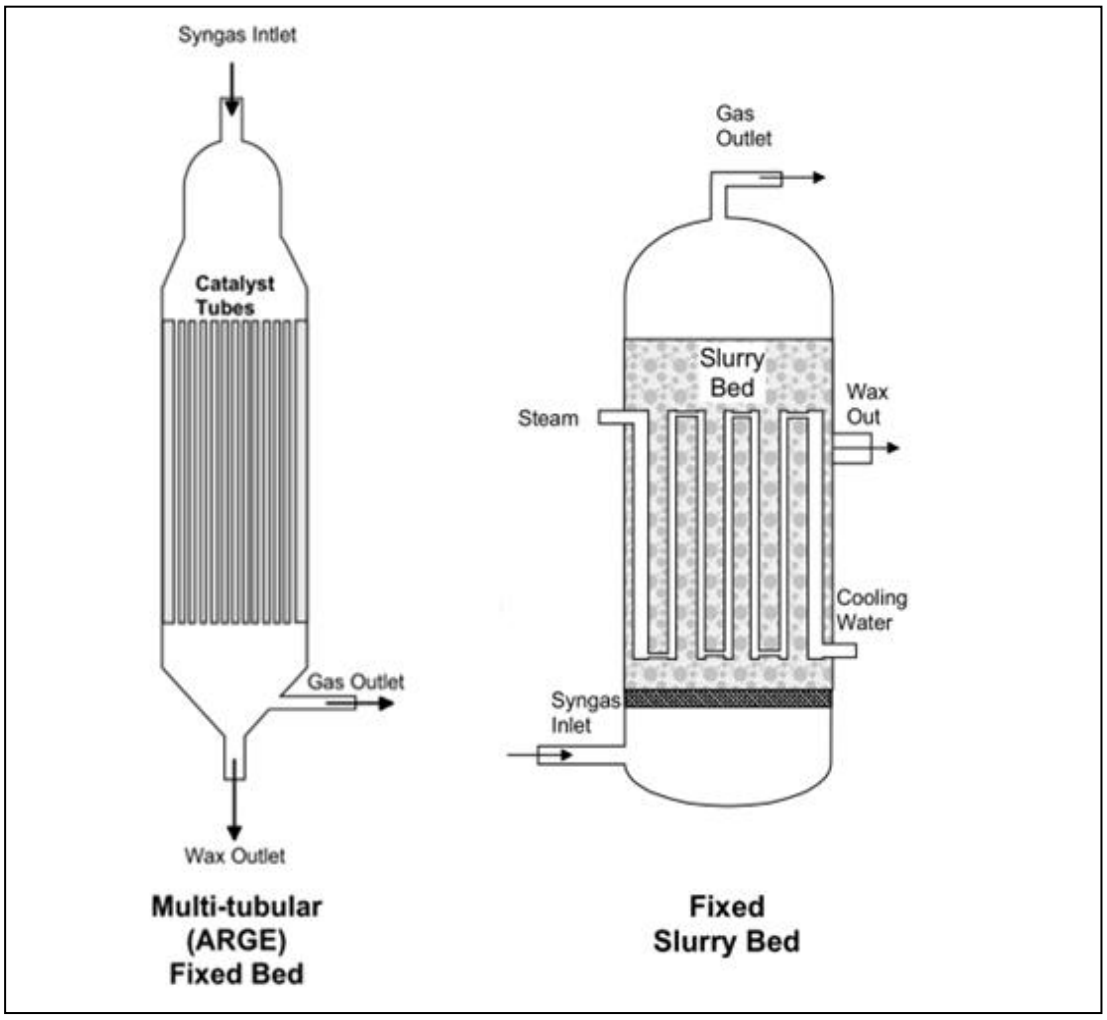

Figure 2.4 : Low temperature Fischer Tropsch reactors.

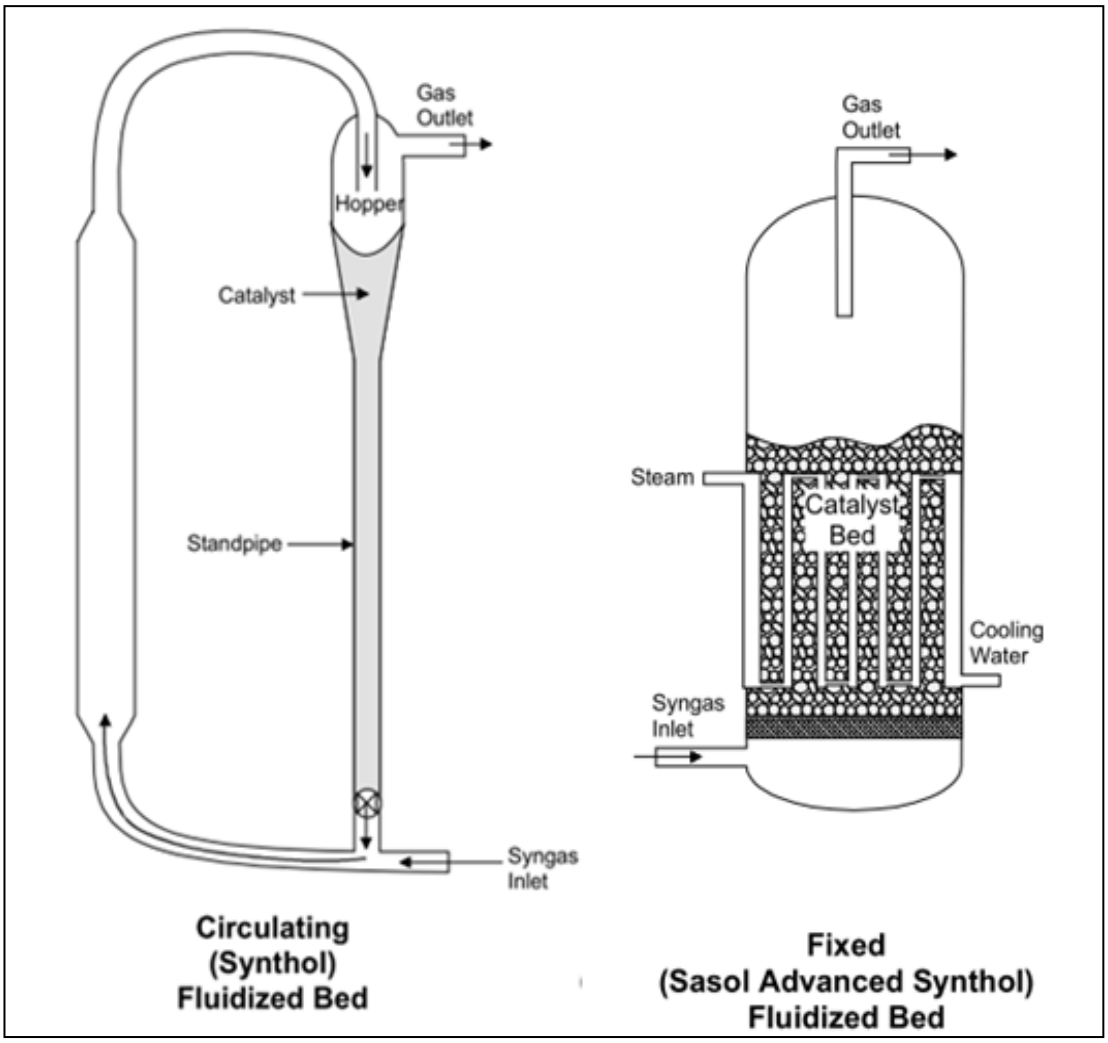

Figure 2.5 : High temperature Fischer Tropsch reactors.

One of the earliest FT reactor designs was the multi-tubular fixed bed reactor.The reactors contain thousands of tubes (i.e. 2.000) filled with Fe catalyst immersed in boiling water for heat removal. The water bath temperature is maintained by controlling the pressure. Syngas introduced to the top of the reactor, flows through the tubes, and the products exit at the bottom of the reactor. The reactor is operated at 20-30 bar pressures 220-260ºC temperatures. Wax accounts for 50% of the total products. Additional temperature control is applied by using high gas velocities and gas recycling. Catalyst lifetimes are around 70-100 days (Wender, 1996) and catalyst removal can be quite difficult.

High-temperature circulating fluidized-bed reactors have been developed for gasoline and light olefin production. These reactors are known as Synthol reactors and operate at 350°C and 25 bars. The combined gas feed (fresh and recycled) enters at the bottom of the reactor and entrains catalyst that is flowing down the standpipe

and through the slide valve. The high gas velocity carries the entrained catalyst into the reaction zone where heat is removed through heat exchangers. Product gases and catalyst are then transported into a large diameter catalyst hopper where the catalyst settles out and the product gases exit through a cyclone. These Synthol reactors have been successfully used for many years, however, they have a number of limitations. They are physically very complex and involve circulation of large amounts of catalyst that leads to considerable erosion in particular regions of the reactor (Lutz, 2001).

The fixed fluidized bed Sasol Advanced Synthol reactor was replaced the circulating fluidized bed Synthol reactor. Gas is introduced through a distributor and bubbles up through the catalyst bed. Heat is removed by an internal heat exchanger immersed in the catalyst bed. These new reactors are half the cost and size of the circulating reactors for the same capacity. They also have better thermal efficiency with a less severe temperature gradient and a lower pressure drop across the reactor. Operating costs are considerably lower and there is greater process flexibility in terms of product distribution (Lutz, 2001).

Another reactor design is the low-temperature slurry reactor (Dry, 1996; Dry, 2002).These 3-phase reactors consist of a solid catalyst suspended and dispersed in FT wax product. Syngas is bubbled through the liquid phase achieving excellent contact with catalyst while keeping the catalyst particles dispersed. Slurry reactors are optimized at low temperatures for high FT wax low methane productions. Compared to the fluidized bed reactors, the liquid slurry bed offers the advantages of better temperature control, lower catalyst loading, and significantly lower catalyst attrition rates. Slurry bed reactors also cost 75% less than the much more complex multi tubular fixed bed reactors. These reactors have only recently been put into commercial FT production primarily because one of the technical barriers, which required considerable development, was reliable catalyst separation from the FT waxes.

New types of reactors, such as monolith structured, micro structured and membrane reactors have also been studied for FT synthesis (Zang, 2010). In the Fischer–Tropsch synthesis the removal of the by-product water has several advantages on the reactor performance such as reduced catalyst de-activation, lowered kinetic inhibition, etc. Therefore, it was proposed to use hydrophilic membranes to increase

reactor productivity (Rohde, 2007). The in situ-water removal by a sol–gel silica-based membrane and a ceramic supported polymer membrane in presence of a WGS active Fe-based catalyst resulted in increased total carbon conversion to hydrocarbons.

2.4 Fischer Tropsch Catalysts

The FT reactor is the core of the whole coal/natural gas to liquid fuel process. The gasification, the gas cleaning/conditioning and the product up-grading sections are designed and configured according to FT reactor. The characteristics of FT reactor, i.e. product selectivity, gas purification and conditioning needs, are mainly determined by the FT catalyst used.

Only four metals from group VIII, namely, Fe, Co, Ni and Ru have sufficiently high activities for the hydrogenation of carbon monoxide to be applicable in FT synthesis. Of these four metals ruthenium is the most active but its high cost and low availability pushes it out of scope for large scale application. On a relative basis, taking the price of scrap iron as 1.0 the approximate costs of Ni, Co and Ru are 250, 1000 and 50000, respectively (Dry, 2002). Nickel is also very active but has two crucial disadvantages. Nickel is a powerful hydrogenating catalyst resulting in a very high unwanted methane selectivity. Furthermore, nickel forms volatile carbonyls resulting in continuous loss of the metal at the temperatures and pressures at which practical FT plants operate. Therefore only iron and cobalt based catalysts can be considered as practical FT catalysts (Gonzalez and Fierro, 2010; Steynberg, 2004).

There are three broad classes of FT catalysts having commercial importance. These are i. Fused iron catalysts, ii. Precipitated iron catalysts, iii. Supported cobalt catalysts (Steynberg, 2004).

2.4.1 Conventional catalysts

2.4.1.1 Fused iron catalysts

Fused iron catalysts are used only for high temperature Fischer Tropsch processes, because of their lower activies due to low catalyst surface areas. Alkali promoters are used to enhance catalyst activity and selectivity. In addition, structural promoters may be used to enhance the surface areas of the final catalysts. These promoters are

added into a molten bath of magnetite. The magnetite is then cooled to form a solid which subsequently is converted into a fine powder. The magnetite powder is reduced with hydrogen to form the metallic iron catalyst before loading into the reactor (Steynberg, 2004).

To decrease the unwanted methane selectivity, the fused iron catalysts are synthesized with high concentrations of alkali promoters. However there is a practical lower limit for the methane selectivity that can be achieved without causing operational problems in the reactors due to the formation of heavy hydrocarbons in the liquid phase. Nevertheless high alkali content causes increased carbon formation and organic acids. The lowest methane selectivity with fused iron catalysts is about 7% of the carbon in the hydrocarbon products (Steynberg, 2004).

The liquid products obtained from these catalysts are highly olefinic. This makes fused iron the most desirable catalyst for the production of olefins which are widely used in the petrochemical industry (Steynberg, 2004).

The activation procedure is very critical step in respect to the catalyst catalytic activity and selectivity. This type of iron catalysts generally are reduced at high temperatures ($T > 673$ K) under hydrogen atmosphere. Reduction under syngas or CO is considered to be ineffective (Brian, 1996).

2.4.1.2 Precipitated iron catalysts

To increase fuel/chemical yield of the process, it is needed to decrease the methane selectivity. To shift the catalyst selectivity towards higher hydrocarbons, the operating temperature of the reactor should be lowered. Using low temperature Fischer Tropsch operation, methane selectivities can be decreased to as low as 3%. In order to compensate for the decreased reaction rates at the lower operating temperature, higher catalyst surface areas are required. An inevitable consequence of these higher surface areas is weaker catalyst particles. Hence structural promoters are used in the catalyst preparation process to enhance catalyst strength (Steynberg, 2004).

Iron metal is used as raw metal instead of cheaper iron oxide used in fused iron preparation. The metal is dissolved into an aqueous acidic solution (e.g. nitric acid) and promoters are added in the desired quantities. As for fused iron catalysts, alkali promotion is important. The catalyst is then precipitated from the acidic solution by

the addition of a basic solution, i.e. a solution containing sodium carbonate or ammonia. The precipitate is then filtered, washed, dried and formed into the shape required for use in the FT reactor. Extrusion techniques are typically used to provide the catalyst shapes used in fixed bed reactors.

Promoters and supports are the essential catalyst components. Fe catalysts can be prepared by precipitation of iron onto catalyst supports such as SiO_2 or Al_2O_3. The promoter type and concentration are important factors to have low selectivity to methane and a high selectivity to heavy hydrocarbon products with the desired olefin and oxygenate content in the products. Alkali promoters are generally used to increase the basicity of the catalyst and thereby enhancing the adsorption of CO to the metal surface and increasing the chain length of the products. The most commonly used promoters are potassium, copper, manganese and cobalt (Steynberg, 2004).

The reduction of precipitated iron catalyst could be carried out under carbon monoxide. Even though the CO reduction gives better results, at industrial scale activation with hydrogen is easier and cheaper. Because pure hydrogen could be produced from synthesis gas via membrane separation (Brian, 1996). Direct activation with syngas is also one of the proposed methods.

2.4.1.3 Supported cobalt catalysts

Cobalt based catalysts are only used in low temperature Fischer Tropsch operation, since their methanation activity and consequently unwanted methane selectivity are very high at elevated temperatures. In the applications, it is tended to use the lowest possible amounts of these catalysts due to their high prices. In order to increase the reaction rate per unit active site, the catalyst surface area should be maximized. This is achieved by means of support materials (Steynberg, 2004).

Modern cobalt catalysts are prepared by impregnation of cobalt on a pre-shaped stable refractory oxide support with high surface areas. Some typical materials used as support are silica, alumina, titania and zinc oxides or their combinations. Catalyst loadings on supports mostly change between 10-30 g catalyst/100 g support. The supports can typically be prepared by using a spray drier or extrusion techniques. Cobalt is then deposited onto the support together with promoter metals such as lanthanum, platinum, palladium, rhenium and ruthenium. These metals are known to

facilitate the reduction of the catalyst. Promoters are not essential to produce a good supported cobalt catalyst but enhance the reduction of the cobalt oxide to metallic state. The support geometry is an important issues in producing of a good supported cobalt catalyst. The catalyst is then dried and reduced using hydrogen at high temperatures (Steynberg, 2004).

In spite of their higher prices, Co catalyst are very important alternatives of iron catalysts due to their higher FT activity. Co catalysts show activity at low pressures, so that the decreasing reactor operating costs may compensate for their higher costs (Dry, 2002).

Given their higher prices, cobalt catalysts are not suitable for coal applications due to the risk of catalyst poisoning by various impurities in the coal. It is difficult to reduce the amounts of these impurities to the desired levels. The syngas compositions obtained from coal gasification are in any case generally considered to be better suited for processing by iron catalysts (Gonzalez and Fierro, 2010).

Continuous catalyst regeneration is proposed for slurry reactors. This is achieved by contacting the catalyst with hydrogen at an elevated temperature. In this way, cobalt that has been oxidized under synthesis conditions is converted back to the metal state. Heavy hydrocarbons that may foul the catalyst are simultaneously removed.

The hydrocarbon products obtained by supported cobalt catalysts comprise predominantly of paraffins. This is in contrast with products from the iron catalysts that usually produce olefins as the predominant product. The best cobalt catalysts have about 5% selectivity (% C) for methane. The cobalt catalysts do not show water gas shift activity, consequently no carbon dioxide is produced in the FT reactor (Steynberg, 2004)

2.4.2 Fischer tropsch reaction mechanism

The understanding of the fundamental processes taking place on metal surfaces during the Fischer-Tropsch synthesis may lead to improved catalyst design and process efficiencies (Laan, 1999; Steynberg, 2004). Although FT process has been extensively studied, a certain reaction mechanism supported by definitive experimental evidences is not available in literature yet.

It is widely accepted that FT reaction is a polymerization reaction with the following steps (Laan, 1999): 1. reactant adsorption; 2. chain initiation; 3. chain growth; 4. chain termination; 5. product desorption; 6. readsorption and further reaction.

There are a number of proposed mechanisms for FT reactions. Most of the FT mechanisms proposed in the literature may be divided into four groups; i. carbide mechanism, ii. hydroxy-carbene mechanism, iii. CO-insertion mechanism, iv. Alkyl mechanism (Gonzalez and Fierro, 2010).

Carbide mechanism is proposed by Fischer-Tropsch and currently is remains to be one of the most plausible reaction route for Fe, Co and Ru catalysts (Gonzalez and Fierro, 2010; Laan 1999). A schematic representation of the initiation, growth and termination of chains according to this mechanism is shown in Figure 2.6. The monomer of the carbide mechanism is a methylene (CH_2) species. CO and H_2 are assumed to adsorb dissociatively. Several species like CH, CH_2 and CH_3 can be formed in this way. These species polymerize by successive addition of C_1 units to yield larger surface alkyl chains. The presence of methylene species has been identified by using isotopic-tracer techniques on Fe/Al_2O_3, Ru/Al_2O_3, Ni/SiO_2. Chain termination occurs by hydrogen addition to yield paraffins or by β-hydrogen abstraction to form alpha olefins.

Various detailed mechanisms have been proposed since the discovery of FT synthesis and this matter still remains controversial (Anderson, 1984; Dry, 1996). The question is asked whether detailed knowledge of the chemical reaction sequences occurring will in fact result in improvements in catalyst activity, selectivity and life. Better catalyst formulations and synthesis process conditions are more likely to result in improvements (Dry, 2002).

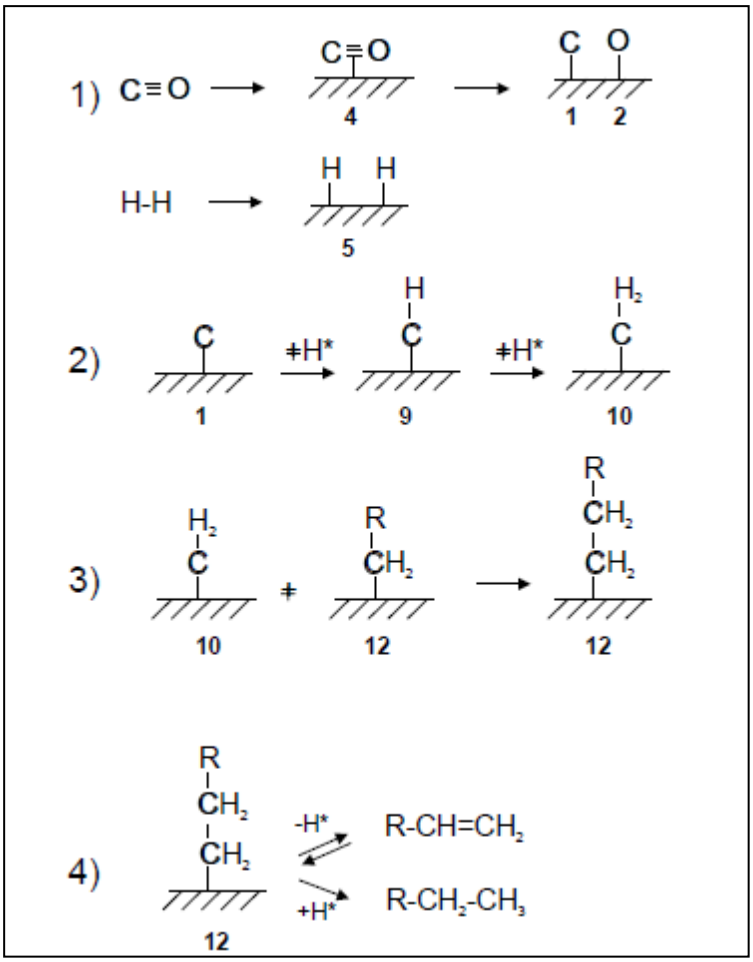

Figure 2.6 : Carbide mechanism for the FT reactions.

2.4.3 Fischer tropsch reaction kinetics

The major problem in describing the FT reaction kinetics is the complexity of its reaction mechanism and the large number of species involved. As discussed before, the mechanistic proposals for the FT used a variety of surface species and different elementary reaction steps, which result in empirical power law expressions for the kinetics (Laan, 1991; Dry, 2002).

For the purpose of comparing the FT kinetics of iron-based (equation 2.8) as against cobalt-based catalysts (equation 2.9) the following two kinetic equations can be used:

$$r = \frac{m p_{H_2} p_{CO}}{p_{CO} + a p_{H_2O}} \qquad \textbf{(2.8)}$$

$$r = \frac{k p_{H_2} p_{CO}}{(1 + b p_{CO})^2} \qquad \textbf{(2.9)}$$

Where, r = the rate of reaction, k; m = reaction rate constant, p_i = the partial pressure of species i, a; b = coefficient of P_{H2O} and P_{CO}, respectively.

Based on the rate equation for the Fe based catalysts, the following important conclusions could be drawn (Dry, 2002):

- The rate decreases with increasing water vapor pressure for Fe based catalyst.
- CO_2 partial pressure has no influence on the FT rate.
- The reaction rate increases with hydrogen partial pressure and at low conversion levels, the rate was solely dependent on H_2 partial pressure.
- The conversion level remains constant when the total pressure was increased while keeping all other variables constant, i.e. feed gas composition, residence time, etc.

The major difference between the iron and cobalt rate equations is the effect of water vapour pressure. The rate decreases with increasing water vapor pressure for Fe based catalyst, while this term is absent for Co based catalyst. Iron is oxidised at much lower H_2O/H_2 ratios than is cobalt metal.

The reaction rate for cobalt catalyst is much higher, so that much higher conversions per pass can be achieved (see Figure 2.7). If the iron catalyst was made to have an initial activity five times higher than that of the cobalt catalyst, the iron catalyst would be superior up to about 50% conversion but beyond this level it would again drop well below that of cobalt. The calculations indicate that high conversions can be achieved with cobalt catalysts in single stage reactors without the need of tailgas recycling or a two stage reactor system with water knock-out between stages. For iron-based catalysts high conversions, e.g. 90%, can be achieved. But this requires two stage operation with gas recycling which has higher capital and running costs. But it should be noticed that, very small Co crystals could be deactivated at high H_2O/H_2 ratios, i.e. high conversions.) To avoid this, a two stage reactor system with inter-cooling or alternatively, a two stage reactor system with inter-cooling and tailgas recycling after inter-cooling may be used (Dry, 2002).

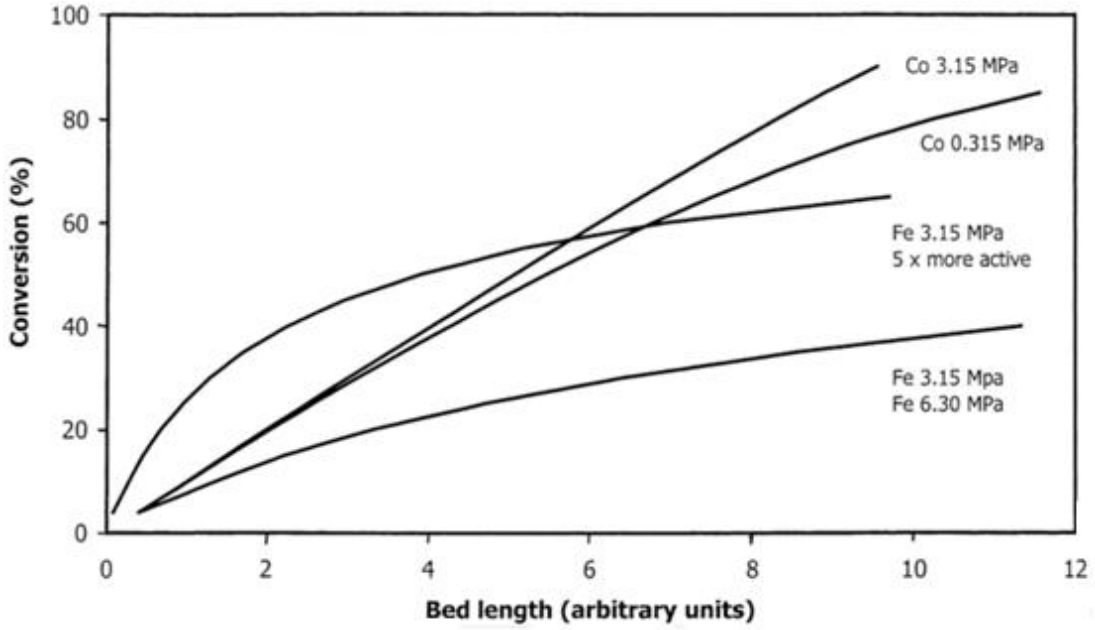

Figure 2.7: FT conversion along the reactor bed for Fe and Co catalysts.

2.4.4 Catalyst deactivation

Catalyst lifetime is one of the most crucial parameters determining FT plant availability and thereby system profitability. FT catalysts can loose activity as a result of i) conversion of the active metal site to an inactive oxide site, ii) sintering, iii) loss of active area by carbon deposition, and iv) chemical poisoning (Spath, 2003).

Some of these mechanisms are unavoidable. Others can be prevented or minimized by insuring that the impurity levels in the syngas are acceptable for the given process. Carbon deposition is the most important mode of catalyst deactivation. Carbon deposition, however, can be affected by promoters added to the catalysts, reaction temperature and pressure. It can be substantially reduced by operating FT reactor under proper operating conditions. Therefore, this deactivation is largely unavoidable. However, FT processes must be operated in a manner so that the decrease in output due to the coke deposition is balanced with improvement in the economics of catalyst regeneration or replacement (Dry, 2002).

One of the easily controlled modes of catalyst deactivation is one that induced by poisoning of the active sites by impurities in the syngas. High water partial pressures lead to irreversible catalyst oxidation and consequently a loss in its activity (Steynberg, 2004). The most abundant, important, and studied FT catalyst poison is sulfur. Sulfur is present in both natural gas and coal. In the steam reforming and

gasification processes it is primarily converted into H_2S, and to the lower extent into other organic sulfur compounds. Sulfur compounds rapidly deactivate both iron and cobalt catalysts, presumably by forming surface metal sulfides that do not have any FT activity. Ideally, there should be no sulfur in the syngas. However, there is, always a small amount of sulfur that gets through to the catalyst. There is really no safe sulfur level in FT process. Again, the level of gas cleaning required is based on economic considerations; namely how long the catalyst remains active versus the investment in gas cleaning.

2.4.5 Selectivity

FT synthesis always produces a wide range of hydrocarbons ranging from C_1 to C_{40} and even higher, containing paraffins, olefins and oxygenated products (alcohols, aldehydes, acids and ketones). There is, however, always a fixed interrelation between the individual products irrespective of what variables were altered. The basis of these interrelation lies in the stepwise growth mechanism of the FT reaction. FT's product selectivities are determined by the ability of a catalyst to catalyze chain propagation versus chain termination reactions. The CH_2 units, formed by the hydrogenation of CO, are taken as the "monomers" in a stepwise oligomerization process. At each stage of growth the adsorbed hydrocarbon species has the option of desorbing or being hydrogenated to form the primary FT products or of adding another monomer to continue the chain growth (Spath, 2003; Gonzalez and Fierro, 2010; Laan, 1999).

Based on the polymerization mechanism described above, the product distribution of hydrocarbons can be described by the Anderson-Schulz-Flory (ASF) equation (Anderson et al., 1980):

$$W_n/n = (1-\alpha)^2 . \alpha^{n-1} \qquad \textbf{(2.10)}$$

where, Wn is the weight fraction of a hydrocarbon with chain length n and α is the growth probability factor. α determines the total carbon number distribution of the FT products. The variation of product distribution with α is given in Figure 2.8 (Spath, 2003).

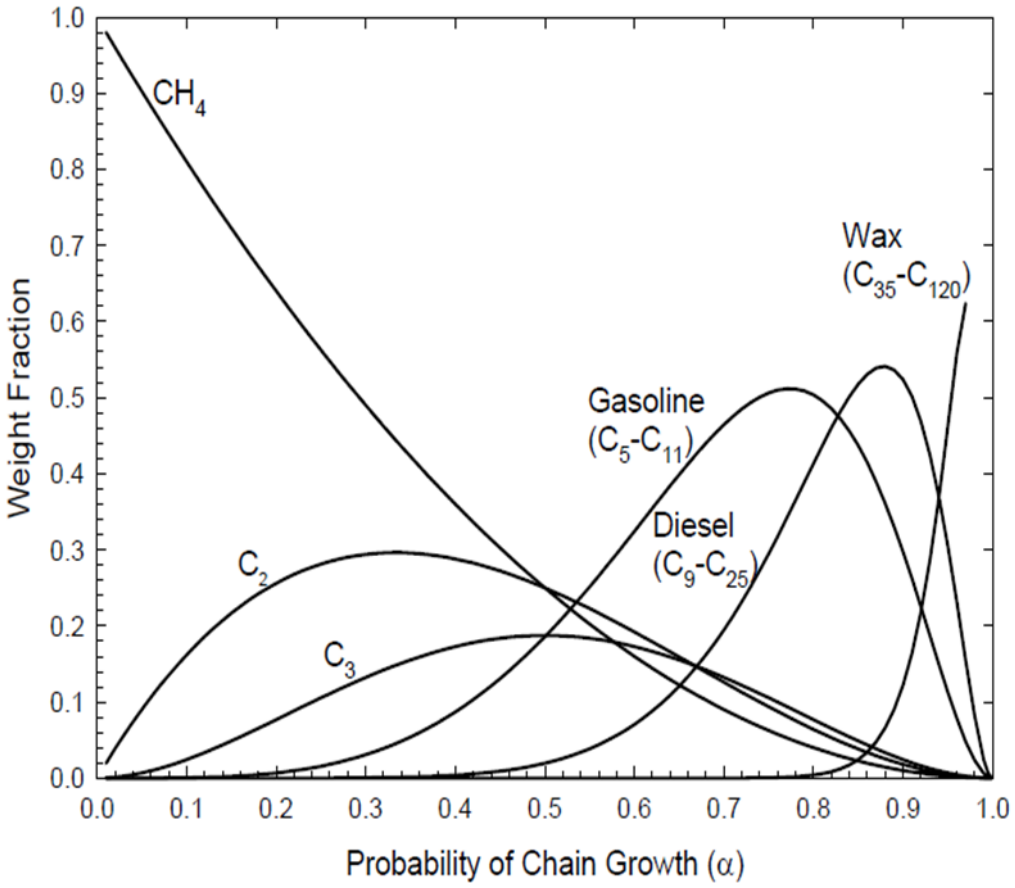

Figure 2.8 : Anderson schulz flory distribution.

The range of α depends on reaction conditions and catalyst type. Dry (2002) reported typical ranges of α on Ru, Co, and Fe to be in the ranges of 0.85- 0.95, 0.70- 0.95, and 0.50-0.70 respectively. However, significant deviations from the ASF distribution are reported in the literature. The foremost deviation from ideal ASF distribution is the relatively higher methane selectivity.

The major process parameters determining the spread of the products are temperature, feed gas composition and pressure, the catalyst type and promoters.

For all FT catalysts, an increase in operating temperature results in a shift in selectivity towards lower carbon number products and increasing amounts of hydrogenated products. Since Co is a more active hydrogenating catalyst, the products in general are more hydrogenated and the CH_4 selectivity rises more rapidly with increasing temperature than it does with Fe catalysts.

Lower CO partial pressures result in lower surface area covered by the CH_2 species, lower chain growth probability and higher desorption probability of the n(CH_2) species. The higher the H_2 partial pressure the more likely is the termination of the

surface species to paraffins. Thus, one can expect that as the H_2/CO ratio increases the selectivity will shift to lighter and more saturated hydrocarbons. This can, however, be an over simplification as the presence of CO_2 and of H_2O could complicate matters. For example, since the chemisorption of CO is much stronger than that of H_2 the presence of CO_2 and H_2O could have a greater negative effect on H_2 than on CO chemisorption (Dry, 2002).

For iron-based catalysts the "basicity" of the catalyst surface is very important. The probability of chain growth increases with alkali promotion i.e. Na and K (Gonzalez and Fierro, 2010). The basicity of the catalyst does not only depend on the amount of K added but also on the anion used as well as on the presence and amounts of oxides such as SiO_2, Al_2O_3, etc. with which the alkali can chemically react to form less basic compounds (Perego and Villa, 1997; Spath, 2003). These oxides may either be impurities existed in or deliberately added to the catalysts as supports, binders or spacers.

2.5 Bi-functional Fischer Tropsch Catalysts

A major limitation of the FT technology is the low selectivity of the conventional catalysts toward targeted products. The well known ASF kinetics of the FT reaction imposes a limit to the maximum selectivity of 48% attainable for gasoline range products (Botes and Bohringer, 2004). Using the Fixed Fluidized Bed reactors at about 340 °C with iron catalyst gives a maximum gasoline production, producing about 40% straight run gasoline (Dry, 2002). In order to overcome the selectivity limitation, the FT process is typically operated under conditions that maximize the formation of long-chain n-paraffins (waxes) and then subjecting the waxes to downstream (hydro)cracking and/or (hydro)isomerization steps . Using FT waxes as a potential feedstock for FCC units to produce high-octane iso-paraffin rich gasoline and light olefins for petrochemical applications has also been studied (Martinez et al., 2008). A novel approach to circumvent the above mentioned two-stage processing and thus significantly reduce the overall investment cost of the synfuel production would be to use bifunctional catalysts. They combine the FT active components (Fe or Co) with a co-catalyst which converts the primary FT products into the desired compounds in a single stage operation. Zeolites, being the industrial FCC catalysts, can be used as the co- catalyst.

2.5.1 Zeolites as co-catalyst for FT synthesis

Zeolites are microporous crystalline solids with well-defined structures having unique pores and channels. Generally, they contain silicon, aluminium and oxygen in their framework and cations. Many occur naturally as minerals, and are extensively mined in many parts of the world. Others are synthetic, and are commercially produced for specific uses.

Zeolites are also known as "molecular sieves". The term molecular sieve refers to a specific property of these materials, namely, the ability to selectively sort molecules primarily on a size exclusion process. Zeolites have a very regular pore structures of molecular dimensions. The maximum size of the molecular or ionic species that can penetrate the pores of a zeolite is controlled by the dimensions of the channels.

Zeolite atomic structures are formed by different arrangements of a very simple building block- a group of four oxygen atoms forming a tetrahedron, with a silicon or aluminium atoms at the centre. Each oxygen atom belongs to two tetrahedra, so the structure can be viewed as a network of tetrahedra linked at the corners (see Figure 2.9). Channel dimensions of zeolites are usually defined by the ring size of the opening, where, for example, the term "6-membered ring" refers to a closed loop of 6 tetrahedral silicon (or aluminum) atoms and 6 oxygen atoms is established.

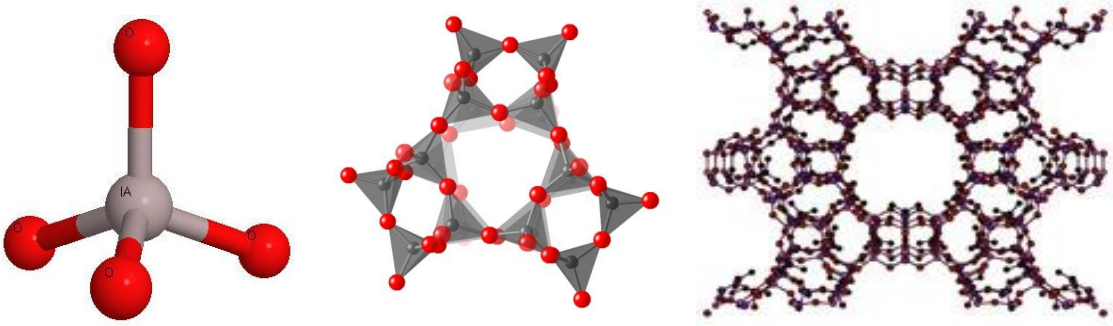

Figure 2.9 : Schematic view of a zeolite structure built from corner-sharing tetrahedral units (Url-2, Url-3).

Zeolites are widely used for water softening, separation and removal of gases and solvents, cleaning agent (detergent) and fuel refining. Besides, the varied molecular diffusion rates in these pores, their shape selectivity and acidic character, makes them widely used. Zeolites are also good hydrocracking/hydroisomerization catalyst due to their acidic nature. Synthetic zeolites are also widely used as catalysts in the petrochemical industry, for instance in fluid catalytic cracking (FCC) and

hydrocracking units. Zeolites confine molecules in small spaces, which caused changes in their structure and reactivity. The hydrogen form of zeolites (prepared by ion exchange) are powerful solid-acids, and can have a variety of acid-catalyzed reactions, such as to facilitate isomerization, alkylation and cracking.

Zeolites have attracted much attention as a co-catalyst for FT synthesis. A variety of zeolites such as ZSM-5 (Pour et al., 2008; Martinez et al., 2008; Botes, 2005), zeolite Y (Yoneyama et al., 2010; Egiebor and Cooper, 1989), zeolite L (Bengoa et al., 2002), beta (Liu et al., 2007) have been used in the synthesis of metal-zeolite bi-functional FT catalysts. ZSM-5 attracted particular attention with its acidic nature and shape selective properties, providing better activity and selectivity. ZSM-5 zeolite is a commercial catalyst and used in the petrochemical industry for fluid catalytic cracking (FCC) units.

If it were possible to precisely design the structural characteristics of the catalysts, then it would be possible to obtain a good activity and selectivity to specific products. It is known that some of the reactions in the Fischer–Tropsch synthesis are "structure sensitive" (Cagnoli, 2002). On the other hand, catalysts with broad metallic crystal size distributions are less selective. Therefore, catalysts with a very narrow metallic crystal size distributions are desirable in FT synthesis.). To attain this purpose, zeolites could be used as support in the FT catalysts.

It is well known that zeolites possess shape-selective features that do not allow the formation of products, intermediates, or transition states larger than the size of the their cavities or channels. Using zeolites as an FT catalyst constituent, may limit chain growth, leading to the formation of lighter hydrocarbons. On the other hand, confinement in nano-sized voids may enhance the readsorption probability and the secondary reactions of α-olefins, leading to long-chain hydrocarbons synthesis. Furthermore, zeolites, due to their acidity, may also catalyze the secondary cracking, isomerization, and aromatization of the primary FT products, contributing to adjustment of the product distributions.

The acidity, surface area, pore structure and cation exchange capability of the zeolite supports are crucial factors affecting the catalytic performance of zeolite–metal FT catalysts with respect to aromatization, oligomerization, isomerization as well as alkylation reactions.

The methods which have been used in the synthesis of bifunctional FT catalysts based on zeolites and metals are as follows:

i. The conventional impregnation (Calleja et al., 1991; Bengoa et al., 2002),
ii. Physical admixing (Martinez et al., 2008; Botes, 2005),
iii. Preparation of encapsulated zeolite – FT catalyst (Li et al; 2009; Yang et al., 2007),
iv. Direct synthesis of aluminoferrisilicate zeolite (Latham, 2000),
v. Ion exchange (Ilton et al., 1983),
vi. Adsorption of carbonyl complexes (Nazar et al., 1983; Suib et al; 1984).

The most widely used methods are physical admixing and conventional impregnation.

2.5.2 Zeolite supported FT catalyst

Supports are expected to play the following roles in heterogeneous catalysis:

i. to disperse the active phase, leading a high surface area of the catalytically active phase,
ii. to stabilize the active phase against the loss of surface area during the reaction,
iii. to maintain the catalyst mechanical strength and facilitate the mass and/or heat transfer in a diffusion-limited or an exothermic reaction.

In addition to these physical effects, the chemical interaction between the active phase and the support may also significantly affect the catalytic behaviors. It is accepted that a balanced interaction between the support and the active phase (or the precursor of active phase) is particularly important for FT synthesis. Although too weak an interaction may lead to a poor dispersion of active phase, too strong an interaction will cause difficulty in the reduction of the precursor of the active phase (Zhang, 2010). Furthermore, the pore structure of the support can have significantly impact on the catalytic performance through changing the reducibility and the size of the active phase or altering the diffusion of reactants or products.

Supports are used for most FT catalysts, especially for Co and Ru catalysts, which are more expensive than Fe catalysts. Oxides, particularly SiO_2, Al_2O_3, and TiO_2, are probably the most extensively investigated supports FT catalysts.The utilization of

materials with well-defined nanoporous structures (i.e. zeolites or carbon nanotubes) as FT catalyst supports has provided new possibilities for tuning the catalytic properties (particularly the selectivity).

Ordered mesoporous materials, have shown many unique characteristics as hosts for the design of structure-defined catalysts. The mesoporous materials typically possess high surface areas (> 400 m^2/g) and uniform porous channels with controllable pore diameters (2–30 nm) and pore lengths, which are favorable for the preparation of suitably dispersed metal particles. It is claimed that some of the reactions in the Fischer–Tropsch synthesis are "structure sensitive" (Cagnoli, 2002) and therefore, catalysts with a broad metallic crystal size distribution are less selective. Inside the zeolite channels, the metallic particles have sizes that do not exceed ca. 10–20 A° diameter, and this allows to modify the catalyst's selectivities and other properties (Bengoa, 2002). Moreover, the mesopores in which the active metal particles are located may function as a nanoreactor to control the chain length, either by shape selectivity or by enhancing the readsorption of a-olefin intermediates. In other words, the nanospaces of mesoporous materials can be expected to regulate the product selectivity.

The most commonly used zeolites as bi-functional FT catalyst constituent are conventional mesoporous materials like as ZSM-5 (Martinez et al., 2008), zeolite Y (Yoneyama et al., 2010) and zeolite L (Bengoa et al., 2002). One the zeolite type studied is MWW zeolite (Ngamcharussrivichai et al., 2004). This zeolite, so-called MCM-22, composing of two different pore channel systems, 1. sinusoidal 10-membered ring channels and 2.large super cages with 10-membered ring pore entrance, have been applied as a support for the Co based FT catalysts. Experiments were conducted under supercritical conditions. MCM-22 supported Co catalysts was found to be active for FT synthesis. And C4+ isoparrafin selectivity was quite high (43-53%). However selectivity towards C12+ HC was not reduced like faujasite supported catalysts (see Figure 2.10). Compared to the results under supercritical conditions, the slurry-phase conditions are more suitable for an active and selective production of gasoline-range hydrocarbons through the Fischer–Tropsch synthesis over MCM-22 supported Co catalysts.

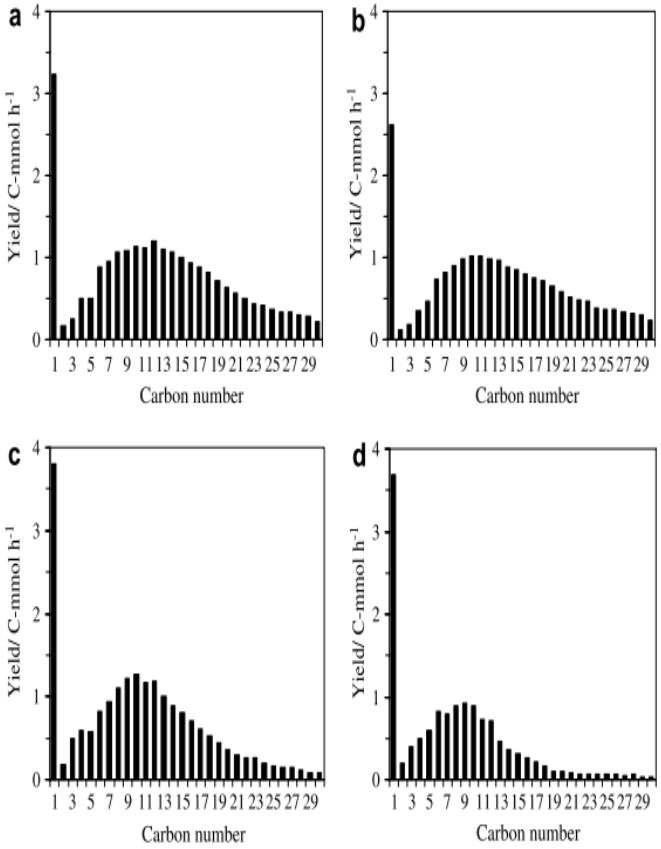

Figure 2.10 : Carbon number distribution in slurry phase FT synthesis catalyzed by (a) Co/SiO_2, (b) Co/Al_2O_3, (c) Co/MONT, (d) Co/USY.

Bessel (2004) studied pentasyl zeolites with different pore structures, including ZSM-5, ZSM-11, ZSM-12, and ZSM-34 as supports for Co catalyst. For these strongly acidic series of zeolites, accessibility of internal acid sites was more important in influencing the secondary acid catalyst restructuring reactions of the primary FT products than was the strength or concentrations of these acid sites. The use of ZSM-12, which possesses the largest pore channels (0.57-0.61 nm) but weaker acidity, provided the highest fraction of gasoline in liquid hydrocarbons and the lowest fraction of n-paraffins. In contrast, ZSM-34, with a more constrained channel structure, produced heavier products containing more n-paraffins. The chain growth occurred on Co particles, and the resultant primary hydrocarbons then underwent secondary reactions at the accessible zeolite acid sites to produce lighter products with more iso-paraffins. Since an important fraction of the Co particles may not be located inside the small zeolite channels, the accessible acid sites mainly include the external acid sites and the internal acid sites close to the pore mouths of the zeolite. The degree of secondary restructuring was the greatest over ZSM-12-supported

catalyst, indicating that the accessibility of primary FT products to the internal acid sites is an important factor.

Bengoa et al. (2002) studied potassic zeolite L to increase the ratio of Fe clusters inside the zeolite channels. In the article it is claimed that, in the case of zeolite supported FT catalysts, active metal goes into the zeolite pore structure after impregnation. But when the catalyst is reduced, some portion of the active metal (Fe, Co) migrates out of the pores. Consequently, the beneficial effect of the zeolite channel structure decreases. It is also claimed that an important fraction of Fe metals could still be kept inside the zeolite structure by using "alkaline microinjection". Potassic zeolite-L (ZLK) with all its exchangeable sites occupied by K^+ ions was used in the study. The impregnating solution goes into the channels of the zeolite, in Fe/ZLK, the K^+ ions exchanged by Fe^{3+}, which fills the channels of the zeolite causing the precipitation. The ratio of Fe in the zeolite channels was determined by means of Mössbauer spectroscopy. 15% of the Fe^0 was observed to be maintained in the catalyst channel. However, the activity of the catalysts in this study are quite low (1.5%- 2.6% CO conversion). There were almost no information on selectivity of the catalyst.

Iron and cobalt are well-known metals to be active for FT synthesis (FTS). Cobalt has been used in many zeolite-FT catalyst studies due to its low water gas shift activity and its convenience for production of heavier hydrocarbons mainly in the diesel range (Dry, 1981). Besides Fe and Co, different metals have been also studied as FT catalyst. Liu and co-workers (2007) studied HZSM5 supported Mo catalysts. Molybdenum carbides and sulfides were reported to be active for FTS reaction. Aromatics and branched/cyclized alkanes are major liquid-phase products produced in FTS by Mo/HZSM-5. FTS by Mo/HZSM-5 proceeds via formation of mixed alcohol as the first step for hydrocarbons production, probably inside the zeolite channels. But the selectivity of liquid (C4+) hydrocarbons is quite low, generally below 25%. On the other hand, CO_2 selectivity is quite high, being %20-%40. Depressing the formation of CO_2 and lower hydrocarbons will be the major task in the further Mo/zeolite-based FT studies.

Ru and bimetallic active metal combinations are also studied. Guczi et al. [159] found that, under the conditions of T=502 K, P=2.1 MPa, and $H_2/CO=2$, Ru/NaY was very active for CO conversion (86%), but the main products were CH_4 and CO_2.

On the other hand, Co/NaY exhibited a very low CO conversion. Faujasite zeolites (X and Y) possess supercages (1.3 nm diameter) and have attracted attention for the preparation of small metal clusters in a confined environment. The addition of Ru to Co/NaY, forming a bimetallic catalyst, significantly enhanced CO conversion from 1.1% to 9%, due to an enhancement in the degree of reduction of Co species. Moreover, the CH_4 selectivity decreased from 44% to 26%, while the C_{5+} selectivity increased from 22% to 38%.

2.5.3 Hybrid FT active metal – zeolite catalysts

An alternative method to prepare a bifunctional catalysts is forming a hybrid catalyst containing the mixture (typically a physical mixture) of an FT active component and a zeolite in a single reactor. In most of the recent studies physical admixing was used for catalyst preparation (Martinez et al., 2008; Botes, 2005; Yoneyama, 2010).

Martinez et al. (2008) studied the catalytic properties of 10- membered ring zeolites (ZSM-5, MCM-22, IM-5, ITQ-2, all with a similar Si/Al ratio of ca. 15) in hybrid Co/SiO2 -zeolite catalysts for the direct conversion of syngas to mainly high-octane gasoline-range hydrocarbons under typical Fischer-Tropsch (FT) conditions: 250°C, 2.0 MPa, and $H_2/CO = 2$. The selectivities of the hybrid catalysts studied are given in Table 2.2The presence of the medium-pore zeolite increased the gasoline yield by about 20–50%, depending on the particular zeolite. The formation of branched products was enhanced with respect to the base Co/SiO2 catalyst, which was explained by the promotion of isomerization and cracking of long-chain (C13+) n-paraffins formed on the FT component.

Pour et al. (2009) studied the effect of proximity of active metal (Fe) with zeolite (HZSM-5) on the activity and products selectivity of hybrid catalysts. Six different conditions were studied. HZSM-5 zeolite and iron catalyst became near to each other step-by-step. The two components of the catalyst were combined via different methods; (a) in separate reactors with a cold trap between reactors, (b) in a single reactor located at upstream and downstream, (c) physical mixture, (d) pelleted physical mixture, (e) pelleted physical mixture by a silica-alumina binder.

Table 2.2 : Product distribution and yield to branched C5-C8 products for hybrid catalysts.

	Co/SiO_2	Base + ZSM5		Base+	Base+	Base+
		Physical Mixture	Double bed*	MCM22	ITQ-2	IM-5
Distribution (%C)						
C_1	12	11	11	13	12	13
C_2-C_4	11	15	16	16	15	15
C_5-C_{12}	41	62	65	50	53	50
C_{13}-C_{22}	28	11	8	18	16	20
C_{23+}	8	1	0	3	4	2
Yield of iso C_{5-8} (%C)	0,2	7,1	6,5	4,3	5,3	4,6

Using catalysts with better zeolite-active metal interaction resulted in cracking reactions in the FT process reduced Brønsted acid sites, increased selectivity to gasoline fraction, suppressed formation of oxygenates, improved isoparaffins (that have a higher-octane number in comparison with normal parrafins) and WGS reaction Presence of zeolite in the catalysts also increased the role of the WGS reaction in FTS. But presence of binder in the these catalysts, on the other hand, resulted in a decrease in the amount of reduced iron species, reduced amounts of Brønsted acid sites, blocked the zeolite pores and weakened the effect of the zeolite on the FTS catalyst activity.

Although the product selectivity could be greatly modified through the various catalyst designs, the activity and stability of the zeolite- supported catalysts were often negatively affected in comparison with the conventional Fe and Co catalysts. This is mainly owing to enhanced coke deposition inside the acidic zeolite cages/channels and metal-support interactions which lowered the reducibility of Fe or Co, consequently retarding the FTS reaction rates and increasing methane formation.

The deactivation of hybrid catalysts has been studied by several groups, Martinez et. al (2008), Pour. et. al. (2008). Martinez et al.(2008) characterized the amount and nature of the carbonaceous deposits by a combination of various characterization techniques. The initial zeolite activity was mostly determined by the surface acidity rather than by the total amount of Brønsted acid sites, pointing out to the existence of limitations for the diffusion of the long-chain n-paraffins through the 10-MR

channels under FT conditions. Thus, ITQ-2 bearing the largest surface area, presents the highest initial yield of branched gasoline-range products, followed by ZSM-5, IM-5, and MCM-22. The yield of iso-C5-C8 components was taken as reference for zeolite activity, which is responsible component for isomerization reactions in the bi-functional catalyst. Change of the relative yield to iso-C_5-C_8 products with time on stream (TOS) is given in Figure 2.11. All zeolites experience a loss of activity with TOS, particularly during the initial reaction stages. This deactivation was governed by the morphological and structural properties of the zeolite, which finally determine the amount and location of the coke species, and not by the acidity.

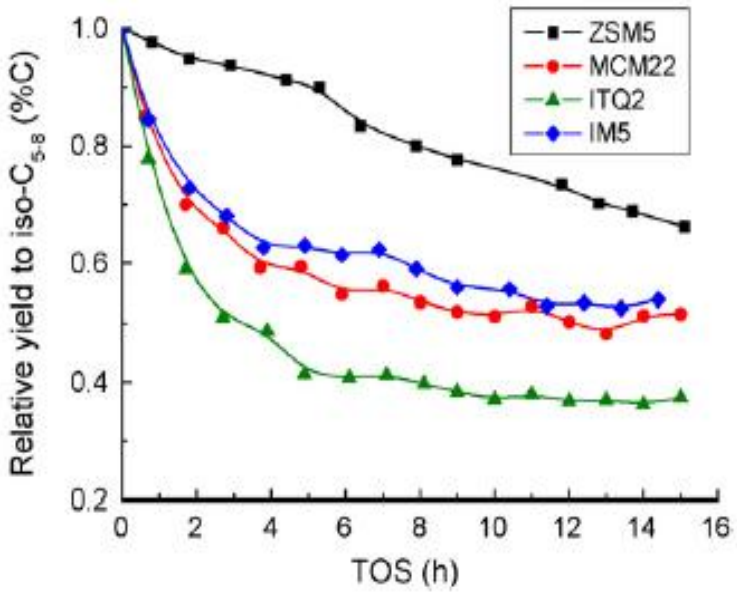

Figure 2.11 : Change of the relative yield to iso-C5-C8 products with TOS.

The total amounts of coke formed in cases of ITQ-2 and MCM-22 were similar and significantly larger than in cases of IM-5 and ZSM-5. In the case of ITQ-2 most of the coke resided on its very large external surface area, which provides an unconstrained space for the formation of bulky (i.e. polyaromatic) species. By contrast, the majority of coke in case of MCM- 22 was located inside the large 12-MR supercages which acting as a trap and preventing their escape through the narrower 10-MR windows. In synthesis by ZSM5, most of the coke was preferentially located on the external surface. This zeolite gave greater stability, at least within in the relatively short range of TOS studied.

2.5.4 Capsule catalysts (core and shell catalysts)

The interaction of, thus contact between the active catalyst components and the zeolite and their arrangement in the catalysts are expected to be very critical for the bifunctional FT process. To enhance this process, Tsubaki et al. (He et al., 2005; Li et al; 2009; Yang et al., 2007; Yang et al., 2008) developed a novel catalysts called capsule-type or core–shell catalysts. They coated zeolite membranes on pellets of a conventional FT catalyst, such as Co/SiO_2 or Co/Al_2O_3, by a hydrothermal synthesis method.

A schematic represenatation of reaction within the capsule FT catalyst is shown in Figure 2.12. Unreacted synthesis gas diffuse through the zeolitic shell of the catalyst and reaches the active metal at the core of the catalyst. FT reactions occur on the this metal (i.e. Co) and hydrocarbons of different chain lengths are synthesized at the core of the catalyst. For long-chain hydrocarbons, their low diffusion rate in zeolite membrane makes them stay in the membrane layer longer. Thus, they can have a higher possibility of isomerization and cracking reactions inside the membrane. Furthermore, compared to conventional membrane reactors, the designed capsule catalysts have larger membran eareas per unit reactor volume.

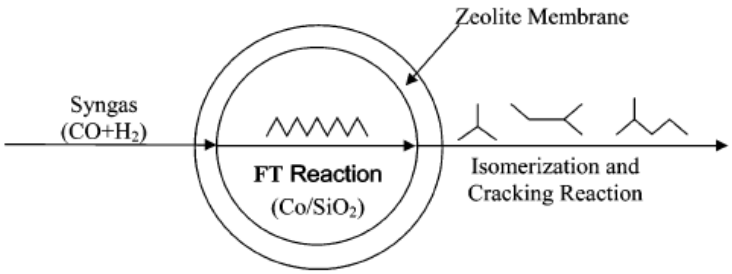

Figure 2.12 : Schematic representation of capsule FT catalyst reaction.

The selectivities obtained by conventional, hybrid and capsule Co-ZSM5 FT catalysts are given in Figure 2.13. H_2 diffuses quickly inside small pores and channels compared to CO. The lower diffusion rate of CO led to a high H_2/CO ratio in the interior part of the catalyst pellets, which might increase methane selectivity for capsule catalysts. The CO_2 in FTS reactions is mainly coming from WGS reaction, and its selectivity hardly changed. Long-chain compounds stayed in the zeolite membrane longer, which caused all long-chain hydrocarbons to crack and isomerize. All capsule catalysts gave a very sharp hydrocarbon distribution that ended at C9-C10, while there were still some C13-C20 hydrocarbons in the products

of the physically mixed catalysts. It is suggested that the membrane cover had an excellent selectivity for short-chain hydrocarbons and inhibit the long-chain hydrocarbons completely.

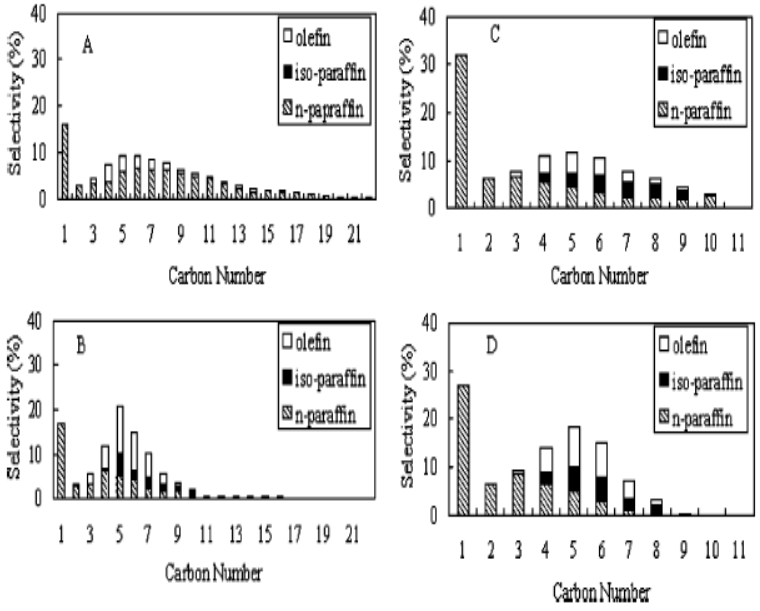

Figure 2.13 : FT synthesis product distribution; (A) Co/SiO_2, (B) Co/SiO_2-zeolite physical mixture, (C) 2-Co/SiO_2-zeolit capsule cat., (D) Co/SiO_2-zeolit capsule cat., $H_2/CO=2$, W/F=10 g.h/mol, T=533 K.

The cross section SEM image and EDS line analysis of the capsule type Ru/SiO_2-ZSM5 catalyst are showed in Figure 2.14. From the SEM image, Fig. 13 A, a clear boundary can be observed between the H-ZSM-5 (shell) and Ru/SiO_2(core), which corresponded with the continuous change of Si-Kα signal showed in its EDS line analysis. Furthermore, no pinhole or crack can be detected either on the SEM image or EDS line analysis, indicating that defect-free H-ZSM-5 zeolite membrane was successfully synthesized on the Ru/ SiO_2 pellets.

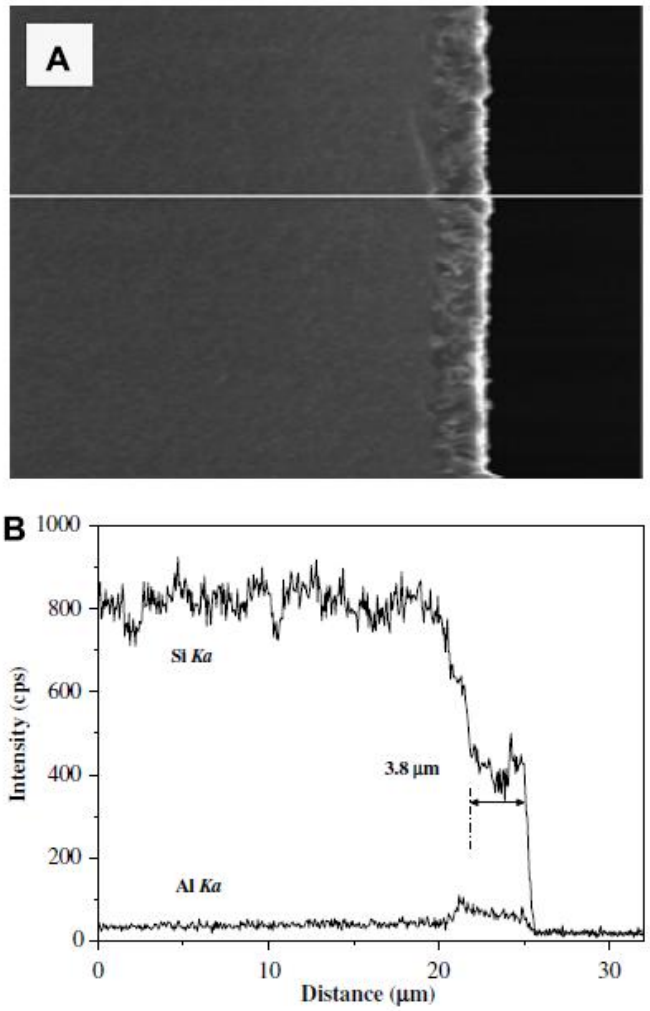

Figure 2.14 : Ru/SiO_2-Z-A capsule catalyst SEM / EDS analysis (A) cross section SEM image (B) EDS line analysis of zeolite capsule catalyst.

The capsule catalysts are expected to have wide applications, if the proper combinations of–core and membrane catalysts can be established for the target reactions. The typical chemical process can be represented as:

$$A \xrightarrow{Cat1} B \xrightarrow{Cat2} C \qquad \textbf{(2.11)}$$

Building catalyst 2 as a membrane on the surface of catalyst 1 pellets can be applied to prepare a lot of different kinds of applications for capsule catalysts. This process can realize the combinations of these two sequential reactions coupled with the in-situ reaction-separation effect. These new kinds of capsule catalysts can be applied to many fields of chemical processes (He, 2005).

2.5.5 Dual bed configuration

Using a dual reactor arrangement with two functional catalysts in separate reactors is another procedure used in literature (Udaya et al., 1990; Zhang et al., 2010; Liu et al., 2007). Shell developed a two-step process for producing branched hydrocarbons from syngas. A conventional FT catalyst was employed in the first step, and the obtained wax products were hydrocracked separately with zeolite component in the second step .

Liu et. al. (2007) studied a consecutive dual reactor system, in which FT reaction was carried out over Co/SiO_2 catalyst in the upper reactor and hydro conversion of the FT HC took place over precious metal/zeolite catalyst in the bottom reactor. Product distribution of traditional FT synthesis was significantly modified and high selectivity to iso-parrafins was achieved with the presence of metal zeolite catalyst in the bottom reactor.

Dual bed configuration process is not only complicated but catalyst deactivation also occurs easily due to the wax deposition. The coexistence of an acidic zeolite with the conventional FT catalyst, as supported or hybrid catalyst, may inhibit the deactivation of the first-step catalyst by simultaneous hydrocracking of waxes (Zhang, 2010).

3. EXPERIMENTAL

3.1 Materials

3.1.1 Chemicals

The chemicals used for catalyst synthesis and characterization were all research grade. Their specifications and suppliers are given in Table 3.1.

Table 3.1 : Chemicals used in catalyst synthesis and characterization.

Chemicals	Formula	Source	Molecular Weight (g/mol)
Iron nitrate nonahydrate	$Fe(NO_3)_3.9H_2O$	Alfa Aeser	404.0
Amonnium hydroxide, 30%	NH_4OH	Alfa Aeser	35.0
Copper nitrate hydrate	$Cu(NO_3)_2$. 2.5 H_2O	Alfa Aeser	232.6
Potassium carbonate	K_2CO_3	Alfa Aeser	101.1
Oxalic acid, 98%	$C_2H_2O_4.2H_2O$	Alfa Aeser	126,1
n-butyl amine	$C_4H_{11}N$	Alfa Aeser	73.14
Water	H_2O	de-ionized water (cond: <1μS/cm)	18
Zeolite Y (CBV 500)	Aluminosilicate	Zeolyst International	-
Zeolite Y (CBV 780)	Aluminosilicate	Zeolyst International	-
ZSM-5 (CBV 28014)	Aluminosilicate	Zeolyst International	-
Beta (CP 814C)	Aluminosilicate	Zeolyst International	-
Mordenite (CBV 21A)	Aluminosilicate	Zeolyst International	-
Ferrierite (CP914C)	Aluminosilicate	Zeolyst International	-

The schematic view of pore structure and dimensions of the zeolite pores are given in Figure 3.1.

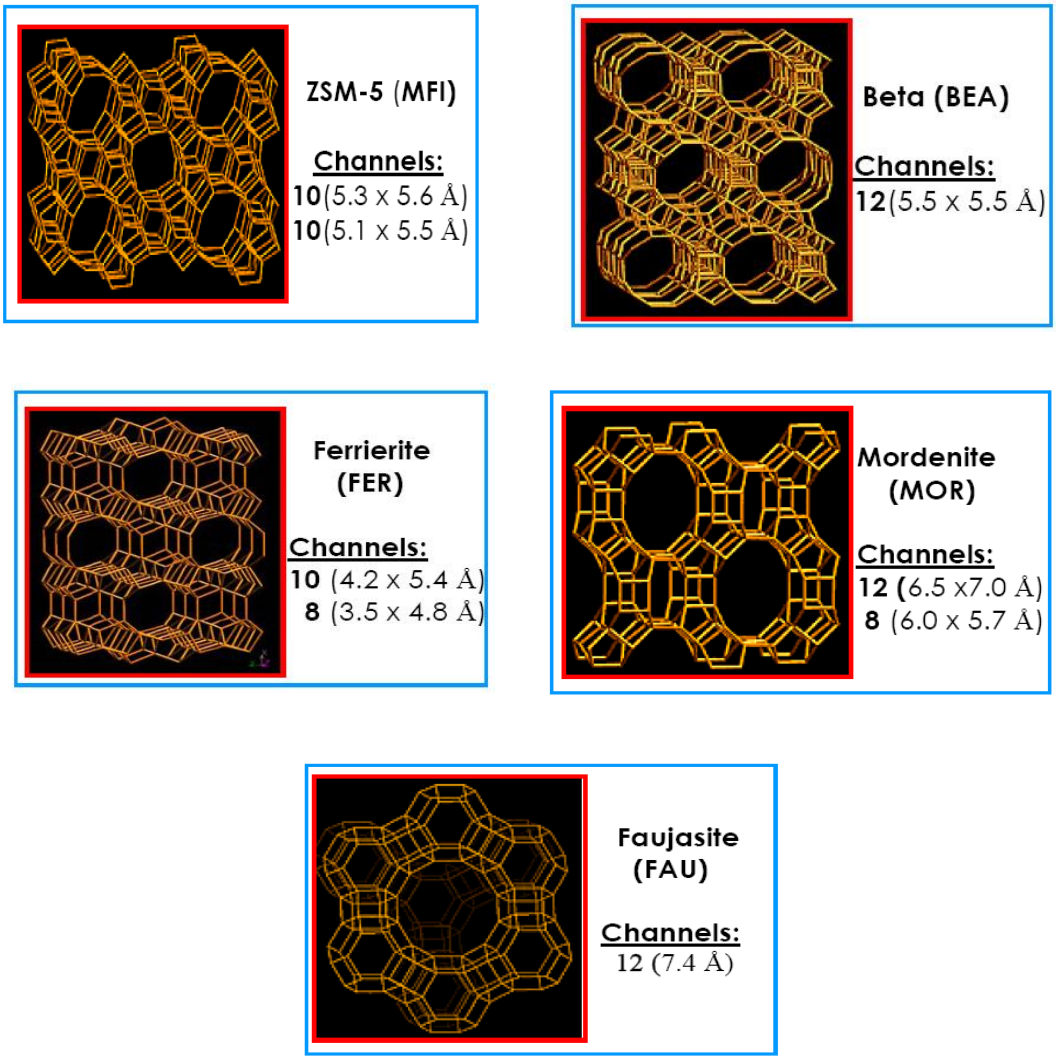

Figure 3.1 : Pore structure of the zeolites used in the study.

ZSM-5 crystalline framework consists of two types of intersecting channel systems made up of ten membered ring openings. One channel system is sinusoidal and has a cross section of 5.1 × 5.5 Å. The other channel system has 5.3 × 5.6 Å openings which run straight and perpendicular to the first system (Viswanadham, 1997).

Zeolite Y (faujasite) framework consists of sodalite cages which are connected through hexagonal prisms. The pore, which is formed by a 12 MR, has a relatively large diameter of 7.4 Å. The inner cavity has a diameter of 12 Å and is surrounded by 10 sodalite cages. Zeolite Y has a one dimensional pore structure (Url-4).

Ferrierite is a zeolite with a bidimensional pore structure, consisting of 10-membered rings (42 x 54 nm) channel intersected by 8-membered rings (35 x 48 nm) channel.

Zeolite Beta is a relatively large pore zeolite with a three-dimensional 12-MR system (straight channels of diameter 6.6 × 6.7 Å and sinusoidal channels of 5.6 × 5.6 Å (Gonzalez, 2007).

Mordenite has an essentially two-dimensional intersecting pore system, constituted by two channel types. The micropore system of mordenite consists of two pore channels; an elliptical pore channel (6.7 × 7.0 Å) and another pore channel (2.6 × 5.7 Å) (Aly et al., 2012).

3.1.2 Gases

All gases except calibration gases, used in the study were supplied by HABAŞ and Linde Companies, İstanbul. Calibration gases were supplied by Air Products, United Kingdom. Table 3.2 lists the specifications and applications of the gases employed in this research.

3.2 Catalyst Preparation and Pretreatment

In the scope of the thesis study four different types of catalysts have been synthesized and tested. They are given bellow:

- Zeolite supported iron based catalyst,
- Base iron catalyst,
- Conventional promoted iron based catalyst (conventional catalyst),
- Hybrid catalyst (physical mixture).

Table 3.2. Specifications and applications of the gases used.

Gas	**Specification (%)**	**Application**
Argon	99.999	GC Carrier Gas
Carbon monoxide	99.5	Reactant
Dry Air	99.999 (21.6 O_2 + Balance N_2)	Oxidizing Agent, GC Pneumatic Valve
Helium	99.999	GC Carrier Gas
Hydrogen	99.999	Reactant, Reducing Agent
Nitrogen	99.999	Reactor Feed Gas Constituent (Inert)
Calibration Gas -1	CH_4: 0.9 O_2: 1 CO: 1.5 CO_2: 14.5 N_2: 34 H_2: 48.1	GC Calibration
Calibration Gas -2	CH_4: 89.76 C_2H_6: 8 C_3H_8: 1.6 n-C_4H_{10}:0.22 i-C_4H_{10}:0.17 N_2: 0.1 CO_2: 0.1 C_6H_{14}: 500 ppm	GC Calibration

3.2.1 Synthesis of zeolite supported iron based catalyst

The zeolite supported catalysts were prepared by the incipient wetness impregnation method. Iron nitrate ($Fe(NO_3)_3 \cdot 9H_2O$) solution was used as the iron source. In the synthesis of the catalysts, zeolites were impregnated with iron nitrate solution under continuous stirring. The concentrations of iron nitrate solutions (molarity) were adjusted, by trial and error procedure, to obtain the final impregnated catalysts in the form of incipient to wetness. The concentration of iron nitrate solutions were 4.5 M (3.63 gr, 2 mL). The impregnated catalysts were dried in the ambient air of 383 K overnight and then calcined at 748 K for 8 hours. The zeolite supported catalysts with approximately 4 wt. %Fe was first synthesized and then it was used to prepare catalysts with 9 wt. %Fe and 18 wt. %Fe by repeating the procedure mentioned above (Figure 3.2).

In order to obtain high catalytic activities, a pretreatment involving catalyst calcination and reduction of the catalysts is required. The last calcination and the reduction of the catalysts were done in the activity test system, following the loading of catalyst into the reactor.

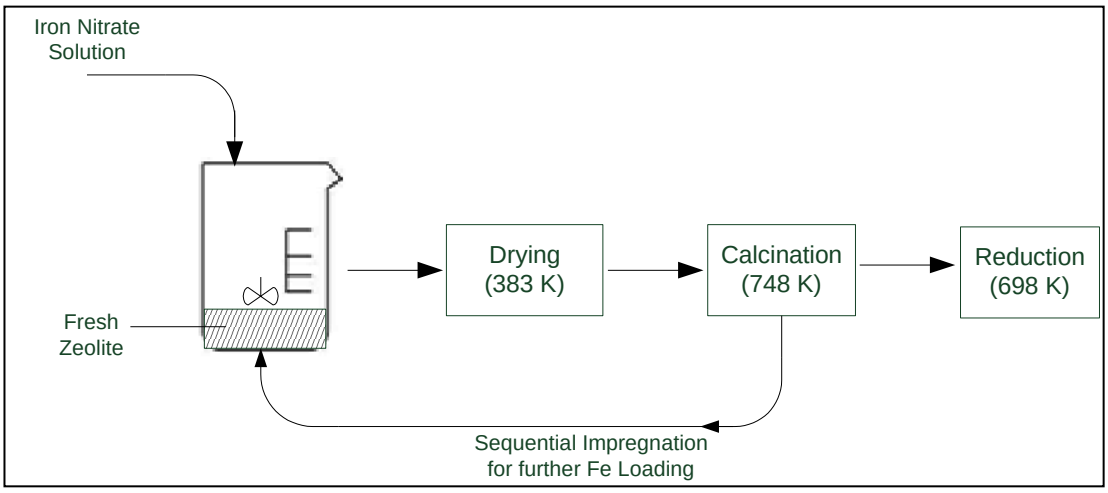

Figure 3.2 : Synthesis procedure of zeolite supported catalyst.

The calcination of the catalysts were conducted under a dry air flow at atmospheric pressure. The catalysts were heated up from ambient temperature to 748 K at a heating rate of 2.5 K/min., and held at 748 K for 8 hours. The time – temperature history of the calcination procedure is given in Figure 3.3. The dry air flow rate was fixed to and kept at 3.0 l/h during the calcination.

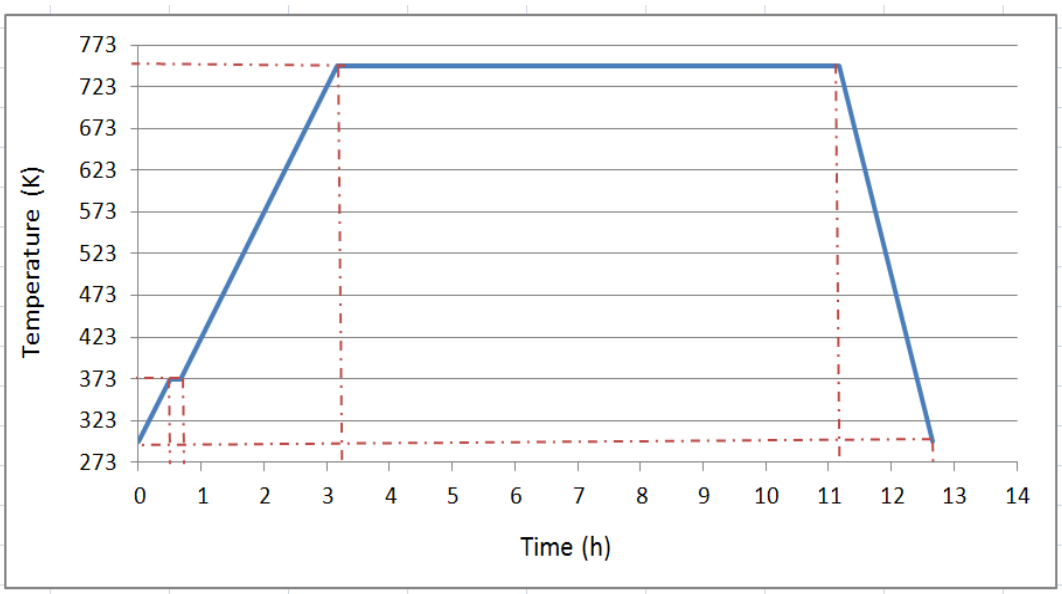

Figure 3.3 : Calcination procedure of zeolite containing catalysts.

The reduction of the active metal (Fe) from the oxide state, formed during calcination, to the metallic state is required since the catalysts in their oxide forms are usually inactive for the FT reactions. Therefore, the prepared fresh catalysts in the oxide form were subjected to a reduction process in which the catalysts were heated up from ambient temperature to 698 K at a heating rate of 2.2 K/min., and held at 698 K for 10 hours. The reduction was carried out done under a 4.5 l/h hydrogen flow at atmospheric pressure. The detailed history of the catalyst heating process applied during reduction is shown in Figure 3.4. Because of the strong interaction between the zeolite support and active metal, the calcination and reduction periods lasted longer than usual, being 8 hours and 10 hours, respectively. After the reduction completed, the temperature was reduced to reaction temperature. The total duration of the calcination and reduction procedures, involving time for heating of catalysts to the calcination and reduction temperatures and cooling them back to the targeted temperatures, was about 27 hours.

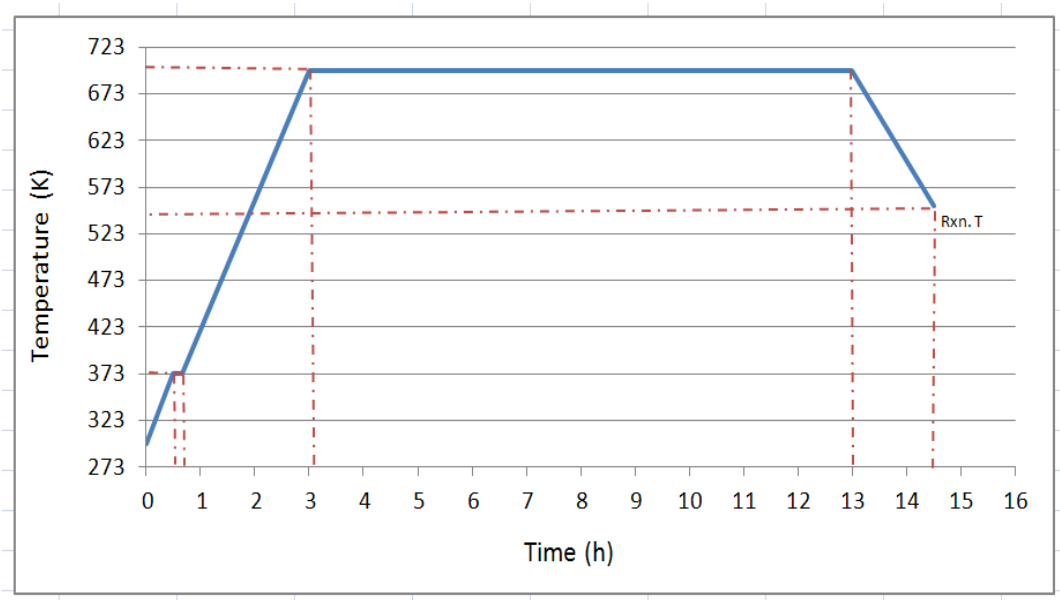

Figure 3.4 : Reduction procedure of zeolite containing catalysts.

3.2.2 Synthesis of base iron catalyst

In the studies, pure base iron was used both as a catalyst in the FT activity tests and as a hybrid catalyst constituent. It was prepared by co-precipitation method from $Fe(NO_3)_3.9H_2O$.

The system used for preparing catalysts by co-precipitation technique includes three beakers, two pumps, a stirred water bath, a temperature controller, a pH meter, a pH controller and a thermocouple. The schematic diagram of the co-precipitation system is shown in Figure 3.5.

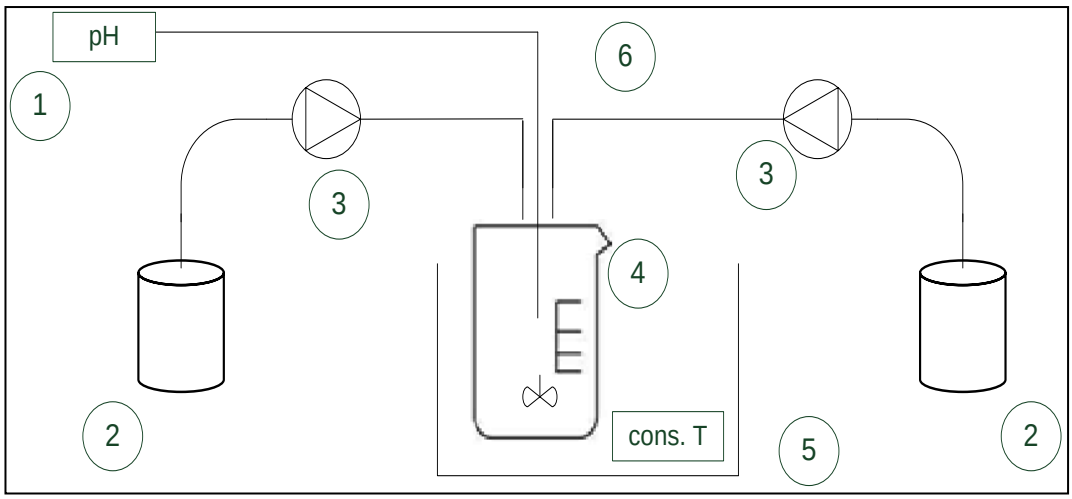

Figure 3.5 : Schematic diagram of the co-precipitation system. (1) pH meter, (2) solution, (3) pump, (4) beaker, (5) constant temperature water bath, (6) silicone tubing.

1M aqueous $Fe(NO_3)_3.9H_2O$ (80.8 gr, 0.25 L) and 15% NH_4OH solutions were separately prepared. Iron nitrate solution was prepared by dissolving of 80.8 g iron nitrate salt in 2.25 L distilled water while ammonium hydroxide solution was obtained by dilution of 30% NH_4OH solution. Both solutions were simultaneously fed into a precipitation beaker which was continuously stirred (Figure 3.5). The feed rates of $Fe(NO_3)_3.9H_2O$ and NH_4OH solutions were set to 20 ml/min and 5 ml/min, respectively. A Masterflex automatic peristaltic pump with silicon tubing was used to feed the $Fe(NO_3)_3.9H_2O$ solution. NH_4OH solution was fed by means of an HPLC pump. Both the feed solution and the precipitation beakers were held at 80 °C in a constant temperature water bath during this process. The apparatus was designed to fix the precipitating holding time to 6 minutes. After the precipitation completed, the solution was centrifuged to recover the precipitate, by using a Backman Coulter Allegra^{TM} 25R centrifuge equipment. Centrifuging was repeated for 5-6 times using 1-1.5 l distilled water to remove ammonia from the precipitate. The precipitate (precursor) then was dried overnight at 110 °C in an oven. The dry iron catalyst precursor was crushed by using of an agate mortar and sieved to 300-425 microns.

The catalyst calcination was done at 643 K for 4 hours in a muffle furnace. The temperature was increased from room temperature to 643 K with 2 K/min temperature ramp.

3.2.3 Synthesis of promoted iron based catalysts

The promoted iron based catalysts were prepared from base iron catalyst via incipient to wetness impregnation method. K and Cu were used as promoters.

The procedure applied for catalyst preparation by impregnation method is schematically shown in Figure 3.6. The experimental set up used for this purpose was consisted of an ultrasonic mixed water bath, a beaker, a flask, a pH-meter, a Masterflex peristaltic pump and a vacuum pump.

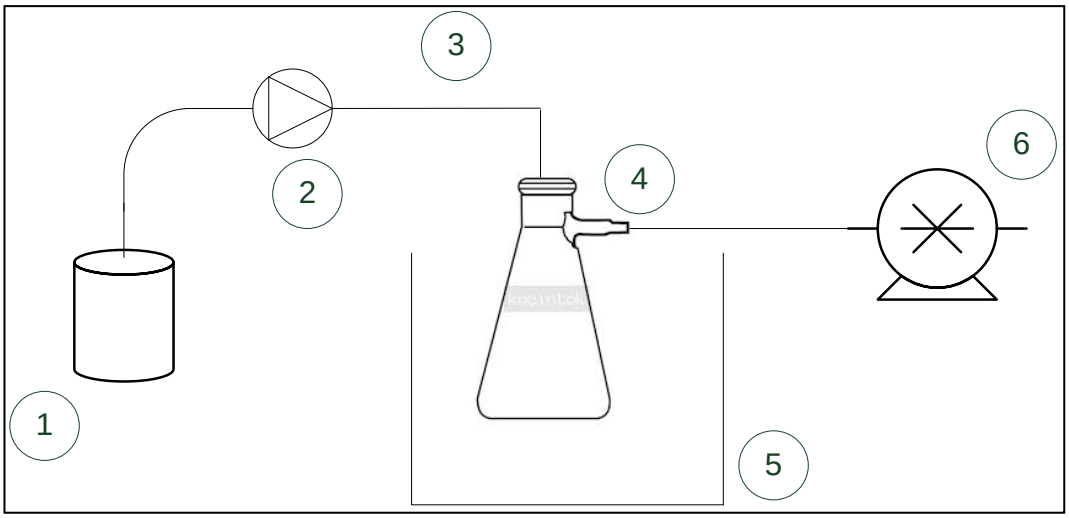

Figure 3.6 : Schematic diagram of the catalyst impregnation system.(1) Precursor solution, (2) peristaltic pump, (3) silicone tubing, (4) flask, (5) ultrasonic mixer, (6) vacuum pump.

The iron catalysts were sequentially impregnated with pre-determined amounts of aqueous $Cu(NO_3)_2$ and K_2CO_3 solutions to produce promoted catalysts with desired Fe/Cu/K weight ratios. For the catalyst preparation, a specified amount (4 gr) of iron precursor was put in a Büchner flask and kept under vacuum at room temperature for 30 minutes by using a vacuum pump to remove the air trapped in procure pores (Figure 3.6). During impregnation, the precursor was mixed in an ultrasonic mixer in order to maintain uniform precursor distribution. 3.2 ml aqueous solution containing 0.709 g $Cu(NO_3)_2.2.5\ H_2O$ was prepared and fed to the flask at a rate of 0.5-1.0 ml/min. After solution feeding completed, the slurry in the flask was ultrasonically mixed for further 90 min. and dried overnight in an oven at 383 K. Applying the same procedure, 3.2 ml solution having 0.049 gr of K_2CO_3 was impregnated on the already prepared copper added iron precursor. The resulting composition of this catalyst was 100Fe7Cu3K.

The resulting slurry was dried overnight at 383 K and calcined in situ under 50 ml/min dry air flow for 4 h at 643 K. Catalyst samples were activated in situ under a flow of synthesis gas with a H_2/CO ratio of 3/1 at 1 bar. During the activation, first temperature was increased from 298 to 423 K with a rate of 10 K/min and then from 423 to 523 K at a rate of 1 K/min. The typical synthesized catalyst samples are shown in Figure 3.7.

Figure 3.7: Samples of synthesized catalysts.

3.2.4 Synthesis of hybrid catalyst

Hybrid catalyst was prepared by physical admixing of the base iron and ZSM-5. Both components were grinded, sieved to 250–350 mesh and then mixed completely. Calcination and reduction of the catalysts were performed according to the procedure given in Section 3.2.1.

3.2.5 Synthesis of de-aluminated zeolite-supported catalysts

The ZSM-5 zeolite was de-aluminated by the following procedure: The zeolite was treated with 0.5 M oxalic acid ($C_2H_2O_4 \bullet 2H_2O$) solution at 353 K under continuous stirring for 1 h. The resulting material was separated from liquid phase via centrifuging and washed several times with distilled water. The obtained de-aluminated zeolite was impregnated with iron nitrate solution by incipient to wetness impregnation procedure as explained in Section 3.2.1. Calcination and reduction procedures described in Section 3.2.1 were also applied to this catalyst.

3.3 Characterization

3.3.1 Catalyst characterization systems

The prepared catalysts were characterized by various methods which are briefly described below

X-Ray Diffraction (XRD). The crystalline phases of the zeolites and catalyst samples were identified by X-ray diffraction (XRD) analyses. Analyses were performed by using an XRD 6000 Shimadzu X-ray diffraction equipment with monochromatized Cu(Kα) radiation. The relative crystallinities of the zeolite in the final catalysts were calculated from the XRD patterns, using the ASTM D5758 Standard. Hematite phase crystallite sizes were calculated by Scherrer's equation.

Inductively Coupled Plasma (ICP). ICP analyses were carried out by using a Thermo Jorrel Ash Atom Scan 25 instrument in order to determine the wt. % of iron in the synthesized catalysts.

Nitrogen Physisorption. The BET surface area, the total pore volume and the pore size distribution of the catalysts were measured by N_2 physisorption at 77 K using a Quantachrome Autosorb Automated Gas Sorption System. The samples were degassed under vacuum at 393 K for 6 h prior to measurements.

Thermo Gravimetric Analysis (TGA). The acidity of the zeolites was measured by using n-butyl amine adsorption and subsequent TGA measurements. TGA measurements were done by using a Mettler Toledo TGA/STDA851 instrument.

Scaning Electron Microscopy (SEM). SEM and EDS tests were conducted on both the freshly calcined and reduced catalyst samples in order to elucidate their micro-structural properties, using a Jeol JSM-6335F Field Emission SEM system of a maximum resolution of 2 nm. No additional coatings or dispersive liquids were used prior to SEM and EDS measurements.

3.3.2 Product analyses

Gas, liquid and wax products form FT shynthesis reactor, were analyzed by using Gas Chromotography (GC) method. Properties of the gas chromotographs used in the analyses and analysis conditions are given in Table 3.3 and Table 3.4 for liquids-waxy and gaseous products, respectively

Reactants and gaseous product were analyzed by using an on-line gas chromatograph (Hewlett Packard, Model 7890 Series II) equipped with 5 valves, 7 columns and 3 detectors (Table 3.4). The flame ionization detector (FID) channel was configured to analyze the hydrocarbons from C1 to C6. The first thermal conductivity detector (TCD) channel was used to analyze CO_2, CO, and N_2. The second TCD channel was dedicated to the H_2 analysis.

The medium range hydrocarbons, collected in cold trap and heavy hydrocarbons, collected in hot trap, were analyzed via an Agilent 6890 Series GC equipped with a HP-PONA column and FID. Two analysis methods were developed for analysis of these products. In order to prevent any trouble might be originated from contamination in the sample, the liquid products were filtered and collected in vials.

Waxy products were solved in carbon disulfide solution to be fed to GC. The analyses of the waxy products were done by "Simulated Distillation" method. During the wax analysis, the GC oven temperature was raised from 308 K upto 573 K. The GC analyses of the wax and oil lasted 167 min. and 160 min., respectively.

Gas chromotographs were periodically calibrated by using certificated calibration gases and liquids (composed of liquid hydrocarbons ranging between C4-C28). The peak area of each liquid component was measured. In this process, first the peak area was measured and then concentration vs peak area curve was determined for each liquid component.

Table 3.3 : Gas chromotograph and liquid phase and waxy products' analyses conditions.

Detector	FID
Oven Temperature Programme	- 308 K (2 min.) - 1.7 K/min. (from 308 K to 573 K) - 573 K (10 min.)
Column	HP Pona Siloxane
Column Material	100% dimethylpolysioxane
Coloumn Length X ID	0.2 mm x 50 m
Carrier Gas	Helium (23 cm/sec.)
Split Ratio	0.1
Analysis Duration	160 minutes (oil anaysis) 167 minutes (wax analysis)

Table 3.4. Properties of gas chromotographs and on-line gas analyses conditions.

1st Column	0.5 m. Hayesep Q 80/100 mesh
2nd Column	6 ft. Hayesep Q 80/100 mesh
3rd Column	6ft. Molecular Sieve 5A 60/80mesh
4th Column	3 ft. Hayesep Q 80/100 Mesh
5th Column	8ft. Molecular Sieve 5A 60/80mesh
6th Column	123-1015 (cut) 2m x 0,32mm x 5um DB-1
7th Column	19091P-S12 25m x 0,32mm x 8um HP-AL/S
Oven Temperature Programme	- 333 K, 1 min. - 20 K/min., 353 K - 30 K/min., 433 K - 463 K, 1.33 min
Front Detector(FID detector)	- Temp.: 523 K - H_2 flow rate : 40 ml/min. - Air flow rate: 450 ml/min. - N_2 flow rate 45 ml/min. (make up)
Back Detector (TCD detector)	- Temp.: 523 K - Ref. gas flow rate : 45 ml/min. - Make up gas flow rate: 2 ml/min. - Negative Polarity: Off
Auxiliary Dedector (TCD detector)	- Temp.: 523 K - Ref. gas flow rate : 45 ml/min. - Make up gas flow rate: 2 ml/min. - Negative Polarity: On
Inlet Temp.	393 K
Gases Analyzed	C1-C5, CO, CO_2, N_2, H_2
Analysis Duration	7 min.

3.4 Catalyst Performance Test System

The catalytic performances of the synthesized catalysts in the Fischer Tropsch process were investigated by using a fixed-bed reactor system, shown in Figure 3.8. It consisted of feed, reaction, product separation, control and product analysis sections.

Feed section. The feed sub-system was composed of gas cylinderes, mass flow controllers (MFC), 1/4" stainless steel tubings, manual on/off valves, check valves and a three way valve.

The gases supplied from pressurized gas cylinders, sequentially passed through gas pressure regulators, mass flow controllers, check valves and entered into the top of the reactor. The flow rates of gases were measured, adjusted and controlled via mass flow controllers (Bronkhost; Model: F-201CV-100-AGD-22-V) and an attached control unit. Check valves positioned before MFC's to protect them from possible back-pressure fluctuations. Manual on/off valves were used in order to isolate lines one from another, in cases needed. A three-way valve and a by-pass line allowed to bypass the reactor and divert the feed stream directly to the analysis unit. Gas mixtures with desired compositions were preapared by mixed pure gases supplied from gas cylinders at pre-determined flow rates. The exact compositions of the these fresh mixtures were determined in gas analysis unit. Gas mixtures were fed to the reactor through a three-way valve. The MFCs were periodically controlled and calibrated via soap bubble test by using a calibrator device (Gilibrator ®).

Reaction section. A stainless-steel (SS-316) fixed-bed tubular reactor of 15 mm ID and 50 cm length with down-flow was used in the experiments. The reactor was held in a furnace with a programmable heating control system. The temperature of the reactor was controlled to ±1 K by a ORDEL PC 991 temperature controller. The reaction temperature was measured by using a K-type sheathed thermocouple which was placed into the center of the catalyst bed. The temperature profile of the reactor was controlled automatically, by the furnace temperature controller. The catalyst loaded to the reactor was supported by ceramic glass wool both from bottom and top. Both ends of furnace were insulated with glass wool to reduce heat loss and to produce a stable temperature profile in the reactor. A back pressure controller (Bronkoshorst; Model: P-702CV-100A-BGD-22-K) mounted after the traps, was

used to control the reactor pressure. The system were checked and fixed prior to each test run in order to determine and prevent gas leaks at high pressures. A stainless steel filter having 15 micron pore size was placed just before the back pressure controller to prevent blockage of the back pressure controller.

Product separation section. The product stream leaving the reactor would contain a broad range of hydrocarbons ranging from C1 (methane) up to C40 (40 carbon containing hydrocarbon) and even higher, together with steam and unconverted feed gases. A hot trap at 473 K and cold trap at 278 K were sequentially located immediately after the reactor for collecting heavy hydrocarbons and the medium range hydrocarbons/water, respectively. All lines connecting the reactor to the cold trap were heated to and kept at 473 K in order to avoid premature condensation. The temperature of the hot trap and tubing lines were controlled by using heating tapes, K type thermocouples and ENDA ETC 4420 temperature controllers. An additional glass wool insulation layer was put on the heating tapes wrapping lines in order to reduces the heat loss. The cold trap was designed and manufactured as a jacketed cylindrical container. Its shell side was fed with refrigirated water stream to keep the tube side temperature at 278K condensing water and medium range hydrocarbons.

Noncondensed gaseous components in the reactor outlet stream vented from the system at downstream of the back pressure controller.

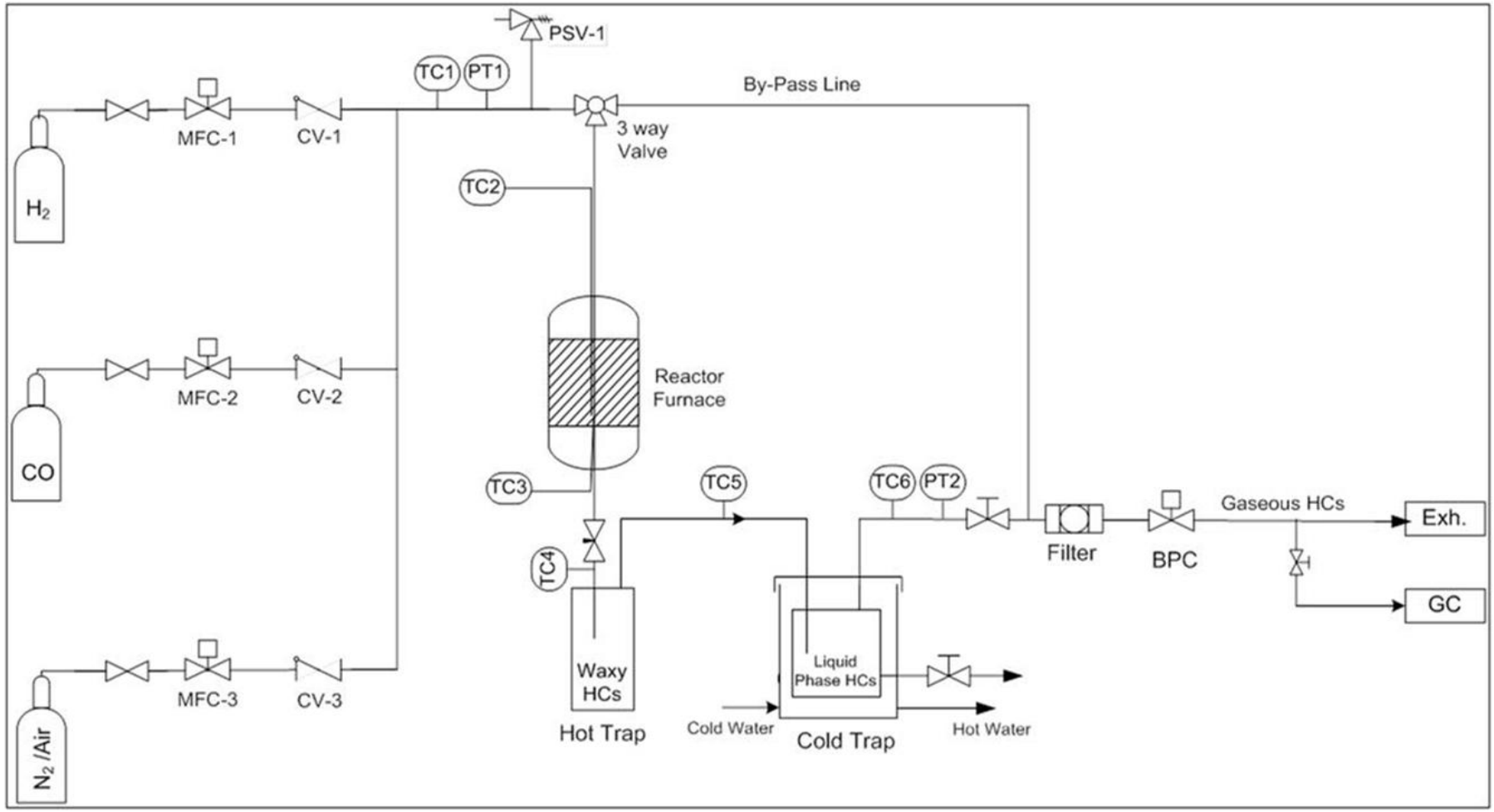

Figure 3.8 : Flow diagram of catalyst activity test system (MFC: mass flow controllers, CV: check valves, TC: thermocouple, PT: pressure transmitter, BPC: back pressure controller, PSV: pressure safety valve).

Control system. A dedicated and comprehensive control system was used to monitor and record the experimental data and control the experimental set up. It allowed to control all flow rates and temperatures as well as reactor pressure. The user interface of the control system software is given in Figure 3.9.

The system was designed to be operated continuously 7 days/24 hours, without continuous monitoring and control of an operator. With the help of the Team Viewer® programme, remote monitoring and control of the system through internet was possible. Controlling system was fitted out with necessary alarms and automatic shutdown procedures. In addition, the furnace temperature was also separately monitored by an attached temperature controller and an electrical switch. To protect the system from excessive temperatures, an electrical switch was used to cut entire electricity supplied to experimental system in case furnace temperature went beyond a pre-determined set value of 1023 K.

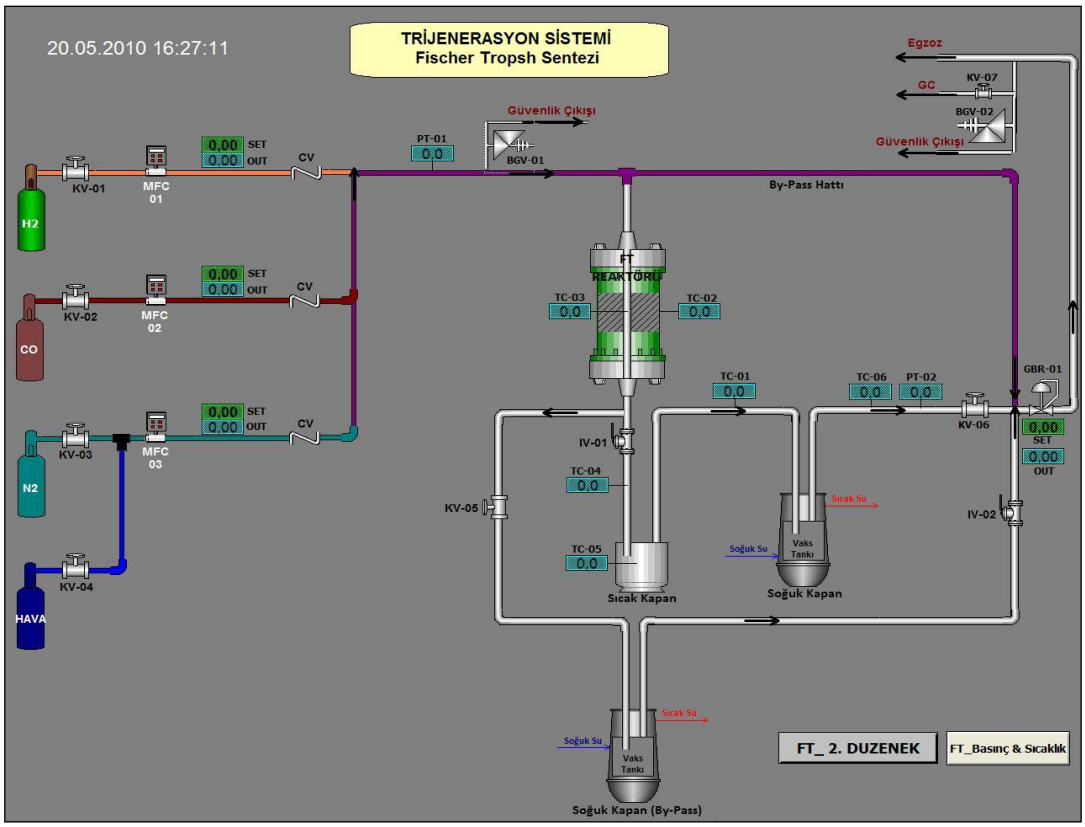

Figure 3.9 : Sofware user interface of the control system of the experimental set-up.

3.5 Running Catalyst Performance Tests

The prepared catalysts were tested for their performances in the FT synthesis. The aim of these experiments was to particularly investigate the activity and selectivity of the catalysts based on the types of supports. Prior to the activity tests, catalysts were reduced under a flow of hydrogen stream at 743 K for 10 hours, as explained in Section 3.3.1. In a typical run, at the end of pre-treatment period, the temperature and pressure were adjusted to pre-determined operating levels. Then the reactant gas mixture was mixed with N_2 in the upstream and introduced to the catalyst bed (reactor) according to the specified experimental conditions and synthesis process was initiated.

The experimental parameters and reactor operating conditions are given in Table 3.5. All of the catalyst were tested at three different reaction temperatures of 523 K, 538 K and 553 K, while other parameter kept constant. N_2 was fed to the reactor as a base for the mass balance calculations. Unless otherwise stated, the flow rates of H_2, CO and N_2 were set to the values given in the table. Moreover, effects of operating conditions (pressure, feed H_2/CO ratio, GHSV) were also studied for one selected catalyst.

Table 3.5 : Experimental parameters considered in experiments carried out to study the performance of catalysts in FT synthesis.

Experimental Parameter		**Symbol**	**Range applied in the experiments**
Reaction temperatures (K)		T	523, 538, 553
Operating pressure (bar a)		P	19
The H_2/CO ratio		H_2/CO	2/1
Gas hourly space velocity (1/h)		GHSV	750
Gas flow rates (Nl/h)	H_2	Q_{H2}	3.0
	CO	Q_{CO}	1.5
	N_2	Q_{N2}	0.45

3.6 Activity and Selectivity Calculations

The activity, selectivity and hydrocarbon yields obtained from the catalyst activity tests were calculated by using the results of the on-line gas analysis and off-line liquid and wax product analysis.

The activity test system has two traps, located just downstream of the reactor, collecting hydrocarbon products: a hot trap hold at 523 K, condensing mainly hydrocarbons heavier than C18 and a cold trap hold at 278 K, condensing mainly hydrocarbons ranging between C4 and C18. The gas phase leaving the reactor contained the non-condensed light C1-C4 hydrocarbons, unconverted synthesis gas, steam and nitrogen leaved the system.

The conversion calculations, the C1-C4 and CO_2 selectivity were calculated based on the on-line GC gas analysis results. On-line GC analyses were repeated at least three times for each condition and each of these analyses was done with at least three successive runs. A constant nitrogen gas stream fed to the reactor was taken as the basis of calculations. The carbon monoxide and hydrogen conversions and the CO_2 selectivity (molar) were calculated using equations 3.1 – 3.3 given below.

CO conversion:
$$X_{CO} = \frac{\left[F_{CO,i} - \left(y_{CO,o} \cdot \frac{F_{N_2}}{y_{N_2,o}}\right)\right]}{F_{CO,i}} \quad \textbf{(3.1)}$$

H_2 Conversion:
$$X_{H_2} = \frac{\left[F_{H2,i} - \left(y_{H2,o} \cdot \frac{F_{N_2}}{y_{N_2,o}}\right)\right]}{F_{H2,i}} \quad \textbf{(3.2)}$$

CO_2 Selectivity:
$$S_{CO_2} = y_{CO2,o} \cdot \frac{F_{N2}}{y_{N2,o} \cdot F_{CO} \cdot X_{CO}} \quad \textbf{(3.3)}$$

where, X_a = the conversion of species a, F_a= molar flow rate of species a at reactor inlet, y_a= the ratio of species a, S_a=selectivity of species a and subscript “i" stands for inlet while subscript “o” stands for outlet.

The distribution of produced hydrocarbon were calculated by using the GC analysis results of the liquid and waxy products accumulated in the cold and hot traps and the on-line gas analyses. The total carbon content of the hydrocarbons from FT synthesis is equal to the amount of converted CO excluding the amount of CO_2 produced. The

hydrocarbon distribution were calculated for the intervals between two sample collections.

The calculation procedure is as follows;

i. Total amount of converted CO was calculated,

ii. Total amount of produced CO_2 was calculated,

iii. Total amount of hydrocarbons, based on carbon content, produced by FT synthesis was calculated,

iv. The amount of gas phase hydrocarbons produced by FT synthesis was calculated from the on-line GC analyses,

v. Total amount of hydrocarbons collected in the trap was calculated by subtracting the amount of gas phase hydrocarbons and CO_2 from total amount of converted CO,

vi. Weight fraction of product hydrocarbons were calculated by dividing weight of individual hydrocarbon to total weight of produced hydrocarbons.

An overall mass balance was established for performance runs. Using N_2 as an internal reference standard, the mass flow rate of gas phase in the reactor effluent stream was calculated. The liquid and waxy products were collected in the traps and then weighed.

Three additional performance indicator parameters were defined and used in order to quantify the performance (activity + selectivity) of the catalysts. 1. *HC productivity* which is the total mass flow rate of hydrocarbons produced by FT synthesis per unit iron mass content of the catalyst (Eq.3.4) . 2. *HC yield* which indicate the total mass flow rate of hydrocarbons produced by FT synthesis per unit mass of the fresh syngas fed to the system reactor (Eq. 3.5). 3. *Gasoline yield* is the total mass flow rate of gasoline range HC produced by FT synthesis per unit mass of fresh syngas fed to the reactor (Eq. 3.6). These parameters were calculated by using the following equations:

HC Productivity: $$P_{HC} = \frac{\dot{m}_{HC,o}}{m_{Fe}} \quad \textbf{(3.4)}$$

HC Yield: $$Y_{HC} = \frac{\dot{m}_{HC,o}}{Q_{syngas,fed}} \quad \textbf{(3.5)}$$

Gasoline Yield: $$Y_{Gasoline} = \frac{\dot{m}_{gasoline,o}}{Q_{syngas,fed}} \quad \textbf{(3.6)}$$

where, $\dot{m}_{HC,o}$ = mass flow rate of hydrocarbons produced by FT synthesis, m_{Fe}= the iron mass of the catalyst, $Q_{syngas,\ fed}$ = the volumetric flow rate of fresh syngas fed to the FT reactor, $\dot{m}_{gasoline,o}$= the mass flow rate of gasoline range HC (C5-C11) produced by FT synthesis.

4. RESULTS AND DISCUSSION

In this study, zeolite–supported iron-based bi-functional catalysts were prepared and tested for their performances in the FT synthesis. They were composed of two components: an active component (iron) and a support (zeolites). The results of the experimental studies carried out on different aspects of the synthesized catalysts are presented and discussed in this chapter with different subtitles.

4.1 Effect of Zeolite Type on The Performance of Bi-functional Fischer Tropsch Catalysts

The acidity, surface area, pore structure, pore dimensions and cation exchange capability of zeolites are crucial factors affecting the catalytic performance of zeolite-metal FT catalysts due to their cracking, oligomerization and isomerization activities. Each zeolite type, having intrinsic pore structure, dimensions, acidity etc., shows different catalytic activities towards above-mentioned reactions. Furthermore, the pore structure and pore dimensions of the zeolite determine the shape selectivity capability of the catalysts. By virtue of the zeolite shape selectivity, the chain-growth process is restricted to give low molecular weight products. On the other hand, the efficiency and selectivity of a supported catalysts are closely related to the dispersion and particle size of the active metal component and to the nature of the interaction between the metal and the support. Zeolites with their high surface areas generally yield well dispersed catalysts.

Recently, microporous molecular sieves were used as supports for preparing FT catalysts, aiming to improve of the FT activity and selectivity as mentioned above. The majority of the studies on bi-functional FT catalysts are devoted to microporous zeolite materials such as ZSM-5 (Pour et al., 2008; Martinez et al., 2008; Botes, 2005) and zeolite Y (Yoneyama et al., 2010; Egiebor and Cooper, 1989). The use of alternative/new micro and mesoporous materials with controlled acid– base properties might be the key to control the FT selectivity.

A variety of methods, mentioned in Section 2, could be used for synthesis of bi-functional catalysts. The most commonly used methods are the physical admixing and conventional impregnation. In most of the recent studies the physical admixing was used for catalyst preparation (Martinez et al., 2008; Botes, 2005; Yoneyama et al., 2010). However, the conventional impregnation could be a superior catalyst preparation route over physical admixing, since it can result in a better dispersion of active component, a greater zeolite–metal interaction and a better utilization of shape selectivity of the zeolite structure.

Iron, cobalt and ruthenium are well-known metals to be active for FT synthesis. Cobalt has been used in many zeolite-FT catalyst studies due to its high activity and low water gas shift activity and its convenience for production of heavier hydrocarbons mainly in the diesel range (Dry, 1981). In order to have the desired reactions using zeolite catalysts, process temperatures need to be slightly higher than 573 K. However, at these temperatures, cobalt based bi-functional catalysts have very high methane selectivity (Schulz et al., 1991). The methane selectivity of iron catalysts at the same temperature level is lower. Furthermore, iron catalysts favor the production of primary olefins, which can be converted into the gasoline range hydrocarbons via zeolite in the bifunctional catalyst.

In this section, the effects of types of zeolites, which were used as supports in the catalyst synthesis, on the selectivity and activity of iron- based Fischer Tropsch catalysts were investigated. Five different zeolites, namely ZSM-5, mordenite, beta, Zeolite Y and ferrierite were used as supports in the preparation of the iron-based bi-funtional FT catalysts. Of them, mordenite and beta zeolites have very rarely been used as bi-functional catalyst component, while no study dedicated to ferrierite supported FT catalysts have been reported. Ferrierite, however, with its acidic nature and high isomerization activity, seemed to be a promising zeolite for FT applications. It is commercially used for isomerization of n-butenes to isobutene. Its pore dimensions resembles to ZSM-5, one of the leading zeolite constituent alternatives of bi-functional FT catalyst. Both zeolites are belong to 10 membered ring (10-MR) zeolite family**.** On the other hand zeolite Y molecular sieves with different Si/Al ratios (5; 80) were used as supports for preparing iron-based FT catalysts, to see the effect of zeolite acidity on behavior of the catalysts.

The catalysts were synthesized by incipient to wetness impregnation. Iron was used as the FT active metal, in all catalysts in order to take the advantage of low methane and high olefin selectivity. Iron ratio of the catalyst was fixed to approximately 17 wt.%. A *base iron catalyst* was also synthesized and tested for comparison purposes, aiming to determine the contributions of zeolite supports to catalytic activities of the resulting catalysts. Seven catalysts, six bi-functional and one base iron, catalyst were prepared using ZSM-5 (Z), mordenite (M) , beta (B) and ferrierite (F) and zeolite Y as support. The catalysts prepared are shown in Table 4.1.

Table 4.1 : The prepared zeolite supported bi-functional iron FT catalysts and preparation methods.

Catalyst	Active component	Support	Preparation Method
SFeZ	Fe	ZSM-5	IWI*
SFeM	Fe	Mordenite	IWI
SFeB	Fe	Beta	IWI
SFeF	Fe	Ferrierite	IWI
SFeY5	Fe	Zeolite Y (SAR: 5)	IWI
SFeY80	Fe	Zeolite Y (SAR: 80)	IWI
BFe	Fe	-	Co-precipitation

* IWI: Incipient to wetness impregnation method

4.1.1 Catalyst characterization

The synthesized catalysts and mother zeolites were characterized by using X-ray diffraction, N_2 physisorption, ICP and TGA techniques. The acidities of the synthesized catalysts were determined by n-butyl amine desorption TGA analyses. The characterization results for mother zeolites and catalysts are given in Table 4.2 and Table 4.3, respectively.

The surface area of the support is very important for an effective iron dispersion in the catalysts. Supports with high surface areas generally provide a better dispersion and consequently results in higher catalytic activity. All zeolite samples used in the study have displayed the N_2 adsorption/desorption isotherms which were typical of

microporous materials. As seen in Table 4.2, they have the BET Surface Area (m^2/g) in a decreasing magnitude as Zeolite Y > Beta > Mordenite > ZSM5 > Ferrierite. Zeolite Y gave the highest surface area, due to its larger pore dimensions. Similarly, Beta zeolite which also belongs to 12-MR zeolite family had the second largest surface area. On the other hand, ZSM-5 and Ferrierite, with smaller pore channel dimensions (10-MR) and Mordenite possessing a pseudo one-dimensional pore system, displayed lower surface areas. A similar trend was observed in pore volumes of zeolites which were in decreasing sequence of: Zeolite Y > Beta > Mordenite ≥ ZSM5 > Ferrierite.

Table 4.2 : The textural properties of the mother zeolites.

Zeolite	Beta	ZSM5	Ferrierite	Mordenite	Y (SAR:5)	Y (SAR:80)
BET Surface Area (m^2/g)	675.8	447.9	362.8	550.7	869.4	898.5
External Surface Area (m^2/g)	200.1	90.74	80.25	151.8	119.5	290.5
Micropore Surface Area (m^2/g)	475.8	357.1	282.6	398.8	749.9	608.0
Micropore volume (ml/g)	0.192	0.159	0.110	0.160	0.290	0.248
Silica Alumina Ratio (-)	38	280	20	20	5	80

The iron loadings of the catalysts were measured by ICP technique, and determined to be 17.5%, 17.6%, 16.4%, 16.3%, 16.4% and 15.5% for SFeB, SFeZ, SFeF, SFeM, SFeY5and SFeY80, respectively. Iron loading of the zeolite supported catalysts were around 16.5 wt. %, within the ± 1% range. Therefore, the catalysts have similar average iron contents of 16.5 wt. %, with a deviation less than ± 1%.

High surface areas were measured for all of the synthesized zeolite supported catalysts, being above 275 m^2/g, while the base iron (BFe) catalyst had a poor surface area of 39.0 m^2/g, as expected. As seen in the table, the surface area of the synthesized catalysts followed the order of SFeB (500 m^2/g) > SFeM (456 m^2/g) > SFeY80 (432m^2/g) > SFeY5 (422m^2/g) > SFeZ (292 m^2/g) > SFeF (275 m^2/g) > BFe (39 m^2/g). As for the micropore volume, a slightly different pattern was observed, SFeB exhibited the largest and BFe exhibited the smallest volume.

Table 4.3: The composition and textural properties of catalysts.

Catalyst	SFeB	SFeZ	SFeF	SFeM	SFeY5	SFeY80	BFe
BET Surface Area (m^2/g)	499.9	292.4	274.7	455.7	421.8	432.3	39.0
External Surface Area (m^2/g)	157.1	95.83	60.58	102.9	127.9	146.5	39.0
Micropore Surface Area (m^2/g)	342.8	196.6	214.1	246.8	293.9	285.8	0.0
Micropore volume (ml/g)	0.137	0.089	0.083	0.113	0.1201	0.124	0.00
Metal crystallite size (nm)	20.3	25.3	23.3	19.7	10.9	25.6	21.3
Iron loading (wt. %)	17.5	17.55	16.4	16.3	16.4	15.5	100

Comparing data in Table 4.2 and Table 4.3 reveals a considerably decrease both in the surface area and micropore volume of the support zeolites upon loading of iron. On average, the surface area and pore volume of the catalysts were decreased in the range of 26-52% and 25-59%, respectively. This suggests the clogging of support pores by iron species within the pore channels or at the pore mouths that makes them less accessible for nitrogen adsorption. This effect was more pronounced for Y zeolites, with a decrease of 52%, 59% for surface area and pore volume, respectively. The greater difference seen for Zeolite Y may be due to its one dimensional pore system and hydrophilicity nature. In the case of one-dimensional pore structure (Y-zeolite), the blockage of the reactant access occurs easily because the whole channel becomes inactive due to the pore plugging of both ends. Besides, because of its hydrophilicity, during impregnation procedure, the iron solution can more readily diffuses into the zeolite pores and iron can deposit inside the zeolite channels. Consuquently, a substantially decreases in surface area and the micropore volume of the zeolite were observed.

On the other hand, the differences observed between external surface areas of the zeolites after iron loading were generally quite smaller in comparison with differences seen in their total surface areas. Upon iron loading, the external surface areas of beta, ferrierite, mordenite, Y(SAR:80) zeolites decreased. This may indicate that the metal was partially located at the external surface of the zeolite particle as a bulky mass. Conversely, the external surface areas of ZSM5 and Y (SAR5)

zeolites slightly increased. This may be attributed to the additive contribution of iron and zeolite to the external surface area. In this case, if the iron loading were further increased, it is predicted that, a decrease in the catalyst external surface areas would occur. This subject will be analyzed in more detail in Section 3.2.1.

XRD analyses of mother zeolites and synthesized catalysts are presented in Figure 4.1 and Figure 4.2, respectively. All XRD patterns display characteristic peaks and crystal structures of related zeolites. On the other hand, XRD patterns of the catalysts, Figure 4.2, indicate that the characteristic patterns of each zeolite structure still were maintained after the metal impregnation. The peak intensions, however, decreased upon iron loading due to accumulation of iron oxides and its dilution effect. XRD analyses also show an intense peak at $2\theta = 33.2^{o}$ and 35.7^{o}, which were attributed to the α-Fe_2O_3, (hematite) particles located on the external surfaces of the zeolites. From XRD analyses, the average crystallite size was calculated from the half width (HW) of the diffraction peak at $2\theta = 33.2$. This peak is a typical hematite phase peak with the highest intensity. The sizes of hematite crystallite of the catalysts calculated from XRD by Scherrer' equation were pretty similar, ranging between 20-25 nm. The results of calculation are given in Table 4.3.

As seen in Table 4.2, the silica to alumina molar ratios (SAR) of the zeolites widely varied, in a large range of 5-280. ZSM-5 has substantially higher SAR, while Zeolite Y5 has the lowest ratio. The chemical structure of the support is considered to be responsible for metal-support interactions which can influence the reducibility of the catalysts. Zeolites of higher alumina contents (i.e: ferrierite and mordenite) have higher cation exchange capabilities. In these catalysts, reduction of iron species bound to the exchange sites can hardly be completed. This situation could result in a decrease in the catalyst activity.

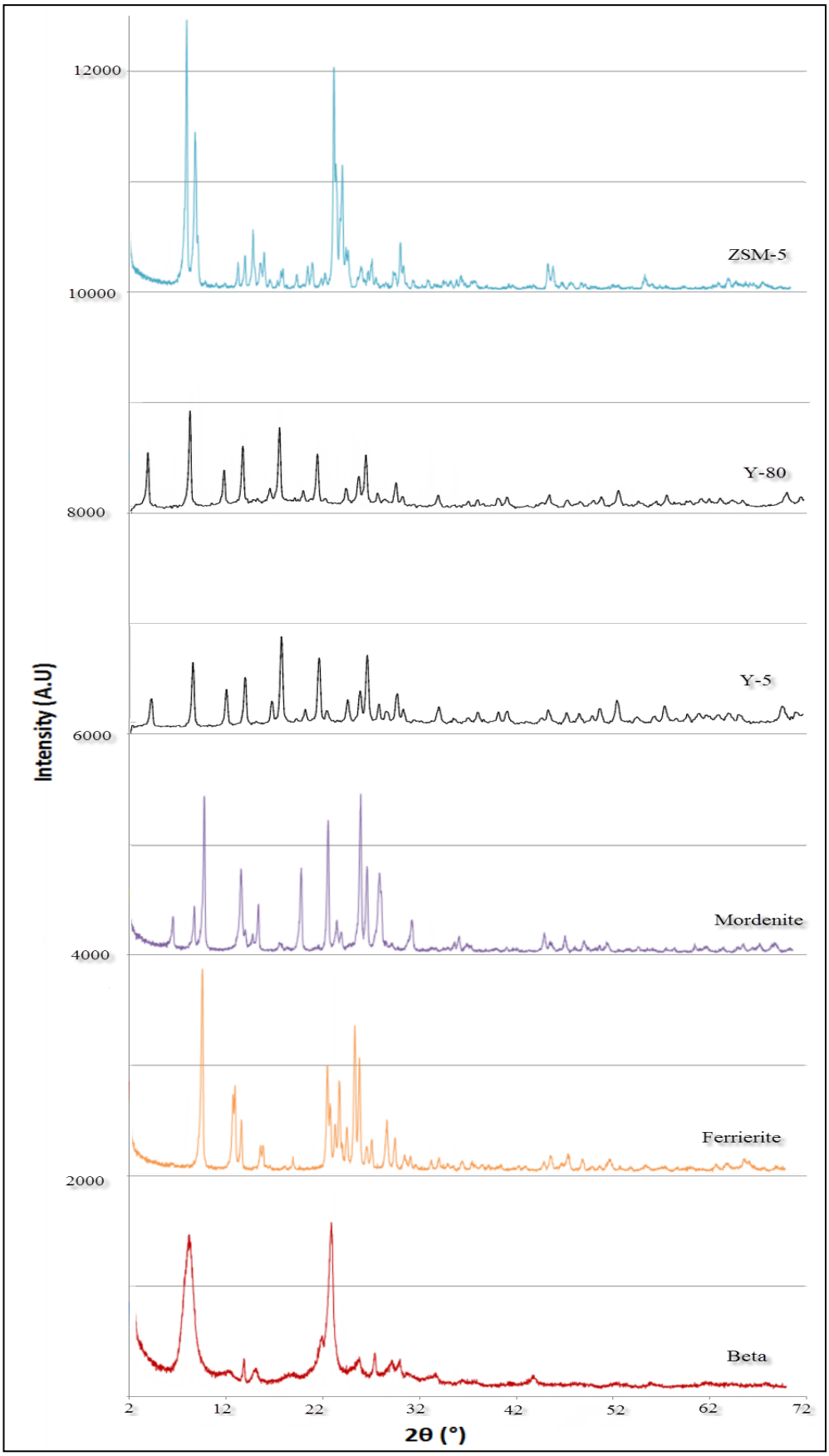

Figure 4.1 : X-ray diffraction patterns of mother zeolites.

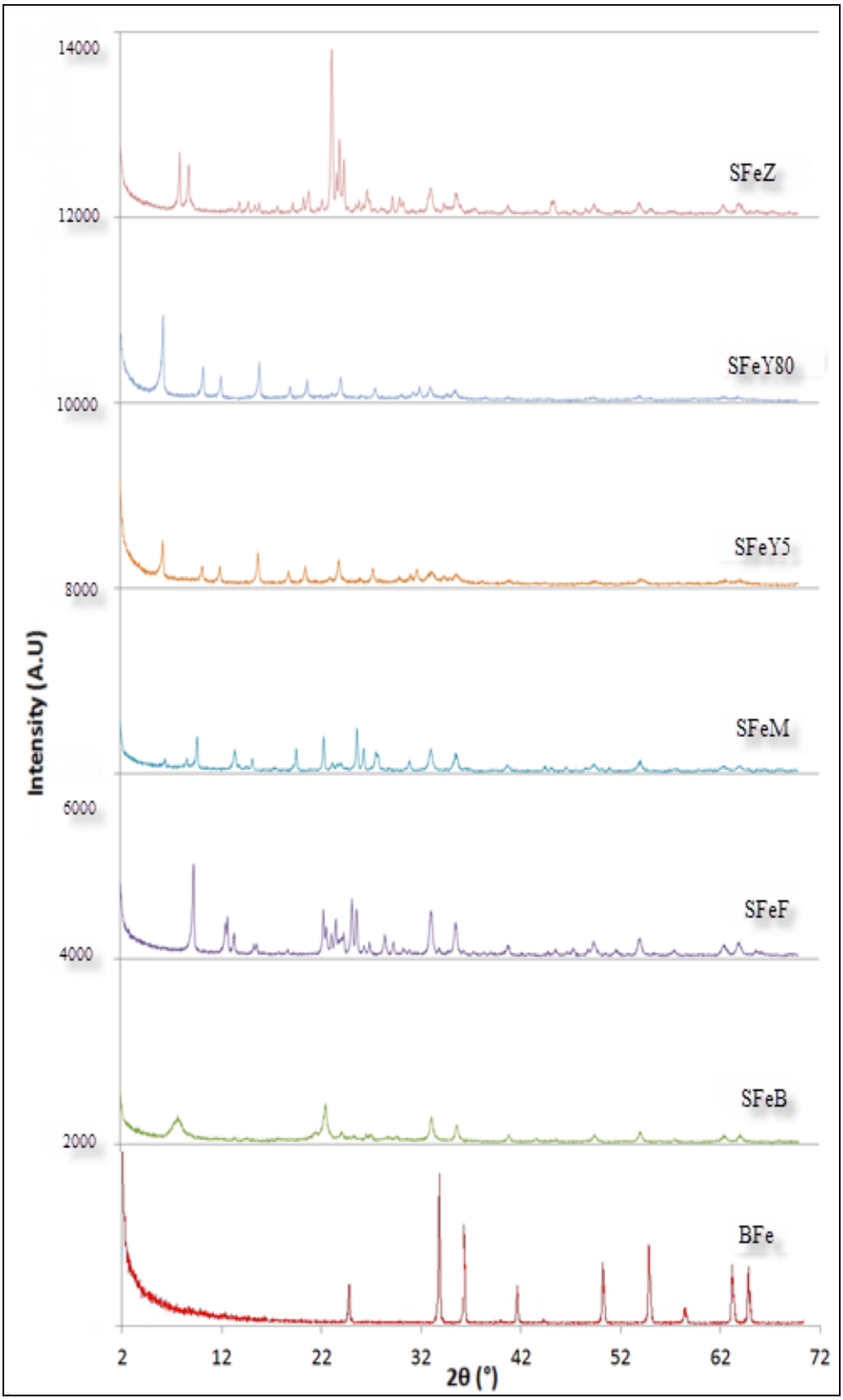

Figure 4.2 : X-ray diffraction patterns of calcined catalysts.

Catalysts were examined by n-butyl amine (n-BA) adsorption method to measure their acidity. This method can be used for measurements of zeolite acidity (Gao et al., 2004; Glosh and Curthoys; 1984). The method is based on the adsorption of n-BA on zeolite and then its desorption from zeolite in a TGA oven by evaporation under inert atmosphere (N_2) with a pre-determined temperature program. The loss in the sample weight below 373 K is attributed to humidity, while low temperature (i.e. 400 K– 500 K) and high temperature (i.e. 550 K – 675 K) losses are attributed to weak and strong acidity of the zeolite, respectively.

The results of catalyst TGA analyses are given in Table 4.4. Weight losses observed at low (400 K – 500 K) and high (550 K – 675 K) temperature ranges are related to desorption of n-butyl amine from the weak and strong (Bronsted) acid sides, respectively. The total acidity followed a decreasing order of SFeY5 > SFeB > SFeY80 > SFeF > SFeZ > SFeM. On the other hand, the numbers of strong acid sites (Bronsted acidity) of catalysts were decreased in sequence of SFeY5 > SFeF > SFeB > SFeM > SFeY80 > SFeZ, which generally fitted well to the silica to aluminum ratio in the zeolite. Strong acidities of catalyst prepared with zeolite Y samples, on the other hand, differ considerably as seen from the table. SFeY5 (Si/Al = 5) and SFeY80 (Si/Al=80) catalyst have 1.09 mmol/g and 0.25 mmol/g acidity, respectively.

Table 4.4 : Acidity of the zeolite supported catalysts.

Acidity (mmol n-BA/g catalyst)	**SFeB**	**SFeZ**	**SFeF**	**SFeM**	**SFeY5**	**SFeY80**
Weak Acidity (400–500 K)	0.52	0.37	0.06	0.13	0.49	0.74
Strong Acidity (550-675K)	0.52	0.25	0.60	0.48	1.09	0.25
Total Acidity	1.03	0.62	0.66	0.61	1.58	0.99

4.1.2 Fischer-Tropsch activities of catalysts

A series of tests were carried out to investigate the effect of zeolite type and the reaction temperature on the catalytic activities of the catalysts for FT synthesis reactions. Experiments were carried out at 3 different temperatures of 523 K, 538 K and 553 K. Operating pressure was fixed to and kept at 19 bar a for all experiments. The experimental conditions for FT activity tests are given at Table 4.5. Results are compiled in Table 4.6, Table 4.7 and Table 4.8.

Table 4.5 : Experimental conditions of zeolite-supported iron catalysts' FT activity tests.

Exp. Set	Zeolite Type	Temperature (K)	Pressure (bar a)
1	ZSM-5	523	19
2	ZSM-5	538	19
3	ZSM-5	553	19
4	Faujasite (SAR:5)	523	19
5	Faujasite (SAR:5)	538	19
6	Faujasite (SAR:5)	553	19
7	Faujasite (SAR:80)	523	19
8	Faujasite (SAR:80)	538	19
9	Faujasite (SAR:80)	553	19
10	Mordenite	523	19
11	Mordenite	538	19
12	Mordenite	553	19
13	Beta	523	19
14	Beta	538	19
15	Beta	553	19
16	Ferrierite	523	19
17	Ferrierite	538	19
18	Ferrierite	553	19
19	Base Iron	523	19
20	Base Iron	538	19
21	Base Iron	553	19
22	Blank Test (ZSM-5)	538	19

A blank test was carried out in order to distinguish possible the catalytic effect of zeolite support and stainless steel piping (reactor wall) etc. in the syngas converion reactions. In test, reactant gas introduced to reactor loaded with pure support (zeolites) and under the same FT synthesis conditions that applied for catalysts. Since the zeolites used in study are known to have no catalytic activity for reactant gas, this test was only applied for ZSM-5.

All synthesized zeolite–supported catalysts displayed a CO conversion ranging from 53% to 79% at 553 K. The base iron catalyst (BFe), the only unsupported catalyst, however, displayed a relatively poor performance with a CO conversion of 40%. Although the performances of the catalysts were widely different, these results indicate that presence of zeolite supports can considerably enhance the catalytic activities of catalysts due to their high surface areas. Zeolites also improved the hydrocarbon productivity of catalysts, likely due to the better dispersion of iron on zeolite supports and iron utilization.

As seen in Table 4.6 - Table 4.8, the CO conversions of catalysts with different zeolite supports clearly indicated that catalytic activity was strongly dependent on the type of zeolite. The CO conversions of the catalysts were determined to be in the following order: SFeB > SFeZ >SFeF > SFeY5 > SFeM > SFeY80. The highest reactant (H_2, CO) conversions were obtained with Beta supported catalysts at all temperatures. Conversion increased with surface area of the support for SFeB, SFeZ, SFeF and BFe catalysts. Mordenite and Y zeolites (SAR: 5 and SAR: 80) however, did not follow this trend. This may be due to one dimensional pore structure of these zeolites, pore channels of which are easily blocked by iron deposited on both ends of pore channels. Therefore, the contribution of iron deposited inside the pore channels to catalytic activities of catalysts remained limited.

Tests were carried out at reaction temperatures in the range of 523 K - 553 K in order to observe the effect of the reaction temperature on the catalytic activities of the catalysts. Results shown in Figure 4.3 and Figure 4.4 indicated that conversions were strongly and positively affected by reaction temperature. For example, rising the reaction temperature by a 30 K pushed the CO conversion from 32.1% to 79.2% for SFeB catalyst. A similar trend was observed for all catalysts. Increasing temperature from 523K to 553K resulted in 40-59% and 36-66%, improvement in the CO and H_2 conversions, respectively.

Table 4.6 : The activity of the zeolite-supported iron catalysts in the FT synthesis process at T = 553K (P=19 bara, GHSV = 750 h^{-1}, H_2/CO = 2).

Catalyst	SFeB	SFeZ	SFeF	SFeM	SFeY5	SFeY80	BFe
CO conversion (%)	79.2	72.4	58.7	53.1	56.2	30.4	39.6
H_2 conversion (%)	78.8	61.7	58.6	51.1	47.4	29.9	33.4
CO_2 selectivity (%)	2.4	9.0	6.2	4.6	4.0	7.1	20.5
Productivity							
Hydrocarbon (g/h/g-Fe)	0.83	0.50	0.58	0.49	0.45	0.39	0.03
Yield							
Hydrocarbon (g/Nm^3-syngas converted)	206.3	212.5	197.7	206.0	225.5	197.7	187.0
Hydrocarbon (g/Nm^3-syngas fed)	148.0	118.9	105.4	96.9	103.2	54.1	58.4
Gasoline (g/Nm^3-syngas converted)	124.3	157.0	89.3	121.0	154.2	100.2	76.6
Gasoline (g/Nm^3-syngas fed)	89.2	87.9	47.6	56.9	70.6	27.4	23.9
Rate of syngas converted, mmol (H_2+CO)/g-cat/h	179.8	111.9	132.5	107.6	89.7	88.3	8.2
Product Composition (wt.%)							
C_1	8.81	7.90	20.90	9.98	6.42	14.67	15.58
C_2-C_4	13.08	14.00	24.12	19.15	15.82	31.54	35.94
C_5-C_{11}	60.23	73.90	45.19	58.73	68.40	50.68	40.96
C_{12}-C_{18}	17.76	4.00	9.62	9.75	9.24	2.91	6.83
C_{19}+	0.13	0.30	0.17	2.40	0.12	0.20	0.69
Olefin ratio (mol%) (C_2-C_4)	10.3	6.7	17.8	31.4	7.1	28.0	37.2

Table 4.7 : The activity of the zeolite-supported iron catalysts in the FT synthesis process at T = 538K (P=19 bara, GHSV = 750 h^{-1}, $H_2/CO = 2$).

Catalyst	SFeB	SFeZ	SFeF	SFeM	SFeY5	SFeY80	BFe
CO conversion (%)	51.2	43.8	32.4	37.9	21.91	19.37	31.98
H_2 conversion (%)	56.0	46.6	35.5	33.9	21.54	19.61	27.56
CO_2 selectivity (%)	4.4	5.5	2.8	3.3	5.7	5.5	16.72
Productivity							
Hydrocarbon (g/h/g-Fe)	0.52	0.33	0.44	0.36	0.17	0.25	0.029
Yield							
Hydrocarbon (g/Nm^3-syngas converted)	189.5	190.8	190.8	218.9	200.8	197.3	193.2
Hydrocarbon (g/Nm^3-syngas fed)	93.8	78.5	79.2	70.1	39.5	35.0	49.4
Gasoline (g/Nm^3-syngas converted)	79.1	125.4	77.8	121.5	87.7	84.7	89.5
Gasoline (g/Nm^3-syngas fed)	39.1	51.6	32.3	38.9	17.3	15.0	22.9
Rate of syngas converted, mmol (H_2+CO)/g-cat/h	124.0	78.2	103.1	73.3	38.6	57.3	6.7
Product Composition (wt.%)							
C_1	21.3	10.9	23.7	11.7	14.8	15.1	14.1
C_2-C_4	32.2	18.4	25.7	21.2	31.0	30.5	29.0
C_5-C_{11}	41.8	65.7	40.8	55.5	43.7	42.9	46.3
C_{12}-C_{18}	4.6	4.9	9.6	9.3	9.8	11.0	10.0
C_{19}+	0.1	0.1	0.1	2.3	0.8	0.4	0.6
Olefin ratio (mol%) (C_2-C_4)	18.3	17.5	26.4	40.8	26.3	31.0	38.5

Table 4.8 : The activity of the zeolite-supported iron catalysts in the FT synthesis process at T = 523K (P=19 bara, GHSV = 750 h^{-1}, $H_2/CO = 2$).

Catalyst	SFeB	SFeZ	SFeF	SFeM	SFeY5	SFeY80	BFe
CO conversion (%)	32.13	33.04	26.58	22.81	14.89	12.78	23.6
H_2 conversion (%)	35.04	33.08	27.10	17.39	14.80	11.60	21.5
CO_2 selectivity (%)	1.78	3.18	2.04	1.80	3.67	3.84	17.3
Productivity							
Hydrocarbon (g/h/g-Fe)	0.338	0.258	0.276	0.219	0.120	0.169	0.02
Yield							
Hydrocarbon (g/Nm^3-syngas converted)	195.0	203.7	203.7	245.8	203.6	215.77	185.52
Hydrocarbon (g/Nm^3-syngas fed)	60.4	61.2	49.9	42.9	27.5	23.5	36.3
Gasoline (g/Nm^3-syngas converted)	78.2	114.9	83.4	134.65	83.21	79.30	84.50
Gasoline (g/Nm^3-syngas fed)	24.2	34.5	20.4	23.5	11.2	8.6	16.5
Rate of syngas converted, mmol (H_2+CO)/g-cat/h	77.6	56.7	60.8	39.9	26.4	35.2	5.1
Product Composition (wt.%)							
C_1	20.23	11.90	21.72	13.30	13.69	16.79	17.08
C_2-C_4	30.21	22.80	21.56	21.65	25.55	28.95	28.70
C_5-C_{11}	40.10	56.41	40.93	54.78	40.87	36.75	45.55
C_{12}-C_{18}	9.40	8.40	15.36	8.25	16.51	12.75	8.20
C_{19}+	0.07	0.49	0.44	2.03	3.38	4.75	0.46
Olefin ratio (mol%) (C_2-C_4)	22.6	49.1	31.2	42.7	41.0	37.0	35.7

The yields and hydrocarbon productivity calculated for the catalysts are also shown in Table 4.6 - Table 4.8. At 553 K, zeolite supported catalysts exhibited productivity changed between 0.39 and 0.83 g/h/g-Fe. The highest productivity was obtained from SFeB catalyst which also had the highest BET surface area and micropore volume. Similar to activity, productivity of catalysts could not be correlated with BET surface area and pore volume. High productivity of SFeB catalyst could be a result of the combining effect of high activity and low CO_2 selectivity. The higher accessibility to the catalytic sites due to large pore diameter and three dimensional pore system of the Beta zeolite support might contribute to high activity of this catalyst. On the other hand, as may be expected, the base iron catalyst showed a very poor productivity since a significant amount of iron in the catalyst did not effectively take place in the reaction due to the restricted accessibility originating from lack of support and resulting low dispersion. As will be discussed in the following section, the water gas shift activity of this catalyst was much higher than that of others. This also could adversely affect its productivity.

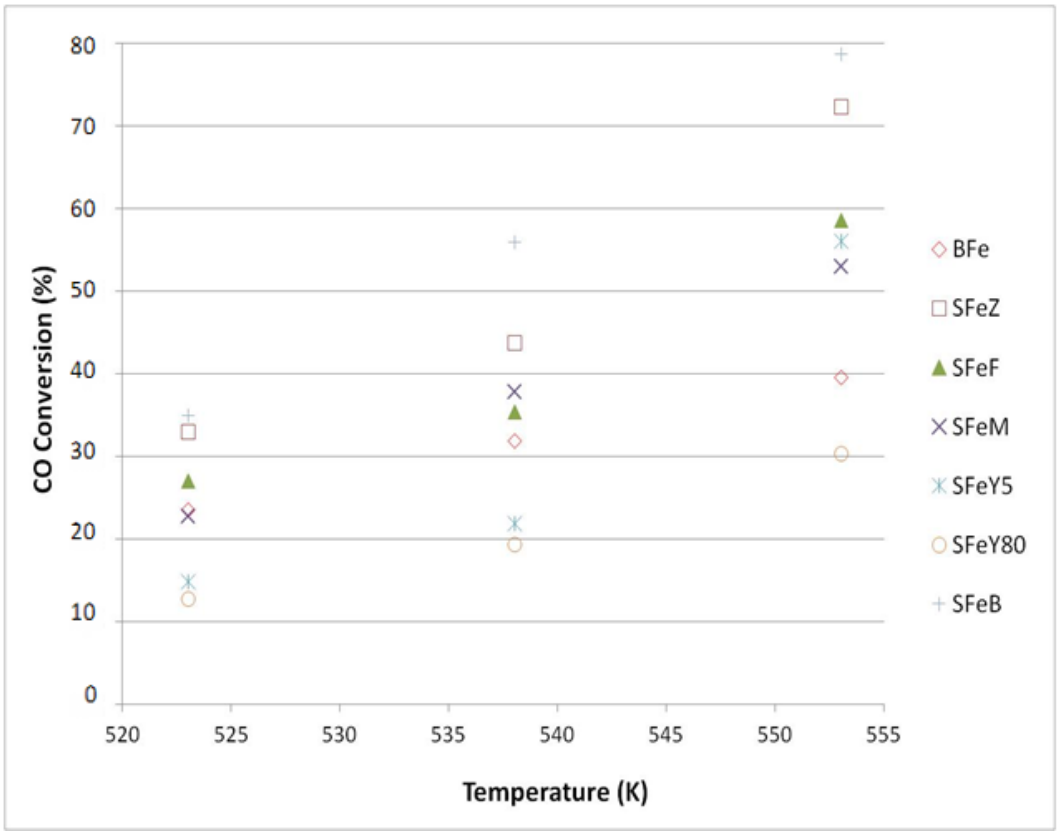

Figure 4.3 : Changing of CO conversion performance of catalysts with type of support and reaction temperature.

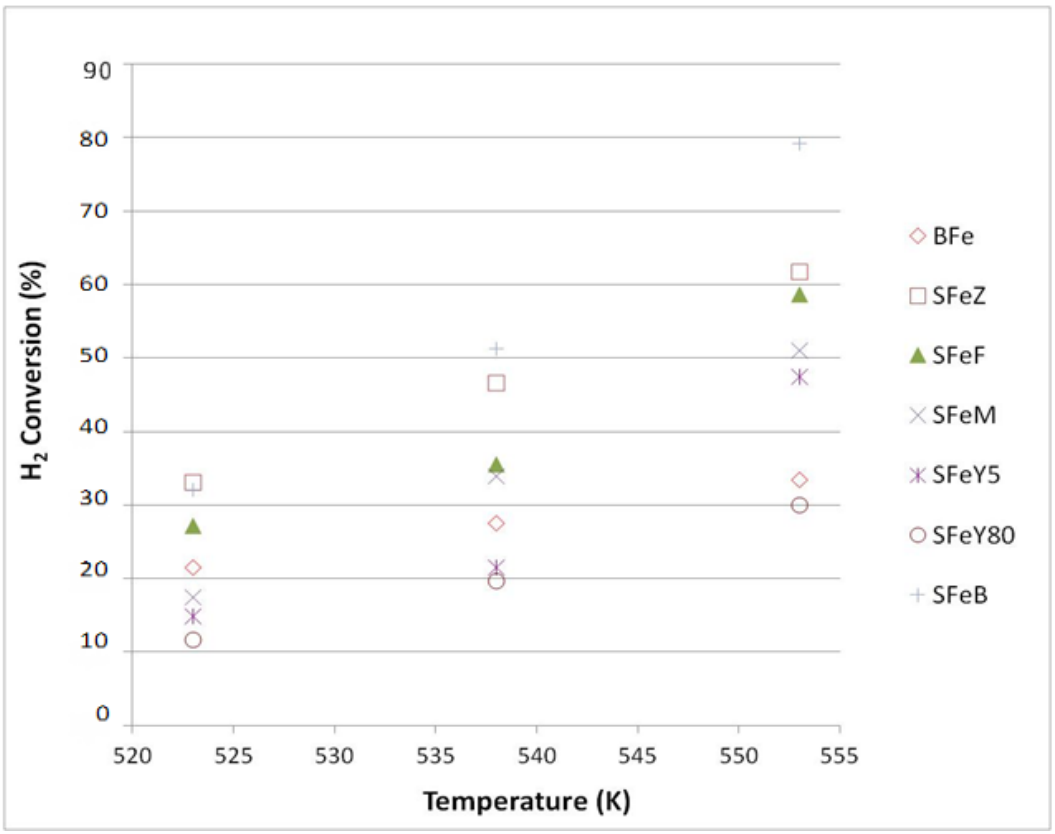

Figure 4.4 : Changing of H_2 conversion performance of catalysts with type of support and reaction temperature.

4.1.3 Water gas shift reaction

It is known that FT reactions on iron catalyst is accompanied by the water gas shift (WGS) reaction. In this reaction, CO reacts with water which is generated during FT synthesis and produces CO_2 and hydrogen. In the presence of WGS reaction activity, the effective H_2/CO ratio increases. This slightly reduces the olefin selectivity and the deactivation rate of the catalyst. The WGS reaction consumes CO, thus the amount of carbon available for hydrocarbon synthesis decreases, which lead the lower hydrocarbon yields in case of feed streams with high H_2 to CO ratios. A typical process of this kind is FT process in which syngas produced from natural gas is used as feedstock. One measure of the WGS activity is the CO_2 selectivity (S_{CO2}) which is defined as:

$$S_{CO2} = \frac{CO_2 \ \mathrm{Pr}oductionRate}{CO \ Consumption Rate} x100 \qquad \textbf{(4.1)}$$

The CO_2 selectivity of the synthesized catalysts are presented in Table 4.6 - Table 4.8 and Figure 4.5. The WGS activities of the zeolite supported catalysts were significantly lower than that of the base iron (BFe). At 553 K, the CO_2 selectivity of the BFe was determined to be 20.5%. The CO_2 selectivity of zeolite supported catalysts varied in the range of 2.4 – 9.0 %, indicating an obvious and higher WGS activity of base iron in this respect, with a 2-5 times higher selectivity. These results suggested that, presence of zeolite in the catalyst formulations could suppress the WGS activity of the iron.

In Figure 4.5, the CO_2 selectivity of catalysts are given as a function of temperature. As seen in the figure, although there are some deviations, the CO_2 selectivity generally increases with increasing temperature for the major of the catalysts. These results may show that WGS reaction rate increases faster than FT reactions.

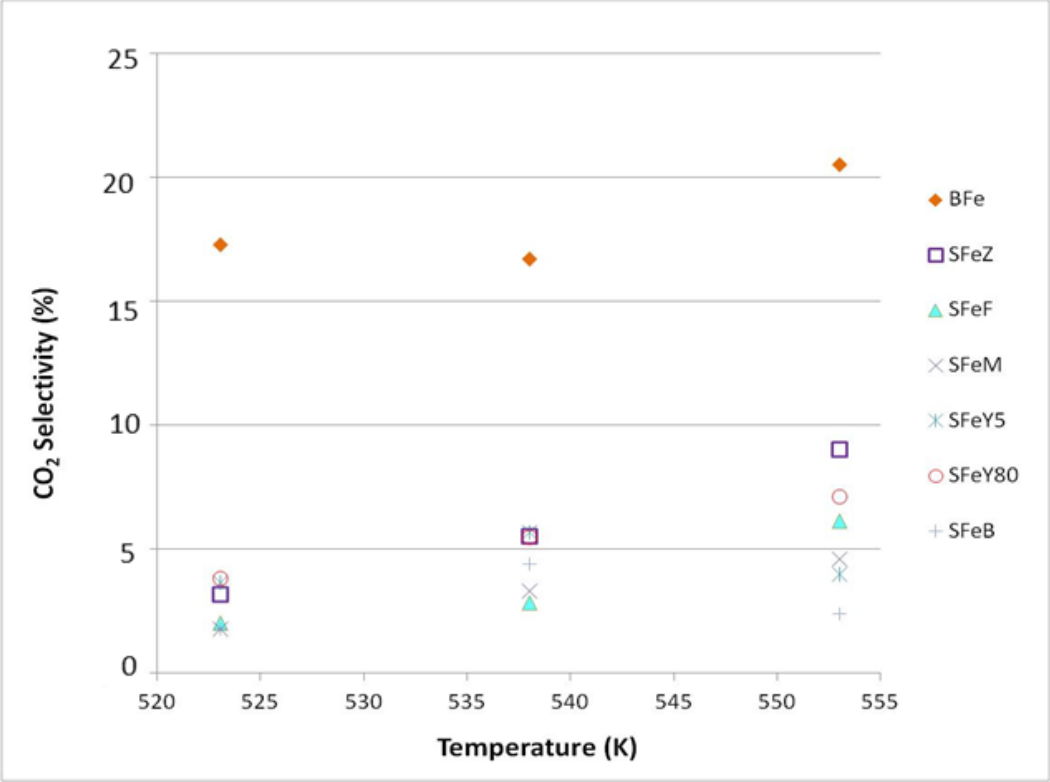

Figure 4.5: Effect of support type and temperature on CO_2 conversion of catalysts.

Suppression of WGS reaction might be due to the higher diffusion rate of hydrogen into the zeolite pores. Hydrogen readily diffuses into the pores of the zeolite with higher rates than CO, which has higher molecular diameter. So, the high hydrogen concentration in zeolite pores might shift the reaction direction, namely to the reverse WGS reaction in presence of iron.

It is well known that alkali promoters, particularly K, can enhance the WGS activity of iron based catalysts (Bukur et al., 1990; Wan et al., 2008). On the other hand, zeolite supports have an acidic nature. This might be a reason for the suppression of the WGS reaction, i.e: decreasing CO_2 selectivity, in the FT synthesis by zeolite-supported catalysts. Comparing acidity (i.e: SAR) of the zeolites used as support (Table 4.2) and the CO_2 selectivity of the catalysts obtained from FT synthesis at 553K (Table 4.6) revealed that, in general, the CO_2 selectivity tended to increase with decreasing acidity of supports as shown below. The only exceptions were Beta-supported catalyst (SFeB) that did not followed the general trend seen in relation between the support acidity and catalyst CO_2 selectivity. The zeolite acidity and catalysts' CO_2 selectivity are compared below:

Zeolite acidity:

ZSM5 (Z) (280) < ZeolitevY80 (Y80) (80) < **Beta (B) (38**) < Ferrierite (F) (20) = Mordenite (M) (20) < ZeoliteY5 (Y5) (5)

Catalyst CO_2 selectivity (553K):

SFeZ (9) > SFeY80 (7.4) > SFeF (6.15) > SFeM (4.62) >SFeY5 (4) > **SFeB (2.4)**

These findings seem to supported our comments that the zeolite acidity likely have negative impact on the WGS reaction and favor reverse WGS reaction.

4.1.4 Hydrocarbon selectivity of catalysts

The gaseous and liquid products obtained from the catalyst activity tests were analyzed to determine their compositions. The liquid and waxy products were collected in two traps, a hot trap at 553 K and a cold trap at 278 K, respectively. However, no waxy product was accumulated in the hot trap, which just placed after the reactor, during the tests. The whole synthesized liquid hydrocarbon products and the produced water were collected in the cold trap. Some typical liquid products obtained from FT synthesis by catalysts are shown in Figure 4.6. The results of the catalyst activity tests are presented in Table 4.6 - Table 4.8**.** Inspection of these data indicated that zeolite presence in the catalysts could considerably influence the product selectivity.

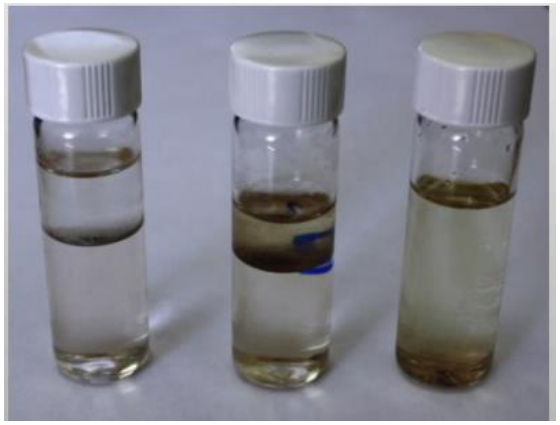

Figure 4.6 : Typical liquid phase products obtained from FT synthesis by zeolite-supported iron catalysts.

The hydrocarbon distribution of the liquid phase products, collected in the cold trap, shown in Figure 4.7, indicated that the C5-C11 range hidrocarbons constituded the major portion of the liquid FT products obtained by the SFeB, SFeZ, SFeF, SFeM, SFeY5and SFeY80 catalysts. The average ratio of C5-C11 range hydrocarbons in liquid products produced by these catalysts ranged from 57.2% to 92.3%. The ratio of C5-C11 hydrocarbons, however, was affected by operating temperature and increased as temperature increased. The highest ratios were obtained from the SFeZ catalyst, being 92.3%, 90.3 % and 77.7% at 553K, 538K and 523K, respectively. Therefore, these results suggested that, upgrading of the raw liquid products from FT synthesis by zeolite-supported catalysts, especiallay SFeZ catalyst, would no longer be needed to produce gasoline due to the low selectivity of these catalyst towards the long chained HCs. The remaining zeolite-supported catalysts, however, produced a considerable amount of diesel range (C12-C18) hydrocarbons, on average of 20%.

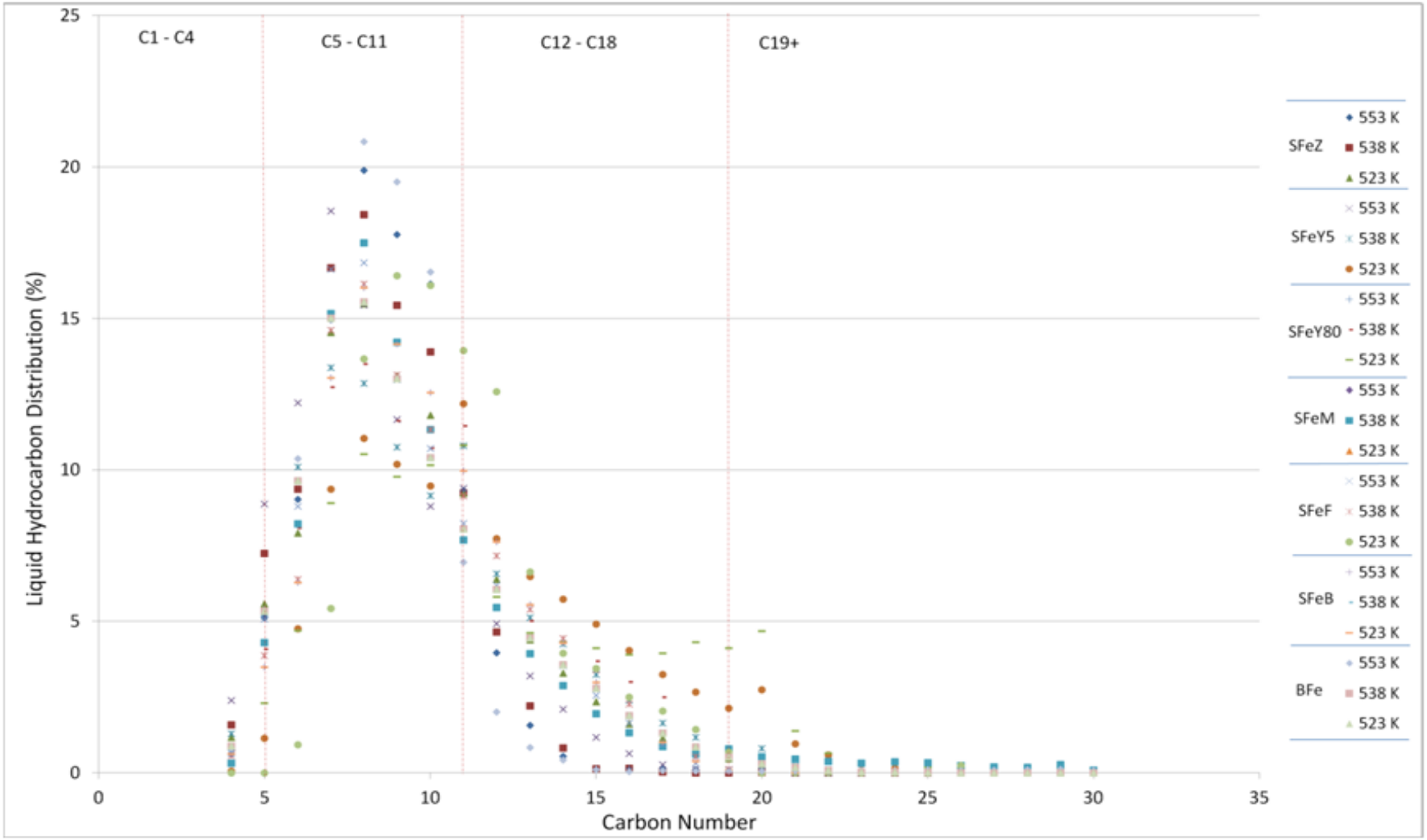

Figure 4.7 : Composition of liquid phase products obtained by zeolite supported catalysts (cold trap) (P=19 bara, GHSV=750 h^{-1}, H_2/CO=2:1).

Analysis results of FT liquid products are separately presented for each catalyst in Appendix A. Generally, there is a shift through higher hydrocarbons with increasing temperature. The effect of temperature on product selectivity will be discussed at the end of this section.

Hydrocarbon product distributions of all synthesized catalysts are given in Figure 4.8. As seen in the figure, the base iron catalyst (BFe) displayed a higher selectivity towards light hydrocarbons (C1-C4) in comparison with other catalysts. Zeolite supported catalysts except the ferrierite supported catalyst (SFeF) narrowed the spectrum of the products by reducing the amount of light hydrocarbon fractions and maximizing the gasoline and diesel range hydrocarbons, especially at 553 K. These catalysts, due to the acidic character of zeolite supports, could catalyze oligomerization of the low molecular weight olefins. On the other hand, heavy hydrocarbon production in FT processes using zeolite containing catalysts could be substantially hindered by the shape selectivity nature of the zeolite. Similarly, zeolites with their acidic nature might catalyze the hydrocracking reactions, so that the heavy hydrocarbons formed during the process could be converted into lighter hydrocarbons. Furthermore lack of alkali promoters in the catalyst formulation has also contributed to resulting low heavy hydrocarbon selectivity.

ZSM-5 supported catalyst (SFeZ) had a considerably better selectivity towards gasoline range hydrocarbons (C5-C11) than the other catalysts. At 553 K, the selectivity of SFeZ towards this hydrocarbons fraction was 74%, while the selectivity of the base iron catalyst (BFe) towards the same fraction was about 41%.

So, SFeZ catalysts, with its high gasoline selectivity and reasonable activity, provides opportunity to design a gasoline producing FT process without product up-grading section. The ZSM-5 zeolite, also being an industrial FCC catalyst, with its high SAR ratio and moderate cracking activity may be the source of this positive results.

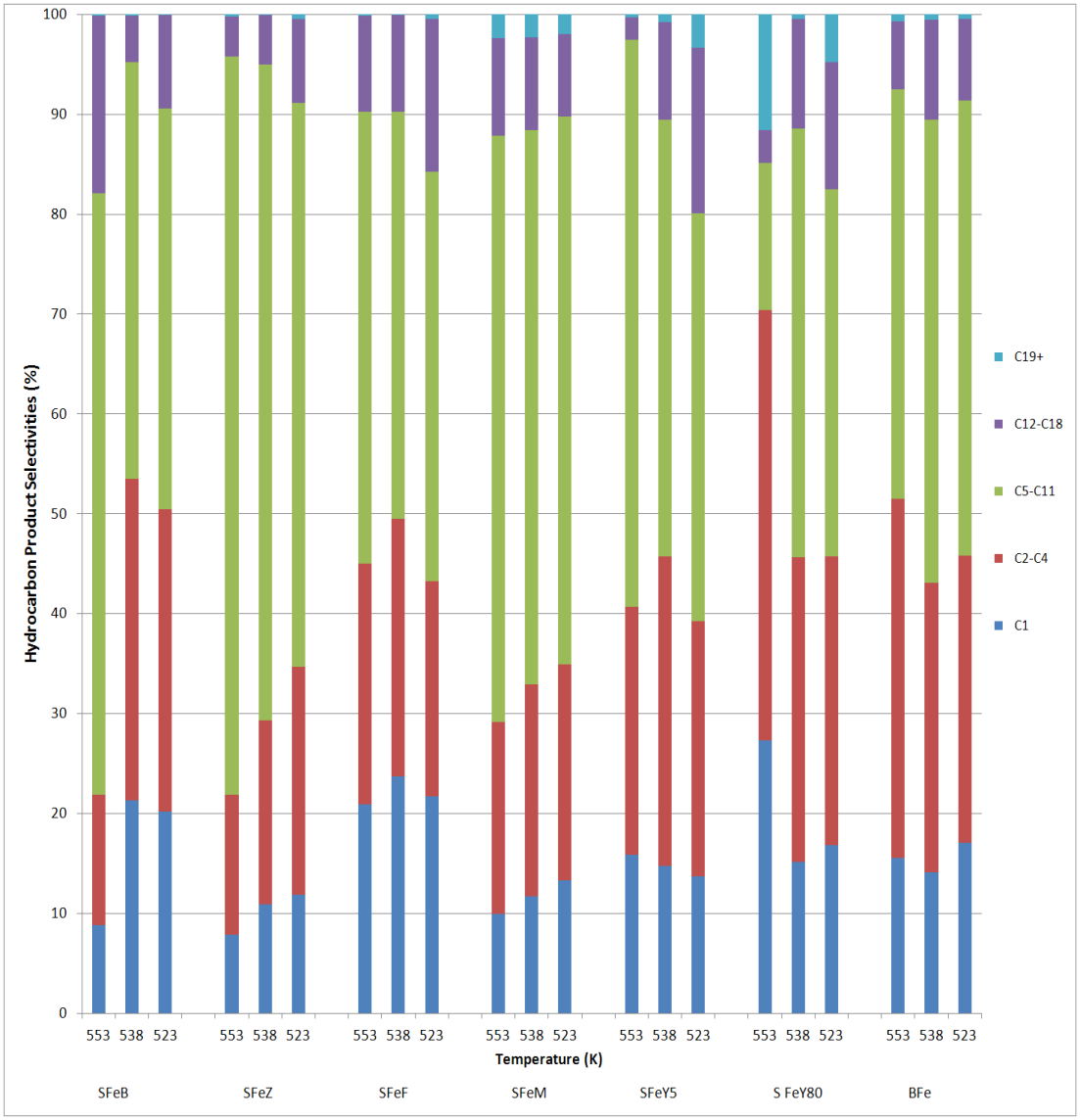

Figure 4.8 : Hydrocarbon distribution of FT synthesis products obtained by zeolite-supported iron catalysts (P=19 bara, GHSV=750 h^{-1}, H_2/CO=2:1).

Of the zeolite-supported catalysts, ferrierite supported-catalyst (SFeF) had the lowest selectivity towards the liquid fuel range hydrocarbons and the highest selectivity towards un-wanted light hydrocarbons. Product distribution obtained by SFeF is similar to that obtained from the unsupported base iron catalyst (BFe). However, experimental findings indicated that using the ferrierite support remarkably enhanced the activity and the productivity of the iron catalyst. Low selectivity of the SFeF catalyst may be due to the small pore dimensions of the ferrierite. Amongst the zeolites used in the study, this zeolite has the smallest pore dimensions, with 4.2 x 5.4 Å (10 membered ring) and 3.5 x 4.8 Å (8 membered ring) channels. To maximize the utilization of the zeolite support via shape selectivity and zeolite-metal interaction, some portion of the active metal (Fe) needs to be located into the pores

of the zeolite. Since ferrierite has small pore sizes, in SFeF catalyst iron may not penetrate inside the zeolite channels. Moreover, the diffusion and the reaction of HC products in the channels would be slower for this zeolite. Consequently, it seemed that the zeolite utilization and zeolite – active metal (support-Fe) interaction remained limited for this zeolite.

The methane selectivity of zeolite-supported catalysts varied between 6.4% -20.9% at 553 K BFe exhibited a 15.6 % methane selectivity, which was the second highest methane selectivity among synthesized catalysts while SFeF had the maximum of 20.9%. The ferrierite and beta-supported catalyst (SFeF, SFeB), which had the highest strong acidities after SFeY5 displayed the highest selectivity towards methane. Methane selectivity may be related to the strong acidity of the catalysts which could strongly increase their hydrocracking activity.

Both of the zeolite Y-supported catalysts (SFeY5 and SFeY80) exhibited low selectivity towards gasoline and diesel range HCs, especially at low temperatures. Zeolite Y catalysts suffer from few inherent disadvantages. They tend to coke too readily. They are also strongly hydrophilic (i.e. oleofobic) tending to repel HCs, which we seek to catalytically convert. Because of the deactivation of the zeolitic component of the bi-functional catalysts induced by coking and/or very limited diffusion of the produced hydrocarbons into the zeolite pores, the selectivity of these catalysts generally were low, resembling to the unsupported catalyst (BFe).

The percentages of C2-C4 range gas olefins obtained from activity tests of catalysts are compared in Figure 4.9, as a function of temperature. The base iron (BFe) catalyst produced about 37% olefins at 553 K, which was considerably higher than that produced by zeolite-supported catalysts. In other words, the zeolite containing catalysts synthesized in this study remarkably reduced the formation of the olefins in the gas phase. The amount of olefins decreased with increase in temperature, due to a better activity displayed by the zeolites at high temperatures. As previously mentioned, decrease in gas phase olefins, that might be originated from the oligomerization by zeolite, favors the production of C5-C11. The lower light HC selectivity of SFeZ, SFeB, SFeY5 in comparison with others may be due to the higher olefin oligomerization activity at 553 K. As seen from Table 4.6 - Table 4.8, olefin selectivities of these catalysts were very low at 553K. As reaction temperature

decreased the olefin selectivity of these catalysts increased and thereby their selectivity gradually approached that of others.

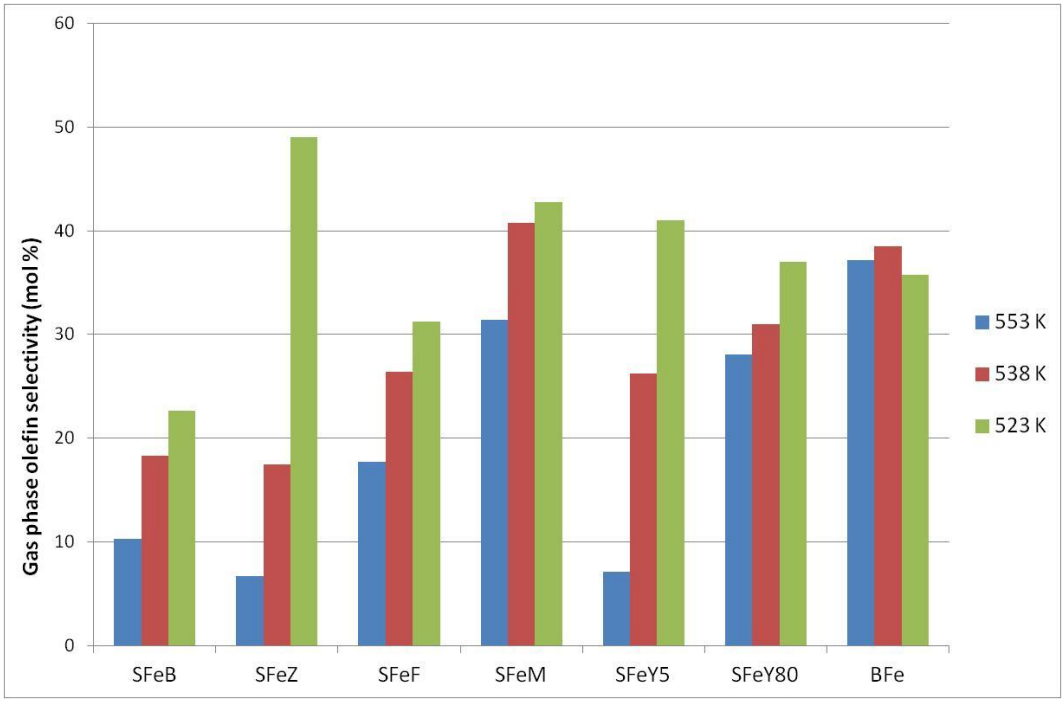

Figure 4.9 : Variation of olefin selectivity in the gas phase products from FT synthesis by zeolite-supported iron catalysts with reaction temperature.

It is known that, for conventional FT catalysts an increase in operating temperature generally results in a shift in selectivity towards lower carbon number hydrocarbons and hydrogenated products (Dry, 2002). This shift is in line with thermodynamic expectations and the relative stability of the products. Zeolite catalytic activity also increases with increasing temperature. As previously mentioned, zeolite activity contribute to reducing of average chain length by its hydrocracking activity. However, on the other hand, oligomerization of light olefins, realized by zeolite activity, results in an increase in the average chain length. Since the olefin selectivity of base iron catalyst for C1-C4 HC is high, being around 40%, this effect may become prominent depending on the rate of oligomerizing activity of zeolitic component of bi-functional catalysts. The light olefin selectivity of zeolite containing catalysts are quite lower than that of the BFe catalyst, indicating high oligomerizing activity of bi-functional catalysts. So the effect of reaction temperature on product selectivity is complex phenomenon, determined by collective effect of competing reactions.

4.2 Low acidity ZSM-5 Supported Iron Catalysts For Fischer-Tropsch Synthesis

This section covers experimental studies carried out on the synthesis of iron based bi-functional FT catalysts by using low acidity ZSM-5 and de-aluminated ZSM-5 as supports and their catalytic performances in the FT process. As mentioned in section 4.1., this zeolite gave the highest selectivity towards gasoline range hydrocarbons among the synthesized catalysts with reasonable activity.

The ZSM-5 type zeolite with silica to alumina ratio (SAR) of 280 was used in the studies because of its low acidity. The purpose for choosing this type of zeolite was to take advantage of its shape selectivity while suppressing acid-catalyzed reactions like hydrocracking originating from its acidic nature. It was aimed to reduce the light hydrocarbon selectivity and to enhance the stability of the catalysts. In order to decrease role of the external surface which might favor hydrocracking reactions and to improve the internal surface utilization, the zeolite was selectively de-aluminated further and so resulting in an decrease in the number of active sites for hydrocracking.

Iron was used in the synthesis of the catalysts in order to take the advantage of its low methane and high olefin selectivity. The target was to maximize the gasoline yield in the FT process through synthesizing a stable and effective zeolite supported catalyst. The two catalyst preparation routes, namely impregnation and physical mixture, were compared with respect to their impact on the activity, selectivity and hydrocarbon yields of the synthesized catalysts.

Zeolite-supported and de-aluminated zeolite –supported catalysts were synthesized by using incipient wetness impregnation method and hybrid catalyst was prepared by physical admixing of ZSM-5 and the base iron.

In the study, in total 7 different catalysts were prepared and tested for their performances in the FT synthesis process. Of them, three were ZSM-5–supported, one was de-aluminated ZMS-5-supported, one was hybrid (physical admixing), one was conventional (promoted and with no support) and one was base iron. The iron ratio of the supported catalysts was also studied. ZSM-5 supported catalysts with 4 wt. %, 9 wt. % and 18 wt. %.iron were synthesized and tested. The ZSM-5-supported

catalysts, de-aluminated ZSM-5-supported catalysts and hybrid catalyst were designated as SFeZX, SFeDZX and HFeZX, respectively, where X is for the iron wt.% in the catalyst. The base iron catalyst and the promoted iron based catalyst (conventional catalyst) were also prepared and denoted as BFe and CFe, respectively, in the text. The prepared catalysts are compiled in Table 4.9.

Table 4.9 : Bi-functional iron-based FT catalysts prepared by using low acidity zeolites and preparation methods.

Catalyst	Support	Iron Loading (wt. %)	Preparation Method
SFeZ4	ZSM-5	4	IWI*
SFeZ9	ZSM-5	9	IWI
SFeZ18	ZSM-5	18	IWI
SFeDZ9	De-aluminated ZSM-5	9	IWI
HFeZ9	Physical admixing of iron and ZSM-5	9	Physical admixing
BFe	-	100	Co-precipitation
CFe	Promoted	90	Co-precipitation + IWI

*IWI: Incipient wetness impregnation

4.2.1 Catalyst characterization

The synthesized catalysts were characterized by using X-ray diffraction (XRD), N_2 physisorption, inductively coupled plasma (ICP), thermogravimetric analyses (TGA) and scanning electron microscopy (SEM-EDS) techniques.

Figure 4.10 shows the XRD patterns of the mother ZSM-5 and the calcined catalysts. Results indicated that the characteristic patterns of ZSM-5 structure were mostly maintained after iron impregnation. Relative intensities of the peaks representing zeolite crystallinities, however, decreased upon iron loading due to inclusion of iron oxides and their dilution effect. On the other hand, no obvious loss of crystallinity in the zeolite structure was observed after de-alumination. Relative crystallinities of the ZSM-5 in the zeolite and catalysts were calculated from the XRD patterns, using the ASTM D5758 Standard. Relative crystallinities of de-aluminated sample was determined to be around 99.0 % with reference to that of the mother ZSM-5, which is

assumed to be 100%. This suggested that the de-alumination did not result in a considerable deterioration in the structure of the zeolite. This may be due to the molecular diameter of the de-aluminating agent (oxalic acid) which is larger than the pore diameter of the ZSM-5. Therefore, it seemed likely that mainly the surface of the zeolite was de-aluminated and it proceeded rather gradually deep into the zeolite structure.

The position and relative intensity of the XRD peaks recorded at 2θ = 33.2 and 35.7 were attributed to α-Fe_2O_3 (hematite) proving the formation of crystalline Fe_2O_3 particles on the zeolite surface upon calcinations (Zola et al., 2002). Intensities of these peaks increased with increasing iron loading. Using the Scherrer's equation, the average crystallite sizes of the samples were calculated from the half-width (HW) of the diffraction peak at 2θ = 33.2 (hkl : 104). This is a typical hematite phase peak with highest intensity and no overlapping with the rest of the hematite and zeolite peaks. The calculation results given in Table 4.10 indicated that the crystal size increased with iron loading degree, from 15.3 for SFeZ4 to 25.3 for SFeZ18.

Table 4.10 : Composition and textural properties of low acidity zeolite- supported bi-functional iron catalysts.

Catalyst	Base ZSM-5	D-ZSM5	SFeZ4	SFeZ9	SFeZ18	SFeDZ9	BFe	CFe
BET surface area (m^2/g)	447.9	416.6	452.3	382.6	292.4	432.3	39.0	35.0
External surface area (m^2/g)	90.7	62.3	115	135.8	95.8	146.5	39.0	34.0
Micropore surface area (m^2/g)	357.1	353.4	337.3	246.8	196.6	285.8	0.0	0.0
Micropore volume (ml/g)	0.159	0.159	0.158	0.113	0.089	0.124	0.00	0.00
Metal crystallite size (nm)	na	na	15.3	21.0	25.3	16.6	21.3	34.7
ZSM-5 relative crystalinity (%)	100	98.99	73.16	58.71	51.47	51.62	na	na
Iron loading (wt. %)	na	na	4.14	9.35	17.55	9.5	100	100

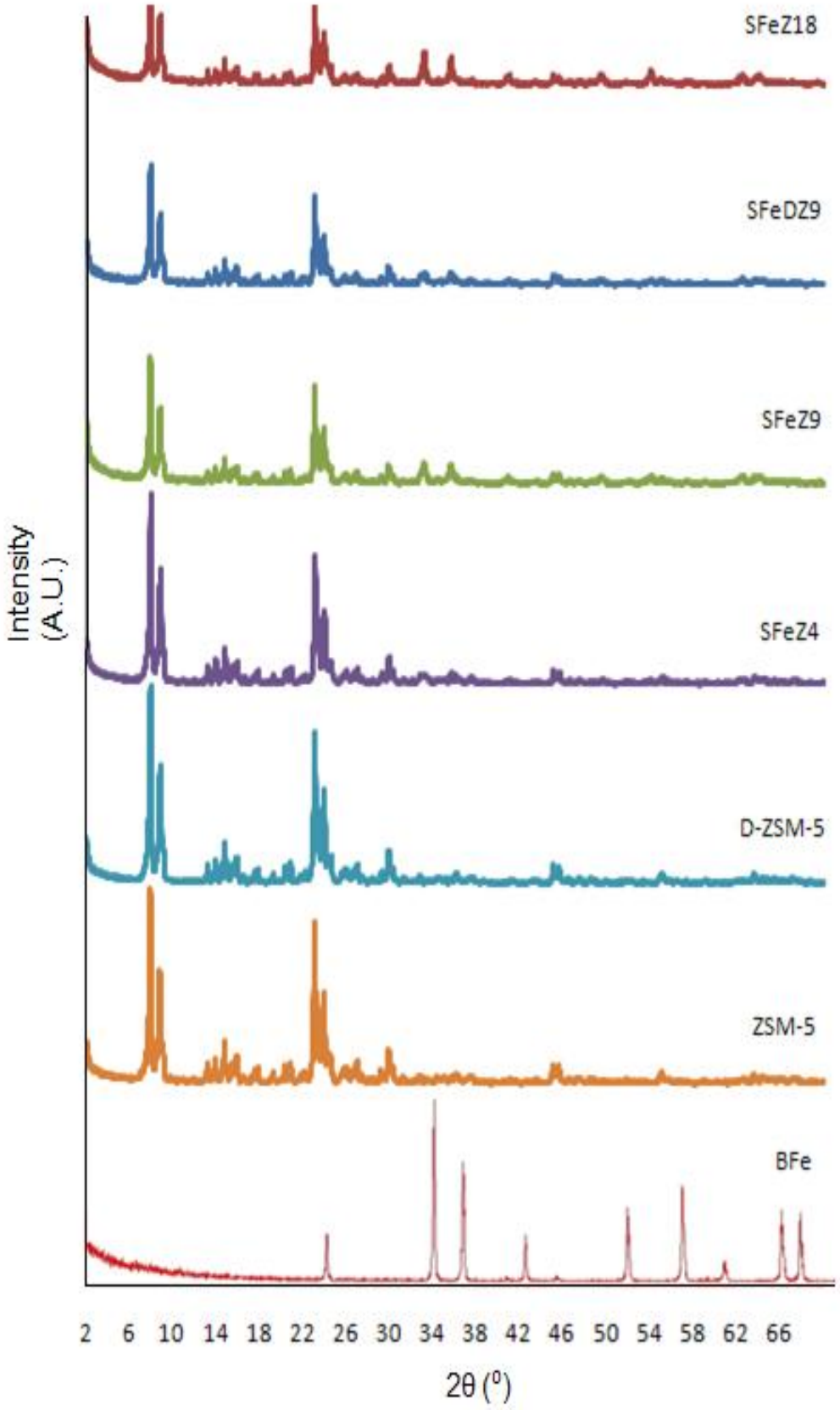

Figure 4.10 : X-ray diffraction patterns of ZSM-5 and calcined bi-functional iron catalysts prepared by using low acidity ZSM-5 and de-aluminated ZSM-5.

As seen from Table 4.10 and Figure 4.11, in general, total BET and micropore surface areas and micropore volumes of the supported catalysts decreased with increasing iron loading. This might be due to the clogging of zeolite pores by iron species, making them less accessible for nitrogen adsorption. External surface areas of catalysts increased in parallel to iron loading up to 9 wt % Fe and then decreased for 18 wt.% Fe. During the synthesis of catalysts, iron was simultaneously loaded on both the external surface and pore channel surfaces of the crystal. The internal surface area gradually decreased as iron deposition in the pores/cavities and pore entrances proceeded. On the other hand, the iron loaded on the external surface also has a surface area. Therefore, the total external surface area of the catalysts could increase to some extent with increasing iron loading through additive contributions of iron and zeolite. After loading exceeded some degrees (i.e. high loading cases), iron would continue to deposit, but mostly on the external surface rather than on internal surfaces as a bulky mass and resulted in a decrease in external surface area. This was confirmed by experimental results indicating that the external surface area of the catalysts increased with iron loading up to 9%, and then decreased on further loading. It should be noticed, however, that the catalyst with 18% iron still had a higher external surface area than that of mother ZSM-5. Considering the simultaneous substantial loss occurred in the BET surface area, this result might be taken as an indication of existence of iron deposited on the zeolite external surface.

Unsupported iron catalysts (BFe, CFe) have a very poor micropore volume, external and total surface areas in comparison to the zeolite supported catalysts.

Acidity measurements showed no considerable acidity for mother and de-aluminated zeolites and catalyst samples, conforming the low acidity of the zeolite as pointed out before. The acidity of the zeolites and synthesized catalyst samples were measured by n-butyl amine (n-BA) adsorption method.

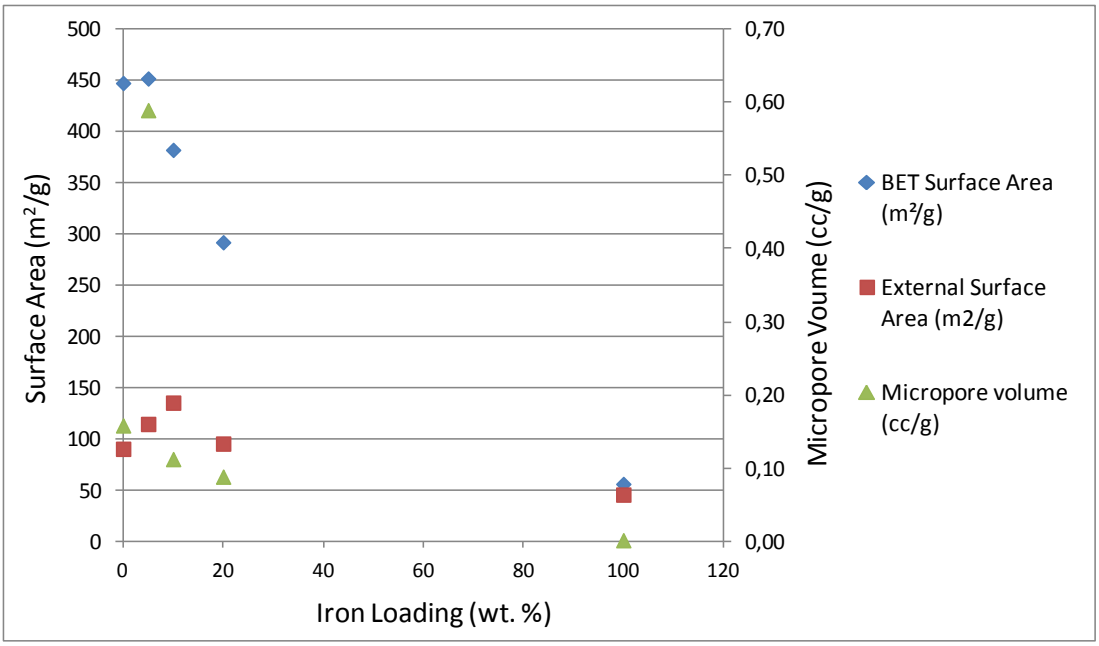

Figure 4.11 : Variation of surface areas and micropore volumes of low acidity zeolite-supported iron catalysts with iron loading.

The results of TGA analysis of the mother ZMS-5, de-aluminated ZMS-5 and the synthesized catalysts treated with n-BA are shown in Figure 4.12. No considerable acidity has been measured for the zeolite and catalyst samples. TGA measurements done before and after the de-alumination indicated de-alumination did not significantly alter the thermal behavior of ZSM-5. This suggested that de-alumination did not result in an obvious loss in its acidity. This might be attributed to the low acidity of the mother zeolite and the fact that de-alumination occurred mainly on the zeolite surface with lesser extend in the deep structure. These results are in line with studies describing ZSM-5 with SAR of 280 as low acidity zeolite (Botes, 2005; Botes and Bohringer, 2004). In studies, working with the same zeolite from the same provider, acidity measurements have been done (Baros and Zotin, 2007; Gaoh et al., 2004; Gonzalez and Hermez, 2007). Barros and Zotin (2007) measured the acidity of ZSM5 of different SAR with NH_3 TPD method and reported the acidity of ZSM-5 with SAR = 280 and SAR = 30 as 216 mmol/g and 1628 mmol/g, respectively. This indicated an 8 fold increase in the acidity as result of SAR decreased from 280 to 30 (Baros and Zotin, 2007). Comparable results have also been published by others (Gaoh et al., 2004; Gonzalez and Hermez, 2007). Considering results of these studies, the ZSM-5 zeolite with SAR = 280 used in this study was classified as *the low acidity ZSM-5*.

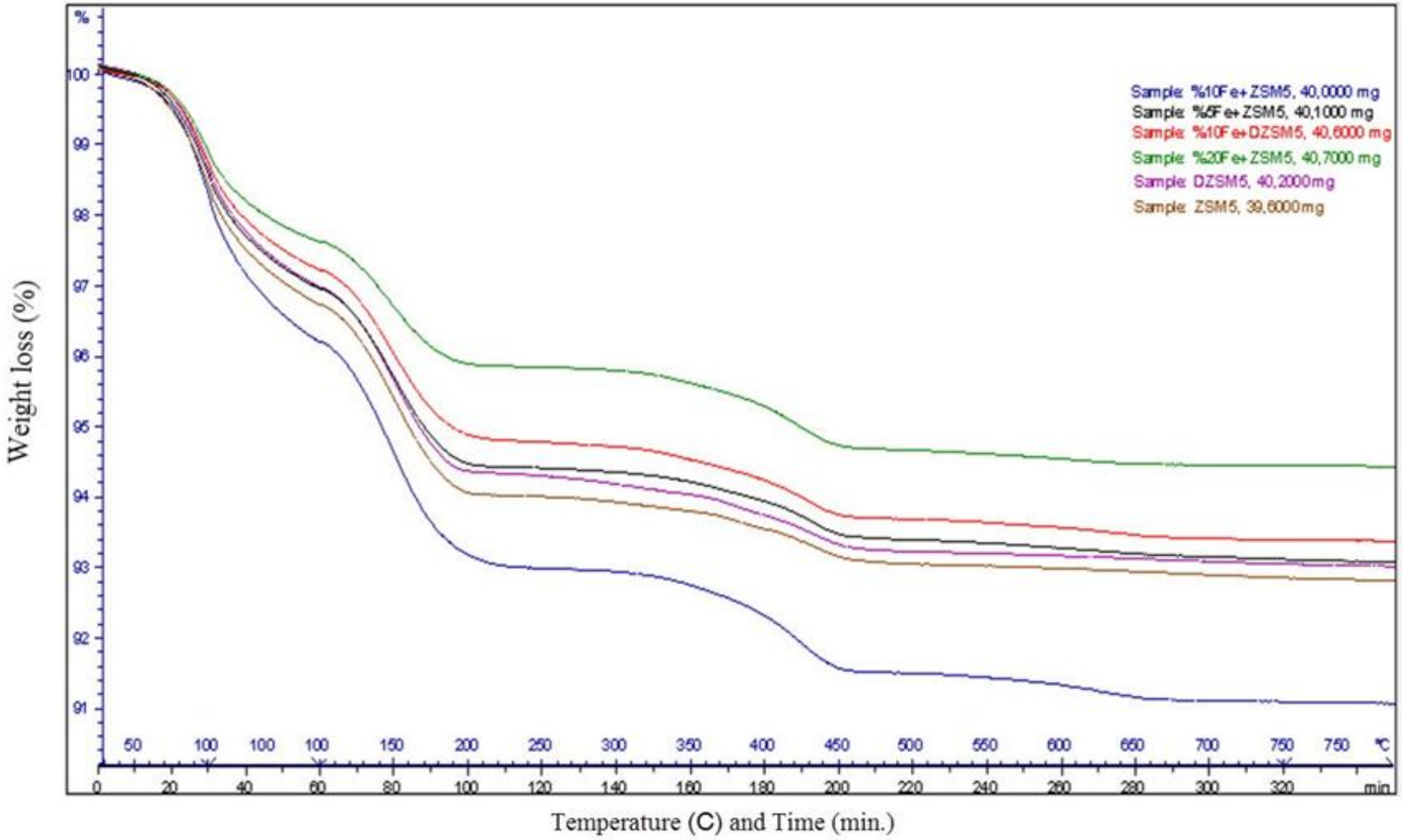

Figure 4.12: TGA analysis of catalysts.

Freshly calcined and reduced Fe-based catalyst samples were examined using SEM-EDS to obtain information on their microstructural properties and metal dispersion. SEM images obtained for different samples are given in Figure 4.13 - Figure 4.14.

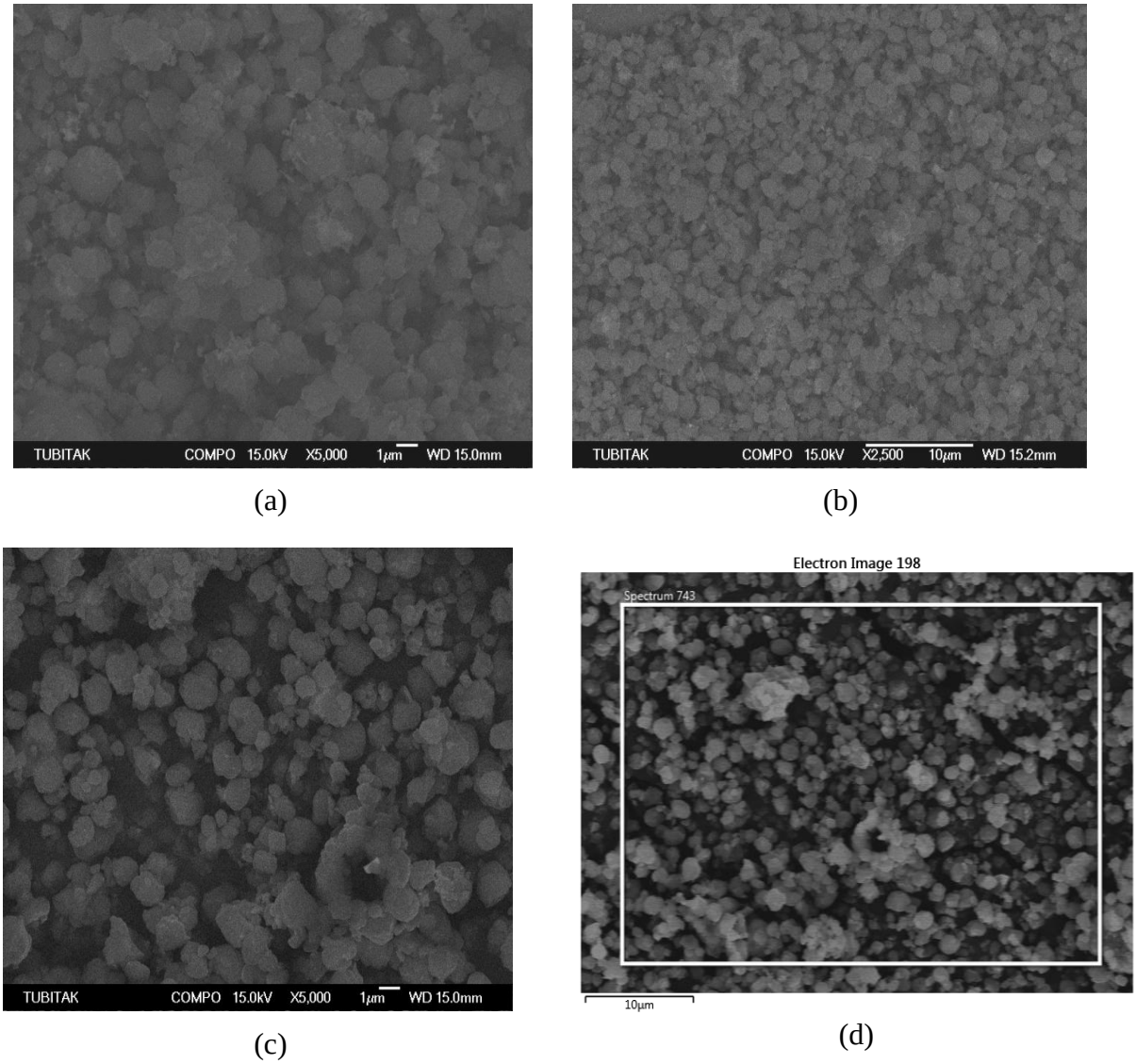

Figure 4.13 : SEM images of the catalysts: General perspective (a) SFeZ18, (b) SFeZ9, (c) SFeZ9 (calcined), (d) SFeZ4.

As seen in Figure 4.13, ZSM-5-supported iron catalysts exhibited a very uniform morphology composed mainly of very small individual crystals with some portions agglomerated into small ensembles. The structures with small open spaces and larger voids of a 2–3 micron diameter resemble to an eroded sponge. These arrangements of the submicron agglomerates well account for the observed high external surface areas and high mesopore volumes. These findings are also compatible with results of

N_2 physisorption analyses, which showed an increase in the external surface area with increase in the iron loading.

EDS analyses of the brighter grains of the catalyst crystals confirmed the presence of iron clusters on the external surface of the zeolite crystals upon reduction, Figure 4.14 The results of EDS analyses are tabulated in Table 4.11. The iron ratios determined by EDS analysis were slightly lower than that measured by ICP. For example, in case of SFeZ9 catalyst, a 8.1 wt.% iron was measured by EDS analysis, which was determined to be 9.4% by the ICP analysis. This difference may be originated from iron located inside the zeolite channels which were not detected by EDS.

Table 4.11 Results of EDS analyses of catalysts (wt%).

Catalyst	Fe	Si	Al	O
SFeZ4 (reduced)	4.5	47.9	trace	47.6
SFeZ9 (reduced)	8.1	46.9	trace	45.0
SFeZ9 (calcined)	4.4	47,8	trace	47,7
SFeZ18 (reduced)	15.6	41.2	trace	42.9

No aluminum was detected in catalysts by EDS analyses. The SAR of the mother ZSM-5 was quite high, being 280. The observed trace amount of Al is believed to be a result of the high SAR of mother zeolite.

The occurrence frequency of iron sites on the catalyst surfaces increased with increase in iron loading, as expected. The iron crystallite sizes were observed to be generally below 50 nm, Figure 4.15, which were fairly compatible with the crystallite sizes (15 - 25 nm) calculated from XRD analysis results by Scherrer equation.

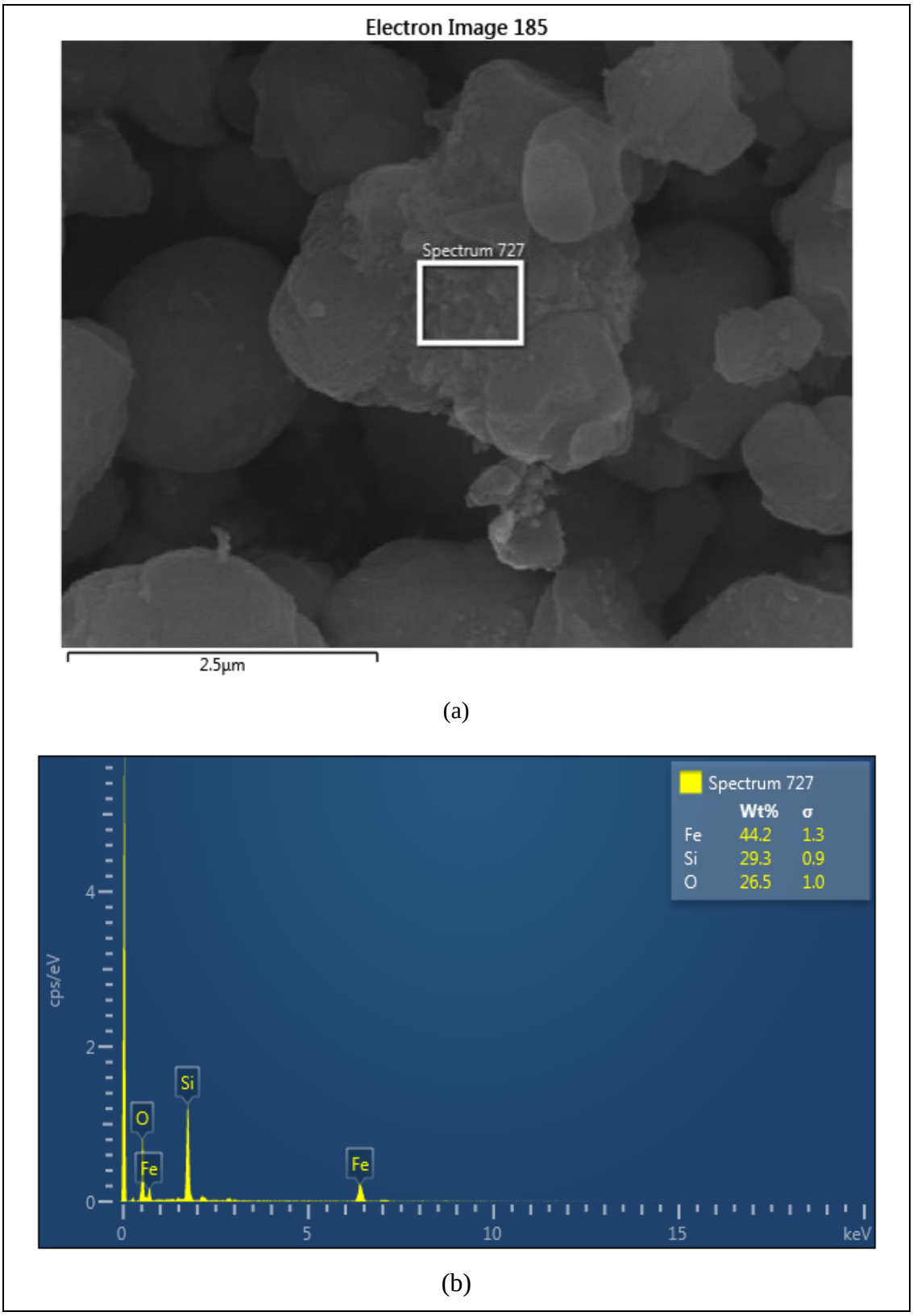

Figure 4.14 : SEM images and EDS analysis of the SFeZ9 catalyst (a) SEM image, (b) EDS analysis.

Since the spaces inside the zeolite channels can not be observed by SEM technique, we are not able to comment on the amount of iron located in these channels.

Furthermore, if all of the iron were deposited on the external surface of the zeolite, then the iron ration measured by EDX would have been much higher than that determined by ICP analysis. However, the SEM and EDS analyses indicated that a considerable iron fraction was located on the external surface of the zeolite. Comparing EDS analyses results of the calcined and the reduced SFeZ9 samples revealed that the latter had much higher iron than the former with 4.4 wt.% and 8.1 wt. %, respectively. This may be attributed to the partial migration of the iron out the zeolite channels during the course of reduction. These findings are in line with that of others (Bengoa, 2002).

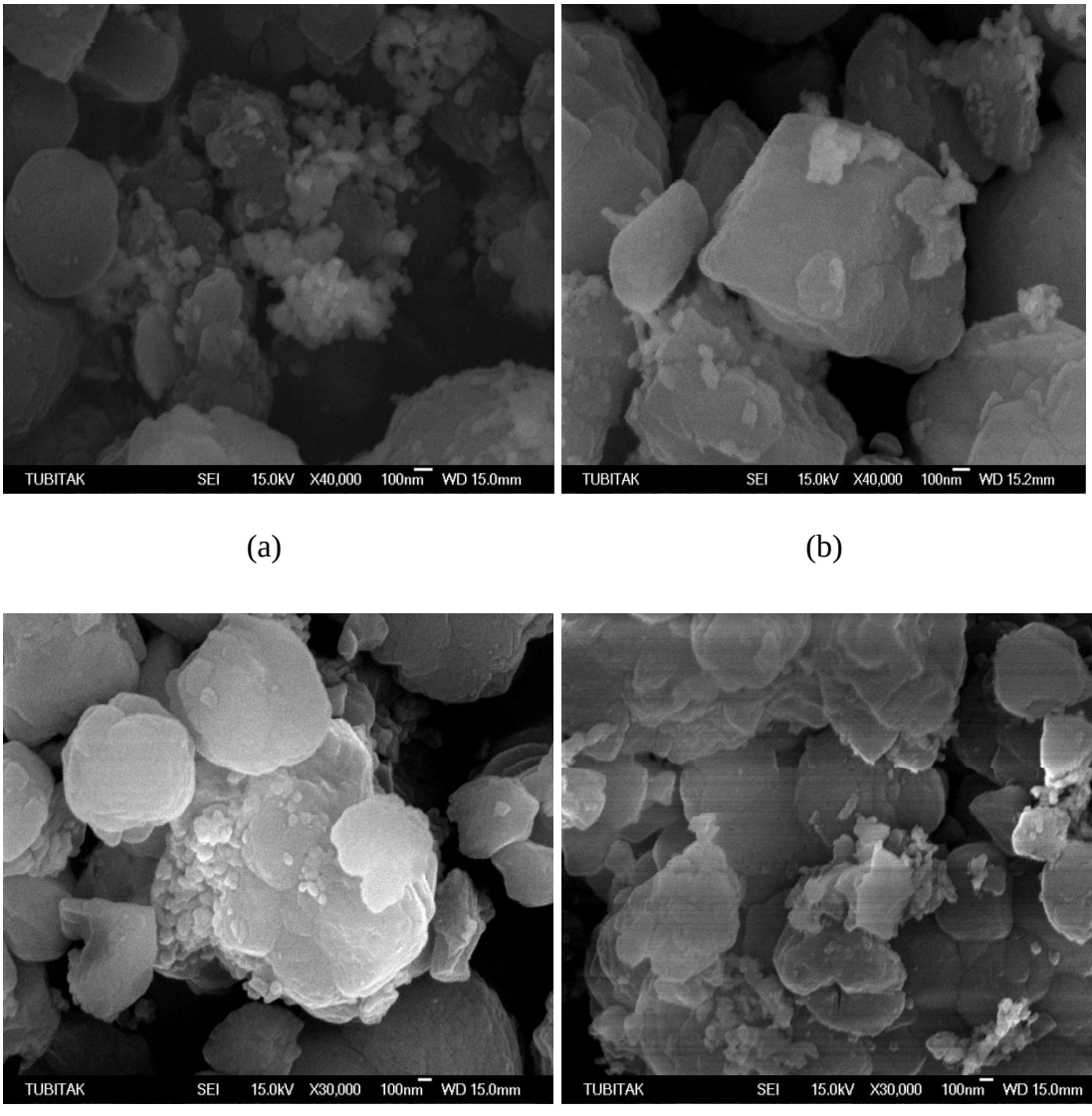

Figure 4.15 : SEM images of the catalysts (a) SFeZ18, (b) SFeZ9, (c) SFeZ9 (calcined), (d) SFeZ4.

4.2.2 FT activity of low acidity zeolite-supported iron catalysts

In this section, we are going to report the results of the experimental studies done to study performances of the low acidity zeolite-supported iron catalysts in the FT synthesis process. A series of tests were carried out to investigate the effects of synthesis method, catalyst composition and reaction temperature on various aspects of catalyst performance such as catalytic activity, selectivity towards various gases, yield and product compositions.

Parameters considered in experiments are presented in Table 3.5. The experiments undertaken to investigate the catalytic performances of the catalysts in FT synthesis are presented in Table 4.12. The catalysts were reduced under a flowing H_2 stream at 743 K for 10 h as explained in Section 3.3.1. The activity tests of the catalysts were performed at three different temperatures of 523K, 538K and 553K.

Table 4.12 : Performance tests undertaken for bi-functional iron-based FT catalysts prepared by using low acidity ZSM-5.

Experimental Run	Catalyst	Temperature (K)
1	SFeZ4	538
2	SFeZ4	553
3	SFeZ9	523
4	SFeZ9	538
5	SFeZ9	553
6	SFeZ18	523
7	SFeZ18	538
8	SFeZ18	553
9	HFeZ9	523
10	HFeZ9	538
11	HFeZ9	553
12	SFeDZ9	538
13	SFeDZ9	553
14	CFe	543

Results in Table 4.13 - Table 4.15 show a clear impact of the iron loading on the catalytic activity of catalysts. The CO conversion, a significant measurement of catalytic activity of the catalysts in the FT synthesis, tended to increase with increase in the iron content of the catalyst. Base iron catalyst (BFe) with 100 wt.% iron, however, did not follow this general trend, likely due to its lower surface area and poor porosity available for gas-metal interaction in comparison with supported catalysts.

Figure 4.16 shows variation of CO conversion with iron loading in FT synthesis by low acidity zeolite-supported catalysts. As seen, increase of the iron loading resulted in a substantial increase in the CO conversion. For example at 553 K, increasing the iron loading from 4% to 18% pushed the CO conversion from 43.3% to 72.4%. Although, in the range of iron content studied, CO conversion seemed to be strongly dependent on the amount of iron in the catalyst, incremental increase in the CO conversion was smaller than that of iron loading. The relatively smaller incremental increase in the CO conversion over catalyst with higher iron loadings was likely due to the increase in the iron particle size and the poor iron dispersion on the supports. The catalyst with highest Fe loading of 18 wt.%, SFeZ18, exhibited the highest activity among the zeolite-supported iron catalysts. The conventional catalyst (CFe) with 90.9 wt.% iron (100Fe/7K/3Cu), on the other hand, yielded the highest CO conversions in all catalysts studied.

Figure 4.17 shows the variation of hydrogen conversion with iron loading for low acidity zeolite-supported catalysts. In parallel to CO conversion, hydrogen conversion increased with increasing iron loading, as a result of the improved catalyst activity. For example, at 553 K, increasing the iron loading from 4% to 18% increased the H_2 conversion from 33.9% to 61.7%. Differences observed between CO and H_2 consumptions originated from the water gas shift activities of the catalysts. This reaction simultaneously consumes CO and generates H_2 thus leads to CO conversions higher than that of H_2. The other reason for these differences could be variation of H_2/CO in the syngas fed to the reactor which is commonly slightly higher than 2.0 . In this study it was 2.0. On the other hand, the variation in the amount of olefins produced during the process can affect the consumption rates of CO and H_2. The alteration of the balance between FT and WGS reaction activities can also have different impact on the H_2 and CO conversion trends.

Table 4.13 : The activity of the low acidity zeolite-supported iron catalysts in the FT synthesis process at T = 553K (P=19 bara, GHSV = 750 h^{-1}, H_2/CO=2).

Catalyst	SFeZ4	SFeZ9	SFeZ18	HFeZ9	SFeDZ9	CFe	BFe
CO conversion (%)	43.3	52.1	72.4	43.0	40.2	97.0	39.6
H_2 conversion (%)	33.9	41.6	61.7	31.1	37.5	92.0	33.4
CO_2 selectivity (%)	8.2	13.2	9.0	17.2	7.4	41.6	20.5
Productivity							
Hydrocarbon (g/h/g-Fe)	1.7	0.7	0.5	1.2	0.89	0.34	0.03
Yield							
Hydrocarbon (g/Nm^3-syngas converted)	226.0	211.3	212.5	213.6	203.9	117.9	187.0
Gasoline (g/Nm^3-syngas converted)	121.5	106.3	156.9	96.7	115.8	17.3	76.6
Rate of syngas converted, mmol (H_2+CO)/g-cat/h	334.4	154.0	111.9	249.4	195.4	127.7	8.2
Product Composition (wt.%)							
C_1	17.4	17.0	7.9	16.9	15.8	27.3	15.6
C_2-C_4	25.7	30.2	14.0	34.6	24.8	43.1	35.9
C_5-C_{11}	53.8	50.3	73.9	45.3	56.8	14.7	41.0
C_{12}-C_{18}	3.2	2.6	4.0	1.5	2.3	3.3	6.8
C_{19}+	0.0	0.0	0.3	1.7	0.3	11.6	0.7
Olefin ratio (mol%) (gas phase)	5.7	10.6	6.7	5.03	11.7	66.7	37.2

Table 4.14 : The activity of the low acidity zeolite-supported iron catalysts in the FT synthesis process at T = 538 K (P=19 bara, GHSV = 750 h^{-1}, H_2/CO=2).

Catalyst	SFeZ4	SFeZ9	SFeZ18	HFeZ9	SFeDZ9	BFe
CO conversion (%)	22.6	31.5	43.8	22.7	19.3	32.0
H_2 conversion (%)	21.4	29.3	46.6	20.6	22.3	27.6
CO_2 selectivity (%)	7.4	7.4	5.5	10.3	2.17	16.7
Productivity						
Hydrocarbon (g/h/g-Fe)	0.89	0.47	0.33	0.68	0.45	0.03
Yield						
Hydrocarbon (g/Nm^3-syngas converted)	202.0	204.2	190.8	201.6	187.1	193.2
Gasoline (g/ Nm^3-syngas converted)	79.6	98.6	125.4	91.3	111.5	89.5
Rate of syngas converted, (mmol (H_2+CO)/g-Fe/h)	196.9	102.5	78.2	151.8	108.4	6.7
Product Composition (wt.%)						
C_1	27.5	19.0	10.9	17.7	16.0	14.1
C_2-C_4	31.2	30.4	18.4	35.9	20.3	29.0
C_5-C_{11}	39.4	48.3	65.7	45.3	59.6	46.3
C_{12}-C_{18}	1.8	2.3	4.9	0.9	4.0	10.0
C_{19}+	0.0	0.0	0.1	0.3	0.2	0.6
Olefin ratio (mol%) (gas phase)	8.99	18.8	17.5	8.4	25.8	38.5

Table 4.15 : The activity of the low acidity zeolite-supported iron catalysts in the FT synthesis process at T = 523K (P=19 bara, GHSV = 750 h^{-1}, H_2/CO=2).

Catalyst	SFeZ9	SFeZ18	HFeZ9	BFe
CO conversion (%)	21.5	33.1	15.5	23.6
H_2 conversion (%)	21.4	33.0	16.0	21.5
CO_2 selectivity (%)	18.4	11.9	7.1	17.3
Productivity				
Hydrocarbon (g/h/g-Fe)	0.33	0.26	0.48	0.02
Yield				
Hydrocarbon (g/Nm^3-syngas converted)	200.5	203.7	191.7	185.5
Gasoline (g/ Nm^3-syngas converted)	113.1	114.9	91.6	84.5
Rate of syngas converted, (mmol (H_2+CO)/g-Fe/h)	73.3	56.7	112.9	5.2
Product Composition (wt.%)				
C_1	18.4	11.9	17.2	17.1
C_2-C_4	33.2	22.8	33.8	28.7
C_5-C_{11}	45.3	56.4	47.8	45.6
C_{12}-C_{18}	3.15	8.4	0.9	8.2
C_{19}+	0.0	0.49	0.26	0.46
Olefin ratio (mol%) (gas phase)	28.9	40.0	14.88	35.7

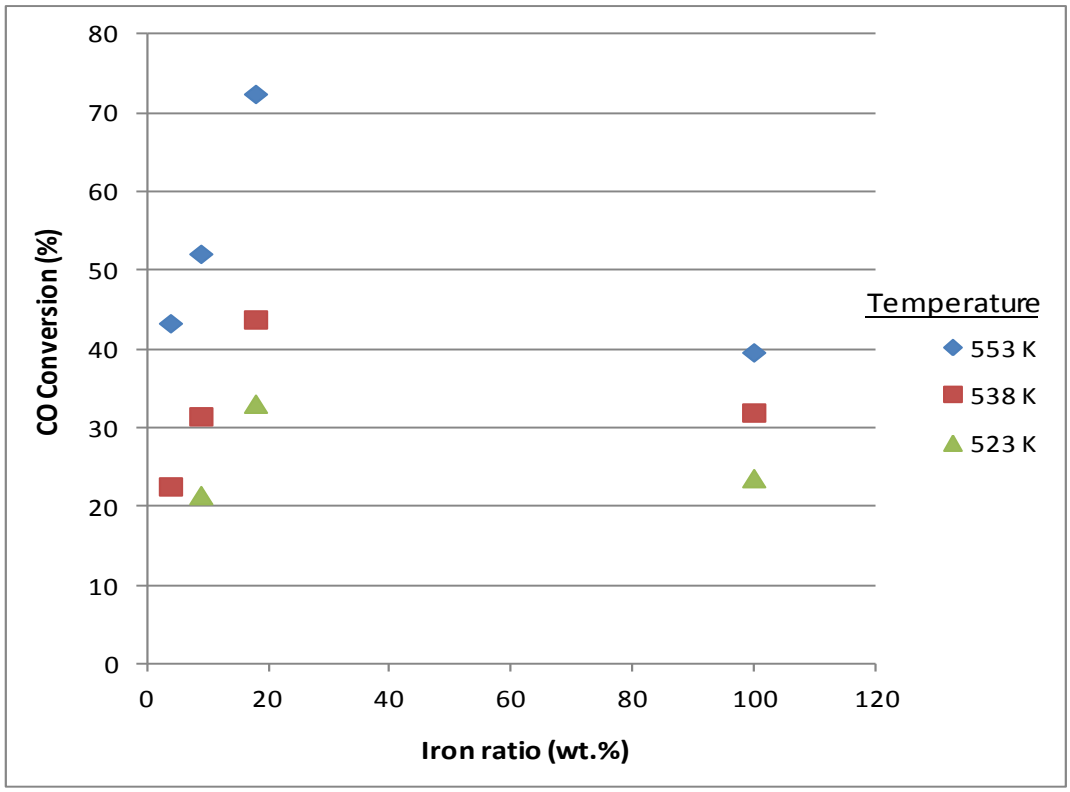

Figure 4.16 : Variation of CO conversion of low acidity zeolite-supported iron catalysts with iron loading.

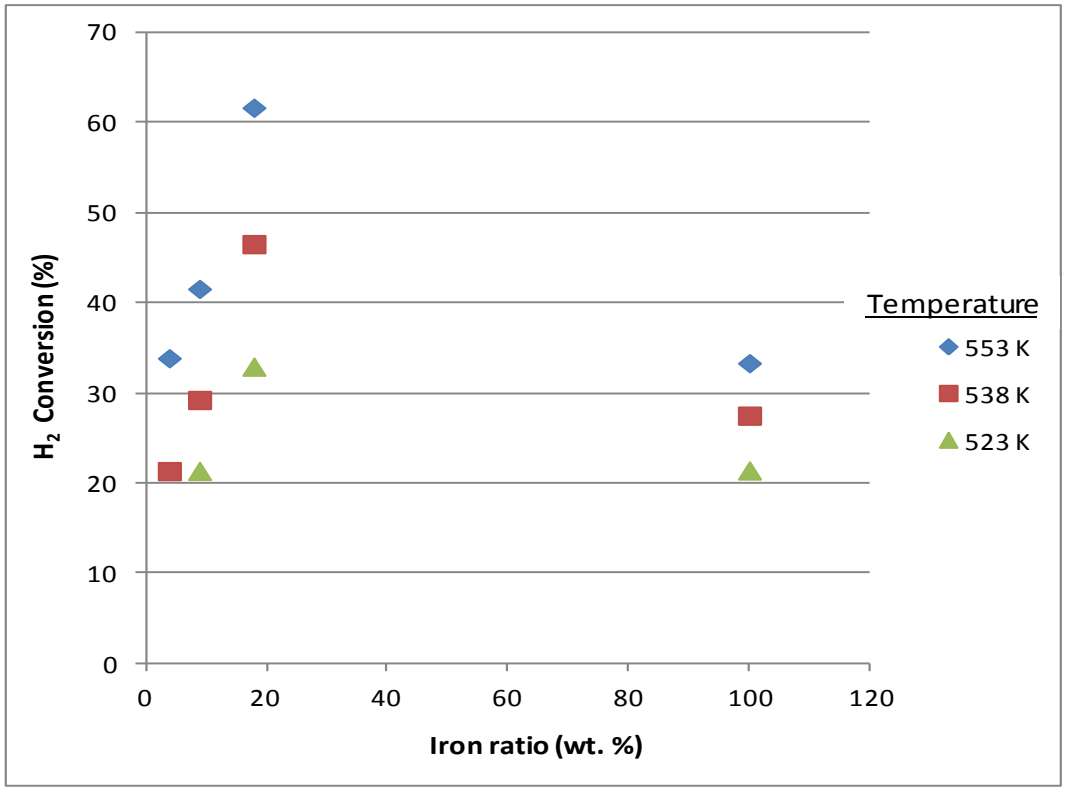

Figure 4.17 : Variation of H_2 conversion of low acidity zeolite-supported iron catalysts with iron loading.

Tests were carried out in the temperature range between 523 K and 553 K in order to observe the effect of the reaction temperature on the catalytic activities and selectivities of the catalysts. Results, shown in Figure 4.16 and Figure 4.17, clearly indicate that conversions were strongly affected by reaction temperature. CO and H_2 conversions increased with temperatures for all catalysts, as expected. An increase of 30 K in the reaction temperature resulted in 39.3% (from 33.1% to 72.4%) and 28.7% (from 33.0% to 61.7%) increase in the CO and H_2 conversions, respectively for SFeZ18 catalyst. The maximum CO and H_2 conversions obtained at 553 K for all catalysts.

Hydrocarbon productivity calculated based on per gram of Fe are shown in Figure 4.18. The hydrocarbon productivities of the catalysts decreased considerably with increase in the iron loading, indicating the impact of dispersion and the particle size of the active component in supported catalysts. These results suggested that a portion of iron did not effectively take place in the reaction due to the restricted accessibility. Base iron catalyst (BFe) with the second lowest BET surface area and porosity, that were 7.5-12 folds and 3.4-6 folds lower, respectively, than that of the zeolite-supported catalysts, displayed the poorest productivity, as expected. Its productivity was 11-30 times lower than that of zeolite-supported catalysts.

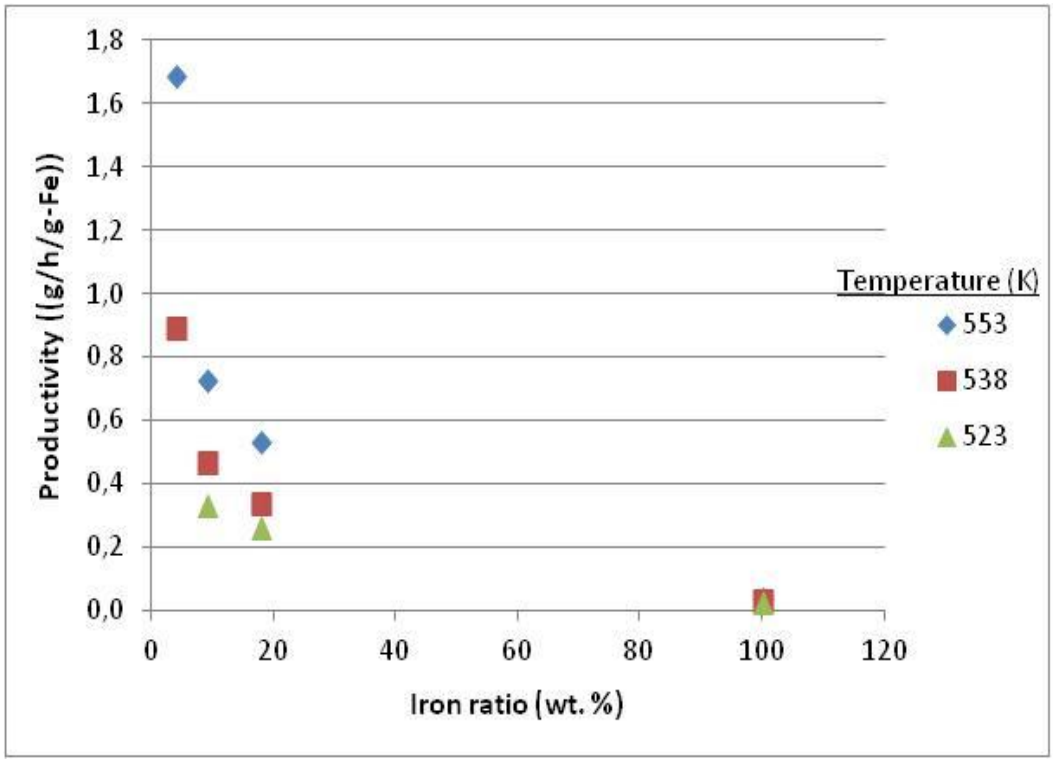

Figure 4.18 : Effect of iron loading on productivities of catalysts.

The catalyst synthesis method seemed to cause a change in the activity of the zeolite containing catalysts. With the same iron loading of 9%, catalyst prepared by impregnation showed a higher activity than the hybrid catalyst (HFeZ9) prepared by physical admixing in respect to CO conversion. A better utilization of zeolite channel structure and better dispersion in the former catalyst is likely to be responsible for that result. In the most of the recent studies physical admixing was used for catalyst preparation (Martinez et al., 2008; Botes, 2005; Yoneyama et al., 2010). However, the conventional impregnation could be a superior catalyst preparation route over physical admixing, since it can result in a better dispersion of active component, a greater zeolite - metal interaction and a better utilization of shape selectivity of the zeolite structure. On the other hand, however, de-alumination of ZSM-5 before impregnation resulted in a decrease in the activity of the resulting catalyst to some extent.

4.2.3 Water gas shift reaction activities of low acidity ZSM-5 containing catalysts

As done in Section 3.1.3., the WGS reaction activities of the synthesized catalysts are evaluated based on their CO_2 selectivity. The CO_2 selectivity of the catalysts are presented in Table 4.13 - Table 4.15. As seen in tables, the WGS activities of the zeolite supported catalysts were significantly lower than that of the base iron (BFe) and promoted conventional catalyst (CFe). At 553 K, the CO_2 selectivity of the BFe was determined to be 20.5%, whereas the potassium promoted conventional catalyst exhibited a 42% CO_2 selectivity. On the other hand, the CO_2 selectivity of zeolite supported catalysts varied between 8.2 – 17.2 %. The conventional catalyst displayed a CO_2 selectivity almost twice higher than that of BFe, and 2.5 – 5 times higher than that of zeolite supported catalysts. These results indicated that, ZSM-5 in the catalyst formulation suppressed the WGS activity of the iron based FT catalyst. It is well known that alkali promoters enhance the WGS activity of iron based catalysts (Bukur and Mukesh, 1990; Wan et al., 2008). Lack of alkali promoters in the base iron and zeolite supported catalysts was one of the possible reasons for their lower CO_2 selectivity.

Experimental results, given in Table 4.13- Table 4.15, clearly indicated that catalyst synthesis methods could affect the WGS activity and consequently can substantially

render the CO_2 selectivity of the catalyst. The CO_2 selectivity of the catalyst prepared via impregnation was quite lower than that of the hybrid catalyst. The WGS reaction proceeds via Eley - Riedal or Mars –Van Krevelen mechanisms in which WGS reaction is taking place through reduction – oxidation of the metals (Ratnasany and Wagner, 2009). It is likely that, the catalysts prepared by impregnation have the ability to suppress the iron WGS activity more effectively through better zeolite-iron interaction, in comparison with the hybrid catalyst (HFeZ9) where interaction between two components was poor. On the other hand, as discussed in Section 3.1.3., hydrogen easily diffuses into the pores of the zeolite where high hydrogen concentration might shift the reaction direction, namely to the reverse WGS reaction in existence of iron there. This was supported by the CO_2 selectivity results in Table 4.13 - Table 4.15 indicating that the CO_2 selectivity of the impregnated catalysts was higher than that of hybrid catalyst whose zeolite component pores expected to be free of iron.

4.2.4 Hydrocarbon selectivity of catalysts

Product distributions obtained from the catalyst activity tests carried out between 523 K and 553 K are given in Table 4.13 - Table 4.15, and Figure 4.19. These results indicated that zeolite presence in the catalyst could considerably influence the product selectivity. Comparison of the selectivity of the zeolite supported catalysts with that of conventional catalyst (CFe), revealed that the main differences were in the selectivity for C12+ and C5-C11 hydrocarbons. Conventional catalyst (CFe) produced considerable amount of heavy hydrocarbons. It exhibited a 12 % selectivity towards C19+. A typical waxy product obtained from FT synthesis by CFe catalyst and its composition are shown in Figure 4.20 and Figure 4.22. Presence of zeolite in the catalyst synthesis lowered selectivity for these hydrocarbons to below 1.7 % at temperatures higher than 538 K.

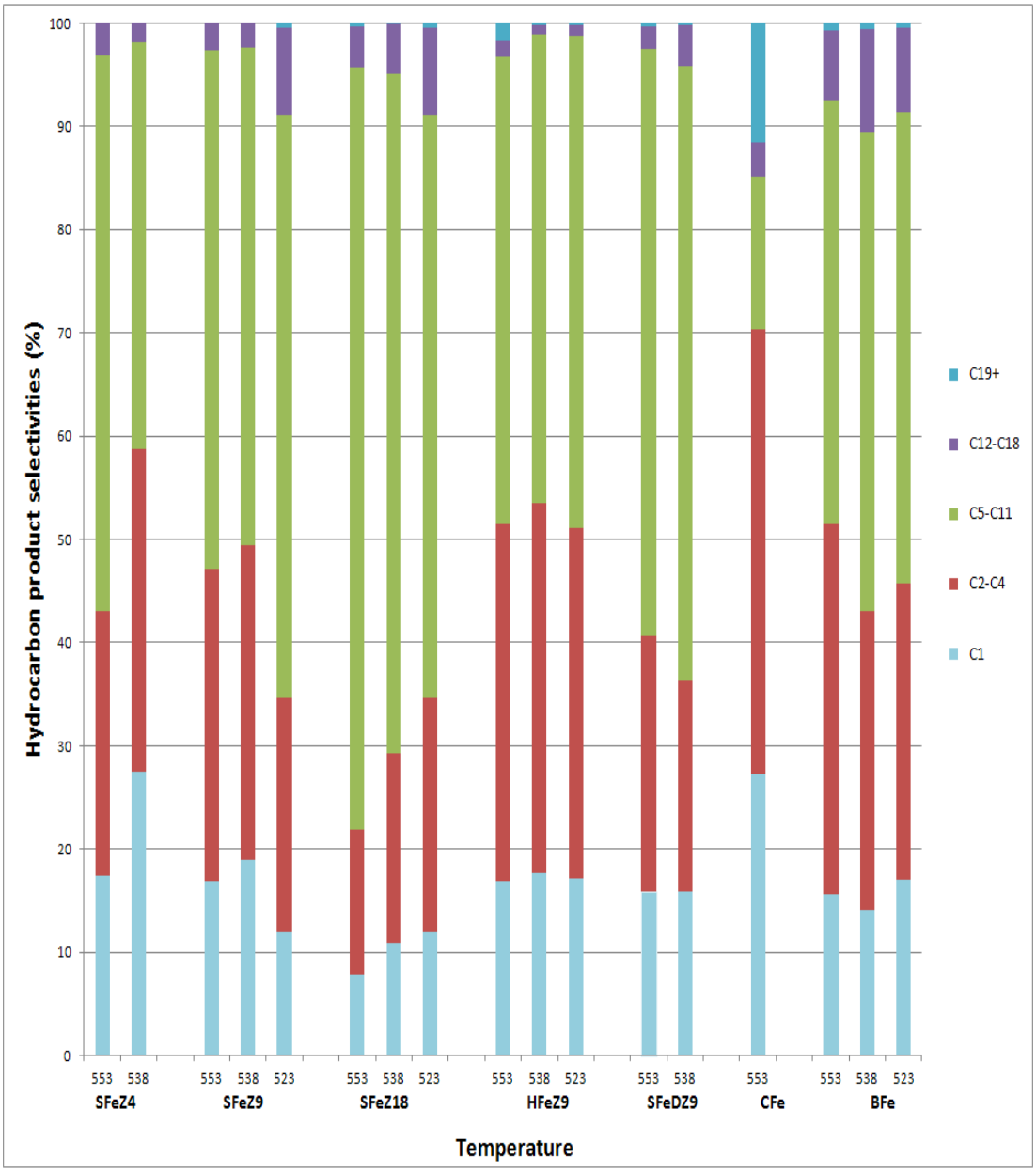

Figure 4.19 : Effects of catalyst composition and reaction temperature on HC distribution in the products obtained from FT synthesis (P=19 bara, GHSV=750 h^{-1}, H_2/CO = 2:1).

Figure 4.20 : A typical waxy product from FT synthesis by conventional catalyst.

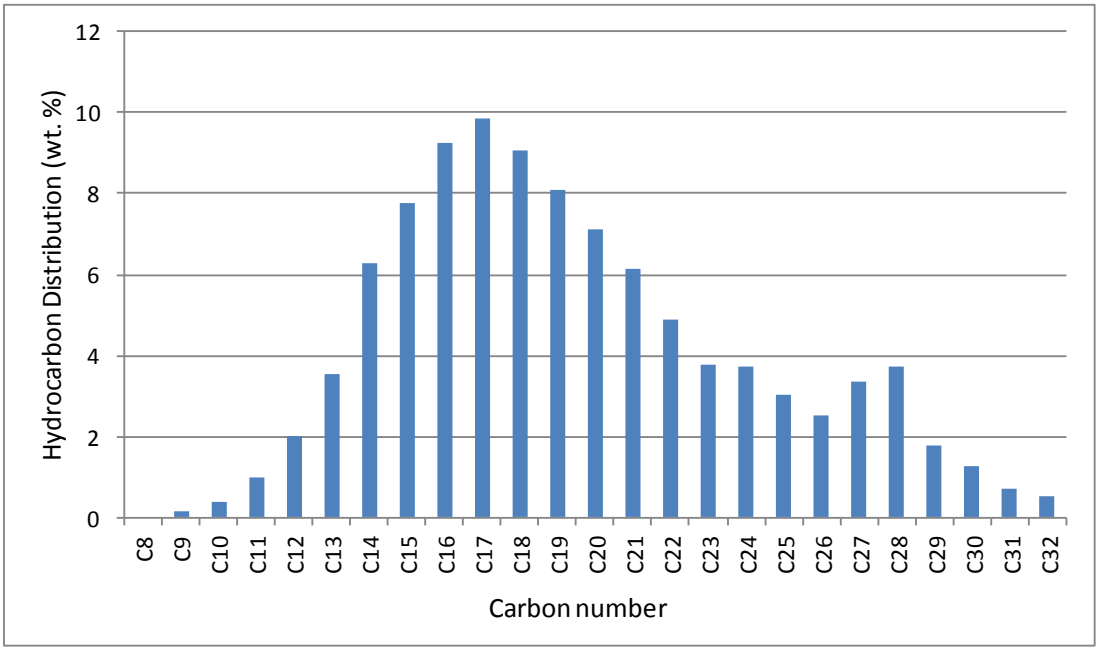

Figure 4.21 : Hydrocarbon distribution of waxy product obtained by CFe catalyst.

Conventional catalyst showed higher selectivity towards light hydrocarbons (C1-C4) in comparison with other catalysts. ZSM-5 containing iron catalysts narrowed the spectrum of the products by reducing the amount of light and heavy hydrocarbon fractions, maximizing the gasoline range hydrocarbons. These catalysts, due to their acidity, could also catalyze oligomerization of low molecular weight olefins. On the other hand, heavy hydrocarbon production in the FT process over zeolite containing catalysts could be substantially hindered by the shape selectivity nature of the zeolites. In spite of its lower acidity degree, the zeolite (ZSM-5) used in the synthesis of catalysts might catalyze the hydrocracking reactions, so that the heavy hydrocarbons formed during the FT synthesis could simultaneously be converted into lighter hydrocarbons in the process. These results are consistent with findings of others who reported that zeolites used in the FT process could produce higher

amounts of low molecular weight hydrocarbons and attributed this to the hydrocracking activities and shape selectivity of these zeolites (Pour et al., 2008; Zola et al., 2007).

GC analyses results of liquid phase obtained by catalyst and collected in the cold trap, are given in Figure 4.22. As seen from the figure, the ratio of C5-C11 range hydrocarbons obtained by catalysts containing low acidity ZSM-5 varied between 77.7% – 94.5% with an average of 89.1%. The vast majority of the catalysts produced liquid phases having C5-C11 range hydrocarbons ratios higher than 90%. A maximum ratio of 94.5% was obtained from SFeZ4 catalyst at 553 K. On the other hand, the average weight percentages of C5-C11 fraction in liquid phases produced by BFe and CFe catalysts and collected in the cold trap, were 82.8% and 65.3%, respectively.The C5-C11 fraction percentages were considerably higher for low acidity ZSM-5 containing catalysts. Therefore, upgrading of the raw liquid product from FT synthesis by these catalysts would be no longer needed to produce gasoline due to the low selectivity of these catalysts towards the long chained HCs.

Figure 4.22 also shows that, the concentration of C16+ fraction in the liquid products vanished almost for all of the ZSM-5 containing catalysts. Cut-off effect of ZSM-5 zeolite, limiting the maximum hydrocarbon chain length, can be seen from this figure. This also support the observation that no waxy hydrocarbon was produced by ZSM-5 containing catalysts. In circumtances waxy product produced in the FT reaction, the hydrocarbons up to C25 should be present in the cold trap liquid phase which would be in vapor- liquid phase equilibrium with the waxy product.

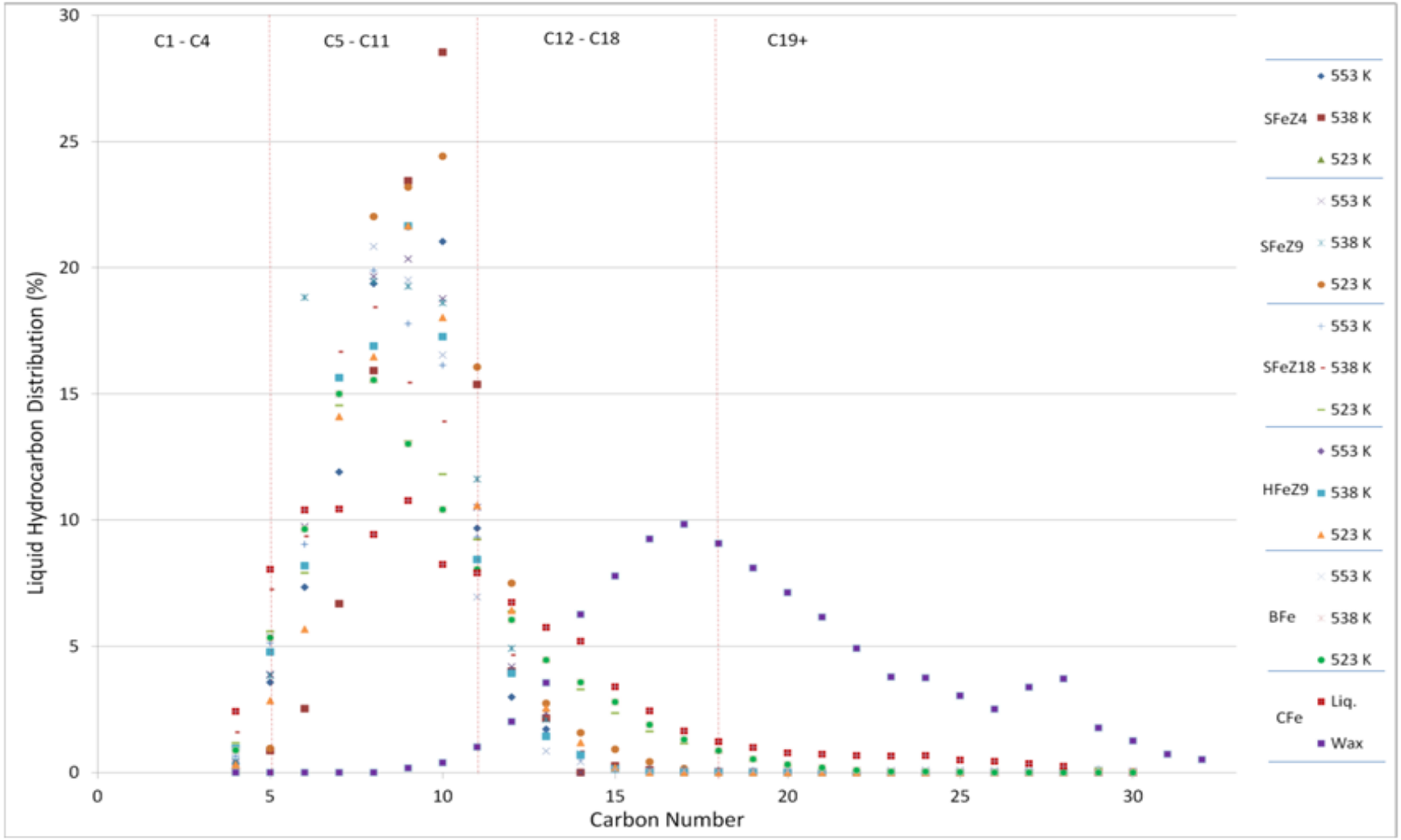

Figure 4.22 : Composition of liquid phase and waxy products obtained by zeolite supported catalysts (P=19 bara, GHSV=750 h^{-1}, H_2/CO = 2:1).

On the other hand, the hydrocarbons upto C20 and C25 were observed in the liquid phase products for BFe and CFe catalyst, respectively. In the FT sythesis conducted by using CFe, in addition to the medium range hydrocarbons (C5-C15) collected in the cold trap, a considerable amount of waxy products were also formed. The detail result of GC analysis of this waxy product obtained in the process catalyzed by CFe presented in Figure 4.21, showed that the hydrocarbons upto C32 were produced.

Methods used for the preparation of catalysts have also an impact on the selectivity of the FT products to a lesser extent. As seen in Table 4.13 - Table 4.15, the catalysts prepared by impregnation method, generally have better selectivity towards C5-C11 hydrocarbons than the hybrid catalyst. At 553 K, the selectivity of zeolite-supported catalysts towards the C5- C11 hydrocarbons fraction, which was the target product in this study, changed between 50% and 74%, while the selectivity of the hybrid catalyst (HFeZ9) towards the same fraction was about 45%. The impregnated catalysts generally displayed higher selectivity for C5-C11 fraction through higher utilization of zeolite shape selectivity and better zeolite iron interaction.

On the other hand, de-alumination resulted in a moderate change in the selectivity of catalyst. The catalyst prepared with de-aluminated ZMS-5, SFeDZ9, had a higher C5-C11 hydrocarbon fraction selectivity than SFeZ9 which had an equal iron loading. Given the fact that these two catalysts had similar physical and textural properties such as BET surface area, pore volume and crystallinity etc., this was likely originated from lower acidity of SFeDZ9 which had undergone de-alumination.

Selectivities of the zeolite-supported catalysts, on the other hand, towards the C19+ fraction were lower than that of the hybrid catalyst (HFeZ9). It seemed that zeolite, as a support, could suppress the reactions which produced high molecular weight hydrocarbons and thus reduced the amount of waxy products. On the contrary, the hybrid catalyst (HFeZ9) produced small amounts of wax, about 2%, under the same process conditions. The superior selectivity of the supported catalysts might also be attributed to the shape selectivity property of the zeolite combined with a better zeolite-iron interaction.

The performance of catalysts with respect to the C2-C4 range olefin hydrocarbons (gas phase) production are compared in Figure 4.23. The conventional (CFe) and

base iron (BFe) catalysts produced about 67% and 37% olefins at 553 K, respectively, which were the highest values obtained in the FT synthesis. As seen from the figure, the zeolite–supported catalysts considerably suppressed the formation of the C2-C4 range olefins. At 553 K, the gas phase olefin selectivity of FT synthesis carried out by these catalysts were at levels of 5% -12%. The amount of olefins smoothly decreased with increase in temperature for all catalysts, due to the better activity of the zeolites at high temperatures. As mentioned before, decrease in the amounts of gas phase olefins which might be originated from the oligomerization induced by zeolites, favor the production of C5-C11.

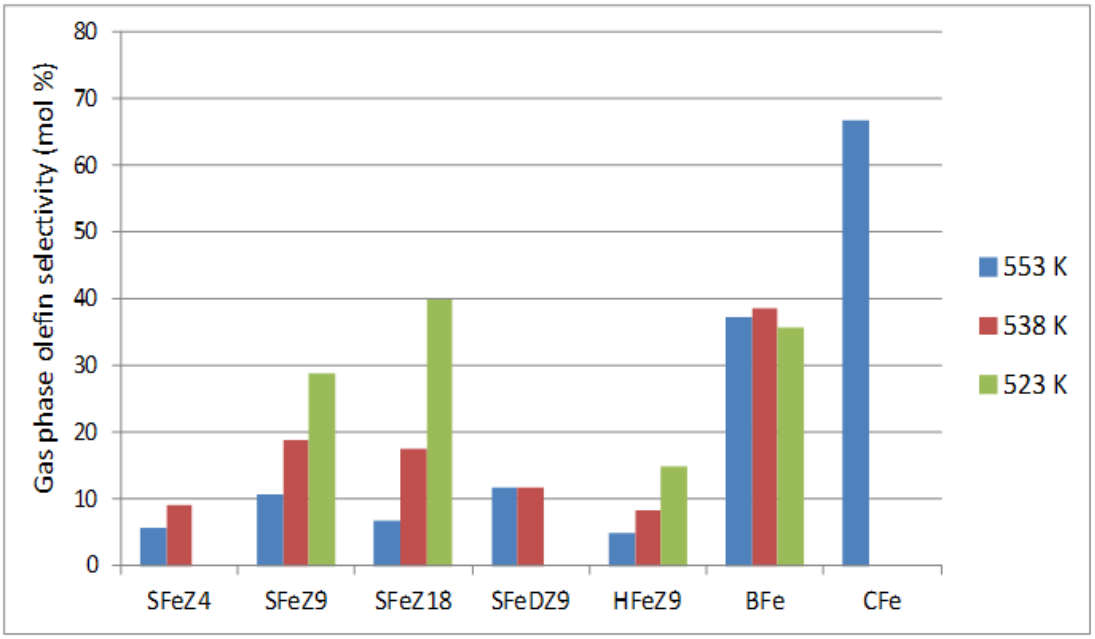

Figure 4.23 : Effect of catalyst composition and operating temperature on gas phase olefin selectivity.

A methane production of up to 7.9%-17.4% was also observed for zeolite supported-catalysts at 553 K, while conventional iron catalyst (CFe) produced 27.3% methane. Methane selectivity of zeolite supported catalysts were much lower than that of the conventional catalyst (CFe).

The selectivity towards C12+ hydrocarbons were increased as the iron percentage in the zeolite-supported catalyst, Figure 4.19. As concentration of iron in the catalyst increased the amount of the iron located out of the pores, which had poor interaction with zeolites was expected to increase as well. This was likely responsible for higher concentrations of long chain hydrocarbons in FT products obtained by catalyst with

higher iron contents. Moreover, the improving conversion with increasing iron content, might also positively contribute to the selectivity for heavy hydrocarbon.

The effect of temperature on product selectivity is given at Figure 4.19. The effect of reaction temperature on product selectivity is complex for bi-functional catalysts, determined by collective effect of competing reactions. This subject was explained in Section 3.1.4. For ZSM-5 supported catalysts, selectivity of heavy hydrocarbons (C19+) was generally decreased with increasing temperature. On the other hand, the light hydrocarbon selectivity was generally decreased with increasing temperature for SFeZ4 and SFeZ18 catalysts. As a result, selectivity towards the C_5-C_{11} hydrocarbons was increased, for these catalysts.

The highest gasoline selectivity, 73.9%, was obtained by SFeZ18 catalyst at 553 K. Furthermore, among the zeolite supported catalysts, the maximum activity was obtained by the same catalyst at 553 K.

In the literature, there are only a few studies, dealing with bi-functional FT catalysts, giving detailed analysis of synthesized hydrocarbon products, including the gasoline (C5-C11), the diesel (C12-C18) and the waxy (C19+) range hydrocarbons fractions. In the majority of these studies the gas phase hydrocarbon (C1-C4) distribution are reported and the rest are simply described and given as C5+ range hydrocarbons. Scattering values ranged from 19% to 62% are reported for the C5-C11 fraction in these studies. Wang et al (2007) studied Na- exchanged ZSM-5, beta, zeolite X and zeolite Y supported iron as FT catalysts. They observed a %19 selectivity of Fe/Na-ZSM-5 for the C5-C9 hydrocarbons. The maximum C5-C9 and C10-C20 selectivity in this study were obtained by Fe/Na-Y catalyst and reported to be 23% and 17%, respectively. Ravishankar et al. (2005) used MCM-22 as support for Co based FT catalyst and obtained up to 36% C5-C9 range hydrocarbon fraction. Pour et al. (2008) reported a 26% C5-C11 selectivity for a Fe/ZSM-5 hybrid catalyst. Botes (2004) also studied the Fe-ZSM-5 hybrid catalyst in the dual bed reaction system. The C5-C11 selectivity was found to be about 35% for hybrid catalyst and 55% for dual bed system. The highest gasoline selectivity was reported by Martinez et al. (2008) for a Co - ZSM-5 hybrid catalyst as 62 wt. %. Compared with the studies cited above, a considerable higher gasoline range hydrocarbon selectivity (up to 74 %) was obtained in this study. Other important aspects of results of this study are that; the heavy hydrocarbon selectivity was quite low and the catalytic activities were

acceptable. It seems that the intrinsic properties of low acidity ZSM-5 zeolite combined with the regulated iron loading and operating temperature resulted in higher selectivity obtained in this study.

4.2.5 Effect of operating conditions on the performance of SFeZ9 catalyst

A systematic study was undertaken in order to investigate the effects of operating conditions on the performance of ZSM-5 supported iron based FT catalyst (SFeZ9) in the FT process. Since almost all of the catalysts tested at three different temperatures, the effect of the operating temperature on catalyst performance is given in preceding sections. In this part, the effect of operating pressure, feed hydrogen to carbon monoxide ratio (H_2/CO) and gas hourly space velocity (GHSV) were studied. Conditions for FT activity tests are given at Table 4.16.

A 260 h long time on stream performance test was also carried out with SFeZ9 catalyst in order to observe its stability.

Table 4.16 : Conditions for FT activity tests (effect of operating conditions).

Set	Pressure (bara)	H_2/CO ratio	GHSV (1/h)
1	8	2	750
2	12	2	750
3	15.5	2	750
4	19	2	750
5	22	2	750
6	19	1	750
7	19	1.5	750
8	19	2	750
9	19	2.5	750
10	19	2	450
11	19	2	600
12	19	2	750
13	19	2	900

Effect of Feed Gas Composition (H_2/CO ratio) on the Performance of Zeolite-Supported Iron Catalysts

The reactant gas composition, particularly the H_2/CO ratio of gas, can considerably affect the performances of the FT catalysts and consequently the properties of products produced by the FT synthesis. In order to investigate the effect H_2/CO ratio on catalysts, the SFeZ9 catalyst was representatively chosen and tested by using reactant gases of varying H_2/CO ratio. Results are presented in Figure 4.24, in which the activity of SFeZ9 catalyst was plotted as function of H_2/CO ratio in the feed stream. The CO conversion increased while that of H_2 decreased with increase in the H_2/CO ratio, as expected.

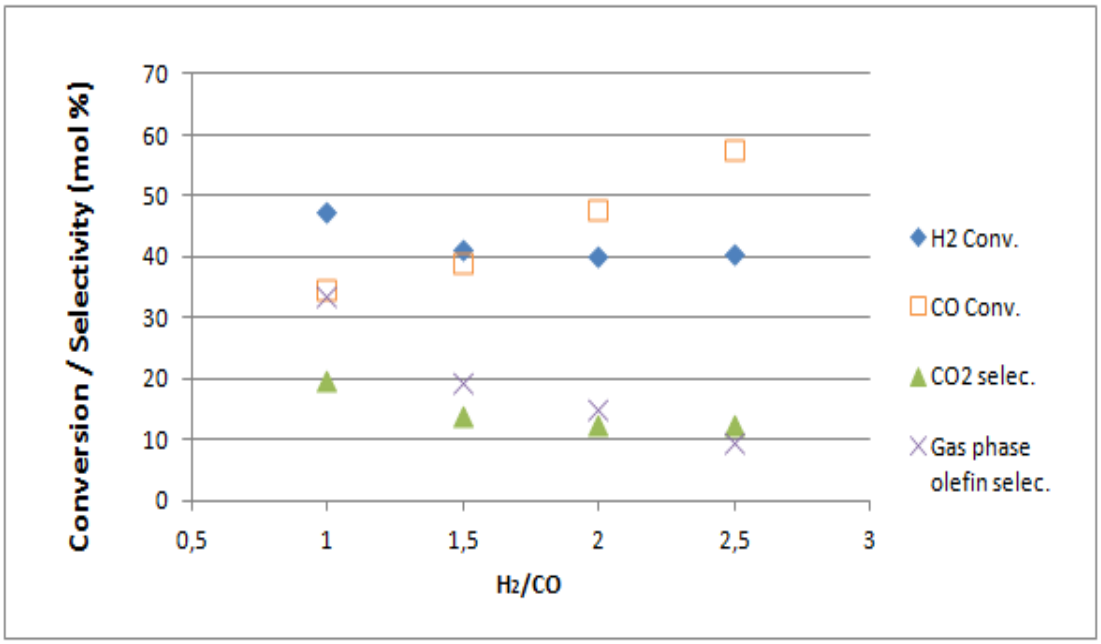

Figure 4.24 : Effect of H_2/CO ratio on the SFeZ9 catalyst activity in FT process (T=553 K).

It is well known that H_2 and CO coverage can have considerable impact on the selectivity of the FT catalysts. The analysis of gaseous hydrocarbon showed that higher H_2/CO ratios produced less olefinic products. This is due to the hydrogenation of olefins producing paraffins. These results are in good agreement with that reported for conventional iron based catalysts (Sarkari et al., 2011; Laan, 1999).

The CO_2 selectivity decreased with increasing H_2/CO ratio. The water gas shift reaction can be considered as an equilibrium reaction over iron catalyst above 523 K.

Decreasing CO and increasing H_2 shifted the reaction equilibrium towards reactants side, resulting in a decrease in the CO_2 selectivity.

Figure 4.25 shows the variation of hydrocarbon selectivity of SFeZ9 catalyst with the H_2/CO ratio. The catalyst selectivity tended to shift towards the lighter hydrocarbons (<C5) as H_2/CO ratio increased, as it may be expected. As the H_2/CO ratio increased, the lower CO partial pressure induces a lower adsorbed CO concentration, so that more H_2 can be adsorbed and dissociated. Due to the combined effect of slower chain growth steps caused by lower CO concentration and faster hydrogenation/chain termination steps resulted from higher H_2 concentration, catalyst selectivity shifted towards lighter hydrocarbons. The selectivity for C5-C11 hydrocarbon fraction followed an opposite trend, decreasing with increase in the H_2/CO ratio. Increasing of the H_2/CO ratio from 1 to 2.5 resulted in a ~30% drop in the C5-C11 hydrocarbon selectivity of the catalyst. The catalyst selectivity towards heavier hydrocarbon fraction (>C12), on the other hand, appeared not to be significantly affected by the H_2/CO ratio. Compared to its selectivity towards C1-C12 hydrocarbons, the catalyst selectivity towards heavier hydrocarbon (> C12) was considerably lower.

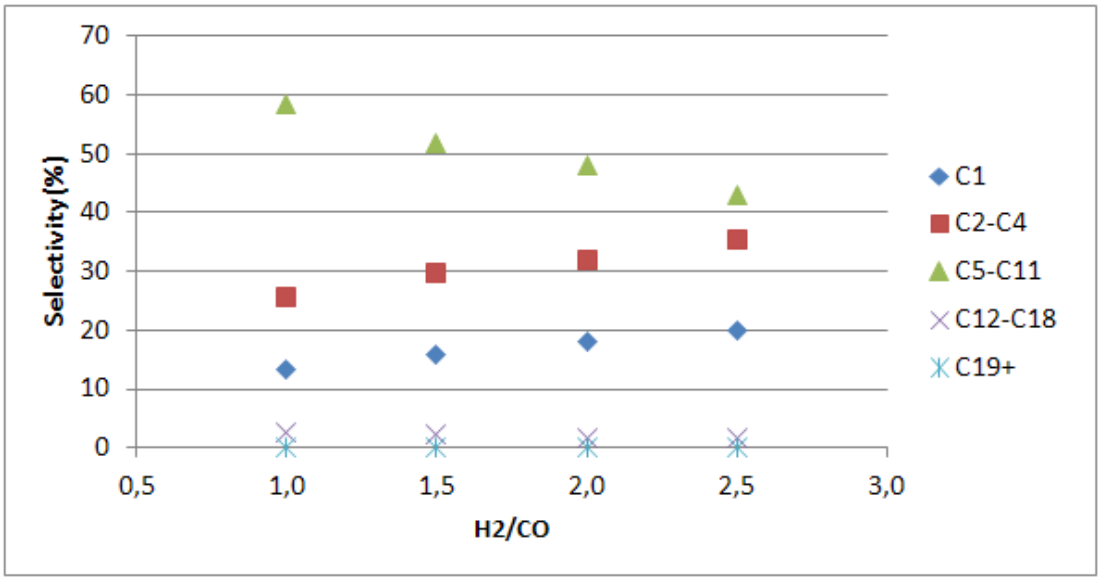

Figure 4.25 : Effect of H_2/CO ratio on the product hydrocarbon distribution for SFeZ9 in FT process (T = 553 K).

Effect of Pressure on the Performance of Zeolite-Supported Iron Catalysts

The effect of the operating pressure on catalyst activity and selectivity was studied for SFeZ9 catalyst by varying the pressure from 8 to 22.5 bars. Figure 4.26 shows the variation of the CO and H_2 conversions in FT synthesis catalyzed by SFeZ9 with pressure. In the pressure range considered the conversion of both gases increased with rising pressure, indicating that a more efficient FT synthesis process could be maintained at high pressures, but with higher operating cost. Increasing pressure from 8 bars to 22.5 bars resulted in a 13% and 16% improvement in the H_2 and CO conversion, respectively. These results are in line with general trend observed in the relationship between pressure and the FT conversion reported by others (Sarkari et al., 2011; Dry, 2002) and with predictions from the FT reaction rate equation given for Fe based catalysts in Section 2.4.3.

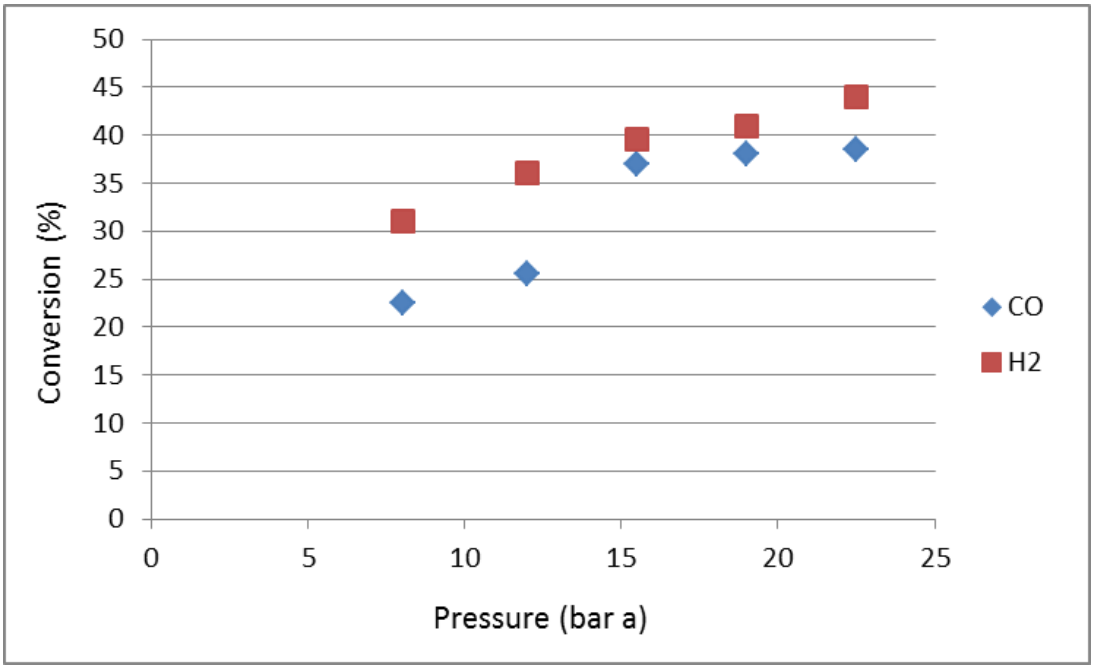

Figure 4.26 : Effect of pressure on CO and H_2 conversions of the FT synthesis by SFeZ9 catalyst (T=553 K).

The effect of pressure on product selectivity is seen in Figure 4.27. Experimental results showed that the catalyst selectivity towards all types of hydrocarbon were strongly affected by pressure, however, with diverse outcomes. The selectivity towards the higher hydrocarbons (C5+) sharply increased while the selectivity towards the lighter hydrocarbons (C1-C4) considerably decreased with increasing pressure. These results are also in good agreement with findings of others reporting that, in FT synthesis with iron based catalysts increasing the pressure results in a

decrease in methane production and an increase in the product average molecular weight (Anderson, 1980; Steynberg, 2004). The catalytic activity of the zeolitic component of the catalyst may also increase with increasing pressure, so that the shift towards the higher hydrocarbons might be retarded.

The effect of pressure on FT process selectivity was attributed to the condensation of hydrocarbons, that are normally in the gaseous state at atmospheric pressures (Anderson, 1980; Sarkari et al., 2011). Higher pressures and higher CO conversions would probably lead to saturation of catalyst pores by liquid reaction products forming a thin liquid hydrocarbons layer. A different liquid phase composition in catalyst pores at high syngas pressures could affect the rate of elementary steps and CO and hydrogen concentrations. As a result, before the reactants reach to the catalyst surface they have to diffuse through this layer, while the reaction products have to do the same thing in the opposite direction before being desorbed. It is well known that olefins, in contrast to the paraffins, can be readsorbed on the active sites, reinserted in the chain growth process, or can be hydrogenated to the corresponding paraffins. This phenomenon is used to explain the higher hydrocarbon selectivity at higher pressures for conventional iron based catalysts (Sarkari et al., 2011). Therefore, one of the reasons of having higher heavier HC selectivity is re-adsorption and oligomerization of olefins. But on the other hand, the diverse results reported in the literature, suggest that the relationship between olefin selectivity and the total pressure can be rather complex. Selectivity was found increasing in some cases and decreasing in others, with increase in the operating pressure (Laan, 1991).

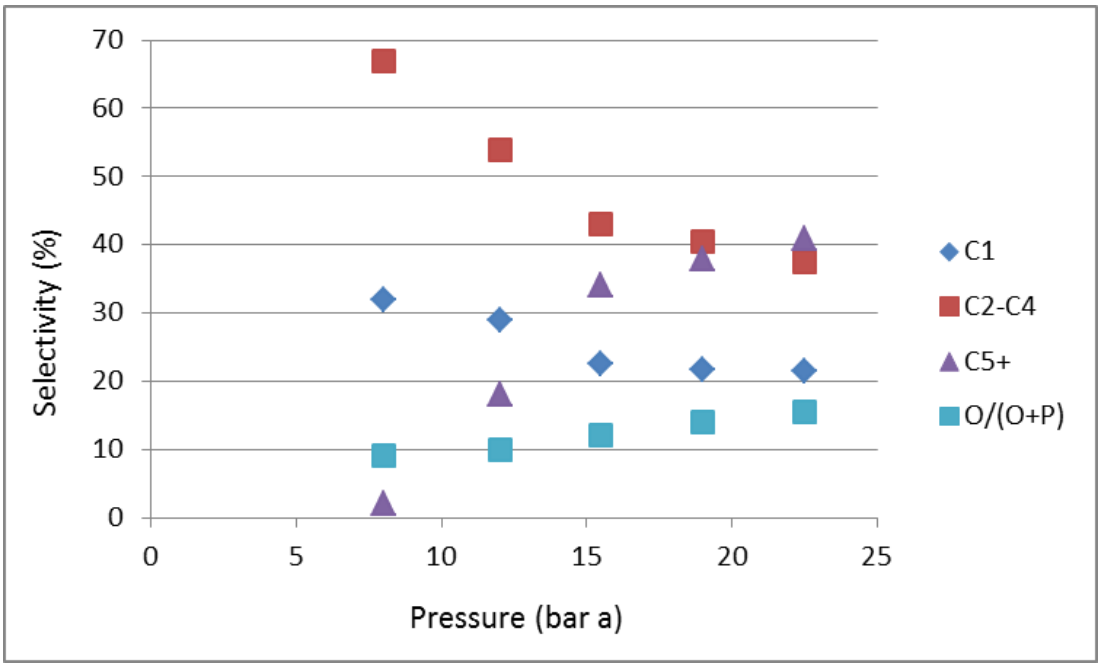

Figure 4.27 : Effect of pressure on the SFeZ9 catalyst activity in FT process (T=553K).

Effect of Space Velocity on the Performance of Zeolite-Supported Iron Catalysts

Results of experimemts carried out to investigate the effect of gas hourly space velocity (GHSV) on catalyst activity and selectivity are presented in Figure 4.29. The GHSV was varied between 450 – 900 h^{-1}. The minimum and maximum GHSV values were determined according to the limits of the mass flow controllers of the activity test system.

Since the amount of catalyst was kept constant during all experiments, the GHSV was changed by varying the syngas flow rate. As expected, the conversion of CO and H_2 declines with increased GHSV. It may be concluded that in this range of GHSV's the external mass transfer restriction is not very high.

Selectivity of the catalyst was hardly changed with changing GHSV. In the literature the relationship between space velocity and hydrocarbon chain length is described a complex phenomena. Bukur et al. (1990) measured no effect of the space velocity on the molecular weight of the hydrocarbons, while Iglesia et al. (1991) observed an increase of the average molecular weight of the products with decrease of the space velocity. They reported that, the selectivity towards methane decreases with a

decrease of the space velocity. As shown in Figure 4.29, the methane selectivity very slightly increased, while C5+ selectivity remained almost unchanged.

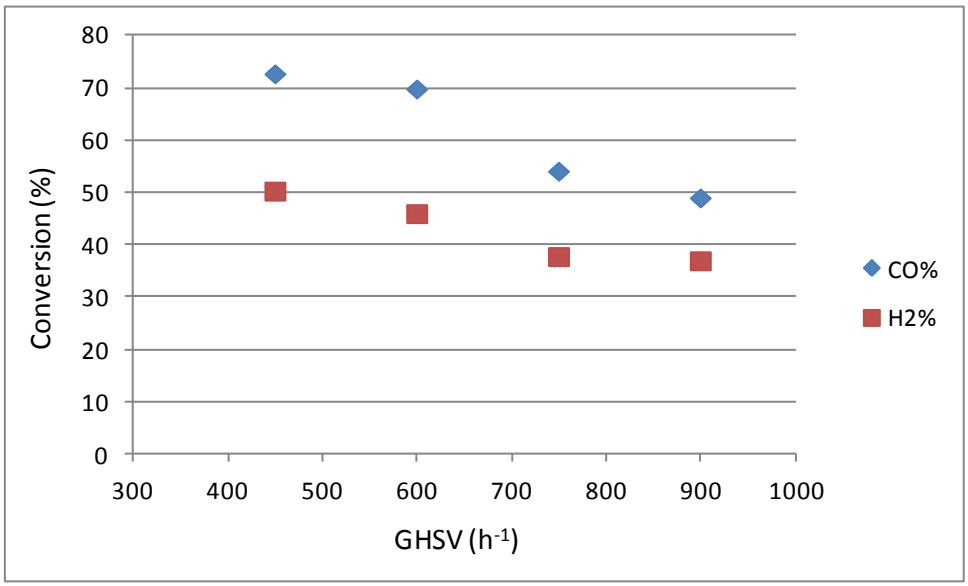

Figure 4.28 : Effect of GHSV ratio on CO and H_2 conversions of catalysts in FT process (T=553 K).

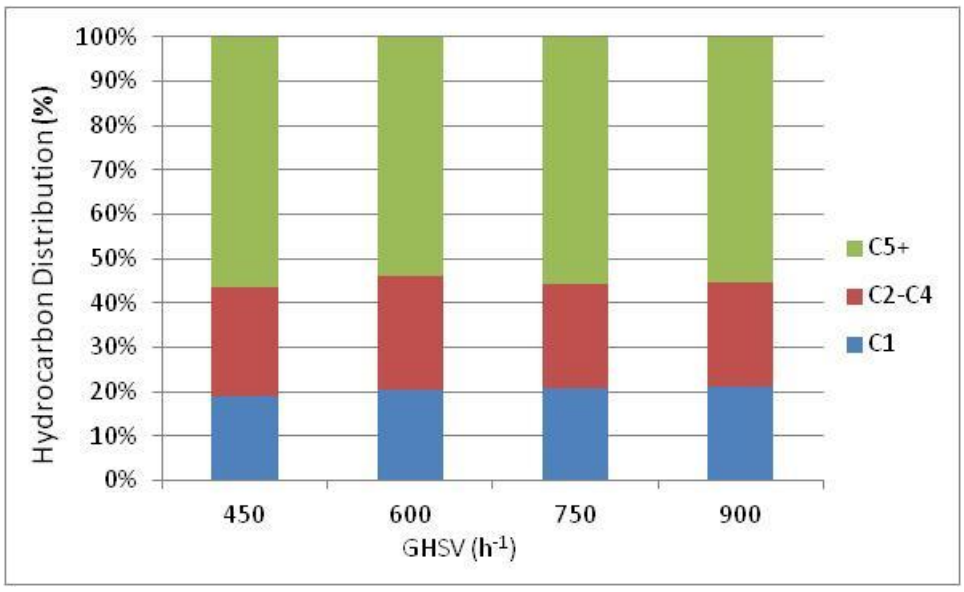

Figure 4.29 : Effect of GHSV on product hydrocarbon distribution for SFeZ9 in FT process (T=553 K).

Time On Stream Test

Change occurred in the catalytic performance of the catalysts over time is of crucial importance in respect of their stability/durability, economic life-time and economics of the FT process. Therefore, the synthesized catalysts need to be tested for their long-terms activities.

A 260 hour long time on stream performance test was carried out with SFeZ9 catalyst in order to observe its stability. The test conditions were : T= 553 K, P = 19 bara, GHSV = 750 h^{-1}, H_2/CO = 2. Test results are shown in Figure 4.30 and Figure 4.31. The catalyst appeared to be fairly stable in respect to CO and H_2 conversions, with no considerable activity losses. The CO and H_2 conversions were calculated to be around 46% ±4 and 40% ±4, respectively, along the course of the test. As seen from Figure 4.31, the isomer selectivity in the gas phase, which was an indication of zeolite activity for the reaction, maintained a steady profile at 20 % during the 260 hours operation. It then slightly decreased, indicating that zeolite activity might be gradually deteriorated with time after that point.

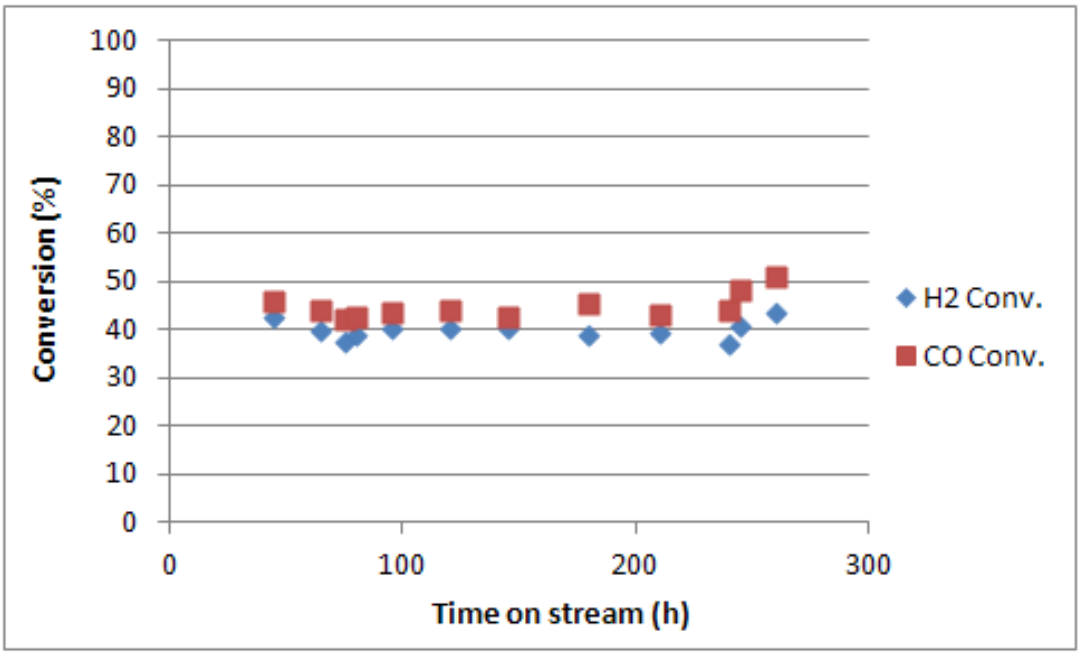

Figure 4.30 : Variation of SFeZ9 catalyst conversions with time on stream (T=553K, P=19bara, GHSV =750 h^{-1}, H_2/CO = 2).

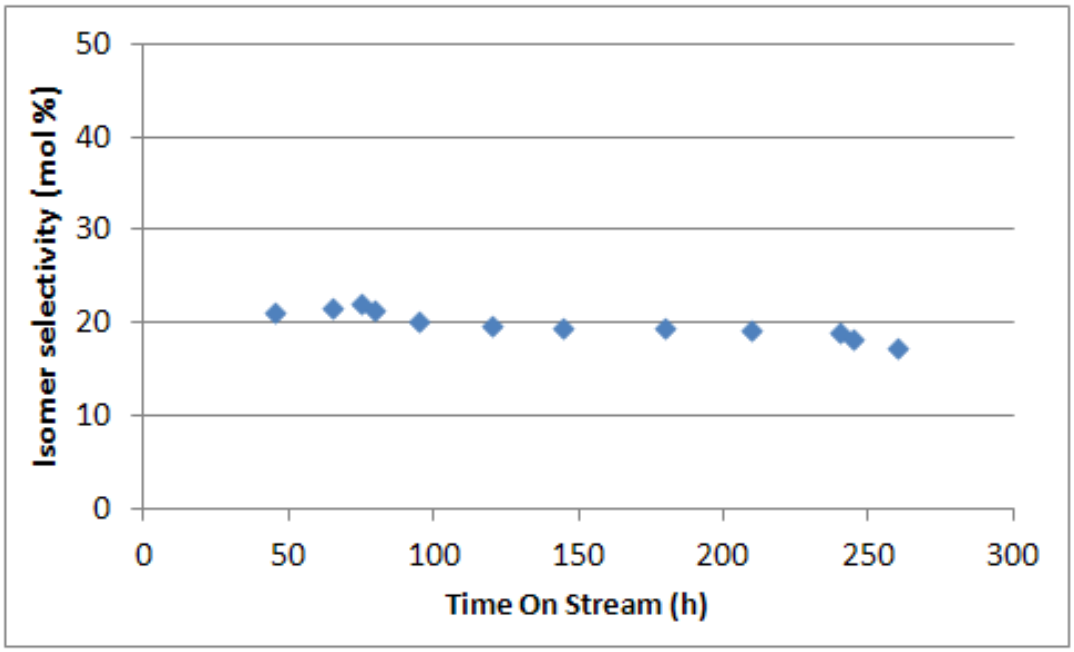

Figure 4.31 : Variation of gas phase isomer selectivity of SFeZ9 catalyst as a function of time on stream T=553 K, P=19 bara, GHSV =750 h^{-1}, H_2/CO =2.

5. SIMULATION OF COAL TO GASOLINE PROCESS USING BI-FUNCTIONAL FISCHER TROPSCH CATALYSTS WITHOUT PRODUCT UPGRADING

Conventional Fischer Tropsch reactor produces so called “syn-crude” containing a wide range of hydrocarbons. The primary FT products can be upgraded by using down-stream conversion units to increase the yield of the desired products. The well-known Anderson–Schulz– Flory (ASF) kinetics of the FT reaction imposes a limit to the selectivity for gasoline-range products. According to ASF model, the maximum selectivity can be 48% obtained (Botes and Bohringer, 2004). Using the Fixed Fluidized Bed reactors at about 340 °C with iron catalyst gives a maximum gasoline production, producing about 40% straight run gasoline (Dry, 2002). Waxes can be selectively hydrocracked to produce diesel fuel with a high cetane number and improved cold flow properties (Sie et al., 1991). Alternatively, FT waxes can be considered as a feedstock for catalytic cracking process to produce gasoline (Martinez et al., 2007). On the other hand, light olefins (propene, butene) can be oligomerized to gasoline (Botes and Bohringer, 2004). The product up-grading section can be regarded as a refinery which processes treated the FT syn-crude and produces liquid fuels and chemicals. Such an up-grading section is generally composed of a syn-crude fractionating unit, a hydrocracking unit, a catalytic (Pt/zeolite) reforming, and isomerization and oligomerization reactors (Liu et al., 2011; Botes and Bohringer, 2004). A hydrogen production system should also be installed to feed hydrocrackers and isomerization reactors. However, the overall complexity of gasoline production makes it less attractive than the diesel fuel option (Dry, 2002).

Above 95% of the transportation fuels is supplied by crude oil. More than 55% of the oil refined is used to produce fuels, especially gasoline and diesel (Sudiro and Bertucco, 2009). Due to the high demand on gasoline in the world and its higher price relative to that of diesel, production of gasoline from the FT process increasingly becomes attractive (Forghani et al., 2009). The direct production of

gasoline range hydrocarbons from Fischer Tropsch synthesis with high selectivity seems very ambitious, particularly, in respect to the catalyst and process development. These obstacles may be overcome by the use of metal/zeolite bi-functional catalysts (Zhang et al., 2010; Martinez et al., 2008; Botes, 2005; Li et al 2005), which can enhance the selectivity of the synthesis towards the gasoline range hydrocarbons, combined with a proper and efficient process design. In the FT process by these catalysts, the active metal (i.e. iron) phase catalyzes FT products that are consisted of a wide range of hydrocarbons. These first products are then converted into gasoline-range products through various mechanisms such as hydrocraking, olefin oligomeration, branching, etc. that are induced by the zeolite component of the catalyst. On the other hand, the formation of heavy hydrocarbons is considerably hindered by zeolite due to their shape selectivity properties (Baranak et al., 2013). Therefore, by using bi-functional catalysts high molecular weight (mw) hydrocarbons (> C15) production could substantially be hindered while gasoline range hydrocarbons selectivity is significantly enhanced.

Depending on the various characteristics of this type bi-functional catalysts, the process scheme and operating conditions need be different to some extent than that of FT using conventional catalysts. The main goal of the Fischer Tropsch process utilizing metal – zeolite bi-functional catalyst would be high gasoline yield with a relatively simpler process and lower investment cost. In case of such a system, the product upgrading section may be almost eliminated, because of the low catalyst selectivity towards long chain HCs.

On the other hands, the light HCs (C1-C4) selectivity of bi-functional catalysts are similar that of conventional catalysts (Nowicki et al., 2001; O'Brien et al., 1997). Bi-functional catalysts can generally produce even more light HCs (Baranak et al., 2013; Pour et al; 2009). Moreover, catalytic activities of these catalysts were found to be generally and considerably lower than that of the conventional catalysts (Baranak et al; 2013). The higher light hydrocarbon selectivity and lower catalytic activity are the major drawbacks for the bi-functional catalysts, which may be overcome through various modifications in and optimization of the process. There are a lot of studies done on zeolite containing bi-functional FT catalysts, including supported catalysts (Bengoa et al., 2002; Calleja, 1991), hybrid catalysts (Liu et al., 2005; Botes, 2005), capsule catalysts (Li et al., 2009; Yang 2007). Good results of

high gasoline selectivities and catalytic activities are published. Martinez and Lopez (2005) have attained selectivity of 50 - 80% for gasoline range HC (C5-C12) via a hybrid catalyst prepared by physically mixing a K-Fe-Co catalyst and HZSM-5 zeolite. Li and coworkers (2009) reported an app. 70% selectivity for gasoline range hydrocarbons, almost without high molecular weight hydrocarbons (>C15) with a "capsule catalyst". On the other hand a number of studies were also carried out on process simulation and optimization of conventional FT process (Sudiro and Bertucco, 2009; Forghani, 2009; Liu et al., 2011; Kim et al., 2009; Bao et al; 2010; Trippe et al., 2011). Liu et al. (2011) have done detailed performance and cost analyses of fuel synthesis from coal and biomass feed stocks via conventional FT process. Forghani (2009) studied integration of a permselective membrane to the FT reactor using bi-functional catalysts to increase gasoline yield. Bao (2010) studied simulation, integration, and economic analyses of gas-to-liquid processes with a specific emphasis given to heat and mass integration (tail gas and water management). Sudiro and Bertucco (2009) investigated the integration of Gas-to-Liquid (GTL) – Coal-to-Liquid (CTL) processes to minimize the CO_2 emissions from them, via using the CO_2 produced by CTL process in the GTL dry reforming. But, to our best knowledge, no study dedicated to process simulation/optimization of CTL or GTL processes utilizing bi-functional FT catalysts have been reported in the literature.

In this study, a process simulation study for a Coal to Gasoline (CTG) FT process using zeolite containing bi-functional FT catalyst has been realized. The ASPEN HYSYS software® has been used as the simulation tool for mass/energy balance and thermodynamic equilibrium calculations. In the study, a process composed of coal gasification, gas cleaning, Fischer Tropsch reactor and a steam reformer reactor unit was considered. The product up-grading section is totally eliminated in this study. The critical operating parameters were defined and their effects on the system performance were investigated. The main of the study goal was to maximize the yield of gasoline range HCs.

5.1 Process Description

Coal-to-liquid processes (CTL) mainly consist of four steps: 1.synthesis gas (syngas) production, 2. syngas purification, 3. Fischer Tropsch (FT) Synthesis, 4. product up-

grading. In this study, by using a zeolite containing FT catalysts, with the aim of gasoline production, the product upgrading section was eliminated based on the favorable catalytic properties of these catalysts. A recycle line and a reformer reactor were integrated into the process aiming to recycle and converted the tail gas from the condensing unit at downstream of FT reactor into syngas which then can be fed to FT reactor. The block diagrams of the conventional indirect Coal to Liquid Process (CTL) and the modified process proposed in this study are given in Figure 5.1 and Figure 5.2, respectively. The major units of CTL process are briefly described below.

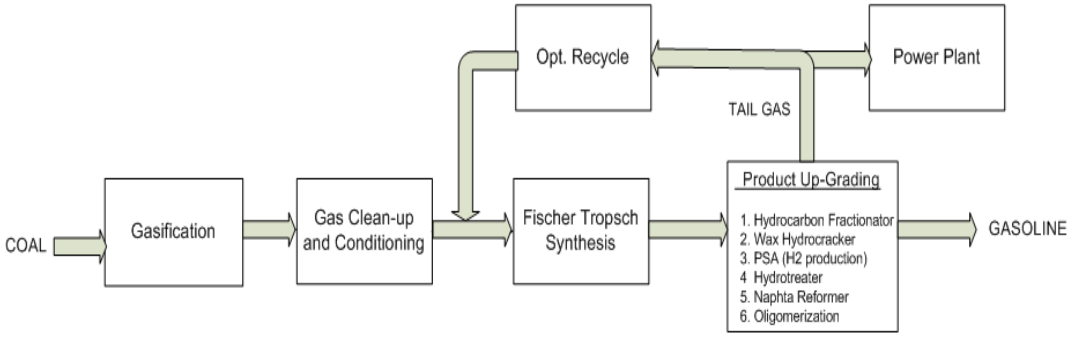

Figure 5.1 : Block Diagram of gasoline production by conventional indirect CTL process.

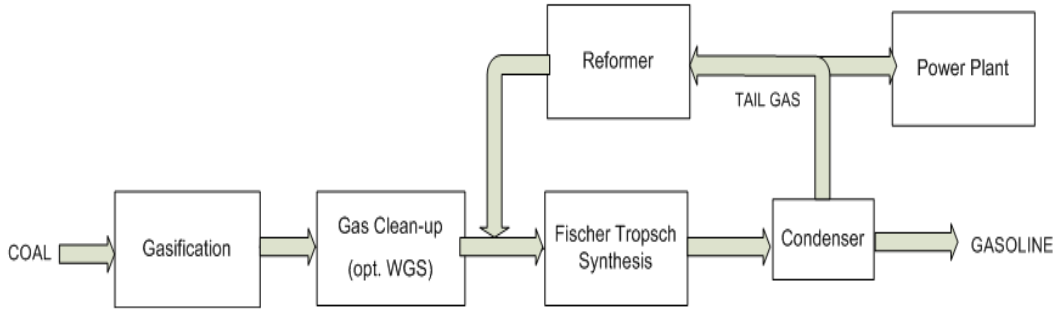

Figure 5.2 : Block Diagram of gasoline production by CTL process using bi-functional FT catalysts.

Gasification unit. Gasification reactor converts the coal feedstock to syngas by process in which coal is gasified under gasifying agent with sub-stoichiometric oxygen at elevated temperature and pressure. In the simulation, a fluidized bed oxy gasifier was involved in the process. This type of gasifiers is particularly suitable for the gasification of low grade coals (Karatas et al., 2013). The gasifier was operated in

the 800-950 °C temperature range at 20 bar pressure. Compared to entrained flow gasifiers, fluidized bed gasifiers provide lower carbon conversions but superior energy efficiencies due to their lower effluent gas stream temperature which results in a lower sensible heat loss.

Syngas Purification. Synthesis gas from gasifier contains various impurities/contaminants/poisons including particulate matters, tar, NH_3, sulfur compounds (H_2S, COS etc.) which needed to be substantially reduced or almost totally removed before it is introduced to the catalytic reactors in the process. This is accomplished via a gas cleaning section. The gas cleaning section, considered in this study, consisted of a granular filter, a metallic filter and a water scrubber unit. Syngas from gasifier fist is fed to the filters where particulate matters are removed. Then it proceeds to the water scrubber unit which removes tar, NH_3 and other water soluble contaminants and the fine particulates escaped from filters. The commercial Rectisol® process downstream of water scrubber removes H_2S, COS, CO_2 and NH_3 from the syngas. The Rectisol process is able to reduce the amount of sulfur compounds and other impurities down to the ppm levels and can operate at elevated pressures. The major disadvantage of this process is its high electricity consumption (Mondal et al., 2011).

Oxygen Supply Unit. A cryogenic Air Separation Unit (ASU) was used to supply pure oxygen needed for gasification of the coal. A high purity oxygen is required to minimize the inert gas build up in the systems involving gas recycling. ASU is one of the most intensive energy consuming units of the process.

Gas Conditioning. A water gas shift (WGS) reactor was used to adjust the hydrogen to carbon monoxide (H_2/CO) ratio of the syngas before it is introduced to the FT reactor which requires a to stoichiometric consumption ratio of approximately 2 (Dry, 2002). The H_2/CO ratio of the syngas from oxy-gasifiers is generally about 0.5 (Nieto et al., 2008). The FT catalysts, such as conventional iron-based ones, that are also active in WGS reaction, can be used for the processing of syngas with H_2/CO ratios lower than stoichiometric levels. On the other hand, bi-functional iron based FT catalysts are reported to be having much lower WGS activity compared with the conventional iron-based catalysts (Li et al., 2009; Baranak et al., 2013; Aydinoglu et al., 2012). Therefore, a separate WGS reactor is needed to be involved prior to the FT reactor in order to enhance the overall syngas conversion. In the simulation

studies, a sour WGS reactor which can tolerate high sulfur concentrations was considered (Hla et al., 2011; Gul et al., 2010). The application of sulfur-resistant sour shift catalysts could significantly simplify the process scheme of coal-based syngas production by the removal of acid gases (H_2S and CO_2) in one step by means of absorption methods, e.g. Rectisol after shift reactor (Antonaik et al., 2012).

FT Reactor. The FT reactor is the core of the whole process. The gasification, the gas cleaning/conditioning and the product up-grading sections are designed and configured according to this reactor. A wide range of hydrocarbons may be produced in the conventional FT reactor. The product distributions from conventional FT catalysts are generally well correlated with so called the "*Anderson Schulz Flory*" (ASF) distribution. The hydrocarbons products obtained from conventional FT reactors can have a wide spectrum, ranging from C1 to C40 or even higher. On the other hand, the ASF distribution does not match with the distribution of products produced by using bi-functional catalysts. It is reported in the literature that the FT products obtained with a zeolite containing bi-functional catalyst are generally very rich in the C5-C11 range hydrocarbons (Zhang et al., 2010; Martinez et al., 2008; Bengoa et al., 2002; Botes, 2005; Calleja et al., 1991). On the contrary, selectivity of these catalysts towards heavy hydrocarbons is very low. The variation of product distribution with the chain propagation probability (α) is given in Figure 5.3. In the figure, the distribution of FT product we obtained from our experimental FT synthesis studies using a zeolite containing iron based catalyst, designated as SFeZ18, is also involved (Baranak et al., 2013).

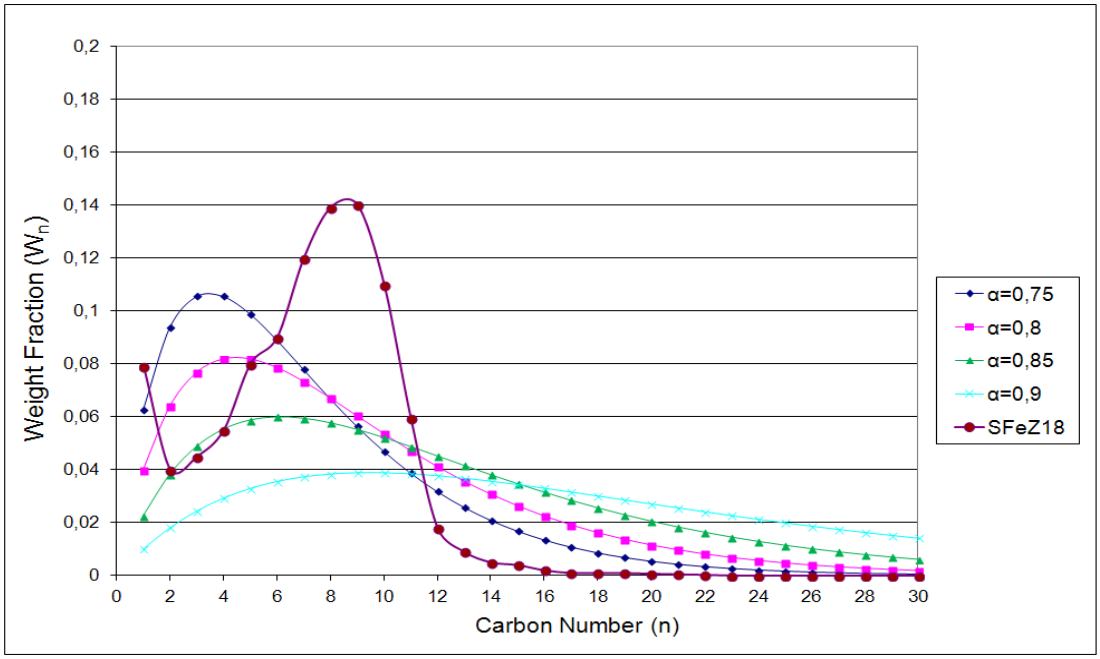

Figure 5.3 : Variation of product distribution of FT products obtained from ASF model (α=0.75 - 0.9) and a zeolite containing iron based catalyst.

Compared to the conventional catalysts, the catalytic activity of the bi-functional catalysts are lower but they generally exhibit higher selectivity for un-wanted light hydrocarbons. A recycle line and a reformer reactor were used in the simulated process in order to overcome these drawbacks. The FT outlet gas was processes and recycled back to the FT reactor in order to increase the overall syngas conversion. The proposed process scheme is shown in Figure 5.4 .

Reformer Reactor. A steam reformer reactor (SR) was integrated into the process to re-convert light gaseous hydrocarbons (C1-C4, the tail gas, synthesized in the FT reactor into the syngas which was to be recycled back to the FT reactor. The conversion of light hydrocarbon is realized through reactions between them and steam represented by reaction 5.1. This reaction is highly endothermic and accompanied with the WGS reaction.

$$C_nH_m + {}^{n}/_{2}\, H_2O \rightarrow nCO + \left(n + {}^{m}/_{2}\right)H_2, \text{ (for } CH_4\text{; } \Delta H = -205.3 \text{ kJ/mol)} \quad \textbf{(5.1)}$$

A compressor was used to overcome pressure drop through the FT reactor. Reformer syngas yield depends tightly on the reformer pressure. Therefore, in some cases the recycle pressure was designated differently from the FT outlet pressure. A turbine was placed in the tail gas recycle line just before the reformer reactor in order to recover the mechanical energy of the tail gas.

In the scope of the study, three different coal-to-gasoline (CTG) process alternatives have been simulated and evaluated.

1. *Coal –to-Liquid (Once-through FT) process* (CTL-OT) . In this process option there is no tail gas recycling.
2. *Coal-to- Liquid Process with tail gas recycling* (CTL-RC). This is modified process involves recycling of the tail gas from FT reactor aiming to increase the total syngas conversion
3. *Coal-to- Liquid Process with tail gas recycling and Processing* (CTL-RC-SR). This process includes both tail gas recycling and a steam reformer reactor to catalytically convert the tail gas into syngas which fed to FT.

These processes are schematically shown in Figure 5.4.

5.2 Technical Approach and Process Simulation

The ASPEN HYSYS® chemical process simulation software was used to develop process models. Material and energy balances were accounted for and solved for each process. Thermodynamic properties of streams were calculated by using the Peng Robinson State Equation. Process was simulated based on a 25,000 bbl gasoline/d (116.5ton gasoline/h) plant capacity. The simulation flow diagram of CTL_RC_SR process, most complex process alternative, is given in Figure 5.5.

Coal feed to the gasifier was simulated as a mixture of C, H, N, O, S, ash and moisture. Properties of the coal used, which represents one of the largest lignite reserves in Turkey, namely Soma, are given in Table 5.1**.** Its elemental analysis indicates that it may be classified as a low grade coal.

Table 5.1 : Elemental analysis of coal used in the gasification.

	%
Ash	24.61
Moisture	13.75
C	45.20
H	2.84
O	11.50
N	0.94
S	1.16
LHV	3773 kcal/kg

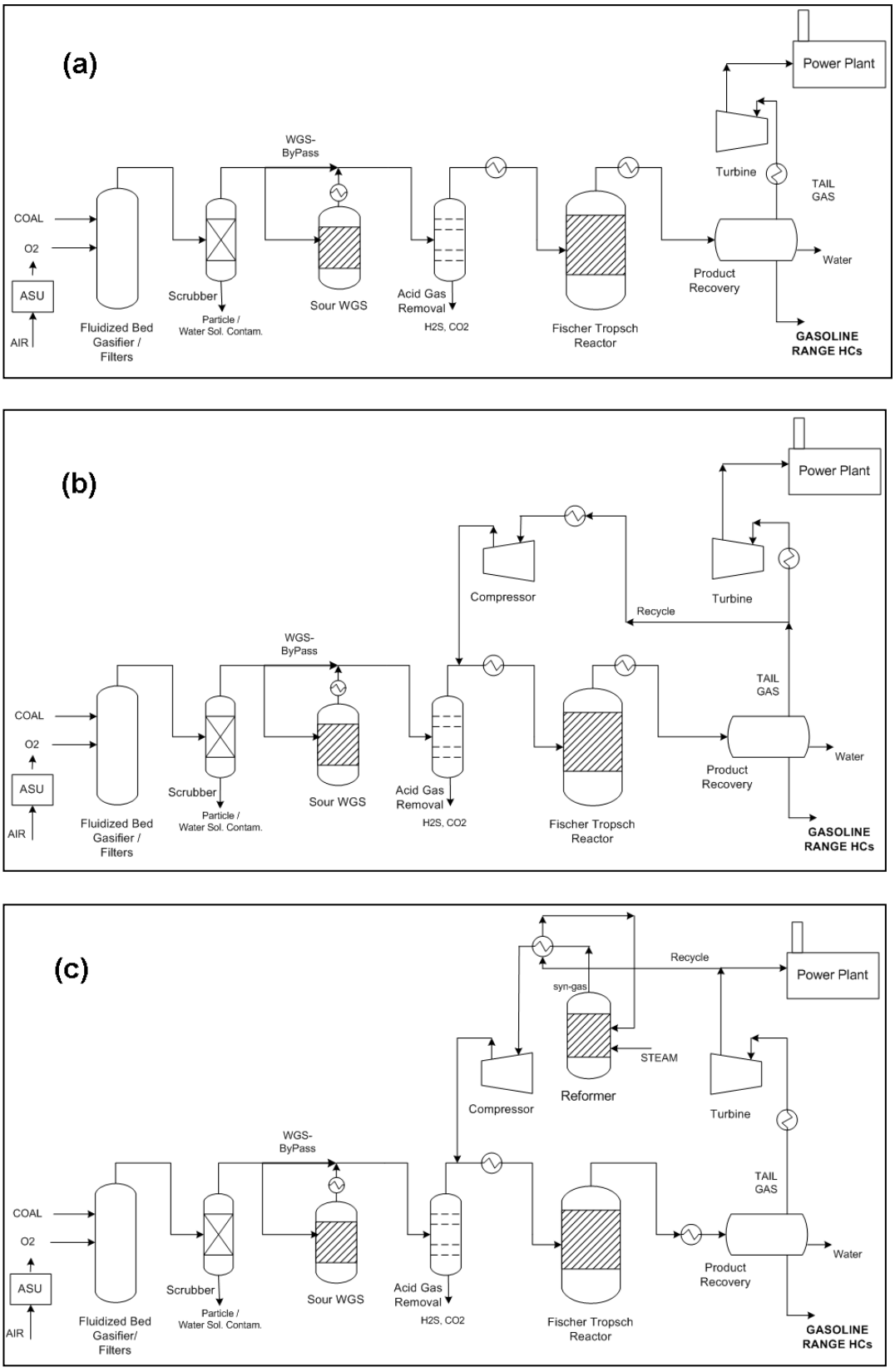

Figure 5.4 : Configurations of coal-to-gasoline processes simulated, (a) CTL-OT, (b) CTL-RC, (c) CTL-RC-SR.

A gasifier could be modeled as an adiabatic, equilibrium reactor with a reasonable accuracy (Gul et al., 2010). Therefore, in this study the gasifier was modeled in this manner. The O_2 stream fed to the gasifier was adjusted to keep the gasifier temperature at 850°C. Its operating pressure was 20 bara. The carbon conversion in the gasifier was fixed to 95%, and 1% of the heat load of the gasifier was assumed lost (Gul et al., 2010). The ASU section was modeled as a separator producing high purity oxygen (99.5% molar) with a 576 kJ/kg O_2 power consumption (Trainer et al., 2009).

The raw syngas coming from the gasifier enters to water scrubber following filters. The outlet temperature of the water scrubber was set to 175 °C. The acid gas removal unit (Rectisol) was modeled as a simple separator, removing 98% of the CO_2 and all sulfur compounds (H_2S, COS) from the gas stream. Its total electricity consumption was taken 0.512 kWh per kmol syngas; 0.329 kWh for refrigeration and 0.183 kWh for other needs (Bell et al., 2011). This consumption figure is in a good agreement with that reported by Liu (2011).

WGS reactor was assumed to be an adiabatic reactor having thermodynamic equilibrium and the WGS reaction was only the reaction (Eq. 5.2) considered. The reactor effluent temperature was set to 427°C. Since this reactor was downstream of the water scrubber, no extra steam injection was needed for the WGS reaction. A by-pass line, upstream of the reactor, was used to keep the molar H_2/CO ratio of gas stream fed to the FT reactor at 2.0.

WGS reaction: $CO + H_2O \leftrightarrow CO_2 + H_2$ (ΔH=-41,1 kJ/mol) **(5.2)**

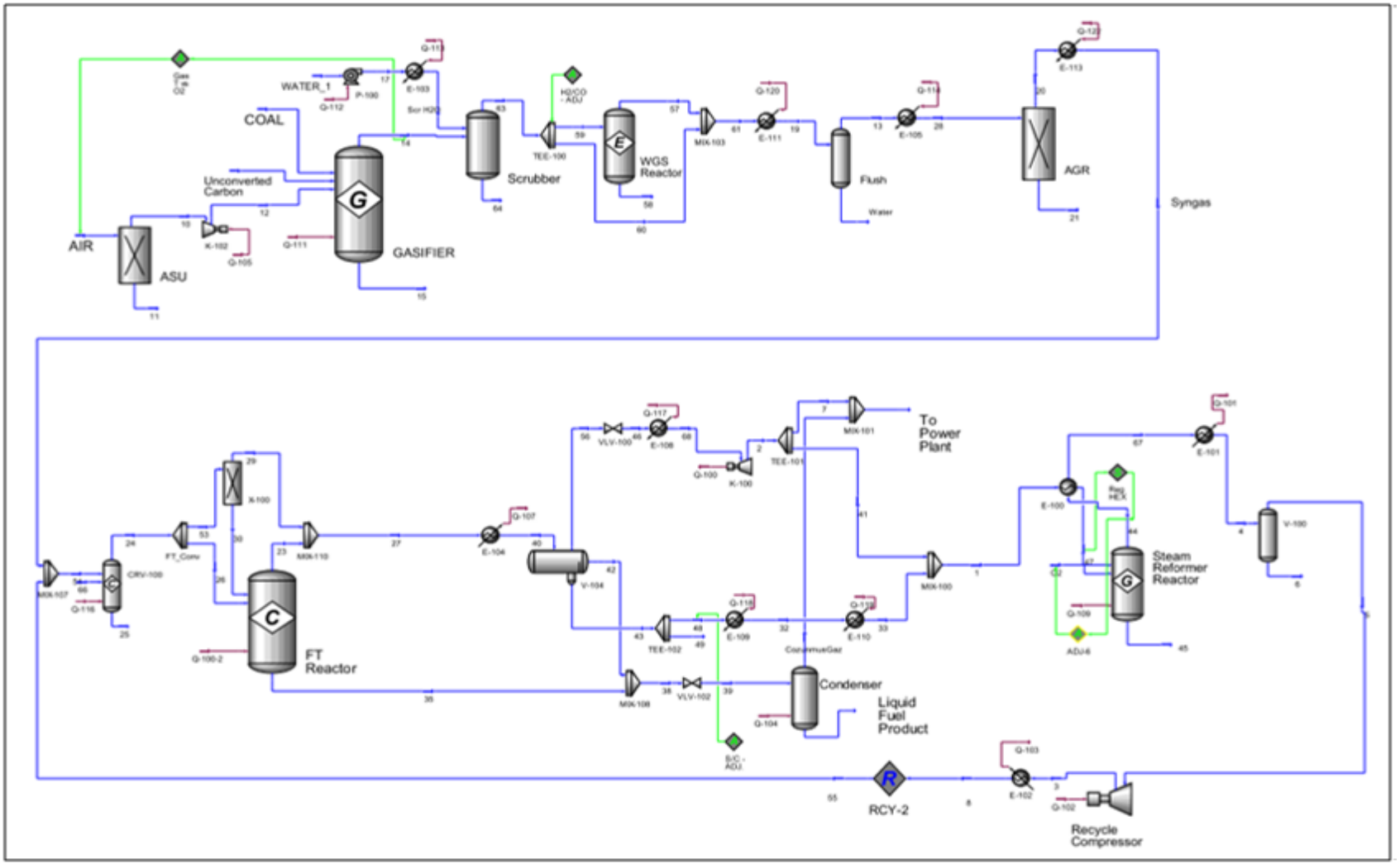

Figure 5.5 : The simulation flow diagram of the CTL_RC_SR process (ASPEN HYSYS®).

The FT reactor was modeled as a "conversion reactor". This type of reactor converts reactants into product species with a given selectivity and an overall conversion. Thirty one different reactions were defined in the reactor, one for WGS and the rest for C_1-C_{30} hydrocarbon production. All hydrocarbons were assumed to be n-paraffins. The FT reactions can be regarded as hydrogenation of carbon monoxide which may be expressed by the following global reaction (Dry, 2002; Kim et al., 2009):

FT reactions: $nCO + 2nH_2 \rightarrow \ -(CH_2)_n- + nH_2O, \ (\Delta H \approx 165 \text{ kJ/mol})$ **(5.3)**

The syngas conversion and the product selectivity data used in the simulation were obtained experimentally and given at Section 3. The catalyst was a bi-functional zeolite supported iron based type containing 18 wt.% iron (SFeZ18). Its CO conversion and the CO_2 selectivity were found to be 72,4 % and 9 wt.%, respectively. The product distribution obtained from the catalyst is given in Figure 5.6. The gasoline range hydrocarbons (C_5-C_{11}) accounted for 74 wt.% of the total hydrocarbon products which is consistent with finding cited in literature (Li et al., 2009; Yang et al., 2007). The operating conditions of FT reactor were: T = 280 °C, P = 20 bara, the inlet gas H_2/CO ratio = 2.0, pressure drop through the reactor = 2.0 bar.

An equilibrium model reactor (Gibbs reactor) has been used to simulate the steam reforming reactor. The tail gas from the FT reactor and steam were fed to the reformer reactor. Steam reformer needed high temperature heat supply which was met by the combustion of a certain portion of tail gas. The steam flow rate into the reactor was determined by the steam to carbon ratio (S/C). S/C ratio was defined as the molar ratio of the steam fed to the SR to the total amount of the carbon, including all hydrocarbons and CO, in the inlet stream. The reactor outlet temperature and the S/C ratio were taken as 850 °C and 1.0, respectively, for the base case. Reactions of all of the hydrocarbons present in the gaseous phase (C1-C6) are covered in the simulation (Eq. 5.1).

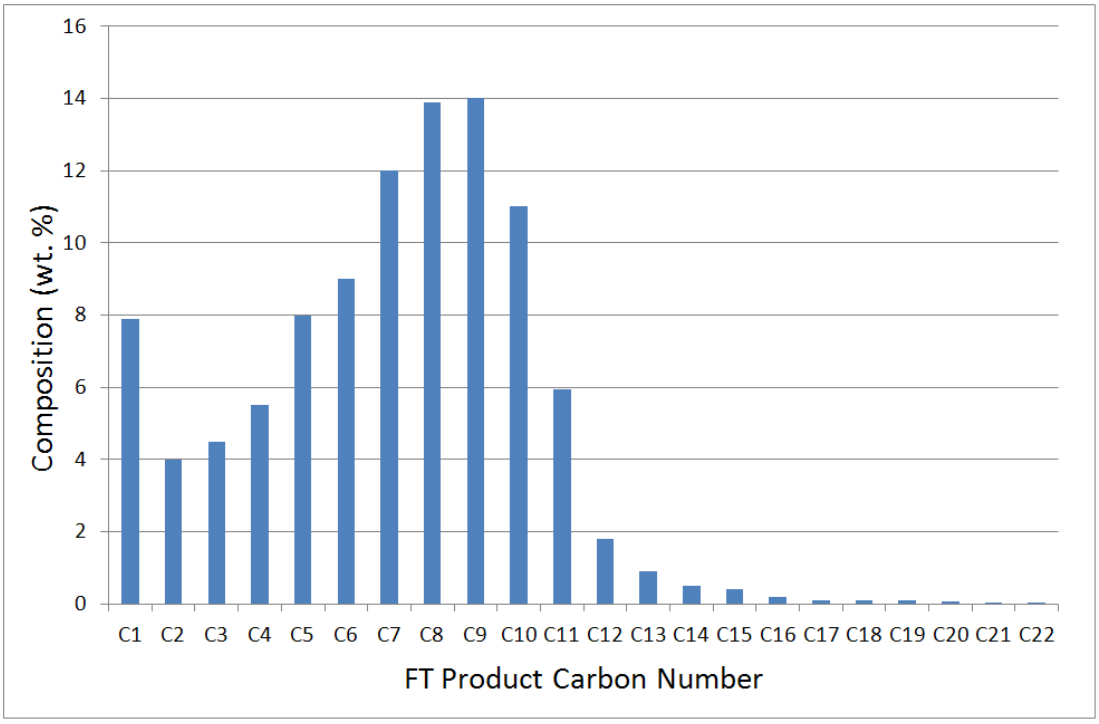

Figure 5.6 : Composition of product obtained from FT process with a bi-functional zeolite-supported iron catalyst (SFeZ18).

Process heat integration and optimization were not included in the scope of the study. However, the balance between heat generation and consumption, on quantity and quality (temperature level) basis, was taken into consideration. In the process there is a need for high temperature heat supply for SR inlet stream, SR reactor and turbine inlet stream. A recuperative heat exchanger was used to heat up the SR inlet stream by the SR outlet stream. The turbine inlet stream was heated to the desire temperature via the WGS reactor outlet stream. In both heat exchangers the minimum temperature approach was taken as 15 ^{o}C. As previously stated, the heat needed for endothermic SR reactor was supplied through combustion of the tail gas. Apart from these, the process generates net waste heat, and the heat needs of the process could be supplied by heat generated within the system itself, for example from FT reactor at 280 ^{o}C. The surplus low temperature heat sources were not considered for electricity generation.

Electricity was produced by the turbine (expander) and a power plant fueled by the tail gas. Tail gas stream was heated before introducing to turbine in order to increase its electricity production. Turbine adiabatic efficiency was assumed to be 90% (Zhanga and Lior, 2008). On the other hand, the power plant was envisaged as a

combined cycle power plant (gas turbine plus steam cycle) with a gross thermal electrical efficiency of 55% (LHV basis).

The gas cleaning unit (Rectisol®), the recycling compressor, ASU, the oxygen compressor and several pumps are electricity consumer units. A compressor was needed in the recycling line to rise the tail gas pressure to that of FT reactor. Adiabatic efficiencies of these turbo machinery were assumed to be as follows; O_2 compressor: 75%, recycle compressor: 88%, pumps: 85% (Zhanga and Lior, 2008).

Critical operating parameters were determined and their effects on the process have been investigated parametrically. The recycling ratio, the recycling pressure, the steam reforming S/C ratio, the reformer temperature and the FT reactor conversion/selectivity were addressed as the main critical operating parameters. The main operating parameters of the base case, their low and high bounds are tabulated in Table 5.2.

Table 5.2 : The main operating parameters and their low and high bounds.

Operating parameters	Base Case	Low Bound	High Bound
Recycle Ratio (-)	0.8	0.5	0.9
SR Temperature (°C)	850	700	1050
Recycle Pressure (kPa)	500	250	1500
Steam reformer S/C (-)	1	0,12	2.25
$X_{FT,CO}$ (%)	72.4	50.0	90.0

Four different performance criteria were taken into account in the simulation of the process.

1. The gasoline production efficiency ($\mu_{th,gas}$) is the ratio of energy of the product to the energy of the coal fed to the system (Eq. 5.4).

$$\mu_{th,gas.} = \frac{LHV_{Gasoline}.\dot{m}_{Gasoline}}{LHV_{Coal}.\dot{m}_{Coal}} \quad \textbf{(5.4)}$$

where, LHV = lower calorific value of gasoline, m = mass.

2. *The process electrical efficiency* ($\mu_{th,elec}$) is defined as the ratio of the produced electrical energy to heating value of the coal feedstock (Eq. 5.5).

$$\mu_{th,elec.} = \frac{W_{elec.}}{LHV_{Coal}.\dot{m}_{Coal}} \quad \textbf{(5.5)}$$

where, $W_{elec.}$ = the amount of electricity.

3. *The total efficiency* (μ_{tot}) is the sum of the electrical and the gasoline production efficiencies (Eq. 5.6).

$$\mu_{tot.} = \mu_{th,gas.} + \mu_{th,elec.} \quad \textbf{(5.6)}$$

where, $\mu_{th,elec.}$= electrical production efficiency, $\mu_{th,gas.}$= gasoline production efficiency

4. *Carbon efficiency* (μ_C) is the ratio of amount of carbon in the gasoline to the amount of carbon in the coal feedstock (Eq. 5.7).

$$\mu_C = \frac{\dot{m}_{C,gas.}}{\dot{m}_{C,Coal}} \quad \textbf{(5.7)}$$

where $m_{c,gas.}$ = mass of gasoline, $m_{c,coal}$ = mass of caoal.

Conversions in various units of the process used in the simulation are described below. The FT reactor conversion and overall process conversion were calculated on the CO basis.

FT reactor conversion ($X_{FT,CO}$) is the molar ratio of the un-converted CO in the FT outlet stream to that of FT inlet stream (Eq. 5.8).

$$X_{FT,CO} = \frac{F_{CO,FTin}}{F_{CO,FTout}} \quad \textbf{(5.8)}$$

Where, $F_{CO,FTin}$ = the molar flow rate of the un-converted CO in the FT inlet stream, $F_{CO,FTout}$ = the molar flow rate of the un-converted CO in the FT outlet stream,

Process overall CO conversion ($X_{TOT,CO}$) is defined as the molar ratio of the un-converted CO in the power plant feed stream to the CO in the clean syngas stream (Eq. 5.9).

$$X_{TOT,CO} = \frac{F_{CO,PowerPlantIn}}{F_{CO,AGRout}} \quad \textbf{(5.9)}$$

where, $F_{CO,Power\ plant}$ = the molar flow rate of the un-converted CO in power plant feed stream, $F_{CO,AGRout}$ = the molar flow rate of the CO in the clean syngas stream.

Steam reforming conversion ($X_{SR,C}$) is the ratio of amount of carbon in the steam reforming reactor inlet stream to that of its outlet stream (Eq. 5.10). In this definition carbon means carbon which is contained by hydrocarbons.

$$X_{SR,C} = \frac{F_{C_{HC,SRout}}}{F_{C_{HC,SRin}}} \quad \textbf{(5.10)}$$

where, $Fc_{HC,SRout}$ = the amount of carbon in the stream reforming reactor inlet stream, $Fc_{HC,SRin}$ = the amount of carbon in the stream reforming reactor outle stream.

The recycle ratio (R_{rcyl}) was defined as the ratio of the recycle stream flow rate to that of the FT reactor **outlet** stream after condenser just before recycling.

$$R_{rcyl} = \frac{F_{\textbf{tail gas,rcyl}}}{F_{\textbf{tailgas,FT}}} \quad \textbf{(5.11)}$$

where, $F_{tailgas,rcyl}$ = the flow rate of recycled tail gas, $F_{tailgas,Ft}$ = the flow rate of tail gas from the FT reactor.

5.3 Results and Discussion

This section presents the results of the simulation study of Coal-to-Gasoline process alternatives mentioned above. The results obtained for three process schemes were compared based on the gasoline production, electrical efficiencies and other main process performance indicators. Furthermore, the effects of selected operating parameters on the process efficiencies and operation were systemically investigated.

The up-grading section of a conventional CTL gasoline production process is generally composed of a syn-crude fractionating and hydrocracking units, catalytic (Pt/zeolite) reforming and isomerization and oligomerization reactors (Dry, 2002; Liu et al., 2011). In the proposed process schemes, the product up-grading section was involved due to the composition of the raw syn-fuel produced from FT synthesis using bi-functional catalysts. Studies by Boerrigter at al. (2008) indicated that the cost of the product up-grading section can make up 15% of the total investment cost of a plant producing fuel from biomass. The gasoline production process without an up-grading section proposed in this study is not only simplified and more compact but also has a considerably lower cost in comparison to the conventional process.

The composition of the synthesized liquid fuel given in Figure 5.7 for the base case CTL-RC-SR indicates that almost 92 wt.% of the liquid fuel composes of C5-C11 range hydrocarbons which represents the gasoline range. The liquid fuels obtained from different schemes displayed similar composition with C5-C11 hydrocarbons ratios higher than 90 wt.%. The density of the produced gasoline, measured as 704 - 705 kg/m^3, is comparable with, 720 - 775 kg/m^3, specified in commercial standard (ISO, 1996). According to the related standard, the gasoline sulfur content should be below 10 mg/kg. Because of the high sulfur removal efficiency of AGR unit (Rectisol), the gasoline obtained from CTL process has negligible sulfur content and satisfy the gasoline standard.

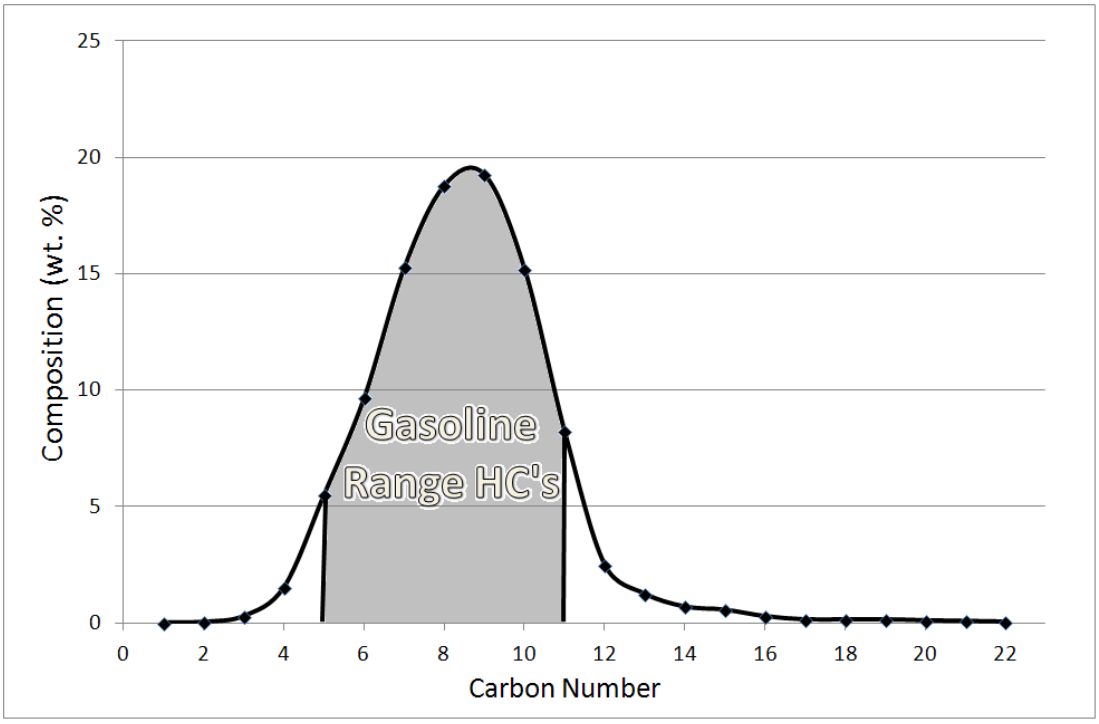

Figure 5.7 : Composition of liquid fuel obtained from CTL-RC-SR scheme for base case conditions.

Since the straight run gasoline produced by the conventional FT reactor had a low octane number, a severe Pt reforming was used to increase the gasoline octane number (Dry, 2002). On the other hand, the zeolite, in the structure of bi-functional FT catalyst, enhances the hydro-isomerization reactions. This results in an increased amount of isomerized and branched hydrocarbons and thus the octane number. Therefore, it was supposed that Pt reforming or any other upgrading unit may not be needed in the proposed process. However, to our best knowledge, no information of the octane number of the liquid fuel produced by the zeolite containing catalyst was reported in the literature. In any case, additives like the di-isopropyl ether, synthesized from propene and water, could be used to boost the liquid fuel octane number, if needed (Dry, 2002).

5.3.1 Comparison of process alternatives

The results obtained from the simulation of the three proposed process schemes based on the essential performance indicators for the base case operating conditions are given in Table 5.3. As seen in the table recycling of the tail gas fed back to FT reactor, as may be expected, enhanced the gasoline production. The process with tail gas recycling and processing, CTL-RC-SR displayed the best performance with a maximum gasoline production efficiency. In this respect the processes follow the

order of CTL- RC-SR (50.02%) > CTL-RC (31.41%) > CTL-OT (22.31%). An opposite trend, however, was observed for the electrical efficiency with order of CTL-OT (22%) > > CTL-RC (16%) > CTL- RC-SR (0.5%).

Table 5.3 : Efficiencies of the process schemes for the base case operating conditions.

Process	CTL-OT	CTL-RC	CTL- RC-SR
Gasoline Production Efficiency (%)	22.31	31.41	50.02
Electrical Efficiency (%)	22.56	15.82	0.51
Total Efficiency (%)	44.87	47.22	50.53
Carbon Efficiency (%)	14.54	20.45	32.62

The maximum electrical efficiency, 22.6%, was obtained from the CTL-OT process. The electrical efficiency decreased to 15.3% for CTL-RC, while CTL-RC-SR had the poorest efficiency. The net electrical efficiency of the CTL-RC-SR process was pretty close to zero. For some particular conditions even negative electrical efficiencies were observed for this process. However, it should be noticed that, supplying the onsite power needs for the same process could be another critical issue besides maximizing the gasoline production efficiency. The differences occurred in processes output efficiencies originated from the tail gas utilization way. In the CTL-OT process the whole FT outlet gas was directly fed to the power plant for electrical production. The tail gas recycling, on the other hand, increases the total syngas conversion. As previously mentioned, In case of CTL-RC-SR process had a SR reactor incorporated into the FT recycle line, so that the light hydrocarbons (C1-C4) produced in the FT reactor were converted into syngas which was recycled back to FT reactor. Although including a reformer reactor and recycling line may also increase the complexity of the process to some extent, this modification also resulted in a substantial increase the gasoline range hydrocarbons yield. A similar trend can cobe seen for the carbon efficiency.

As seen from the table, the maximum total efficiency was observed for the CTL-RC-SR process indicating that, in spite it very law electrical efficiency it has best overall performance. The total efficiency decreased in the order CTL- RC-SR > CTL-RC > CTL-OT. However, compared to the differences observed for process gasoline

productions efficiency, the differences determined in their total efficiencies appeared to be relatively moderate. It seemed that the large gaps emerged in process gasoline efficiencies were substantially compensated by the electricity produced from the tail gas.

In respect of maximizing the gasoline production efficiency, the CTL-RC-SR process appeared to be the best alternative. Streams compositions and operating conditions at CTL-RC-SR for the base case are given at Table 5.4. The simpler CTL-OT and CTL-RC processes, however, may regarded to be better options if a simultaneous electricity and gasoline productions is to preferred. Streams compositions and operating conditions of these processes for the base case are given in Appendix B. It should be noticed that, it is also possible to shift the electricity and gasoline production balance of CTL-RC-SR process and obtain higher electrical efficiencies through altering the process operating parameters.

In the CTL-RC-SR process proposed in this study, the SR reactor was utilized to produce syngas from gaseous hydrocarbons. The Partial Oxidation Reactor (POX) and Autothermal Reforming Reactor (ATR) are the other alternative reactor types which can be used for the same purpose. These three reactors have different product compositions as well as different heat characteristics. The steam reformer operates at high temperature and needs considerable amount of heat supply, while the partial oxidation reactor, although similarly operates at high temperature, produces heat through partial combustion. The autothermal reformer, on the other hand, can be considered to be an adiabatic reactor with a need for neither heat input nor output. The heat need for autothermal reforming reactions is supplied through the combustion of certain portion of feed gas stream in the reactor itself.

Table 5.4 : Operating Conditions and Streams Compositions of CTL-RC-SR process for the base case.

Stream Name	Operating Conditions			Composition (molar)							
	T (°C)	P (kPa)	F (ton/h)	H_2	CO	CO_2	H_2O	O_2	N_2	CH_4	Bal.
Coal Input	20	2000	496.9	0.22	-	-	0.12	0.06	0.01	-	0.59
ASU Air Inlet	25	100	1260.6	-	-	-	-	0.21	0.79	-	0.00
Gasifier O_2 Inlet	460	2000	280.1	-	-	-	-	0.99	0.01	-	0.00
Gasifier Outlet	848	2000	761.8	0.21	0.51	0.13	0.06	0.00	0.01	0.08	0.00
Scrubber H_2O Inlet	20	2000	1187.5	-	-	-	1.00	-	-	-	0.00
Scrubber Gas Outlet	176	2000	1231.0	0.12	0.28	0.07	0.47	-	0.00	0.04	0.02
WGS Inlet	176	2000	728.2	0.12	0.28	0.07	0.47	-	0.00	0.04	0.02
WGS ByPass	176	2000	502.8	0.12	0.28	0.07	0.47	-	0.00	0.04	0.02
Flush Outlet	40	2000	875.1	0.39	0.22	0.31	0.00	-	0.01	0.06	0.01
AGR Effluent	16	2000	541.7	-	-	0.98	-	-	-	-	0.02
AGR Syngas Outlet	16	2000	333.4	0.56	0.32	0.01	0.01	-	0.01	0.09	0.00
FT Inlet	280	2000	780.9	0.59	0.29	0.04	0.01	-	0.02	0.05	0.00
FT Outlet	280	2000	829.0	0.29	0.12	0.10	0.31	-	0.03	0.10	0.05
3 Pha. Sep. Vap Out.	20	2000	477.8	0.44	0.18	0.15	-	-	0.05	0.15	0.03
3 Phas Sep. H_2O Out.	20	2000	230.6	-	-	-	0.998	-	-	-	0.00
3 Phase Sep. HC Out.	20	2000	120.6	0.01	0.01	0.04	-	-	-	0.01	0.93
Condenser Vap. Out.	20	100	3.8	0.08	0.08	0.41	-	-	0.02	0.16	0.25
Liquid Fuel Product	20	100	116.6	-	-	-	-	-	-	-	1.00
Turbine Inlet	415	1800	477.8	0.44	0.18	0.15	-	-	0.05	0.15	0.03
Turbine Outlet	265	500	477.8	0.44	0.18	0.15	-	-	0.05	0.15	0.03
Power Plant Feed	258	100	992.4	0.44	0.18	0.16	-	-	0.05	0.15	0.02
Recycled Tail Gas	265	500	382.2	0.44	0.18	0.15	-	-	0.05	0.15	0.03
Reg. HEX Inlet	300	500	543.7	0.31	0.13	0.11	0.29	-	0.03	0.10	0.03
Reformer Water Inlet	400	2000	161.5	-	-	-	1.00	-	-	-	0.00
Reformer Syngas Inlet	835	500	543.7	0.31	0.13	0.11	0.29	-	0.03	0.10	0.03
Reformer Syngas Out	850	500	543.7	0.52	0.24	0.06	0.14	-	0.03	0.01	0.00
Rec. Condenser Inlet	340	500	543.7	0.52	0.24	0.06	0.14	-	0.03	0.01	0.00
Rec. Compressor In.	25	500	447.5	0.60	0.28	0.07	0.01	-	0.03	0.02	0.00
Recycle Gas to FT	250	2000	448.1	0.60	0.28	0.07	0.01	-	0.03	0.02	0.00

The ATR reactor was seen to be the advantageous natural gas reforming alternative for CTL systems. This may be due to the its milder operating conditions, soot free operation as well as relatively simple design and construction, with no need of

internal heat exchangers (Vosloo, 2001). Since the main goal of this study was maximizing the gasoline production efficiency, the SR reactor was selected. Some portion of FT tail gas was burned to meet the heat required for the reforming reactions. The stream recycling was used only for syngas production through reforming reaction, thus gasoline production efficiency increased at expense of electricity generation. Since oxidation reactions do not take place in the SR reformer, the CO_2 build up in the system decreases. Also it should be remembered that, in contrast to ATR or POX reactors, the SR reactor does not need any oxidant in the feed stream. Thus ASU capacity and need for O_2 compressor will be lower resulting in advantages of lower operating and investment costs.

The SR and POX reactors produce syngas with the highest and the lowest the H_2/CO ratio, respectively. The H_2/CO ratio produced by SR reactor is about 2.5-3.0. Therefore, SR reactor also could be used as a tool to adjust and increase the H_2/CO ratio in the syngas stream fed to FT reactor. Thus, a WGS reactor might not be needed. However in order to eliminate WGS reactor, the gasification would be needed to be carried out with a mixture of steam and oxygen so that the H_2/CO ratio could be high enough for this purpose.

The energy flow diagram of the CTL-RC-SR process is shown in Figure 5.8. The diagram was arranged based on the lower heating value of the flow streams. At the base case, gasoline production efficiency was calculated to be 50.2%. The theoretical maximum efficiency of CTL process is reported to be 60%, while 50% energy efficiency seems to be achievable (Steynberg and Nel, 2004). The existing coal conversion plants operating with thermal efficiencies close to 40% were regarded to be cash positive. But it should be noted that the price of the oil has increased considerably since then. Therefore economic value of the liquid fuel produced by this process has increased as well, which allows these plants to be cash positive even for lower thermal efficiencies these days (Steynberg and Nel, 2004). For a CTL process, the production of the liquid fuel with an efficiency of 50% indicates a considerable improvement in the process performance with reference to theoretical maximum efficiency of 60%. This improvement was achieved by simplifying the process and optimizing the operating parameters.

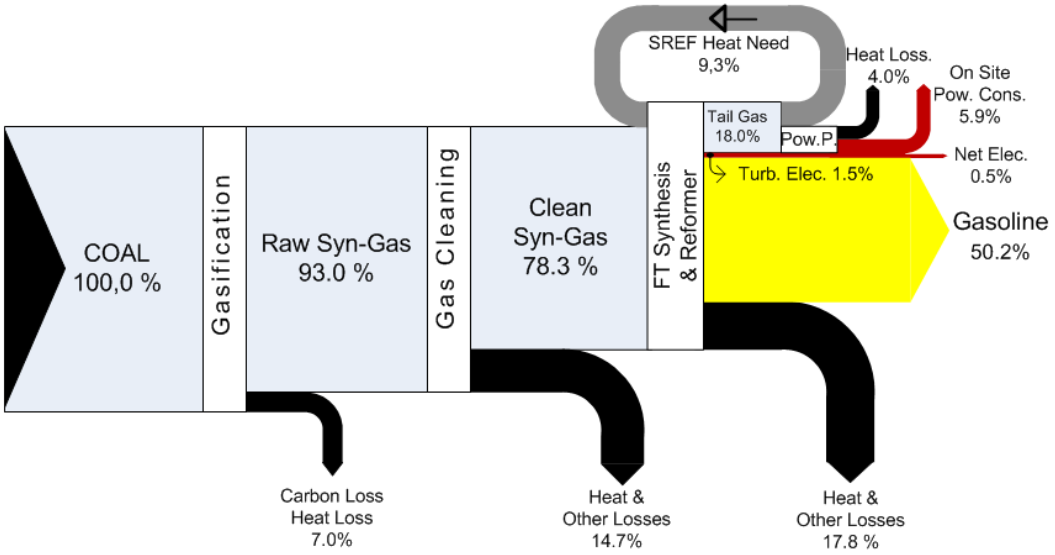

Figure 5.8 : Energy flow diagram of the CTL-RC-SR process for base case scenario.

As seen from Figure 5.8, the highest energy losses occurred in the gas cleaning and the FT synthesis stages. The total loss in these two units is about 32%. The tail gas leaving FT carries 18% of the total energy fed to the process. Nearly half of this energy is used for heat production which is utilized in SR. The rest of the tail gas energy is transferred to power station to produce electricity.

Table 5.5 shows the carbon balance of the CTL processes. In the table, the amounts of carbon in various output streams are given as a percentage of carbon in the coal fed to the process which assumed to be 100. The schematic carbon flow diagram of CTL-RC-SR process is given in Figure 5.9. The carbon balance indicates that the largest carbon loss come from CO_2 stream exiting AGR unit which is suitable for carbon capture and sequestration (CCS). If CCS is used for AGR vent, the only source of greenhouse gas emission of the process would be power plant exhaust gas. The sum of CO_2 amount vented from power plant and the carbon amount in the gasoline is about 45% for all process schemes, while the sharing of these two streams differs considerably according to process scheme. The CTL-RC-SR process appeared to have the highest gasoline production efficiency, and consequently the highest carbon percentage in gasoline stream. On the other hand, the CTL-OT process with the highest electrical efficiency has the highest carbon percentage in the power plant vent. Based on gasoline production rate, the CTL-RC-SR process emitted the greenhouse gas at the lowest rate. The CO_2 emissions (kg CO_2/GJ FT fuel), coming

from power plants of processes were descending in order of CTL-OT (135.07) > CTL-RC (80.28) > CTL-RC-SR (26.84).

Table 5.5 : Carbon balances of the simulated CTL processes for base case operating conditions.

	CTL-RC-SR	CTL-RC	CTL-OT
Carbon in (%)			
Carbon in feed coal	100.0	100.0	100.0
Carbon out*(%)			
Carbon in ash	5.0	5.0	5.0
Carbon in AGR vent	49.3	50.3	51.6
Carbon in power plant exhaust	12.9	24.1	28.8
Carbon in gasoline	32.8	20.5	14.6
CO_2 emission (kg CO_2/GJ FT fuel)	26.84	80.28	135.07

*As percentage of carbon in feed coal.

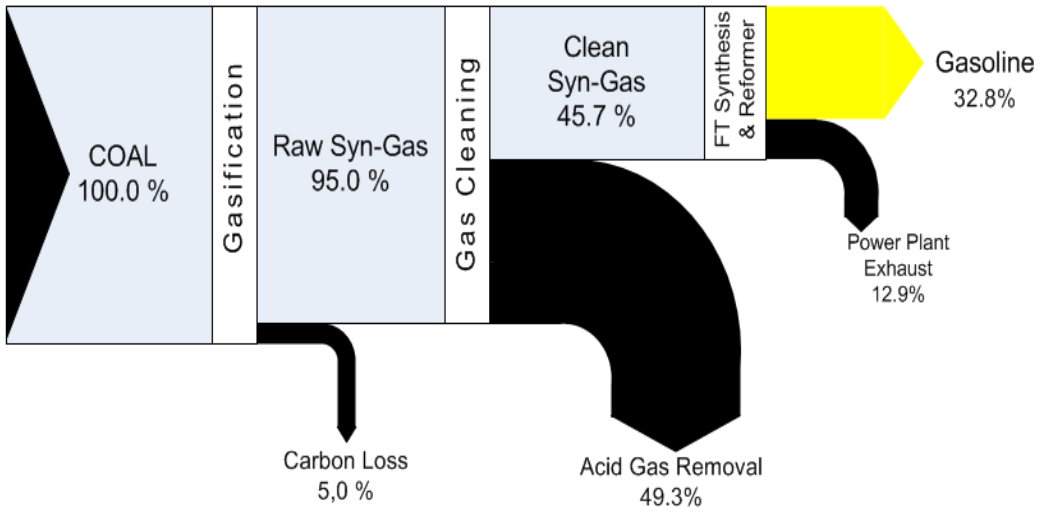

Figure 5.9 : Carbon flow diagram of the CTL-RC-SR process for base case scenario.

The electricity production and consumption figures of the three processes with a capacity of 25000 bbl gasoline/d for base case are presented in Table 5.6. As seen from the table, all process alternatives may operate with a net electrical production. The highest net electricity production is achieved with CTL-OT, following by CLT-RC. The net benefit from CTL-RC-SR is substantially low in comparison with that of other two. In all processes, the AGR unit has the largest share in electricity consumption which ranging from 27.1% for CTL-RC-SR to 37.3% for CTL-OT. The

second largest electricity consumer unit is ASU for all processes. The total consumption occurred in these two units makes up 53.5%, 71.6% and 73% of total plant electricity consumption for CTL-RC-SR, CTL-RC and CTL-OT, respectively. Although the lowest net electricity production is gained from CTL-RC-SR, this is not surprising as its operating conditions are optimized with emphasis on gasoline production. A comparison of Table 5.3 and Table 5.6 indicates that the lowest electricity production may be compensated with a higher gasoline production. The gasoline and electricity efficiencies of the processes can be amended through adjustment of major operating parameters such as tail gas recycling ratio.

Table 5.6 : The electricity production and consumption of processes with a capacity of 25000 bbl gasoline/d for base case conditions

	CTL-RC-SR	**CTL-RC**	**CTL-OT**
Electrical Production (MWe)			
Turbine	43.5	18.0	43.3
Power Plant	139.9	916.2	1704.3
Total electricity production(MWe)	**183.4**	**934.2**	**1747.6**
Electrical consumption (MWe)			
Recycling compressor	45.4	3.5	-
ASU	44.7	71.4	100.4
Gasifier oxygen compressor	33.2	52.9	74.5
AGR (RECTISOL)	46.2	74.2	105.3
Total electricity consumption	**170.3**	**203.4**	**282.0**
NET electricity production	**13.1**	**730.8**	**1465.8**

It is clear from Table 5.6 that the net electrical output of the coal-to-liquid fuels plants are strongly affected by electricity consuming units. One of leading electrical consumers is gas cleaning unit. The Rectisol® system considered in this study is widely used for its capability to effectively remove the impurities (i.e. hydrocarbons, H_2S, NH_3, etc.) from syngas to few ppm levels. But this technology is more energy intensive compared to the other gas purification alternatives. In cases, as proposed here, when the up-grading section is eliminated and only the FT reactor is involved as a catalytic unit downstream of the gas purification unit, the impurity constraints can be specified accordingly so that other AGR systems with lower electricity

consumption may be adapted. This can enhance the electrical and total efficiencies of the system, resulting in an increase in the net electricity production.

5.3.2 Effects of operating parameters on performance of the CTL-RC-SR process.

In this section the results of simulation studies carried out to investigate the impact of various parameters such as the tail gas recycling ratio and pressure, the reformer reactor temperature, the steam to carbon rati (S/C) of the reformer, the FT conversion and selectivity on the performance of the coal-to-liquid fuel process with tail gase recycling and processing (CTL-RC-SR).

5.3.2.1 Effect of the tail gas recycle ratio on the performance of CTL-RC-SR process

The tail gas recycle ratio is one of the most significant parameters determining the performance of a CTL process. Its effect on the performance of CTL-RC-SR process is shown in Figure 5.10 and Figure 5.11. In Figure 5.10, the gasoline production efficiency ($\mu_{th,gas}$), the total process efficiency (μ_{tot}), the carbon efficiency (μ_C) and SR conversion (X_{SR}) are plotted as a function of the tail gas recycling ratio. Gasoline and total efficiencies increase with increase in the recycling ratio. Rising of recycling ratio from 0.5 to 0.9 results in a considerable improvement in the gasoline and carbon efficiencies, while increase in the total efficiency remains rather modest.

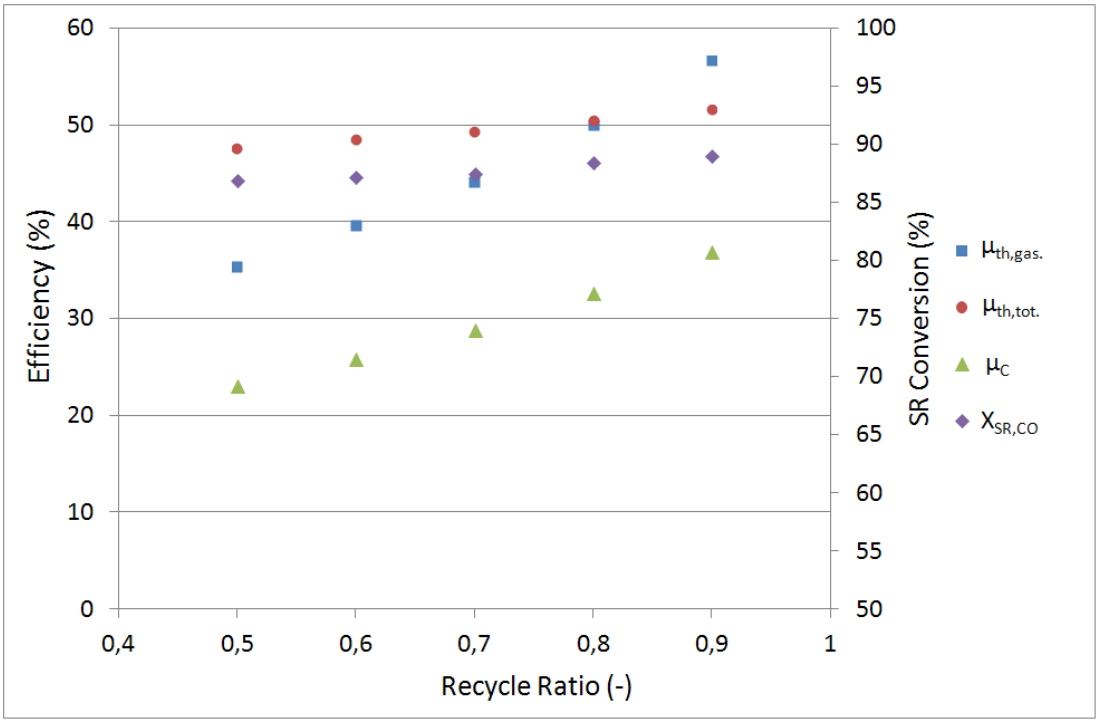

Figure 5.10 : Variation of the efficiency of CTL-RC-SR process with the tail gas recycling ratio.

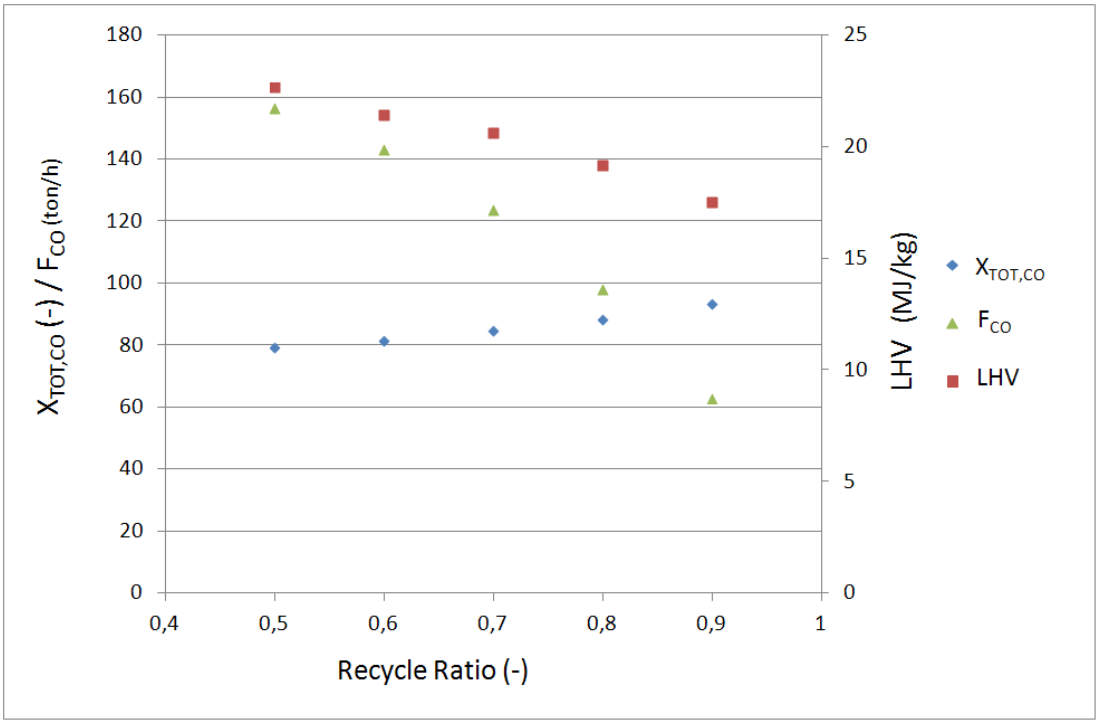

Figure 5.11 : Effect of process tail gas recycle ratio on overall syngas conversion ($X_{TOT,CO}$) of CTL-RC-SR process and tail gas lower heat value (LHVtail gas).

Increase in recycle ratio, on the other hand, means lower amounts of tail gas fed the power plant, Figure 5.11. Furthermore, the lower heating value of the tail gas ($LHV_{tail\ gas}$) decreases with increase in recycling ratio due the increased reactants' conversion in the FT reactor producing a tail gas with higher inert (N_2, CO_2….etc.) ratios. Therefore, increase in the recycling ratio results in a decrease in the electricity production. For tail gas recycling ratios higher than 0.8, the electricity consumption exceeds its production and the CTL-RC-SR process becomes a net electricity importer. Therefore, a recycle ratio of 0.8 appears to be appropriate value to maximize gasoline production without importing electricity. The recycling ratio can be used as a tool to shift the gasoline and electricity production balance of the system in direction favoring of the desired one. The recycling ratio, however, does not have an obvious impact on the conversion of steam reforming, Figure 5.10.

5.3.2.2 Effect of the tail gas recycling pressure on the performance of CTL-RC-SR process

Since the lower pressures favor the steam reforming conversion, all tail gas leaving product separator unit was fed to the expander (turbine) where its pressure was reduced to the reformer operating pressure in the CTL-RC-SR process, as seen in Figure 5.4 (c). On the other hand, in the CTL- OT and CTL-RC processes not the whole but only the tail gas stream from the separator which was to be sent to power plant was passed through the expander, Figure 5.4 (a, b). The CTL- OT process had no compressor since there was no tail gas recycling while in the CTL-RC scheme the compressor operated only against the pressure loses in the FT reactor. Therefore, in these two process configurations electrical load of turbines, except CTL-OT, and compressors decreases as seen in Table 5.6. Consequently, the capacity and investment costs of turbine and compressor are considerably lower for them.

The pressure of the recycled tail gas stream affects the reformer conversion and the electrical generating and consuming capacities of the expander and compressor. As seen from Figure 5.12, the reformer conversion decreases considerably and almost linearly with increase in recycling pressure. This also means a decreasing conversion of light hydrocarbon into gasoline and thus a diminishing gasoline production efficiency. As seen from the figure, however, compared to reformer conversion decrease in the gasoline production efficiency ($\mu_{th,gas}$) is very slow. Although the

process efficiencies (i.e. $\mu_{th,gas}$, μ_c, $\mu_{th,gas}$) slightly worsen with tail gas pressure, in general, they do not seem to be considerably influenced. The highest efficiencies are attained in the 250-750 kPa pressure range.

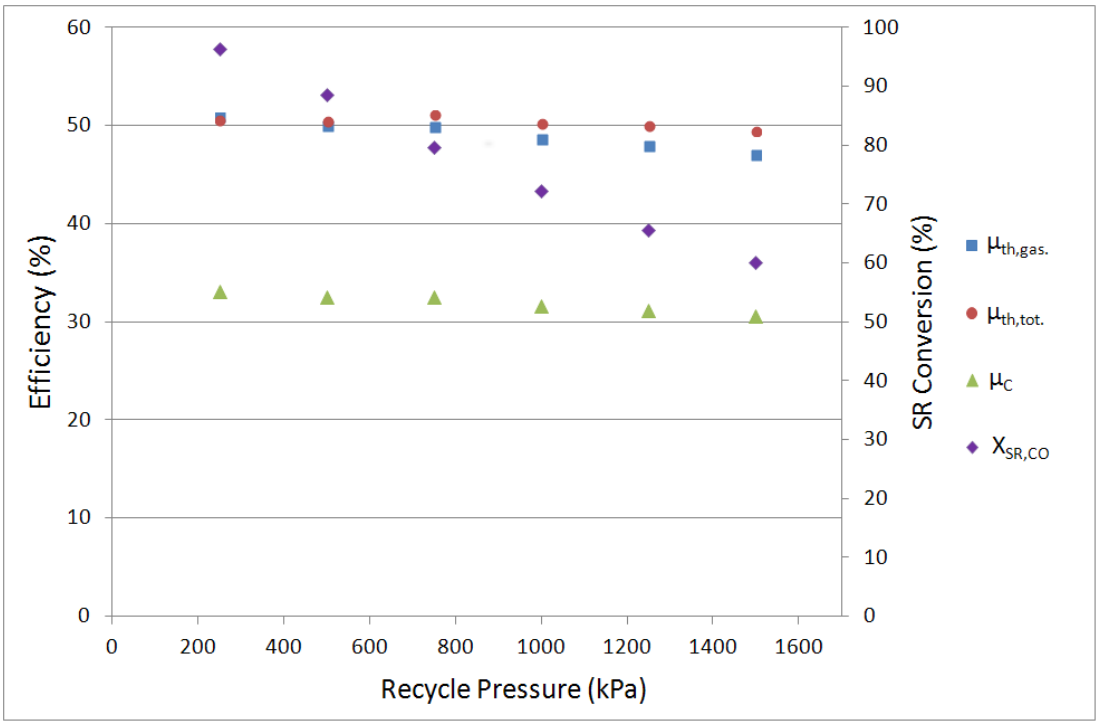

Figure 5.12 : Variation of the CTL –RC-SR process efficiency and reformer conversion with tail gas pressure.

Variation in pressure did not considerably change the difference occurred between electrical capacities of the turbine and compressor. But increase in pressure enhanced the electrical efficiency of the process because of tail gas having higher LHV and flow rate at elevated pressures and the fact that a portion of which this gas is fed to the power plant.

5.3.2.3 Effect of the reformer temperature and S/C ratio on the performance of CTL-RC-SR process

The degree of conversion of light hydrocarbons back into the syngas is determined by the reformer operating conditions; i.e. temperature and S/C ratio. The variations of CTL-RC-SR process efficiencies with reformer temperature and S/C ratio are plotted in Figure 5.13 and Figure 5.14, respectively. These figures indicate that both operating parameters have a strong impact on the reformer conversion. Conversion rises quickly with increasing temperature and reaches a degree higher than 80% at 850 ^{o}C and S:C ratio = 1, after which it seems to attain an asymptotic profile.

Conversion appears to be completed at temperature higher than 950 °C and exceeds 90% for S/C >1.20

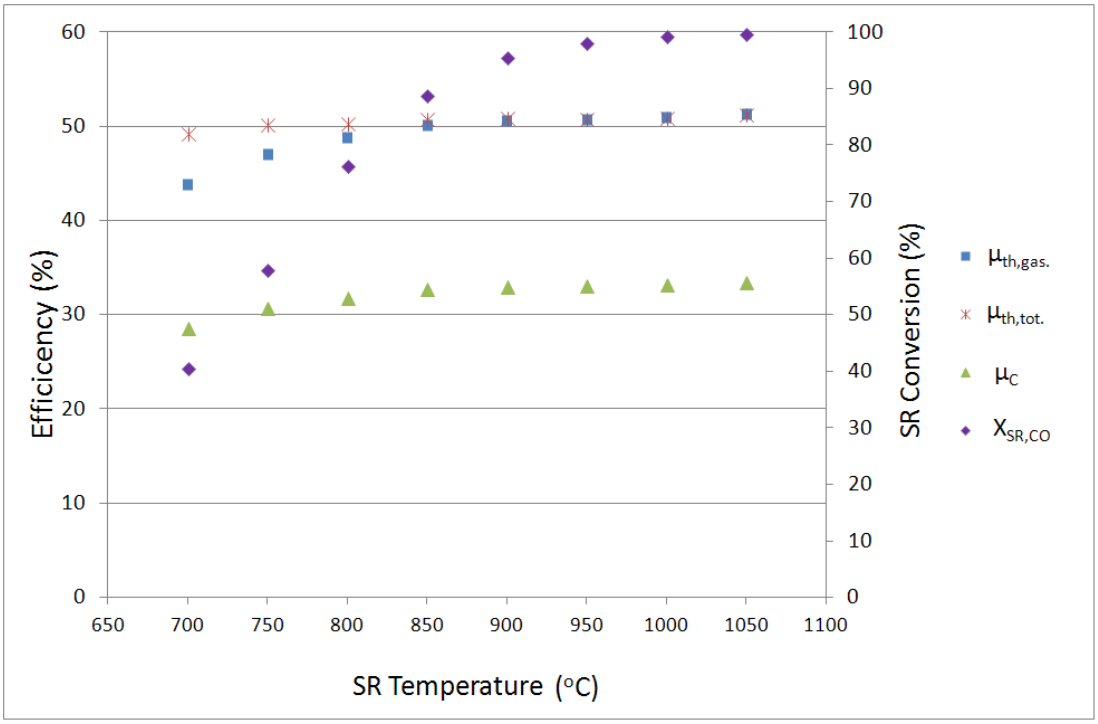

Figure 5.13 : Variation of CTL–RC-SR process efficiencies and reformer conversion with reforming temperature.

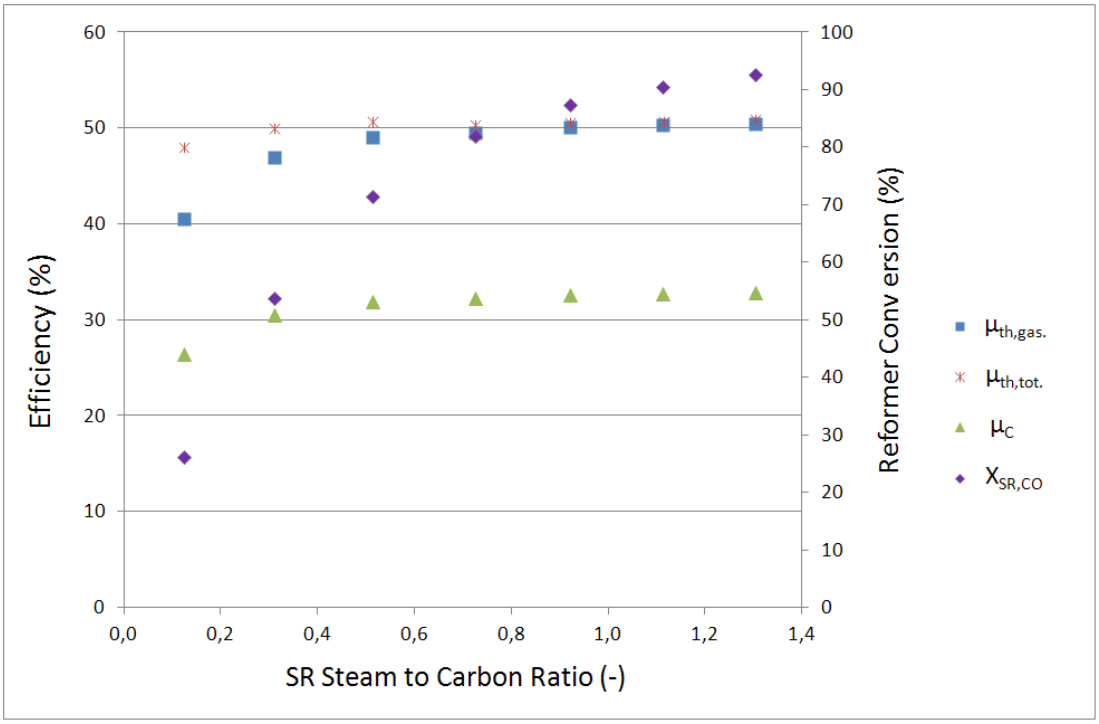

Figure 5.14 : Variation of CTL–RC–SR process efficiencies and reformer conversion with S/C ratio.

As result of increasing reformer conversion, the gasoline production efficiency also increases to some extend via re-converting of light hydrocarbons into syngas which is recycled back to the FT reactor. At T > 850 °C and S/C >1, however, all efficiencies reach a maximum degree with no further change after that. Since the heat required for reformer is supplied through a regenerative heat exchanger and steam needed for reforming reactions is produced via waste heat, further increase in operating parameters (i.e. temperature and S/C ratio) up to T = 1050 °C and S/C=1.5 can hardly deteriorate the overall process efficiency. But these harsher operating conditions are needed to be justified economically. The results presented in Figure 5.13 and Figure 5.14 reveal that a satisfactory (optimum) process performance may be achieved with a reformer operating under conditions of $T \geq 850\ ^{o}C$ and $S/C \geq 1.0$.

5.3.3 FT conversion and selectivity

Studies published in the literature on activity and selectivity of the bi-functional FT catalysts repoted considerably diverse and contradictory results (Li et al., 2009; Pour et al., 2009; Yang et al., 2007; Ravishankar et al., 2005). It is common fact that catalyst is key parameter affecting the FT process performance and product properties. Therefore, the FT conversion and selectivity were considered as parameters in the process simulation and their effects on the composition of raw liquid fuel and process efficiencies were studied. Results are presented in Figure 5.15, Figure 5.16, Figure 5.17 and Table 5.7.

The FT synthesis conversion degree also determines the amount of the unconverted syngas, namely tail gas, leaving the reactor. As the FT conversion increases, the amount and heating value of tail gas, which is used for electricity production, decrease. Consequently, the gasoline production efficiency improves while the electricity production capacity decreases, Figure 5.15. Since a reduction in electricity production is compensated by increase in gasoline production, the total efficiency of the process slightly improves. For FT conversion > 75%, process electricity consumption exceeds its electricity production.

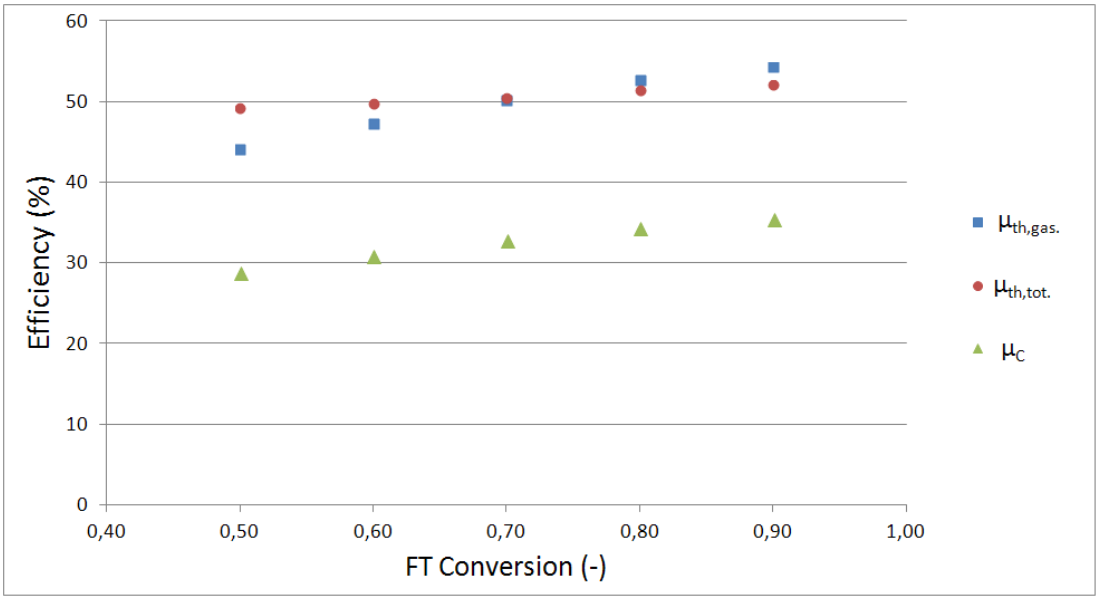

Figure 5.15 : Variation of the CTL–RC-SR process efficiencies with FT conversion degree

The effect of the selectivity on the process efficiencies and liquid product composition was investigated for three different selectivity degrees which classified as reference, lighter and heavier, as shown in Figure 5.16. Results are presented in Table 5.7 and Figure 5.17. Shifting the selectivity to the heavier fractions is accompanied by decreasing amount of lighter C1-C4 hydrocarbons which are used for power generation, so that electrical efficiency decreases while liquid fuel production efficiency increases. As seen from table, the carbon and total efficiencies are also steadily enhanced as the selectivity moved from lighter to heavier hydrocarbon fractions. For the base case scenario, the ratio of C5-C11 hydrocarbons, which represent gasoline, is determined to be 92,0%. For the lower selectivity case, however, the liquid fuel mainly composes of C4-C8 range hydrocarbons (83,6%) , which means that the condensed product obtained from FT is not gasoline anymore and exhibits different properties. For example, the liquid fuel produced with reference selectivity has a density of 706 kg/m^3 while that of the liquid fuel obtained with lighter selectivity is around 675,5 kg/m^3. On the other hand, for the heavier selectivity case, the C5-C11 fraction decreased to 60,4%, while C12+ fraction increased to 38.7%. Therefore, further processing (i.e. separation, hydrocracking) is needed to upgrade the raw liquid fuel obtained from FT synthesis to the gasoline. All these results indicate that the selectivity of FT catalyst is one of the most important parameters with regard to the quality of liquid fuel. In order to eliminate the need for a product up-grading section, catalysts which can maximize C6-C10 production and

minimize the selectivity toward C1-C4 and C13+ fractions are required. Maximizing liquid fuel efficiency also requires a selectivity toward C1-C4 as low as possible. Bu it should be noticed that this fraction may be desired for the electricity production, therefore, a flexible restriction should be imposed in case it needed.

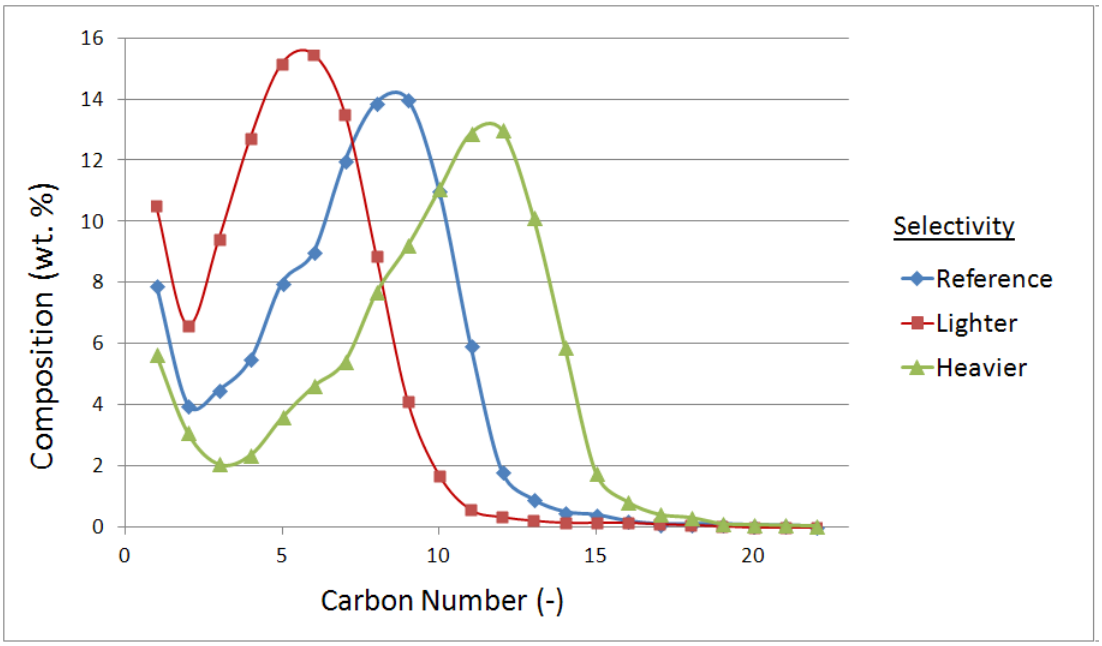

Figure 5.16 : Variation of FT synthesis product composition with catalyst selectivity.

Table 5.7 : Effect of FT reactor selectivity on process efficiencies.

Efficiency (%)	Selectivity		
	Lighter	Reference	Heavier
Liquid Fuel Product Efficiency	42.68	50.02	53.27
Electrical Efficiency	1.99	0.51	0,20
Total Efficiency	44.67	50.53	53.47
Carbon Efficiency	27.64	32.62	34.92

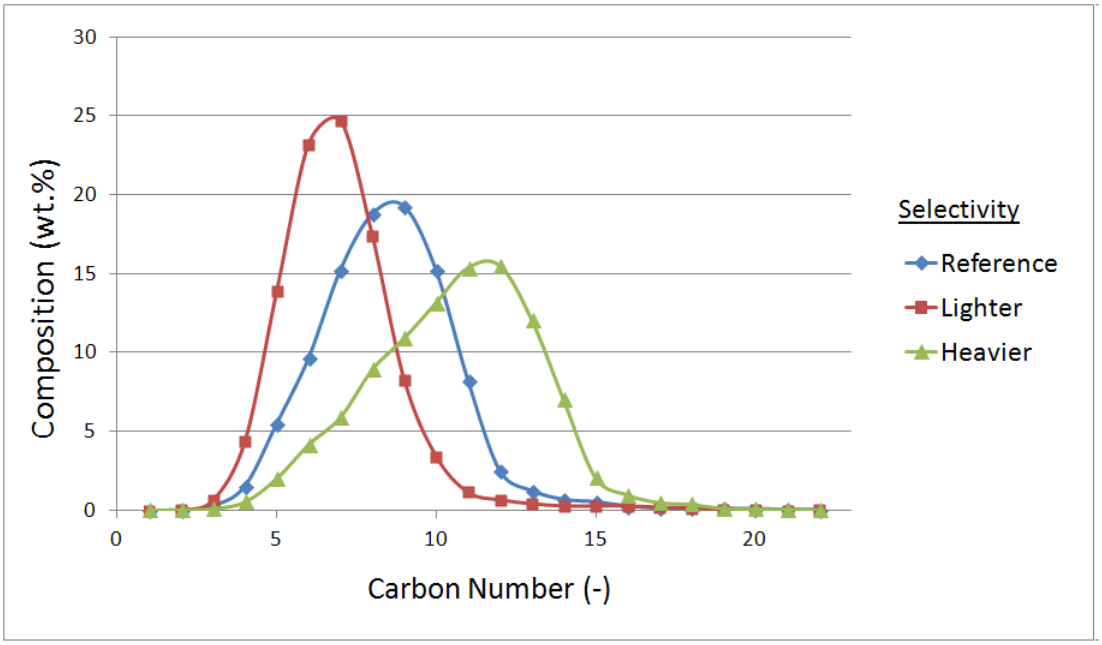

Figure 5.17 : Variation of FT liquid fuel composition with catalyst selectivity.

6. CONCLUSIONS

A major limitation of the Fischer-Tropsch (FT) technology is the low selectivity of the conventional catalysts towards targeted compounds. Conventional Fischer Tropsch reactor produces so called "syn-crude" containing a wide range of hydrocarbons, ranging from C1 (methane) to C40 and even higher. The direct production of gasoline through FT reactions is a great challenge related to catalyst and process development. This may be overcome by the use of metal/zeolite bifunctional catalysts, which can enhance the selectivity of the synthesis toward the desired products, i.e. gasoline range hydrocarbons. In the thesis study, bi-functional FT catalysts have been studied with a special focus on zeolite supported iron based catalysts. The main goal of the study was to develop bi-functional FT catalysts with high selectivity towards gasoline range hydrocarbons as well as acceptable activity and durability. The thesis study is composed of three parts.

In the first part, iron based FT catalysts with different types of zeolite supports were prepared by incipient wetness impregnation. Five different zeolites, namely ZSM-5, mordenite, beta, Zeolite Y and ferrierite were used as supports in the preparation of the iron-based bi-funtional FT catalysts. Their catalytic activities were tested under different temperatures. The following are the major conclusions:

- The activity and selectivity of the catalysts were found to be affected by the type of zeolite.
- Presence of the zeolite in the catalyst synthesis considerably enhanced the catalytic activity. Zeolites also improved the hydrocarbon productivity of catalyst through better dispersion and utilization of iron in catalysts.
- The CO conversions of catalysts with different zeolite supports clearly indicated that catalytic activity was strongly dependent on the type of zeolite. All zeolite-supported catalysts displayed CO conversion ranging from 30% to 79% at 553 K. The CO conversions of the catalysts were determined to be in the following order: SFeB > SFeZ >SFeF > SFeY5 > SFeM > SFeY80.

- The highest reactant conversions were obtained with Beta supported catalysts at all temperatures. At 553 K the highest hydrocarbon productivity was obtained for SFeB catalyst as 0.83 g/h/g-Fe.
- Catalysts'conversions were strongly affected by reaction temperature. CO and H_2 conversions increased with temperature for all catalysts. The maximum increase in selectivity with temperature was measured for SFeB. An increase of 30 K in the reaction temperature increased its CO conversion from 32.1% to 79.2%.
- The hydrocarbon distribution of the liquid phase concentrated between C5-11 range hydrocarbons. The average ratio of C5-C11 range hydrocarbons was determined to be 79.2%, 86.7%, 73.5%, 78.4%, 71.8% and 57.2% for SFeB, SFeZ, SFeF, SFeM, SFeY5and SFeY80, respectively. Therefore, upgrading of the raw liquid products from the FT synthesis by the zeolite supported catalysts, especially SFeZ catalyst, to produce gasoline would be no longer needed due to the low selectivity of these catalysts towards the long chained HCs.
- ZSM-5 supported catalyst displayed better selectivity towards gasoline range hydrocarbons (C5-C11) than other catalysts. At 553 K, the selectivity of SFeZ towards this hydrocarbon fraction was 74%, while that of the base iron catalyst (BFe) towards the same fraction was about 41%.
- The ferrierite supported-catalyst (SFeF) had the lowest selectivity towards the liquid fuel range hydrocarbons and the highest selectivity towards un-wanted light hydrocarbons. Product distribution obtained by SFeF is similar to that obtained from the BFe. However, ferrierite as a support remarkably enhanced the activity and the productivity of the iron catalyst.
- Both zeolite Y-supported catalysts (SFeY5 and SFeY80) exhibited low selectivity towards gasoline and diesel range HCs, especially at low temperatures.
- The zeolite supported catalysts considerably reduced the formation of the olefins in the gas phase. The synthesized catalysts have produced a gas phase products with 5% -10% olefins content. The amount of olefins decreased with increase in temperature, due to the better activity of the zeolites at high temperatures.

- Zeolite in the catalyst suppressed the WGS activity of the iron catalyst.
- The effect of reaction temperature on product selectivity is complex pnenomenon realized through the combined effects of olefin oligomerization reaction by zeolite and FT reaction by iron.
- Compared to the pure iron catalyst (BFe), the main advantages of zeolite supported-catalysts can be enumerated as follows,
    - Higher activity,
    - Lower active metal (i.e. iron) consumption,
    - Lower CO_2 selectivity,
    - Lower selectivity towards unwanted light hydrocarbons,
    - Higher selectivity towards gasoline and diesel range hydrocarbons,
    - Higher hydrocarbon yield per unit syn-gas fed.

The second section is allocated to ZSM-5 supported catalyst, which had the highest gasoline selectivity among the zeolites studied. In this section, the effect of catalyst preparation route, zeolite de-alumination, iron loading and operating conditions (T, P, GHSV, H_2/CO ratio) were studied. A 260 hours long time on stream test was also carried out. In addition to the activity tests, characterization of the catalysts was also done by using ICP, N_2 physisorption, XRD, TGA and SEM techniques. The following are the major conclusions:

- Catalytic activities of all catalyst were found to be considerably affected by catalyst preparation method, iron loading, and the reaction temperature.
- The activities of the catalyst enhanced as the iron percentage in the catalyst and the reaction temperature increased. All synthesized catalysts had CO conversions higher than 40% at 553 K. The conventional catalyst displayed the highest CO conversion, while the ZSM-5 supported iron based catalyst with 18% iron loading exhibited the highest activity among the zeolite containing catalysts.
- Catalyst prepared by impregnation showed higher activity in respect to the CO conversion in comparison with catalyst prepared by physical admixing of zeolite and iron.

- Activity test results indicated that, zeolite in the catalyst formulation could suppress the iron catalyst WGS activity. This was proved by much lower CO_2 selectivity of zeolite containing catalysts, in comparison with that of the conventional and the base iron catalysts which did not contain zeolite.
- The CO_2 selectivity of the catalyst prepared via impregnation was quite lower than that of the hybrid catalyst.
- ZSM-5 supported iron catalysts were found maximizing selectivity of C5-C11 range hydrocarbons through reducing the amount of the light and heavy hydrocarbon fractions. On the contrary, conventional catalysts produced more heavy hydrocarbons fraction. A maximum selectivity of 74% for C5-C11 range hydrocarbon was observed for SFeZ18 catalyst at 553 K.
- The analysis of synthesized liquid fuel (collected at cold trap) for zeolite containing catalysts indicated that >90 wt.% of the liquid fuel composes of C5-C11 range hydrocarbons which represents the gasoline range. A maximum ratio of 94.5% was obtained from SFeZ4 catalyst at 553 K.
- The catalysts prepared by impregnation method, generally have better selectivity towards C5-C11 hydrocarbons than the hybrid catalyst. At 553 K, the selectivity of zeolite-supported catalysts towards the C5-C11 hydrocarbons fraction changed between 50% and 74%, while the selectivity of the hybrid catalyst (HFeZ9) towards the same fraction was about 45%.
- Compared with the studies in the literature, a considerable higher gasoline range hydrocarbon selectivity (up to 74 %) was obtained in this study. It seems that the intrinsic properties of low acidity ZSM-5 zeolite combined with the regulated iron loading and operating temperature resulted in higher selectivity obtained in this study.

- Process operating conditions considerably affected the activity and selectivity of the catalysts The following are concluded from the studies done on the effect of temperature, pressure, feed gas H_2/CO ratio, GHSV catalysts' performances.
    - The CO conversion increased while the H_2 conversion decreased with increase in the H_2/CO ratio, as expected. Catalyst selectivity tended to shift towards the lighter hydrocarbons (< C5) as H_2/CO ratio increased. CO_2 selectivity decreased with increasing H_2/CO ratio.

- In the pressure range considered, the conversion of both reactant gases increased with rising pressure. The selectivity towards the higher hydrocarbons (C5+) sharply increased while the selectivity towards the lighter hydrocarbons (C1-C4) considerably decreased with increasing pressure.
- Both CO and H_2 conversions declined with increased GHSV. The catalyst selectivity, however, seemed not to be considerably affected by changes in GHSV

- A zeolite supported iron catalyst with 9% iron (SFeZ9) was tested for the stability through 260 h time on stream test. It was found to be stable without any obvious loss in catalytic activity.

Finally, a process simulation study for a Coal to Liquid (CTL) FT process utilizing zeolite containing bi-functional FT catalyst has been realized. The main goal of the Fischer Tropsch process utilizing metal – zeolite bi-functional catalyst would be high gasoline yield with a relatively simpler process and lower investment cost. In case of such a system, it might be possible to eliminate the product upgrading section, because of the low catalyst selectivity towards long chain hydrocarbons. Three different CTG process configurations, each consisting of gasification, gas purification and Fischer Tropsch (FT) Synthesis steps, have been simulated. They were designated as CTL-OT, CTL-RC and CTL-RC-SR. They differ in respect to the re-using (recycling) of the unused syngas leaving FT reactor or tail gas. CLT-OT is the process with no recycling of tail gas which was also used as base case, CTL-RC is the process in which the tail gas was cycled back to FT reactor, and CTL-RC-SR represented the process in which the tail gas was first converted into syngas in a steam reformer reactor and then was re-used for FT synthesis. The major difference between these processes, all use a bi-functional zeolite supported iron catalyst for FT synthesis, and the conventional process is that they do not need a product up grading unit downstream of FT reactor. This is also the major superiority they acquired over the conventional process. All processes are compared based on the same process capacity of 25.000 bbl/d. The followings are the major conclusions drown.

- The catalysts used in the FT synthesis are the key factor determining the composition of the liquid fuel product obtained from the FT synthesis. By

using a proper catalyst with a high CO conversion and high selectivity for gasoline range (C5-C11) hydrocarbons, the upgrading of the raw liquid fuel obtained from FT synthesis may not be needed, and thus the whole process can be simplified. Moreover, the investment cost and the operating costs of the process can be reduced.

- The gasoline efficiencies of the processes varied as CTL-RC-SR (50%) > CTL-RC (31.4%) > CTL-OT (22.3%). Their electricity production efficiencies, followed an opposite trend with an descending order CTL-OT (22.6%) > CTL-RC (15.8%) > CTL-RC-SR (0.5%).
- All processes can be a net electricity producer under proper operating conditions. CTL-OT can attain a far higher electrical production as all tail gas was allocated for that purpose. The net electricity production of the CTL-RC-SR process, on the other hand, was the lowest.
- The gas cleaning and air separation unit (ASU) emerged to be the largest electricity consumer units for all three processes. The total share of these two units in the total process electricity consumptions varied between 53.5% and 73%, the lowest for CTL-RC-SR and highest for CTL-OT.
- The major parameters affecting the overall performance of the CTG processes were determined to be the recycling ratio of the tail gas, the recycling pressure, the steam reformer reactor S:C ratio, the reformer temperature and conversion/selectivity of the Fisher Tropsch reactor (catalyst). The effect of this parameters on process performance has been studied for CTL-RC-SR process:
    - The gasoline production efficiency of the CTG processes could be increased by recycling of the tail gas from FT reactor, but this accompanied by a decrease in the electricity production efficiency. A recycle ratio of 0.8 appears to be appropriate value to maximize gasoline production without importing electricity. The recycling ratio can be used as a tool to shift the gasoline and electricity production balance of the system in direction favoring of the desired one.
    - The pressure of the recycled tail gas stream affects the reformer conversion and the electrical generating and consuming capacities of the expander and compressor. Although the reformer conversion decreases

considerably with increase in pressure, the process efficiencies slightly worsen with pressure. The highest efficiencies are attained in the 250-750 kPa pressure range.

- The degree of conversion of light hydrocarbons back into the syngas is determined by the reformer operating conditions; temperature and S/C ratio. Conversion rises quickly with increasing temperature and S/C ratio and reaches a degree higher than 80% at 850 ^{o}C and S/C ratio=1, after which it seems to attain an asymptotic profile. As a result of increasing reformer conversion, the gasoline production efficiency also increases to some extend via re-converting of light hydrocarbons into syngas which is recycled back to the FT reactor.

- The FT catalyst is key parameter affecting the FT process performance and product properties.
  - The gasoline production efficiency improves while the electricity production capacity decreases, with increasing FT conversion.
  - Shifting the FT catalyst's selectivity to the heavier fractions is accompanied by decreasing amount of lighter C1-C4 hydrocarbons which are used for power generation, so that electrical efficiency decreases while liquid fuel production efficiency increases. For the base case scenario, the ratio of C5-C11 hydrocarbons, which represent gasoline, is determined to be 92.0%. For the lower selectivity case, however, the liquid fuel mainly composes of C4-C8 range hydrocarbons (83.6%), which means that the condensed product obtained from FT is not gasoline anymore. On the other hand, for the heavier selectivity case, the C5-C11 fraction decreased to 60.4%, while C12+ fraction increased to 38.7%. Therefore, further processing (i.e. separation, hydrocracking) is needed to upgrade the raw liquid fuel obtained from FT synthesis to the gasoline.
- The CO_2 emissions (kg CO_2/GJ FT fuel) of the processes, which is coming from power plant, in descending sequence are: CTL-OT (135.1) > CTL-RC (80.3) > CTL-RC-SR (26.8).

REFERENCES

Aly, H. M., Moustafa, E. M., Abdelrahman, E. A. (2012). Synthesis of mordenite zeolite in absence of organic template, *Advanced Powder Technology*, 23, 757-760

Anderson, R. B. (1984). *The Fischer–Tropsch Synthesis*, Academic Press, New York.

Anderson, R. B., Karn, F. S., Schultz, J. F. (1980). Kinetics on the Fischer Tropsch synthesis on iron catalysts, *Bulletin 614*, United States Bureau of Mines, 1-50.

Antonaik, K., Kowalik, P., Procniak, W., Konkol, M. , Wach, A. , Kustrowski, P., Ryczkowski, J. (2012). Effect of flash calcined alumina support and potassium doping on the activity of Co–Mo catalysts in sour gas shift process, *Applied Catalysis A: General*, 423-424, 114–120.

Aydinoglu, S. O., Atac, O., Gul, O. F., Kinayyigit, S. , Sal, S., Baranak, M. and Boz, I. (2012). α-olefin selectivity of Fe–Cu–K catalysts in Fischer–Tropsch synthesis: Effects of catalyst composition and process conditions, *Chemical Engineering Journal*, 181-182, 581–589.

Bao, B., El-Halwagi, M. M. and Elbashir, N. O. (2010). Simulation, integration, and economic analysis of gas-to-liquid processes, *Fuel Processing Technology*, 91, 703–713.

Baranak, M., Gurunlu, B., Sarioglan, A., Atac, O. and Atakul, H. (2013). Low acidity ZSM-5 supported iron catalysts for Fischer–Tropsch synthesis, *Catalysis Today*, 207, 57–64.

Barros, Z. S. and Zotin, F. (2007). Conversion of natural gas to higher valued products: light olefins production from methanol over ZSM-5 zeolites, Studies in Surface Science and Catalysis, *Natural Gas Conversion VIII*, 167, 255-260.

Bell, D. A., Towler, B. F. and Fan, M. (2011). *Coal Gasification and Its Applications (1st ed.)*,William Andrew, Oxford,

Bengoa, J. F., Alvarez, A. M., Cagnoli, M. V., Gallegos, N. G., Yeramian, A. A., Marchetti, S. G. (2002). Fischer–Tropsch reaction on Fe/Zeolite-L system. Structure and catalytic behavior, *Materials Letters*, 53, 6-11.

Bessel, S. (1995). Investigation of bifunctional zeolite supported cobalt Fischer Tropsch catalysts, *Applied Catalysis A: General*, 126, 235-244.

Boerrigter, H. (2008). *Economy of Biomass to Liquids (BTL) plants*, ECN-C-08-19, Petten, 16-18.

Botes, F. G. (2005). The effect of a higher operating temperature on the Fischer–Tropsch/HZSM-5 bifunctional process, *Applied Catalysis A: General*, 284, 21-29.

Botes, F. G. and Bohringer, W. (2004). The addition of HZSM-5 to the Fischer–Tropsch process for improved gasoline production, *Applied Catalysis A: General*, 267, 217-225.

Brian, R. (1996). Activation study of precipitated iron FT catalyst, *Energy & Fuels*, 10, 921-926.

Bukur, D. B., Mukesh, D. and Patel, S. A. (1990). Promoter effects on precipitated iron catalysts for Fischer-Tropsch synthesis, *Ind. Eng. Chem. Res.*, 29, 194.

Bukur, D.B., Patel, S.A. and Lang, X. (1990). Fixed bed and slurry reactor studies of Fischer-Tropsch synthesis on precipitated iron catalyst, *Applied Catalysis A: General*, 61, 329–349.

Cagnoli M. V., Gallegos, N. G., Alvarez, A. M., Bengoa, J. F., Yeramian, A. A., Schmal, M., Schmal, M. (2002) Catalytic CO hydrogenation on potassic Fe/zeolite LTL, *Applied Catalysis A: General*, 230, 169–176.

Calleja, G. , Lucas, A. D. and Grieken, R. V. (1991). Cobalt/HZSM-5 zeolite catalyst for the conversion of syngas to hydrocarbons, *Applied Catalysis*, 68, 11–29.

Chang Teng, L. (2004) *Cleaning Thecnologies of Synthesis Gas*, B.Sc. Thesis, The University of Queensland, 41-9.

Chang, C. D., Lang, W.H. and Silvestri, A. J. (1979). Synthesis gas conversion to aromatic hydrocarbons, *Journal of Catalysis*, 56, 268–273.

Dry, M. E. (2002). The Fischer–Tropsch process: 1950–2000, *Catalysis Today*, 71, 227–241.

Dry, M. E. (2008) *Handbook of Heterogeneous Catalysis*, (Vol. 6, pp. 2965-2994) Weinheim

Dry, M. E. (1996) Practical and theoretical aspects of the catalytic Fischer-Tropsch process, *Applied Catalysis A: General*, 138 (2), 319-344

Dry, M., Anderson, J. R. and Boudart, M. (1981). *Catalysis Science and Technology*, vol. 1, Sringer, Berlin, 1981, Chapter 4.

Egiebor, N. O. and Cooper, W. C. (1989). Synthesis of motor fuels from HY-zeolite supported Fischer-Tropsch iron catalysts, *Applied Catalysis*, 55, 47-64.

EN ISO 12185, (1996) Methods of test for petroleum and its products. Crude petroleum and petroleum products. *Determination of density. Oscillating U-tube method*.

Forghani, A. A. , Elekaei, H. and Rahimpour, M. R. (2009). Enhancement of gasoline production in a novel hydrogen-permselective membrane reactor in Fischer–Tropsch synthesis of GTL technology, *International Journal of Hydrogen Energy*, 34, 3965–3976.

Gao, X. , Yeh, C. Y. and Angevine, P. (2004). Mechanistic study of organic template removal from ZSM-5 precursors, *Microporous and Mesoporous Materials*, 70, 27-35.

Ghosh, A. K. and Curthoys, G. (1984). Characterization of zeolite acidity. A thermal study of n-butylamine and ammonia adsorbed on mordenites, *J. Phys. Chem.*, 88 (6), 1130-1132

Gonzalez, L. and Hermes, F. (2007). The acid properties of H-ZSM-5 as studied by NH_3-TPD and 27Al-MAS-NMR spectroscopy, *Applied Catalysis A: General*, 328, 174-182.

Gul, S., Ersoz, A., Baranak, M., Gul, O. F. and Akgun, F. (2010). Comparative evaluation of different coal to liquid process conditions via Fischer-Tropsch synthesis, *27th Annual International Pittsburgh Coal Conference*, PCC 2010 2 , 1471

He, J., Yoneyama, Y., Xu, B., Nishiyama, N. and Tsubaki, N. (2005). Designing a Capsule Catalyst and Its Application for Direct Synthesis of Middle Isoparaffins, *Langmuir*, 21, 1699-1702

Hla, S. S., Duffy, G. J. , Morpheth, L. D. , Cousins, A. , Roberts, D. G. and Edwards, J. H. (2011). Investigation into the performance of a Co–Mo based sour shift catalyst using simulated coal-derived syngases, *International Journal of Hydrogen Energy*, 36, 6638–6645.

Iglesia, E., Reyes, S.C. and Madon, R.J. (1991). Transport-enhanced E-olefin readsorption pathways Ru-catalyzed hydrocarbon synthesis, *J. Catal.*, 129, 238–256.

Iton, L. E., Beal, R. B. and Hodul, D. T. (1983). A new approach to the generation of metal-bearing, medium-pore, shape-selective zeolites for fischer-tropsch catalysis: spectroscopic studies of zeolites, *Journal of Molecular Catalysis*, 21, 151-171.

Karatas, H., Olgun, H. and Akgun, F. (2013). Coal and coal and calcined dolomite gasification experiments in a bubbling fluidized bed gasifier under air atmosphere, *Fuel Processing Technology*, 106, 666–672.

Kim, Y. H., Jun, K. , Joo, H., Han, C. and Song, I. K. (2009). A simulation study on gas-to-liquid (natural gas to Fischer–Tropsch synthetic fuel) process optimization, *Chemical Engineering Journal*, 155, 427–432.

Laan, V. L. (1999). *Kinetics, Selectivity and Scale Up of the Fischer-Tropsch Synthesis*, PhD Thesis, University of Groningen, Netherlands

Latham, K., Round, C. I. and Williams, C. D. (2000). Synthesis, further characterisation and catalytic activity of iron-substituted zeolite LTL, prepared using tetrahedral oxo-anion species, *Microporous and Mesoporous Materials*, 38, 333-344.

Li, X., He, J., Meng, M., Yoneyama, Y. and Tsubaki, N. (2009). One-step synthesis of H–β zeolite-enwrapped Co/Al_2O_3 Fischer–Tropsch catalyst with high spatial selectivity, *Journal of Catalysis*, 265, 26-34.

Lin, T., Schwartz, L. H. and Butt, J. B. (1986). Iron alloy Fischer-Tropsch catalysts: V. FeCo on Y zeolite, *Journal of Catalysis*, 97, 177–187.

Liu, G., Larson, E. D. , Williams, R. H. , Kreutz, T.G. and Guo, X. (2011). Making Fischer−Tropsch Fuels and Electricity from Coal and Biomass: Performance and Cost Analysis, *Energy Fuels*, 25, 415–437.

Liu, S., Gujar, A., Thomas, P., Toghiani, H. and White, M. G. (2008). Synthesis of gasoline range hydrocarbons over Mo/HZSM5 catalysts, *Applied catalysts A: General*, 357, 18-25

Liu, Z. W., Li, X., Asami, K. and Fujimoto, K. (2007). Syngas to iso-paraffins over Co/SiO_2 combined with metal/zeolite catalysts, *Fuel Processing Technology*, 88, 165-170.

Liu, Z. W., Li, X., Asami, K. and Fujimoto, K. (2005). Selective production of iso-paraffins from syngas over Co/SiO_2 and Pd/beta hybrid catalysts, *Catalysis Communications*, 6, 503–506.

Lutz, B., (2001). New age gas-to-liquids processing, *Hydrocarbon Engineering*, 6 11- 23

Martinez, A., Rollan, J., Arribas, M. A., Cerqueira, H. S., Costa, A. F. and Aguiar, E. F. S. (2007). A detailed study of the activity and deactivation of zeolites in hybrid Co/SiO_2-zeolite Fischer–Tropsch catalysts, *Journal of Catalysis*, 249, 162–173.

Martinez, A., Valencia, S., Murciano, R., Cerqueira, H. S., Costa, A.F. and Aguiar, E. F. S. (2008). Catalytic behavior of hybrid Co/SiO_2-(medium-pore) zeolite catalysts during the one-stage conversion of syngas to gasoline, *Applied Catalysis A: General*, 346, 117–125.

Martinez, A. and Lopez, C. (2005). The influence of ZSM-5 zeolite composition and crystal size on the in situ conversion of Fischer–Tropsch products over hybrid catalysts, *Applied Catalysis A: General*, 294, 251–259.

Mondal, P., Dang, G. S. and Garg, M. O. (2011). Syngas production through gasification and cleanup for downstream applications - Recent developments, *Fuel Processing Technology*, 92, 1395–1410.

Nazar, L. F., Ozin, G. A., Hugues, F. and Godber, J. (1983). Metal atoms in solution: versatile reagents for preparing metal cluster-zeolite catalysts; application to the selective reduction of carbon monoxide to butene, *Journal of Molecular Catalysis*, 21, 313-329.

Ngamcharussrivichai, C., Liu, X., Li, X., Vitidsant, T. and Fujimoto, K. (2007). An active and selective production of gasoline-range hydrocarbons over bifunctional Co-based catalysts, *Fuel*, 86, 50-69

Nieto, C., Arenas, E., Arrieta, A., Zapata, Z., Londono, C., Valdes C. and Chejne, F. (2008). Simulation of IGCC technologies: ınfluence of operational conditions (environmental and fuel gas production, *Revise Energetica*, 40, 39

Nowicki, L., Ledakowicz, S. and Bukur, D. B. (2001). Hydrocarbon selectivity model for the slurry phase Fischer–Tropsch synthesis on precipitated iron catalysts, *Chemical Engineering Science*, 56, 1175–1180.

O'Brien, R. J., Xu, L., Spicer, R. L., Bao, S., Milburn, D. R. and Davis, B. H. (1997). Activity and selectivity of precipitated iron Fischer-Tropsch catalysts, *Catalysis Today*, 36, 325–334.

Pour, A. N., Zamani, Y., Tavasoli, A., Shahri, S. M. K. and Taheri, S. A. (2008). Study on products distribution of iron and iron–zeolite catalysts in Fischer–Tropsch synthesis, *Fuel*, 87, 2004–2012.

Pour, A. N., Zare, M., Shahri, S. M. K., Zamani, Y. and Alaei, M. R. (2009). Catalytic behaviors of bifunctional Fe-HZSM-5 catalyst in Fischer–Tropsch synthesis, *Journal of Natural Gas Science and Engineering*, 1, 183–189.

Ratnasamy, C. and Wagner, J. (2008) Water Gas Shift Catalysis, *Catal. Rev.*, 51, 325-440

Ravishankar, R., Li, M. M. and Borgna, A. (2005). Novel utilization of MCM-22 molecular sieves as supports of cobalt catalysts in the Fischer–Tropsch synthesis, *Catalysis Today*, 106, 149-153.

Rohde, M. P., Schaub, G., Khajavi, S., Jansen, J. C. and Kapteijn, F. (2008) Fischer–Tropsch synthesis with in situ H_2O removal – Directions of membrane development, *Microporous and Mesoporous Materials*, 115, 123-136

Sarioglan, A., Senatalar, A. E., Savasci, O. T. and Taarit, Y. B. (2004). The effect of dealumination on the apparent and actual rates of aromatization of methane over MFI-supported molybdenum catalysts, *Journal of Catalysis*, 226, 210-214.

Sarkari, M., Fazlollahi, F., Razmjooies, A., Mirzaei, A. (2011). FisherTropsch Synthesison Alumina Supported Iron-Nickel Catalysts: Effect of Preparation Methods, *Chemical and Biochemical Engineering*, 25, 289-297

Schulz, H., Niederberger, H. L., Kneip, M. and Weil, F. (1991). Synthesis Gas Conversion on Fischer-Tropsch Iron/HZSM5 Composite Catalysts, *Studies in Surface Science and Catalysis*, 61, 313-323.

Sie, S. T., Senden, M. M. G. and van Wechum, H. M. H. (1991). Conversion of natural gas to transportation fuels via the shell middle distillate synthesis process (SMDS), *Catalysis Today*, 8, 371–394.

Spath, P. L., Dayton, D. C. (2003). *Preliminary Screening - Technical and Economic Assessment of Synthesis Gas to Fuels and Chemicals with Emphasis on the Potential for Biomass-Derived Syngas*, pp 90-110, Springfield VA,

Steynberg, A. P. and Nel, H. G. (2004). Clean coal conversion options using Fischer–Tropsch technology, *Fuel*, 83, 765–770.

Steynberg, A. P., Espinoza, R. L., Jager, B., Vosloo, A. C. (1999). High temperature Fischer-Tropsch synthesis in commercial practice, *Appl. Catal. A*, 186 (1-2), 41-54.

Steynberg, A., Dry, M. (2004) Studies Surface Science and Catalysis 152, *Fischer Tropsch Technology*, Elsevier Science and Technology Books.

Sudiro, M. and Bertucco, A. (2009). Production of synthetic gasoline and diesel fuel by alternative processes using natural gas and coal: Process simulation and optimization, *Energy*, 34, 2206–2214.

Suib, S. L., Mcmohan, K. C., Tau, L. M. and Bennett, C. O. (1984). Synthesis, characterization, and Fischer-Tropsch studies of iron-containing zeolites, *Journal of Catalysis*, 89, 20–34.

Trainer, J. P., Dubettier, R. and Perrin, N. (2009). Air Seperation, *1st International Oxyfuel Combustion Conference*, Cottbus.

Trippe, F., Fröhling, M., Schultmann, F., Stahl, R. and Henrich, E. (2011). Techno-economic assessment of gasification as a process step within biomass-to-liquid (BtL) fuel and chemicals production, *Fuel Processing Technology*, 92, 2169–2184.

Udaya, V., Rao, S., Gormley, R. J., (1990) Bifunctional catalysis in syngas conversions, *Catal. Today*, 6, 207 –234

Url-1: <http://fixingtheeconomists.wordpress.com/2013/07/12/oil-price-speculation-an-interesting-battle> date retrieved 04.03.2014.

Url-2: <http://Europhysicsnews.org> date retrieved 02.06.2013.

Url-3: <http://Cmasc.gmu.edu> date retrieved 05.01.2013.

Url-4: <http://en.wikipedia.org/wiki/Faujasite> date retrieved 01.11.2013.

Viswanadham, N., Murali, G. and Prasada Rao T.S.R. (1997). Pore size analysis of ZSM-5 catalysts used in n-heptane aromatization reaction: An evidence for molecular traffic control (MTC) mechanism, *Journal of Molecular Catalysis A: Chemical*, 2-3, L87-L90.

Vosloo, A. C. (2001). Fischer–Tropsch: a futuristic view, *Fuel Processing Technology*, 71, 149–155.

Wan, H., Wu, B., Zhang, C., Xiang, H. and Li, Y. (2008). Promotional effects of Cu and K on precipitated iron-based catalysts for Fischer–Tropsch synthesis, *J. Mol. Catal. A: Chem.*, 283, 33-42.

Wang, P., Kang, J., Zhang, Q., Wang, Y. (2007). Development of Novel Catalysts for Fischer–Tropsch Synthesis: Tuning the Product Selectivity, *Catal. Lett.*, 114, 178 –184.

Wender, I. (1996). Reactions of synthesis gas, *Fuel Processing Technology*, 48, 189-297.

Yalınkılıç, F. (2013) Yüksek kur enerji faturasını büyütebilir. Retrieved from http://realtime.wsj.com/turkey/2013/08/26/yuksek-kur-enerji-faturasini-buyutebilir/.

Yang, G., He, J., Yoneyama, Y., Tan, Y., Han, Y. and Tsubaki, B. (2007). Preparation, characterization and reaction performance of H-ZSM-5/cobalt/silica capsule catalysts with different sizes for direct synthesis of isoparaffins, *Applied Catalysis A: General*, 329, 99–105.

Yang, G., Tan, Y., Han, Y., Qui, J., Tsubaki, N. (2008) Increasing the shell thickness by controlling the core size of zeolite capsule catalyst: Application in iso-paraffin direct synthesis, *Catalysis Communications*, 9, 2520–2524

Yoneyama, Y., Sun, X., Zhao, T., Wang, T., Iwai, T., Ozaki, K. and Tsubaki, N. (2010). Direct synthesis of isoparaffin from synthesis gas under supercritical conditions, *Catalysis Today*, 149, 105-110.

Zhang, Q. , Kang, J. and Wang, Y. (2010). Development of Novel Catalysts for Fischer–Tropsch Synthesis: Tuning the Product Selectivity, *ChemCatChem*, 2, 1030–1058.

Zhanga, N. and Lior, N. (2008). Two novel oxy-fuel power cycles integrated with natural gas reforming and CO_2 capture, *Energy*, 33, 340–351.

Zola, A. S., Bidart, A. M. F., Fraga, A. C., Hori, C. E., Aguiar, E. F. S. and Arroyo, P. A. (2007). Cobalt supported on different zeolites for fischer-tropsch synthesis, *Studies in Surface Science and Catalysis, Natural Gas Conversion VIII*, 167, 129-134.

APPENDICES

APPENDIX A : Hydrocarbon analysis of the catalysts.

APPENDIX B : Operating conditions and streams compositions of CTL-RC and CTL-OTprocesses for the base case.

APPENDIX A: Hydrocarbon analysis of the catalysts.

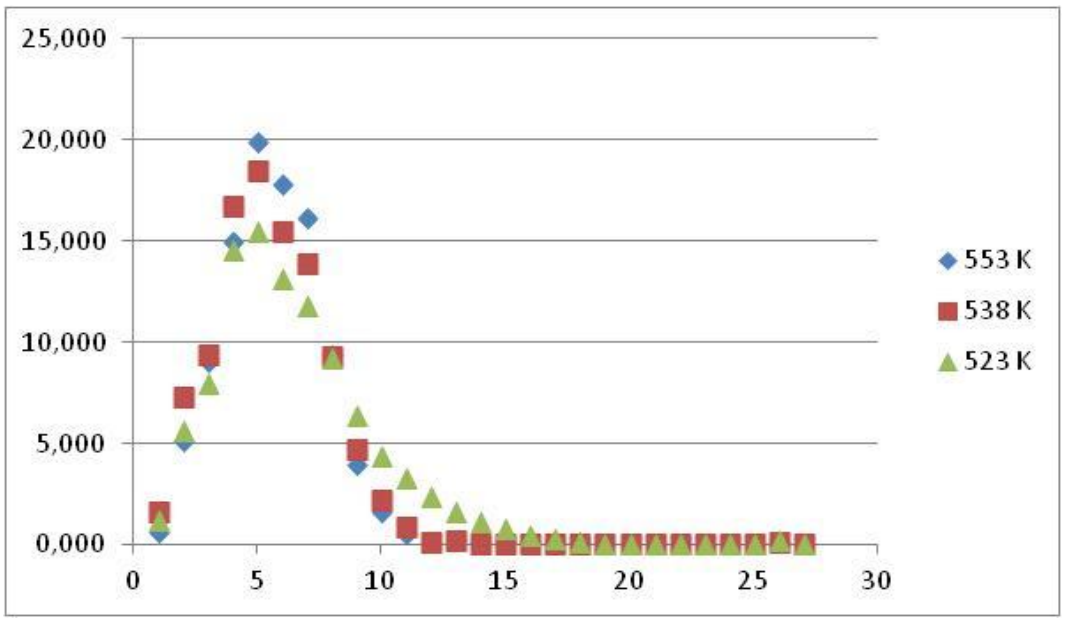

(a) SFeZ20

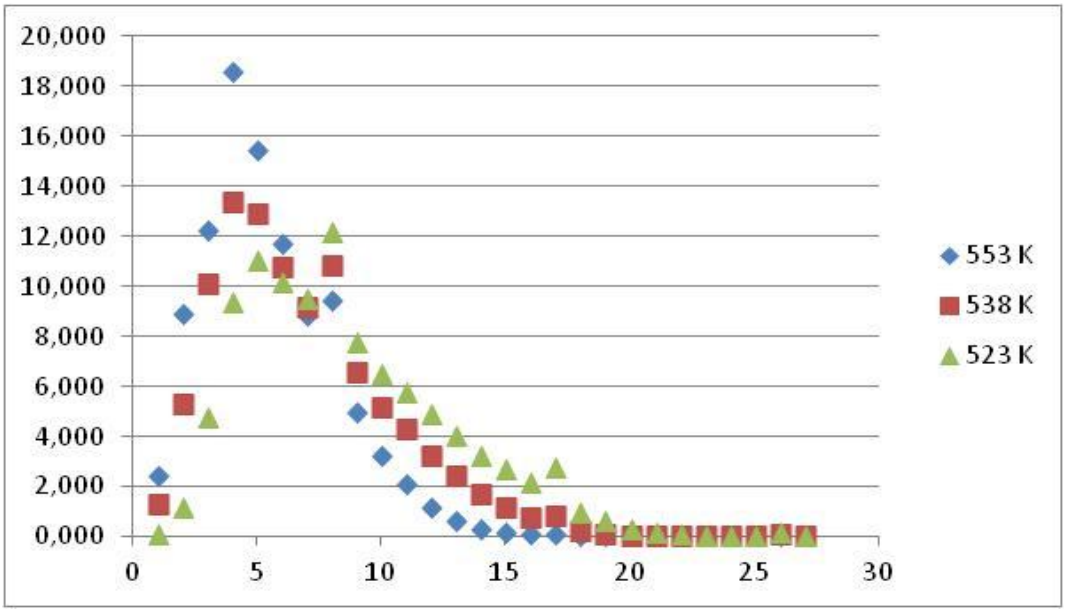

(b)SFeY5

Figure A.1 : Composition of liquid phase products obtained by zeolite supported catalysts (P=19 bara, GHSV=750 h^{-1}, $H_2/CO=2$).

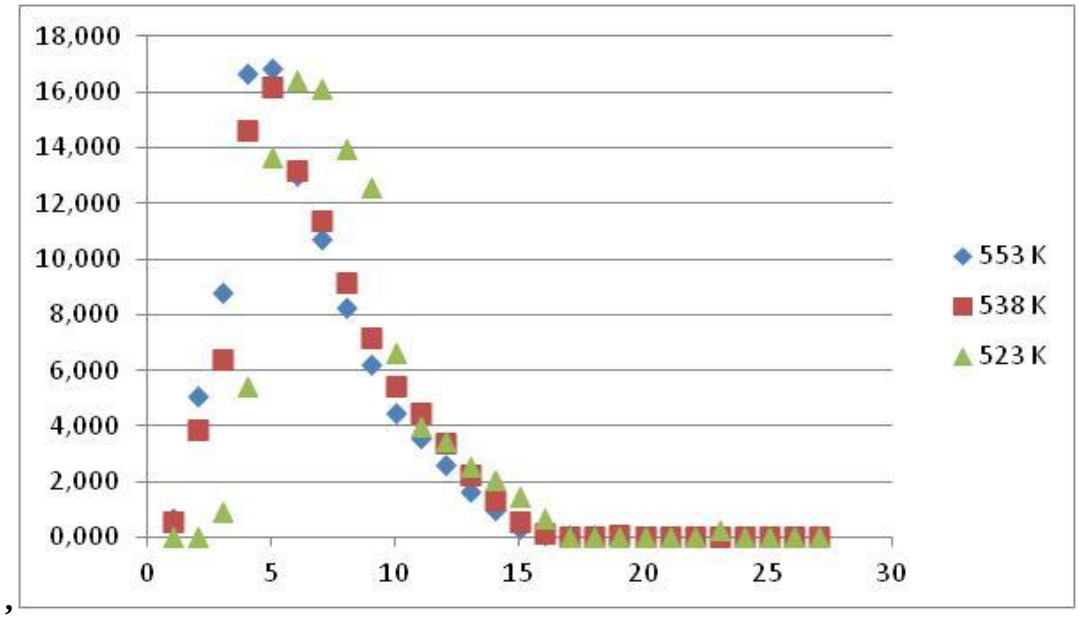

,

(c) SFeF

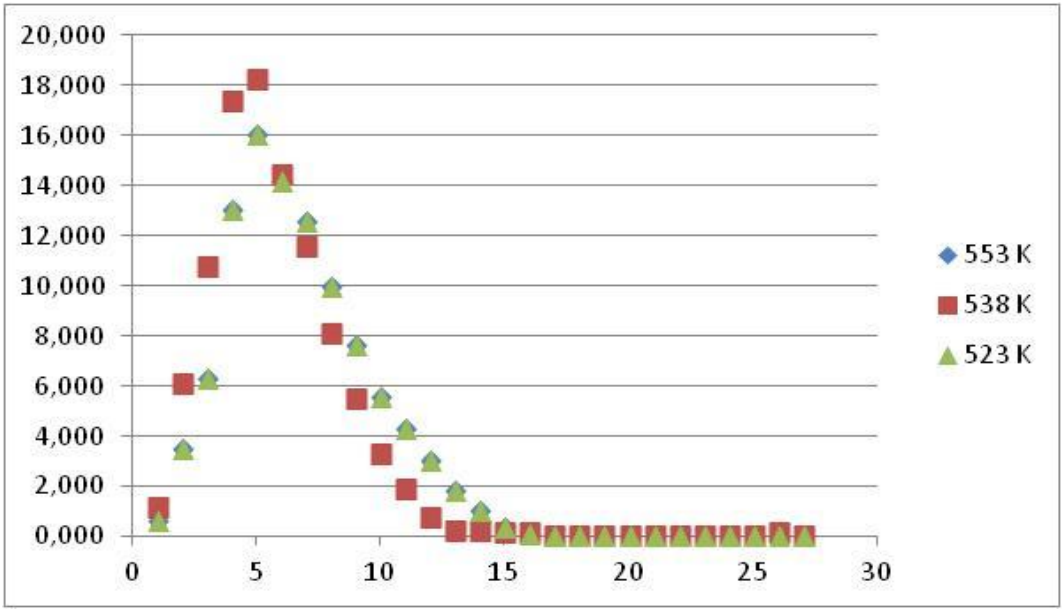

(d) SFeB

Figure A.1 (continued) : Composition of liquid phase products obtained by zeolite supported catalysts (P=19bara,GHSV=750h^{-1},H_2/CO=2).

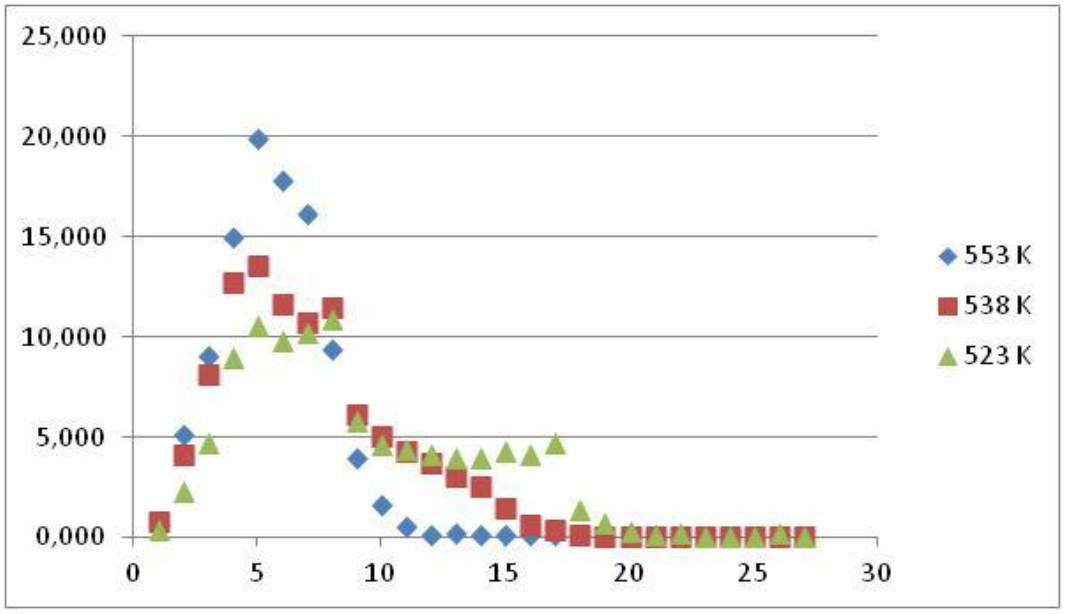

(e) SFeY80

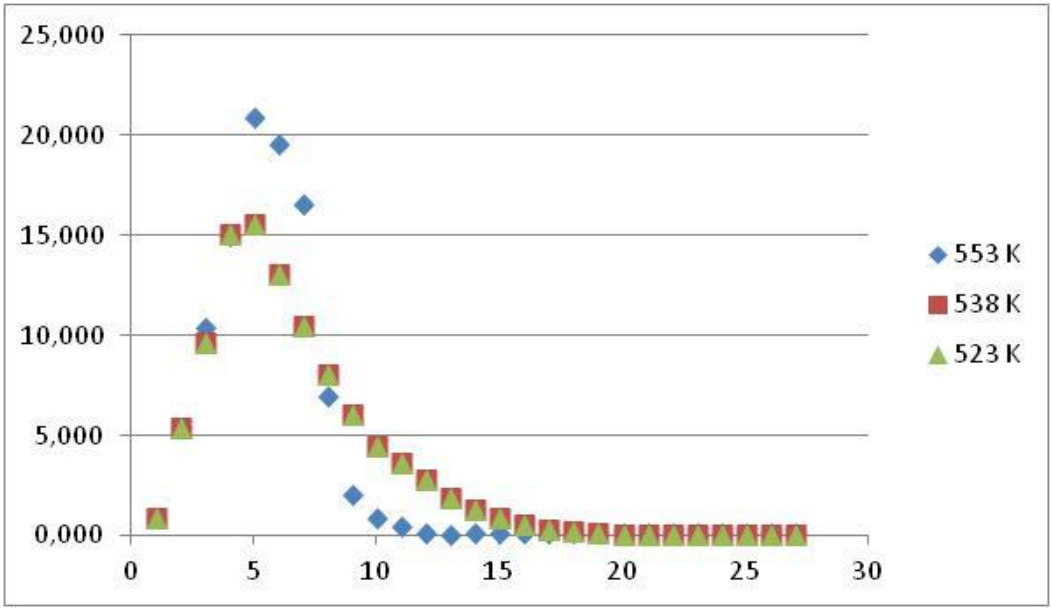

(f) BFe

Figure A.1 (continued) : Composition of liquid phase products obtained by zeolite supported catalysts (P=19bara,GHSV=750h^{-1}, H_2/CO=2).

APPENDIX B : Operating conditions and streams compositions of CTL-RC and CTL-OTprocesses for the base case.

Table B.1 : Operating conditions and streams compositions of CTL-RC process for the base case.

Stream Name	Operating Conditions			Composition (molar)							
	T(C)	P(kPa)	F (ton/h)	H_2	CO	CO_2	H_2O	O_2	N_2	CH_4	Bal.
Coal Input	20	2000	792.3	0.22	-	-	0.12	0.06	0.01	-	0.59
ASU Air Inlet	25	100	2010.2	-	-	-	-	0.21	0.79	-	0.00
Gasifier O_2 Inlet	460	2000	446.6	-	-	-	-	0.99	0.01	-	0.00
Gasifier Outlet	848	2000	1214.7	0.21	0.51	0.13	0.06	0.00	0.01	0.08	0.00
Scrubber Water Inlet	20	2000	1893.6	-	-	-	1.00	-	-	-	0.00
Scrubber Gas Outlet	176	2000	1962.9	0.12	0.28	0.07	0.47	-	0.00	0.04	0.02
WGS Inlet	176	2000	1204.2	0.12	0.28	0.07	0.47	-	0.00	0.04	0.02
WGS ByPass	176	2000	758.7	0.12	0.28	0.07	0.47	-	0.00	0.04	0.02
Flush Outlet	40	2000	1403.9	0.39	0.21	0.32	0.00	-	0.01	0.06	0.01
AGR Effluent	16	2000	883.7	0.00	0.00	0.98	-	-	-	-	0.02
AGR Syngas Outlet	16	2000	520.2	0.57	0.31	0.01	0.01	0.00	0.01	0.09	0.00
FT Inlet	280	2000	1419.6	0.39	0.20	0.09	0.00	0.00	0.02	0.27	0.03
FT Outlet	280	2000	1495.3	0.17	0.07	0.13	0.20	0.00	0.03	0.35	0.05
3 Phase Sep. Vap Out.	20	2000	1124.4	0.21	0.09	0.17	0.00	0.00	0.04	0.44	0.05
3 Phase Sep. H_2O Out.	20	2000	248.0			0.00	0.998				0.00
3 Phase Sep. HC Out.	20	2000	122.9	0.00	0.00	0.05	0.00	0.00	0.00	0.05	0.90
Condenser Vap. Out.	20	100	6.8	0.02	0.02	0.29	0.00	0.00	0.01	0.30	0.36
Liquid Fuel Product	20	100	116.6	-	-	0.00	-	-	-	0.00	1.00
Turbine Inlet	415	1800	224.9	0.21	0.09	0.17	0.00	-	0.04	0.44	0.05
Turbine Outlet	292	500	224.9	0.21	0.09	0.17	0.00	-	0.04	0.44	0.05
Power Plant Feed Gas	285	100	232.2	0.21	0.09	0.17	0.00	-	0.04	0.44	0.05
Recycled Tail Gas	19	1800	899.5	0.21	0.09	0.17	0.00	-	0.04	0.44	0.05
Recycle Gas to FT	250	2000	899.5	0.22	0.09	0.17	0.00	-	0.04	0.44	0.04

Table B.2 : Operating conditions and streams compositions of CTL-OT process for the base case.

Stream Name	Operating Conditions			Composition (molar)							
	T(C)	P(kPa)	F (ton/h)	H_2	CO	CO_2	H_2O	O_2	N_2	CH_4	Bal.
Coal Input	20	2000	1118.9	0.22	-	-	0.12	0.06	0.01	-	0.59
ASU Air Inlet	25	100	2838.8	-	-	-	-	0.21	0.79	-	0.00
Gasifier O_2 Inlet	460	2000	630.7	-	-	-	-	0.99	0.01	-	0.00
Gasifier Outlet	848	2000	1715.5	0.21	0.51	0.13	0.06	0.00	0.01	0.08	0.00
Scrubber Water Inlet	20	2000	2674.1	-	-	-	1.00	-	-	-	0.00
Scrubber Gas Outlet	176	2000	2772.1	0.12	0.28	0.07	0.47	-	0.00	0.04	0.02
WGS Inlet	176	2000	1763.0	0.12	0.28	0.07	0.47	-	0.00	0.04	0.02
WGS ByPass	176	2000	1008.7	0.12	0.28	0.07	0.47	-	0.00	0.04	0.02
Flush Outlet	40	2000	1995.9	0.39	0.20	0.32	0.00	-	0.01	0.06	0.02
AGR Effluent	16	2000	1279.2	-	-	0.98	-	-	-	-	0.02
AGR Syngas Outlet	16	2000	716.8	0.59	0.29	0.01	0.01	-	0.01	0.09	0.00
FT Inlet	280	2000	716.8	0.59	0.29	0.01	0.01	-	0.01	0.09	0.00
FT Outlet	280	2000	823.6	0.27	0.11	0.05	0.37	-	0.01	0.15	0.04
3 Phase Sep. Vap Out.	20	2000	414.0	0.44	0.18	0.08	0.00	0.00	0.02	0.25	0.03
3 Phase Sep. H_2O Out.	20	2000	289.4	-	-	0.00	0.999	-	-	-	0.00
3 Phase Sep. HC Out.	20	2000	120.2	0.01	0.01	0.02	0.00	-	0.00	0.02	0.94
Condenser Vap. Out.	20	100	2.8	0.09	0.09	0.25	0.00	-	0.01	0.31	0.25
Liquid Fuel Product	20	100	116.6	-	-	0.00	-	-	-	-	1.00
Turbine Inlet	415	1800	414.0	0.44	0.18	0.08	0.00	-	0.02	0.25	0.03
Turbine Outlet	269	500	414.0	0.44	0.18	0.08	0.00	-	0.02	0.25	0.03
Power Plant Feed Gas	268	100	417.0	0.44	0.18	0.08	0.00	-	0.02	0.25	0.03

CURRICULUM VITAE

Name Surname: Murat Baranak

Place and Date of Birth: İstanbul – 05.08.1979

E-Mail: murat.baranak@tubitak.gov.tr

EDUCATION:

B.Sc.: İTÜ Chemical Engineering Department

M.Sc. : İTÜ Material Science and Engineering Department

PROFESSIONAL EXPERIENCE AND REWARDS:

In 2001 he started working as a Research Assistant at Istanbul Technical University. He has been working at TUBITAK MRC Energy Institute as researcher (later chief senior researcher) since 2002. He was the coordinator of 4 national/international big size projects and worked as a researcher for more than 10 projects. His research experience includes Fischer Tropsch synthesis and catalysis, cogeneration, flue gas cleaning technologies, hydrogen production and fuel cell systems. He is specialized in the fields of process design and commissioning, reactor design, process simulation and catalysis. He is the author of 6 SCI indexed articles, more than 20 Conference proceedings. He is the owner of 4 TÜBİTAK MRC Project Encouragement Awards.

PUBLICATIONS, PRESENTATIONS AND PATENTS ON THE THESIS:

- **Baranak, M.,** Gurunlu, B., Sarioglan, A., Atac, O. and Atakul, H. (2013). Low acidity ZSM-5 supported iron catalysts for Fischer–Tropsch synthesis, *Catalysis Today*, 207, 57–64.
- **Baranak, M.,** Gurunlu, B., Sarioglan, A. and Atakul, H. (2012). Effect of zeolite type on the performance of bifunctional iron based Fischer Tropsch catalysts, *6th International Ege Energy Symposium & Exhibition*, İzmir / Türkiye
- **Baranak, M.,** Gurunlu, B., Sarioglan, A. and Atakul, H. (2011). Synthesis Of Gasoline - Range Hydrocarbons Over Zeolite Supported Iron Catalysts via Fischer Tropsch Synthesis, *61st Canadian Chemical Engineering Conference*, Ontario/Canada
- **Baranak, M.,** Gurunlu, B. and Atakul, H. (2011). Simulation of Direct Synthesis of Gasoline via Alternative Fischer Tropsch Process – Zeolite Based Fischer Tropsh Catalyst, *61st Canadian Chemical Engineering Conference*, Ontario/Canada
- **Baranak, M.,** Gurunlu, B., Sarioglan, A. and Atakul, H. (2012). Production of gasoline-range hydrocarbons over dealuminated zeolite supported iron catalysts in Fischer Tropsch synthesis, *International Congress on Catalysis*, Munich, Germany

OTHER PUBLICATIONS, PRESENTATIONS AND PATENTS :

- Aydinoglu, S. O. , Atac, O. , Gul, O. F. , Kinayyigit, S. , Sal, S. , **Baranak, M.** and Boz, I. (2012). α-olefin selectivity of Fe–Cu–K catalysts in Fischer–Tropsch synthesis: Effects of catalyst composition and process conditions, *Chemical Engineering Journal*, 181-182, 581–589.
- **Baranak**, **M.** and Atakül, H. (2007). A basic model for analysis of molten carbonate fuel cell behavior, *Journal Of Power Sources*, 172, 831–839.
- Sarioglan, A., Olgun, H., **Baranak**, **M.**, Ersoz, A., Atakul, H. and Ozdogan, S. (2007). Diesel evaporation as the first step of hydrogen production, *International Journal of Hydrogen Energy*, 32, 2895– 2901.
- Yılmaz, O., **Baranak, M.**, Güner, S. and Erciyes, T. (2005). The usage of linseed oil-based polyurethanes as a rheological modifier, *Journal of Applied Polymer Science*, 98, Vol. 3, 1032-1035.
- Güner, S., **Baranak, M.**, Soytaş, S., Erciyes, T. (2004). Flow Behaviour of Oil Modified Polymer Solutions, *Progress in Organic Coatings*, 50 , 172-178.
- Akgün, F., İlhan, N, Özyönüm, G. N., and **Baranak, M.** (2009). **Y**akıt Pilli Mikro Kojenerasyon Sistemi" *3e ELECTROTECH*, 177, 3, 112, 2009.
- İlhan, N., Özyönüm, G. N., **Baranak, M.** and Akgün F. (2010). Enerji Verimliliğinde Evsel Mikro Kojenerasyon Uygulamaları, *Enerji Verimliliği*, 1, 72–75.

- **Baranak, M**., Kaytaz, A., Ersöz, A. et. al. (2008). A Pem Fuel Cell Micro Cogeneration System. *14th Energy and Environment Technologies Systems Exhibition and Conference,* Istanbul.
- Akgun, F., Kaytaz, A., İlhan, N., **Baranak, M.**, Özyönüm, G. N., Akış, C., Ersöz, A,. Sarıoğlan (2007). A Fuel Cell Micro Cogeneration System" *International Hydrogen Energy Congress and Exhibiton,* Istanbul.
- **Baranak, M.**, Ersöz, A.,et. al., (2008). Hydrogen production and utilization for residential combined heat and power applications, *German – Turkish TU9-Workshop on Sustainable Energy*, Kocaeli.
- **Baranak, M.**, Atakül, H., Şener, T. (2005). A Model for Molten Carbonate Fuel Cell, *International Hydrogen Energy Congress and Exhibition*, İstanbul.
- Sarioglan, A., Olgun, H., Ersoz, A., **Baranak, M.**, Atakul, H., Ozdogan, S. (2005). Diesel evaporation as the first step of hydrogen production, *2nd European Hydrogen Energy Conference*, Zaragoza, Spain.
- Gül, S., Ersoz, A., **Baranak, M.**, Gul, O. F., Akgun, F. (2010). Comparative evaluation of different coal to liquid process conditions via Fischer-Tropsch synthesis, *International Pittsburgh Coal Conference*, İstanbul.
- Kaytaz, A., **Baranak, M.**, Akgün, F. (2010) Exergy Analysis of Hydrogen Production Unit Integrated with a PEM Fuel Cell, *18th World Hydrogen Energy Conference 2010*, İstanbul.
- Ünlü, N., **Baranak, M.**, Akgün, F., Tiris, M. (2005). Molten Carbonate Fuel Cell, Naval Applications, *International Cogeneration Conference*, Istanbul.
- Akar E., Genç, F., Sağlam, G., **Baranak, M.**, Korkmaz, Ö., Obut, S., Akgün, F. (2009). Evsel Mikro Kojenerasyon Uygulamaları ile Enerji Verimliliğinin Arttırılması, 2. Enerji Verimliliği Kongresi, İstanbul.
- **Baranak, M.**, Soytas, S., Çalıca, S., Güner, S., Erciyes, T. (2002). Yüksek Katı İçerikli Yüzey Kaplayıcıların Reolojik ve Film Özelliklerinin İncelenmesi, *Ulusal Kimya Müh. Kongresi 5*, Ankara.
- Yılmaz, O., B**aranak, M.**, Güner, S., Erciyes, T. (2004). Üretan yağı yapının tiksotropik akış davranışına etkisinin incelenmesi", Paint 2004, V. *International Paint, Varnish, Ink and Auxiliary Products Industry Conference and Exhibition*, İstanbul.
- **Baranak, M.**, Atakül, H., (2004). Modeling Molten Carbonate Fuel Cells, National *Chemical Engineering Congress*, Izmir.
- Yilmaz, O., **Baranak, M.**, Guner, S., Erciyes, T. (2004). Effect of Urethane Oils on Thixotropic Flow Behaviour, *V. International Paint, Varnish, Ink ad Auxiliary Products Industry Conference and Exhibitions*, İstanbul.